

**THE ROLE OF THE GATA TRANSCRIPTION FACTOR
Gaf1 IN NUTRIENT RESPONSES AND CELLULAR
AGEING**

S. GONZALEZ

Ph.D.

2022



**THE ROLE OF THE GATA TRANSCRIPTION FACTOR
Gaf1 IN NUTRIENT RESPONSES AND CELLULAR
AGEING**

SUAM GONZALEZ

**A thesis submitted in partial fulfilment of the requirements of the
University of East London for the degree of Doctor of Philosophy**

School of Health Sport and Bioscience

March 2022

DECLARATION

I hereby certify that the work presented within this thesis is the result of my own investigation, except where reference has been made to published literature and where acknowledgment is made for unpublished data. During the course of this research programme I have not been registered or enrolled to another award from any academic or professional institutions.

Suam Gonzalez.

School of Health, Sport and Bioscience

University of East London

2022

Abstract

The discovery of the biological bases of ageing continues to be one of the most fascinating challenges in modern science. Current efforts have narrowed the complexity of such task by focusing on mechanisms used by the cell to couple its physiology with environmental stimuli as they are often involved in the regulation of ageing. The Target of Rapamycin (TOR) have been proved to be a rheostat of nutritional status orchestrating cellular growth and homeostasis mainly through the regulation of transcriptional responses that remain to be understood. Recent studies unveiled novel functions of the evolutionarily conserved GATA transcription factor Gaf1 in nutrient sensing pathways and potentially in cellular ageing by regulating transcription downstream of TOR signalling. To elucidate these questions, the robust model organism *Schizosaccharomyces pombe* was used in this study due to its relevant similarity with higher eukaryotes and thoroughly described genetics. The experimental settings involved a combination of *in silico* analyses, fitness assessments, revivability assays, transcriptomics, mutagenesis, chemical-genetics, and interactome to further characterise functions of Gaf1. This study also contributed to the identification of candidate genes that promote longevity and mediate the resistance of mutant cells depleted of *gaf1* gene to the TOR-kinase inhibitor torin1. The results indicate that upon TOR complex 1 (TORC1) inhibition, Gaf1 represses genes that induce protein translation (anabolism) and upregulates genes required for survival (catabolism) under adverse nutritional conditions downstream of TORC1.

Acknowledgements

I would like to express my infinite gratitude to my supervisor Charalampos Rallis for giving me the opportunity to pursue my research interests and passion, for his unconditional help, guidance and valuable advice. I would also like to thank the University of East London for funding my research and our collaborators Jürg Bähler and Maria Rodriguez-Lopez for all the resources provided for the completion of this project. I would like to express my gratitude to my supervisor David Bringloe, academic staff David Guiliano, Sally Cutler, Winston Morgan, and academic coordinators Nazmin Uddin and Richard Bottoms for their support throughout my studies at the university and for their help with my project. My gratitude also goes to all the members of the lab for making my PhD journey a great and enjoyable experience as well as for their unforgettable friendships. I would also like to extend my acknowledgements to my mother for always supporting my dreams, my sister and aunty Vilma for their infinite love, as well as the rest of my family, friends and colleagues for always being present. Special thanks to Roberta Cordeiro for her help, advises, constructive feedback and admirable encouragement throughout my PhD endeavour. Thank you to my father and all the loved ones that accompany me from beyond physical barriers, this work is inspired by you. Thank you all for being part of this wonderful experience.

Resources derived from this thesis

Publications:

- Martinez-Miguel VE, Lujan C, Espie-Caullet T, Martinez-Martinez D, Moore S, Backes C, Gonzalez S, Galimov ER, Brown AEX, Halic M, Tomita K, Rallis C, von der Haar T, Cabreiro F, Bjedov I. (2021). Increased fidelity of protein synthesis extends lifespan. *Cell Metabolism*. S1550-4131(21):00417-4. doi: 10.1016/j.cmet.2021.08.017.
- Rodríguez-López M, Gonzalez S, Hillson O, Tunnaclyffe E, Codlin S, Tallada V, Bähler J, Rallis C. (2020). The GATA Transcription Factor Gaf1 Represses tRNAs, Inhibits Growth, and Extends Chronological Lifespan Downstream of Fission Yeast TORC1. *Cell Reports*. 30(10): 3240–3249.e4. doi: 10.1016/j.celrep.2020.02.058.
- Hillson O, Gonzalez S, Rallis C. (2018). Prospects of Pharmacological Interventions to Organismal Aging. *Biomolecular Concepts*. 9(1):200-215. doi: 10.1515/bmc-2018-0018.
- Gonzalez S, Rallis C. (2017). The TOR Signaling Pathway in Spatial and Temporal Control of Cell Size and Growth. *Frontiers in Cell and Developmental Biology*. 5:61. doi: 10.3389/fcell.2017.00061.

Technical resources:

- Tolerance of fission yeast to cytotoxicity of torin1.
- Chronological lifespan of the fission yeast mutant strains (with and without torin1 treatment): wild type (972), *gaf1*Δ, *toco89*Δ, *tor1*Δ.
- Improvement of the laboratory protocol for generation of query strains for Synthetic Genetic Array experiments applying electroporation.

General resources:

- List of Gaf1-dependent differentially expressed protein-coding genes in the fission yeast genome with and without TOR signalling inhibition (Gaf1-dependent transcriptome). The essential and non-essential genes were integrated with curated data about intronic content to explore potential regulatory functions of non-coding regions.
- List of all non-essential genes in the fission yeast genome showing synthetic genetic interactions with the *gaf1* gene with and without TOR signalling inhibition (Gaf1-interactome).

List of abbreviations

Adenosine Monophosphate (AMP)

Adenosine triphosphate (ATP)

Adenosine Monophosphate-activated protein kinase (AMPK)

Aminoimidazole carboxamide riboside (AICAR)

Analysis of Gene Lists (*AnGeLi*)

Base pair (bp)

Basic Local Alignment Search Tool (BLAST)

Caenorhabditis elegans (*C. elegans*)

Colony forming unit (CFU)

Complementary DNA (cDNA)

Chromatin immunoprecipitation-sequencing (ChIP-seq)

Chronological Lifespan assays (CLS)

Deoxyribonucleic acid (DNA)

Downregulated (DR)

Edinburgh Minimal Medium (EMM2)

EMM2 supplemented with nitrogen (EMM2+N)

Endoplasmic Reticulum (ER)

Ethanol (EtOH)

Ethylenediaminetetraacetic acid (EDTA)

False Discovery Rate (FDR)

Gene Ontology (GO)

gDNA: genomic DNA

Green fluorescent protein (GFP)

Guanosine-5'-triphosphate (GTP)

Messenger RNA (mRNA)

New end take off (NETO)
Nucleotide (nt)
Open reading frame (ORF)
Optical Density (OD)
Phosphate buffered saline (PBS)
Protein-to-Protein Interaction (PPI)
Polymerase chain reaction (PCR)
Pombe PCR Primer Programs (PPPP)
Replicative lifespans (RLS)
Revolutions per minute (rpm)
Ribonuclease (RNase)
Ribonucleic acid (RNA)
RNA interference (RNAi)
RNA polymerase III (RNA Pol III)
Schizosaccharomyces japonicus (*S. japonicas*)
Schizosaccharomyces octosporus (*S. octosporus*)
Schizosaccharomyces pombe (*S. pombe*)
Synthetic Genetic Array (SGA)
Target of Rapamycin (TOR)
Target of Rapamycin complex 1 (TORC1)
Target of Rapamycin complex 2 (TORC2)
Transcription Factors (TFs)
Transfer RNA (tRNA)
University College London (UCL)
Upregulated (UR)
Untranslated Regions (UTRs)
Yeast Extract with supplements (YES)

LIST OF CONTENTS

Page

LIST OF CONTENTS.....	vii
1. Chapter 1. Introduction	1
1.1. Current perspectives on ageing.....	1
1.2. TOR pathway: A conserved rheostat of nutrient-sensing	3
1.3. Pharmacological inhibition of TOR signalling in <i>S. pombe</i>	11
1.4. Functional genetics of <i>S. pombe</i>	15
1.4.1. Biology & life cycle.....	15
1.4.2. Genomic configuration.....	19
1.5. The GATA transcription factor Gaf1	21
1.6. Aims of the project and contribution	23
2. Chapter 2. Materials and methods.....	26
2.1. In-silico analyses of Gaf1 transcription factor	26
2.1.1. Screening for orthologues.....	26
2.1.2. Transcriptional responses of <i>gaf1</i>	26
2.1.3. Protein interactions network of Gaf1.....	27
2.2. General techniques	27
2.2.1. Fission yeast strains, media and treatments.....	27
2.2.2. Collection and storage of <i>S. pombe</i> cells	31
2.2.3. Genomic DNA extraction	32
2.2.4. RNA extraction	34
2.2.5. Polymerase chain reaction (PCR)	35
2.2.6. Gel electrophoresis for DNA visualisation.....	36
2.2.7. Generation of the <i>gaf1</i> Δ query strain	37
2.2.8. Transformation of <i>S. pombe</i> cells into <i>gaf1</i> Δ query strain	40

2.3. Specific techniques	42
2.3.1. Growth assays for fitness assessment	42
2.3.2. Toxicity tests for torin1 sensitivity	43
2.3.3. Chronological lifespan assays	44
2.3.4. Transcriptome analysis.....	46
2.3.5. Genetic interactome analysis.....	50
3. Chapter 3. GATA transcription factor Gaf1 as a relevant model: <i>In silico</i> analyses.....	55
3.1. Introduction.....	55
3.2. Screening for orthologues of Gaf1 transcription factor	56
3.3. Transcriptional response of <i>gaf1</i> under multiple conditions.....	61
3.4. Protein interactions network of Gaf1	64
4. Chapter 4. Growth patterns of <i>S. pombe</i> mediated by Gaf1 transcription factor.....	71
4.1. Introduction.....	71
4.2. Growth assays.....	74
4.2.1. Spot tests for fitness assessment.....	74
4.2.1.1. Viability of <i>gaf1</i> Δ cells.....	74
4.2.1.2. Viability of relevant strains.....	79
4.2.1.2.1. Viability of control cells.....	79
4.2.1.2.2. Viability of mutants for amino acid biosynthesis & metabolism.....	83
4.2.1.2.3. Viability of mutants for amino acid sensing & uptake.....	86
4.2.1.2.4. Involvement of amino acid uptake & metabolism in torin1 resistance.....	93
4.2.2. Toxicity tests for torin1 treatments.....	100

4.2.3. Chronological Lifespan assays.....	106
4.2.3.1. Survival of <i>gaf1</i> Δ and wild type cells with rapamycin treatment in minimal media.....	110
4.2.3.2. Survival of <i>gaf1</i> Δ , <i>tco89</i> Δ , <i>tor1</i> Δ and wild type cells in rich and minimal media.....	112
4.2.3.3. Survival of wild type cells with torin1 treatment in rich and minimal media.....	115
4.2.3.4. Survival of <i>gaf1</i> Δ cells with torin1 treatment in rich and minimal media.....	117
4.2.3.5. Survival of <i>tco89</i> Δ cells with torin1 treatment in rich and minimal media.....	119
4.2.3.6. Survival of <i>tor1</i> Δ cells with torin1 treatment in rich and minimal media.....	121
4.2.3.7. TOR signalling and cellular nutritional context.....	125
4.2.3.8. Survival of <i>ssp2</i> Δ , <i>amk2</i> Δ and wild type cells with compound 991 treatment in rich media.....	127
4.2.3.9. Protein translation accuracy and CLS in the fission yeast.....	129
5. Chapter 5. Gaf1-dependent expression profile and transcriptional network.	135
5.1. Introduction.....	135
5.2. Global expression profile controlled by Gaf1	137
5.3. Transcriptional network controlled by Gaf1	153
6. Chapter 6. High-throughput screening of genetic interactions and functional analyses of <i>gaf1</i> in the context of TOR signalling network.....	170
6.1. Introduction.....	170
6.2. Screening of <i>gaf1</i> -dependent genetic interaction network during global TOR inhibition.....	174
6.3. Data integration between <i>gaf1</i> -dependent genetic interaction network and Gaf1 transcriptional profile in the context of TOR inhibition.....	207

7. Chapter 7. Closing remarks and future work	221
7.1. <i>In silico</i> analyses and growth patterns mediated by Gaf1 transcription factor.....	222
7.2. Gaf1-dependent transcriptome.....	231
7.3. <i>gaf1</i> -dependent interactome.....	234
Bibliography	240
[Appendix I - Computational prediction on PPI with Gaf1]	266
[Appendix II – Genes downregulated in <i>gaf1Δ</i> relative to the wild type during torin1 treatment].....	270
[Appendix III - Genes upregulated in <i>gaf1Δ</i> relative to the wild type during torin1 treatment].....	273
[Appendix IV - Single mutants with decreased fitness]	276
[Appendix V – Single mutants with increased fitness].....	283
[Appendix VI – Single mutants sensitive to torin1]	289
[Appendix VII – Single mutant resistant to torin1]	290
[Appendix VIII –Gene deletions showing reduced fitness when combined with <i>gaf1Δ</i>].....	299
[Appendix IX – Gene deletions showing increased fitness when combined with <i>gaf1Δ</i>].....	309
[Appendix X – Double mutants sensitive to torin1].....	310
[Appendix XI – Double mutants resistant to torin1]	311

LIST OF FIGURES

	Page
Figure 1. The nine hallmarks of ageing.....	2
Figure 2. Potential new roles of mTORC1 and mTORC2.	6
Figure 3. <i>S. pombe</i> TORC1 and TORC2	9
Figure 4. Micro-photograph of <i>S. pombe</i> cells	16
Figure 5. <i>S. pombe</i> meiotic & mitotic cycles	18
Figure 6. <i>S. pombe</i> chromosomal architecture	19
Figure 7. Regulation of nitrogen starvation response by TORC1 via nuclear translocation of Gaf1	22
Figure 8: Steps for the extraction of DNA	33
Figure 9: PCR-mediated gene deletion technique used to construct <i>gaf1</i> Δ yeast strains	38
Figure 10. Growth curve of fission yeast and onset of chronological lifespan...45	
Figure 11. Revivability assay to estimate viable cells in a non-proliferative liquid culture	46
Figure 12. Diagram of expression microarrays setup.....	48
Figure 13. Schematic illustrating Synthetic Genetic Array method.....	52
Figure 14. Multiple sequence alignment comparing Gaf1 with orthologs	58
Figure 15. Phylogram of different Gaf1 orthologs	60
Figure 16. Tilling-chip array profile of <i>gaf1</i> gene in <i>S. pombe</i> chromosome 3. .62	
Figure 17. Predicted and known PPI network of the transcription factor Gaf1 ..66	
Figure 18. PPI network of the transcription factor Gaf1	67
Figure 19. Interacting genes with <i>gaf1</i>	68
Figure 20: Spot test of wild type and <i>gaf1</i> Δ on rich media with torin1 and caffeine + rapamycin	75

Figure 21: Spot test of wild type, <i>car1</i> Δ , <i>car2</i> Δ , <i>aru1</i> Δ , <i>fil1</i> Δ , <i>aca1</i> Δ , <i>gaf1</i> Δ , <i>tco89</i> Δ , <i>tor1</i> Δ with rapamycin, torin1 and arginine.	80
Figure 22: Toxicity tests using torin1.....	102
Figure 23. CLS of wild type and <i>gaf1</i> Δ with rapamycin.....	110
Figure 24. Maximal lifespan of wild type, <i>gaf1</i> Δ , <i>tco89</i> Δ , <i>tor1</i> Δ in rich and minimal media	113
Figure 25. CLS of wild type cells in rich media with torin1	115
Figure 26. CLS of wild type cells in minimal media with torin1.....	116
Figure 27. CLS of <i>gaf1</i> Δ cells in rich media with torin1	118
Figure 28. CLS of <i>gaf1</i> Δ cells in minimal media with torin1	118
Figure 29. CLS of <i>tco89</i> Δ cells in rich media with torin1	120
Figure 30. CLS of <i>tco89</i> Δ cells in minimal media with torin1.....	120
Figure 31. CLS of <i>tor1</i> Δ cells in rich media with torin1	122
Figure 32. CLS of <i>tor1</i> Δ cells in minimal media with torin1	122
Figure 33. CLS of wild type, <i>ssp2</i> Δ , and <i>amk2</i> Δ in rich media with C991	128
Figure 34. CLS of <i>rps23</i> mutant cells in rich media.....	130
Figure 35. Hierarchical clustering of microarray data of <i>gaf1</i> Δ before and after torin1 in rich media.....	142
Figure 36. Functional enrichments of upregulated genes in <i>gaf1</i> Δ after torin1 in rich media	144
Figure 37. Integration between upregulated genes in <i>gaf1</i> Δ after torin1 treatment in rich media.....	145
Figure 38. Functional enrichments of downregulated genes in <i>gaf1</i> Δ after torin1 in rich media.....	147
Figure 39. Integration between downregulated genes in <i>gaf1</i> Δ after torin1 treatment in rich media	149
Figure 40. Integration between Gaf1-binding sites before and after torin1 treatment in rich media	154

Figure 41. Integration between Gaf1-specific targets before torin1 treatment, and differentially expressed genes in torin1-treated <i>gaf1Δ</i> in rich media.....	156
Figure 42. Integration between gene essentiality, intronic regions, and Gaf1-specific targets before torin1 treatment in rich media.....	157
Figure 43. Integration between Gaf1-specific targets after torin1 treatment and differentially expressed genes in <i>gaf1Δ</i> mutants in rich media	158
Figure 44. Integration between gene essentiality, intronic regions, and Gaf1-specific targets after torin1 treatment in rich media.....	159
Figure 45. Functional enrichments of protein-coding genes targeted by Gaf1 after torin1 treatment in rich media.....	161
Figure 46. Model for Gaf1-mediated transcriptional repression of translation downstream of TORC1	168
Figure 47. Classification of SGA experimental samples and comparisons for data analyses.....	178
Figure 48. Single mutant library fitness in rich media.....	179
Figure 49. Single mutant library in rich media treated with torin1.....	180
Figure 50. Integration between single mutants resistant to torin1 and single mutants with affected fitness in rich media.	185
Figure 51. Integration between single mutants resistant to torin1 and previously reported mutants resistant to torin1 in rich and in minimal media	185
Figure 52. Double mutants fitness in rich media	190
Figure 53. Integration between double mutants negatively interacting with <i>gaf1</i> , single mutants sensitive to torin1, and single mutants resistant to torin1.....	193
Figure 54. Integration between double mutants negatively interacting with <i>gaf1</i> , single mutants with reduced fitness, and single mutants with increased fitness in rich media.	195
Figure 55. Double mutants fitness in rich media treated with torin1	198

Figure 56. Integration between double mutants resistant to torin1, double mutants negatively interacting with *gaf1*, and double mutants positively interacting with *gaf1*202

Figure 57. Integration between double mutants resistant to torin1 in rich media, single mutants sensitive to torin1 in rich media, single mutants resistant to torin1 in rich media, and previously reported single mutants resistant to torin1 in minimal media203

Figure 58. Integration between single mutants with reduced fitness, differentially expressed genes in *gaf1* Δ after torin1 treatment, and transcriptional targets of Gaf1 before / after torin1 treatment. All of them grown in rich media.208

Figure 59. Integration between single mutants with increased fitness, differentially expressed genes in *gaf1* Δ after torin1 treatment, and transcriptional targets of Gaf1 before / after torin1 treatment. All of them grown in rich media.210

Figure 60. Integration between single mutants sensitive to torin1, differentially expressed genes in *gaf1* Δ after torin1 treatment, and transcriptional targets of Gaf1 before / after torin1 treatment. All of them grown in rich media212

Figure 61. Integration between single mutants resistant to torin1, differentially expressed genes in *gaf1* Δ after torin1 treatment, and transcriptional targets of Gaf1 before / after torin1 treatment. All of them grown in rich media213

Figure 62. Integration between double mutants positively interacting with *gaf1*, differentially expressed genes in *gaf1* Δ after torin1, and transcriptional targets of Gaf1 before / after torin1 treatment. All of them grown in rich media215

Figure 63. Integration between double mutants negatively interacting with *gaf1*, differentially expressed genes in *gaf1* Δ after torin1 treatment, and transcriptional targets of Gaf1 before / after torin1 treatment. All of them grown in rich media216

Figure 64. Integration between double mutants resistant to torin1, differentially expressed genes in *gaf1* Δ after torin1 treatment, and transcriptional targets of Gaf1 before / after torin1 treatment. All of them grown in rich media218

Figure 65. Integration between double mutants sensitive to torin1, differentially expressed genes in *gaf1* Δ after torin1 treatment, and transcriptional targets of Gaf1 before / after torin1 treatment. All of them grown in rich media.....220

LIST OF TABLES

	Page
Table 1: Details of media supplement, stressors and antibiotics used in this research project.	28
Table 2: <i>S. pombe</i> strains used in this research project.	30
Table 3: List of primers used for the creation of the query strain <i>gaf1Δ::natMX6</i>	39
Table 4: List of primers used to confirm the query strain <i>gaf1Δ::natMX6</i>	40
Table 5: List of genomic location of <i>gaf1</i> gene and primers used for the generation / confirmation of <i>gaf1::natMX6</i> query strain	40
Table 6: Number of genes with showing genetic interactions with <i>gaf1</i> identified in the SGAs analyses.....	205

Chapter 1. Introduction

1.1. *Current perspectives on ageing*

The demographic shift experienced by human populations during the last century called population ageing, involves the widespread re-distribution of the subjects towards older ages, accompanied by a decline in the proportion of the population composed of children (United Nations, 2013).

Recent reports revealed significant increases in the average age of the global population, projected to grow from 12% in the year 2015 (900 million), to 22% in the year 2050 (2 billion), with 434 million people aged over 80 years worldwide (World Health Organization, 2018). This social phenomenon introduces major healthcare challenges to modern societies (Hillson O, 2018), where the improvement in medical interventions is leading to a substantial fraction of the population to live longer (United Nations, 2002), but accumulating age-related chronic ailment such as neurodegeneration, cardiovascular diseases, and cancer (López-Otín, et al., 2013).

The current approach to alleviate some of these socio-economic challenges produced by an increasing world-wide elderly population, is through the study of ageing not only aimed to increase lifespan, which has been arguably accomplished in model organisms (Kenyon, 2010), but on increasing health-span defined as the length of time an individual spends at optimal health free from diseases associated with age (Gems & Partridge, 2013).

Considering that this modern perspective on ageing research only started less than 40 years ago following the identification of long-lived strains in *Caenorhabditis elegans* [*C. elegans*] (Klass, 1983), understanding the molecular mechanisms underlying cellular ageing remains as one of the greatest challenges in science, and is a crucial step to develop effective strategies and therapies for a myriad of age-related pathologies, aiming to improve the quality of life at old age (Partridge, 2010).

By definition, ageing is a multifactorial biological process that leads to the accumulation of cellular and molecular damage, which ultimately introduce physiological decay increasing the risk of development of age-related illnesses and death (Niccoli & Partridge, 2012). The hallmarks of ageing (figure 1) have been described as follows: impaired nutrient-sensing, epigenetic alterations, loss of proteostasis, mitochondrial dysfunction, altered intercellular communication, genomic instability, cellular senescence, stem cell exhaustion and telomere attrition (López-Otín, et al., 2013).

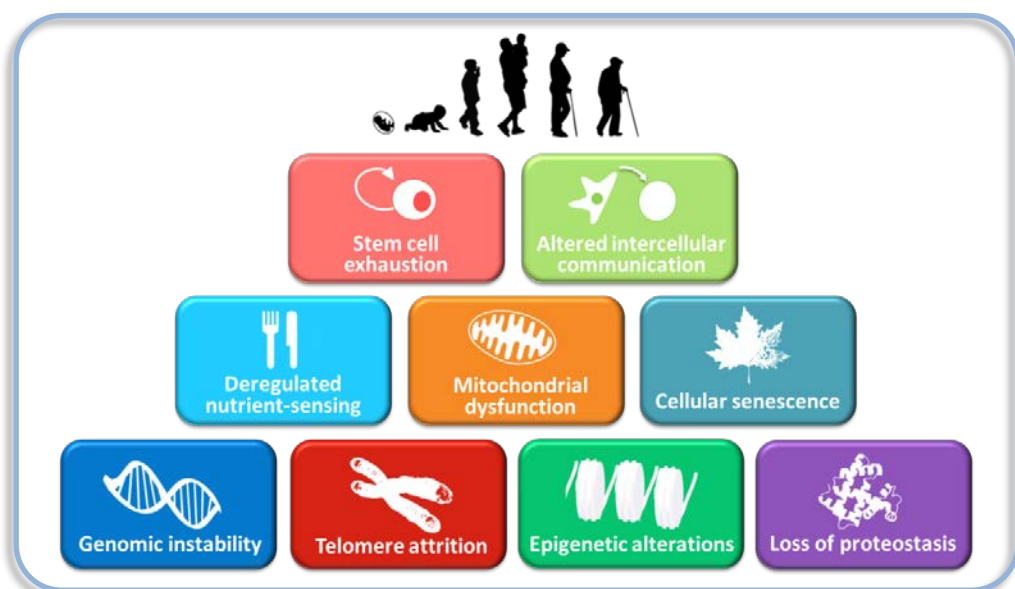


Figure 1. The nine hallmarks of ageing. Figure adapted from (López-Otín, et al., 2013).

It is fascinating that the lifespan of living organisms is determined by environmental and genetic factors that are highly conserved across species (Fontana, et al., 2010). Several studies using established model organisms including yeast, nematodes, flies, mice and monkeys support the idea that ageing is amenable to interventions (de Magalhães, et al., 2012; Gems & Partridge, 2013).

1.2. TOR pathway: A conserved rheostat of nutrient-sensing

A well-documented intervention that influences lifespan in all eukaryotes is dietary restriction (Katewa & Kapahi, 2010). When the food intake of organisms such as yeast and rodents is reduced without malnutrition, they live longer compared to organisms fed with a normal diet (Kenyon, 2010). Similar benefits are achieved when the activity of nutrient-sensing signalling pathways is reduced by mutations or chemical inhibitors (Gems & Partridge, 2013). In rodents, both dietary restriction and decreased nutrient-sensing pathways activity lowered the incidence of age-related loss of function and disease, including tumours and neurodegeneration (Fontana, et al., 2010).

Caloric restriction in rhesus monkeys, increased lifespan and reduced the incidence of cancer, cardiovascular disease, diabetes and brain atrophy (Colman, et al., 2009). Human subjects carrying mutations in the growth hormone receptors, and natural genetic variants in nutrient-sensing pathways present increased lifespan and reduced incidence of cancer and diabetes, indicating that dietary restriction and limited activity of nutrient-sensing pathways may thus slow

ageing by similar mechanisms, a phenomenon that have been conserved throughout evolution (Fontana, et al., 2010).

Among the different nutrient-sensing pathways present in the cell, the Target of Rapamycin (TOR) stands out as a universal sensor of nutrient availability (Gonzalez & Rallis, 2017), controlling cellular metabolism, proliferation and survival (Laplante & Sabatini, 2012). The TOR kinases were initially discovered in the budding yeast through the characterisation of mutants resistant to the growth inhibitor rapamycin (Heitman, et al., 1991). Shortly afterwards, biochemical approaches in mammals resulted in the purification of mammalian /mechanistic TOR (mTOR) and its discovery as the physical target of rapamycin (Sabatini, et al., 1994).

The TOR pathway is only found in eukaryotes and is conserved in multiple species from yeast to mammals (Kapahi, et al., 2010). Eukaryotic TOR protein sequences share approximately 40% to 60% homology, presenting several conserved structural motifs (Janus, et al., 2005). Human TOR protein showed even higher homology of 95% in the primary sequence with other mammalian TOR proteins (Jiang & Liu, 2008).

mTOR is an atypical 289 kilodaltons (kDa) serine/threonine (Ser/Thr) protein kinase that belongs to the phosphoinositide 3-kinase (PI3K)-related kinase family (Querfurth & Lee, 2021). In mammals, it interacts with different proteins in a conserved fashion to form two distinct complexes named mTOR complex1 (mTORC1) and mTOR complex2 [mTORC2] (Laplante & Sabatini, 2012).

The assembly of mTORC1 involves six and mTORC2 seven known proteins (Laplante & Sabatini, 2012). Both of them share the following core components: the catalytic mTOR subunit, the mammalian lethal with sec-13 (mLST8), also known as the positive/negative regulator G protein β -subunit-like [G β L] (Jacinto, et al., 2004), the DEP domain containing mTOR-interacting protein [Deptor] (Peterson, et al., 2009), and the TEL2-interacting protein 1 Tti1/Tel2 complex (Kaizuka, et al., 2010).

The mTORC1-specific components include the regulatory-associated protein of mammalian target of rapamycin [Raptor] (Hara, et al., 2002) and the proline-rich Akt substrate [PRAS40] (Wang, et al., 2007). While the mTORC2-specific components include the rapamycin-insensitive companion of mTOR [Rictor] (Jacinto, et al., 2004), the mammalian stress-activated map kinase-interacting protein 1 [mSin1] (Frias, et al., 2006), and protein observed with Rictor 1 and 2 (protor1/2) (Pearce, et al., 2011). Therefore, both complexes share mTOR, mLST8, Deptor, and Tti1/Tel2 complex, and are distinguished by Raptor and PRAS40 (mTORC1) and Rictor, mSIN1, and Protor [mTORC2] (Querfurth & Lee, 2021).

mTORC1 promotes protein translation, anabolism, ribosome biogenesis, vegetative cell proliferation, and inhibits stress responses such as amino acid uptake and autophagy (Valvezan & Manning, 2019). mTORC2 has opposite functions in these processes and is implicated in DNA damage repair, telomere stability, gene silencing and is required for stress responses (Laplante & Sabatini, 2012).

The role mTORC1 has been mostly related to the regulation of temporal aspects of cell size and proliferation (Balcazar, et al., 2009), mainly by stimulating protein synthesis, inhibiting autophagy, and controlling the activity of cyclin/cyclin-dependent kinases (De Virgilio and Loewith, 2006). On the other side, mTORC2 has been linked to spatial growth by regulating the actin cytoskeleton (Jacinto, et al., 2004), through the activation of several kinases belonging to the AGC family, including the protein kinase B (PKB) also known as Akt, the protein kinase C (PKC), and the serum and glucocorticoid-regulated kinase [SGK] (Zoncu, et al., 2011).

Despite this traditional individualisation of the roles of the two TOR complexes as different entities, recent data suggest that the interplay between them is more complex, where functions usually attributed to mTORC1 may be mediated by mTORC2 and vice versa [figure 2] (Gonzalez & Rallis, 2017).

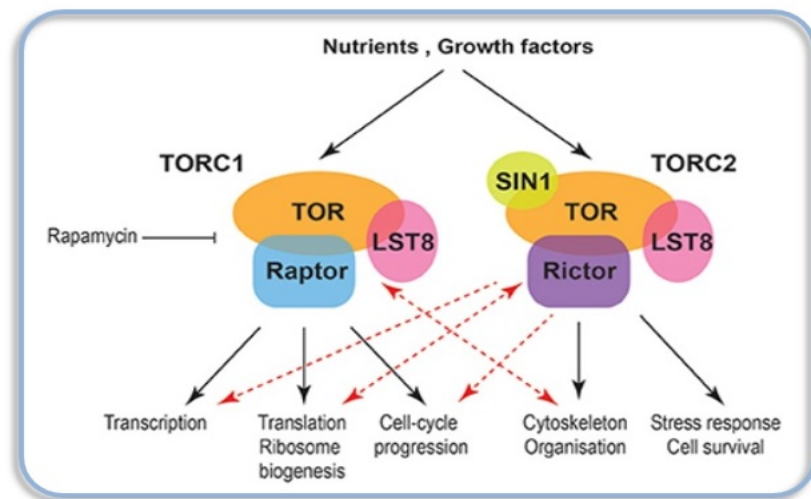


Figure 2. Potential new roles of mTORC1 and mTORC2. Schematic diagram indicating processes affecting cell size and growth downstream of mammalian TOR complexes 1 and 2. Black arrows indicate well-established relationships between TORC1 and TORC2 with temporal and spatial aspects of cell growth respectively. Red arrows indicate new functional connections while double red arrows indicate cross-regulation between TORC1 and cytoskeleton as well as TORC2 and ribosomes, transcription and regulation of proliferation. Figure adapted from (Gonzalez & Rallis, 2017).

The conservation of the TOR signalling facilitates the advance in the elucidation of the pathway (Gonzalez & Rallis, 2017). Recent studies in the budding yeast, revealed that TORC1 is also implicated in the control of spatial cell size and organisation through the activity of one its components. The Las24/Kog1, apart from controlling global protein translation and phosphorylation of the Ser/Thr Npr1p kinase and the Gln3p GATA transcription factor both involved in nitrogen catabolite repression (Loewith & Hall, 2011), it is reported to also regulate the spatial configuration of the actin cytoskeleton (Araki, et al., 2005), normally attributed to TORC2 (Jacinto, et al., 2004).

Polarised cytoskeleton that results in morphological changes, leads to reduced cellular growth and size in yeast by inhibiting TORC1, this process requires the Iml1 complex, proved to inhibit TORC1 activity depending on the availability of nitrogen sources (Goranov, et al., 2013). Proteomics analysis of TOR-containing membrane fractions, also revealed interactions between TORC1 and actin cytoskeleton related functions (Aronova, et al., 2007). These findings indicate that TORC1 can therefore regulate spatial aspects of cell growth and organisation.

Other studies demonstrated that TORC2 signalling requires the physical association with ribosomes, in a process that is independent from protein synthesis, which is promoted by insulin-stimulated PI3Ks, ensuring appropriate levels of TORC2 activity in growing cells (Zinzalla, et al., 2011). In *Drosophila melanogaster*, the core component of TOR complexes Lst8 regulates cell size but not cell cycle progression in a cell-autonomous manner through TORC2 (Wang, et al., 2012).

TORC2 is also implicated in several temporal aspects of the cell cycle, including: the maintenance of genome stability during S phase, and its essential function to return to cell cycle progression after stress (Schonbrun, et al., 2013); control of cell size at division and the correct timing of mitosis, otherwise delaying it and producing longer cells (Yang, et al., 2006) as observed in the elongated cell morphology of mutants for the TOR kinase Tor1 (Kawai, et al., 2001).

These emerging functions of TORC1 implicated in actin cytoskeleton, and TORC2 involved in the timing of cell division, require further scrutiny of the complexes individually (Gonzalez & Rallis, 2017). The conservation of the TOR pathway across eukaryotes together with the thorough functional information currently available for the model organism fission yeast *Schizosaccharomyces pombe* (*S. pombe*), provide an excellent platform to further evaluate such functions (Hoffman, et al., 2015).

In this model, there are two TOR homologues named Tor1 and Tor2 (Weisman, et al., 2007). Tor2 is the catalytic subunit, which together with Mip1 (Raptor), Pop3/Wat1 (Lst8), Toc1 and Tco89 constitute TORC1. On the other side, the assembly of Ste20 (Rictor), Pop3/Wat1 (Lst8), Sin1, Bit61, together with the catalytic subunit Tor1, gives rise to TORC2 [figure 3] (Hayashi, et al., 2007; Ikai, et al., 2011).

Similar to mTORCs, the *S. pombe* TORC1 promotes transcription, protein synthesis, positively regulating vegetative cell proliferation, and inhibiting catabolism, nitrogen-starvation responses, sexual differentiation and amino acid

uptake. In contrast, TORC2 is implicated in DNA damage repair, telomere integrity, appropriate G1 arrest, telomere stability, gene silencing, sexual differentiation, and is required for survival during stress responses (Weisman, et al., 2007).

The presence of two TOR kinases in *S. pombe* (figure 3) facilitates the study of those complexes using mutant strains with disruptions in their components that limit their functionality (Weisman & Choder, 2001). In TORC2, the kinase Tor1 is not essential and can be removed by disruption/deletion of the *tor1* gene. TORC1 contains Tor2, which is essential for cell viability (Weisman & Choder, 2001), thus disruptions to this complex by mutagenesis require targeting other TORC1 components such as the *tco89* gene (Ikai, et al., 2011).

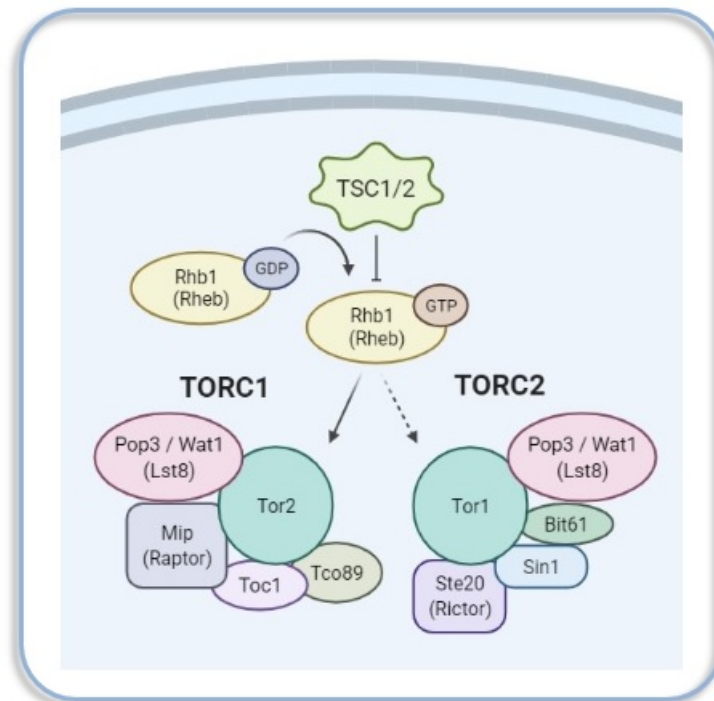


Figure 3. *S. pombe* TORC1 and TORC2. Schematic diagram of the subunit compositions previously determined by mass spectrometry. Mammalian homologues are in brackets. Figure adapted from (Hayashi, et al., 2007; Nakashima A, 2010; Shertz, et al., 2010).

Alternatively, TORC1 could be pharmacologically inhibited, resulting in phenotypic/transcriptional responses that highly resemble nitrogen starvation, involving: cell arrest at the G1 phase, small-round cell size, induction of nitrogen starvation-response genes, and de-repression of sexual differentiation (Rallis, et al., 2013).

Conversely, disruptions in TORC2 by means of mutagenesis (*tor1Δ*, *ste20Δ*, *sin1Δ*, etc.), result in pleiotropic defects, including: inability to initiate sexual development or acquire stationary-phase physiology, sensitivity to oxidative stress, osmotic stress, high or low temperature, sensitivity to low glucose (Weisman & Choder, 2001), delay in entry to mitosis (Petersen & Nurse, 2007), decrease in amino acid uptake (Weisman, et al., 2005), inability to induce gene silencing, tolerate DNA attrition, or maintain telomere length (Schonbrun, et al., 2013). TORC2 operates via phosphorylation and activation of the AGC kinase Gad8 (Cohen, et al., 2014).

The TOR pathway orchestrates all those aspects by sensing the cellular environment to efficiently coordinate processes that require significant energy and nutrient consumption in the cell (Fingar, et al., 2002). During cellular growth, the accumulation of biomass requires extensive amount of protein synthesis to produce cellular components and macromolecules (Perez-Hidalgo & Moreno, 2016), constituting the largest energy-consuming process in actively growing mammalian cells, which accounts for ~30% of the total energy consumption (Buttgereit & Brand, 1995).

Interestingly, various types of nutrients have diverse effects on the duration and strength of TORC1 activity, with specific amino acids proven to have stronger effects on the activation of mTORC1 (Bar-Peled & Sabatini, 2014). Ultimately, the control of the global rate of protein synthesis is fundamental to understand cellular growth (Mak, et al., 2021) and ageing (Filer, et al., 2017), which is the triggering factor of several human chronic diseases (Gems & Partridge, 2013). The therapeutic potential of targeting this process has prompted significant number of clinical studies aiming to pharmacologically inhibit the pathway to increase health and reduce diseases (Laplante & Sabatini, 2012).

1.3. Pharmacological inhibition of TOR signalling in *S. pombe*

Intense research in the areas of cellular and organismal ageing using a variety of model systems has uncovered relevant information about the processes involved in TOR signalling that lead to normal and pathological conditions. Current approaches to study this pathway in eukaryotic cells, involve treatment with pharmacological agents that directly or indirectly inhibit the functions of the two TOR complexes (Hillson O, 2018).

The fission yeast *S. pombe* constitutes a valuable genetic model system to study the mechanism(s) of drug action as well as to determine genetic contexts associated with drug sensitivity or resistance. The drug rapamycin also known as sirolimus, is a macrolide with broad antiproliferative properties that in this model system inhibits TOR activity without reducing vegetative cellular growth (Doi, et al., 2015; Weisman, 2010).

Rapamycin acts through an unusual allosteric mechanism that requires the formation of an intracellular complex with the receptor isomerase Fkh1 (functional orthologue of mammalian FK506-binding protein 12 - FKBP12), which then binds to TORC1 to directly inhibit the intrinsic catalytic activity of this complex (Ikai, et al., 2011; Takahara & Maeda, 2012).

The Fission yeast Tor1 or Tor2 contain FRB domains (FKBP12-rapamycin binding from its mammalian orthologue) which bind to rapamycin in the presence of Fkh1, indicating that the basic structural features for rapamycin-mediated TOR signalling inhibition exist in this model (Weisman, 2010). The activity of TORC2 is differently affected by rapamycin treatment compared to TORC1. The inhibition of TORC2 has been reported to occur only after prolonged treatment with the drug (Weisman, 2010; Sarbassov, et al., 2006). Therefore, rapamycin is commonly used to assess the functions of TORC1 signalling in different processes (Rallis, et al., 2013).

The phenotypes of rapamycin-treated cells resemble that observed in cells deprived of nitrogen, which arrest the cell cycle in G1 phase as quiescent cells with small-rounded shape that are de-repressed for sexual development, they present a hallmark established by the induction of nitrogen starvation-responsive genes (Matsuo, et al., 2007; Rallis, et al., 2013).

Rapamycin in combination with caffeine have been used to enhance the inhibition of TORC1 functions, with reported sensitivity to this compound in *S. pombe* (Rallis, et al., 2013). Caffeine as an ATP-competitor (Takahara & Maeda, 2012),

inhibits in varying degrees the phosphatidylinositol 3-kinase-related kinase family (PIKK) to which TOR proteins belong (Sarkaria, et al., 1999).

Another compound used in this project to study functions of the TOR pathway was torin1, a highly potent and selective ATP-competitor specific for TOR kinase inhibition that directly inhibits both TORC1 and TORC2 complexes. This drug was originally designed as an anti-cancer treatment (Atkin, et al., 2014; Thoreen, et al., 2009).

In contrast to the mild impact of rapamycin on cell division, torin1 impairs cell growth and proliferation to a far greater extent than rapamycin without inducing cell death (Atkin, et al., 2014). The mechanisms of action of this compound are independent from TORC2 inhibition, and is instead triggered by the suppression of rapamycin-resistant functions of TORC1 that are essential for growth and proliferation, including cap-dependent translation and suppression of autophagy (Atkin, et al., 2014; Thoreen, et al., 2009).

Torin1 specificity relies on its interaction with tryptophan-2239 in the catalytic active site of TOR kinases. Crucially, this residue is absent in other kinases, including the mTOR-related phosphoinositide 3-kinases [PI3Ks] (Atkin, et al., 2014). Treatment with torin1 induce autophagy, disrupt protein synthesis and arrest cell cycle progression in G1 with a reduced cell size in mammalian and yeast models (Atkin, et al., 2014; Rodríguez-López, et al., 2020; Thoreen, et al., 2009). This compound constituted the main platform for the pharmacological

intervention of TOR signalling used throughout all the experiments performed in the present study.

Current strategies used to reduce TOR signalling also involve the indirect targeting of the pathway through the activation of negative regulators of TOR functions. One such interplay is conserved in *S. pombe* and is controlled by another rheostat of energy homeostasis, the adenosine monophosphate (AMP) activated protein kinase [AMPK] (Kim, et al., 2016). AMPK is a key regulator of cellular energy, controlling metabolic pathways to balance nutrient inputs such as glucose and fatty acid uptake with energy expenditure via sensing levels of its allosteric activator AMP. AMPK ensures survival during cellular metabolic stress limiting the activity of TOR to redress energy imbalance through the promotion of ATP-generating catabolic processes and inhibition of ATP-consuming processes, including cell growth and proliferation (Kim, et al., 2016).

The fission yeast ortholog of AMPK consists of the α (catalytic) subunit Ssp2, and the $\beta\gamma$ (regulatory) subunits Amk2 and Cbs2 to which AMP binds providing a target for the unique stress-responsive kinase Ssp1, which phosphorylates Ssp2 to activate AMPK (Schutt & Moseley, 2017; Viollet, et al., 2010).

The recently identified small-molecule compound 991 (C991) also known as ex229, is a potent allosteric activator of AMPK as it resembles cellular AMP. It triggers conformational changes in AMPK that allow increased phosphorylation of the α -subunit blocking its de-phosphorylation (Kim, et al., 2016; Xu, et al., 2018). This compound directly binds to a site formed between the small lobe of

the α -subunit kinase domain and the β -subunit carbohydrate-binding module to stimulate AMPK activity of both β 1- and β 2-containing complexes (Lai, et al., 2014). The present study assessed the survival of relevant mutants disrupted in the catalytic and regulatory subunits of AMPK, aiming to elucidate if the compound is effected in *S. pombe* in terms of limiting TOR signalling and subsequently increasing lifespan.

1.4. Functional genetics of *S. pombe*

1.4.1. Biology & life cycle

The species *Schizosaccharomyces pombe* (*S. pombe*) was the first fission yeast to be discovered in 1893 (Lindner, 1893). It belongs to the group ascomycete yeast from the kingdom Fungi. Yeasts can be classified as either ascomycetes or basidiomycetes and they are distinguished from other fungi by both their ability to ferment sugars and their unicellular nature, in contrast to mycelial growth (mass of branching filaments). As an ascomycete, its sexual reproduction leads to spores within specialised structures called an ascus [Latin for “bag”] (Hoffman, et al., 2015). Taxonomic systems establish three species of fission yeast: *S. pombe* is a unique four-spored species, whereas *S. japonicus* and *S. octosporus* are eight-spored species (Sipiczki, 2000). In the present study, the terms fission yeast and *S. pombe* were used interchangeably to refer to *S. pombe*.

The cellular morphology of *S. pombe* is characterised by a cylindrical shape, typically measuring between 3-4 μm in diameter and between 7-15 μm in length

(figure 4), lined by a cell wall mainly constituted of polysaccharides responsible for cell wall rigidity.

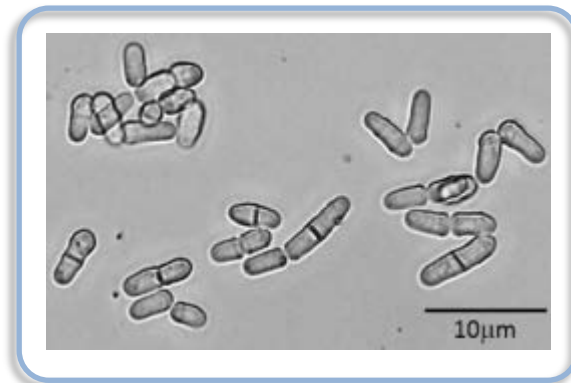


Figure 4. Representative micro-photograph of *S. pombe* cells. Figure adapted from (Ďúranová H, et al., 2019).

This organism contains two alleles (*mat1-P* and *mat1-M*) inherited in the *mat1* locus of chromosome II that define the mating type of the cell, these could be classified as heterothallic: h^+ (*mat1-P*), h^- (*mat1-M*), and homothallic h^{90} which typically switch between h^+ and h^- mating types to reproduce within the culture. The cells can also be distinguished by genomic configuration as haploid cells and diploid cells (Forsburg & Rhind, 2006).

Most of the *S. pombe* laboratory strains currently used in genetics and molecular biology around the world are nearly isogenic. They include 968 h^{90} , 972 h^- , and 975 h^+ derived from a single strain used by Urs Leupold for genetic analysis in the early 1950s (Hoffman, et al., 2015). This represents a technical advantage compared to some of the difficulties experienced in *S. cerevisiae* studies, in which there is considerable genetic variability between wild type strains such as S288c and W303, resulting in differential responses to treatment and genetic interventions (Ralser, et al., 2012).

Cell division occurs by binary fission at a doubling time of ~2-4 hours (depending on the temperature and media used). The cells grow by polar elongation dividing by medial septation or fission, generating two biologically independent and symmetrical daughter cells (Mitchison & Nurse, 1985). After mitosis, cytokinesis is accomplished by the construction of a septum through the middle of the cell. The assessment of septum formation under phase contrast microscopy, allows to monitor physiological responses of growing cells to different conditions in real time. This is achieved by measuring the septation index of the culture (percentage of cells with a complete septum but no invagination at any single time point), which normally peak at G1 phase of the cell cycle with a value between 30% and 60% in synchronised cultures (Willis & Rhind, 2011).

One of the greatest advantages of this model organism is the plasticity to control several aspects of its biology including the duration of the cell cycle, the mating type, the type of media/temperature, and genomic configuration of the strains to confer homogeneity or diversity of the samples depending on the intended applications. The life cycle and cellular division in *S. pombe* occur by mitosis and/or meiosis [figure 5] (Hoffman, et al., 2015).

The reproduction of *S. pombe* consists of two phases: asexually by mitosis under favourable conditions (vegetative), and sexually when haploid cells are starved of nutrients. The meiotic cycle is triggered particularly by nitrogen depletion from the environment. In this context, when stressed cells of different mating type are present, they arrest the cell cycle at G1, and undergo sexual differentiation and conjugation. This produce a diploid zygote that splits into four genetically distinct

spores, which subsequently sporulate into single cells containing diploid nucleus, and restart the meiotic cycle (Kim, et al., 2012). When haploid cells are subjected to nutrient starvation in the absence of a mating partner, they exit the cell cycle and enter stationary phase (Hoffman, et al., 2015).

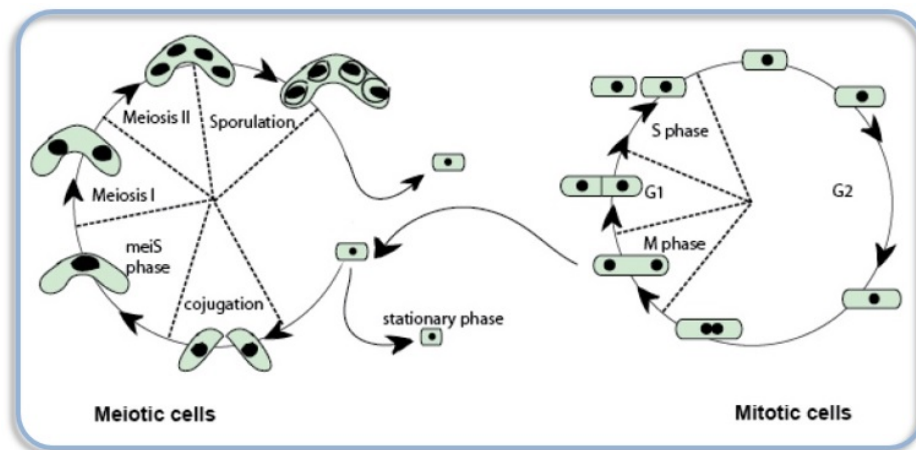


Figure 5. *S. pombe* meiotic & mitotic cycles. Diploid or meiotic cells undergo sexual conjugation producing four spores. The spores germinate and form new diploid cells that can restart the cycle. Haploid or mitotic cells grow in a vegetative manner until reaching the stationary phase. Figure adapted from (Forsburg, 2011).

Depending on their mating-type constitution, diploid cells enter either stationary phase or differentiate to enter the sexual cycle in response to nutrient starvation (Piel & Tran, 2009). Normally, the nucleus enters the meiotic pathway soon after zygote formation, giving rise to four haploid nuclei. Subsequently, the spore wall surrounds each nucleus producing an ascus that contains four spores within the shell of the zygote. Conversely, azygotic asci deriving from vegetative diploid cells are short and linear. Whether zygotic or azygotic, the ascus wall lyses on exposure to growth medium, and spores germinate to develop into vegetative cells that return to mitotic growth (Hoffman, et al., 2015).

1.4.2. Genomic configuration

The genome content of *S. pombe* became available in 2002, it was the sixth eukaryotic model organism to have its genome sequence and annotation published (Wood, et al., 2002). This sequence provides a robust platform for the ongoing functional assessment of the genome, which is constantly developed by linking annotations of genomic features (sequences) with new functional information discovered. In time these efforts will provide a more complete picture of the functional regulation of the *S. pombe* genome (Hoffman, et al., 2015).

The most recent update of the *S. pombe* genome structure and organisation (January 2017), reported a genome size of 12.57 mega base pairs (Mbp), compacted into three chromosomes (figure 6), with a gene count of 5,132 curated protein-coding genes (6,998 genes in total), constituting the smallest number of protein-coding genes amongst eukaryotic genomes. Its mitochondrial chromosome consists of ~20 kilo base pairs [kbp] (Lock, et al., 2019; Wood, et al., 2002).

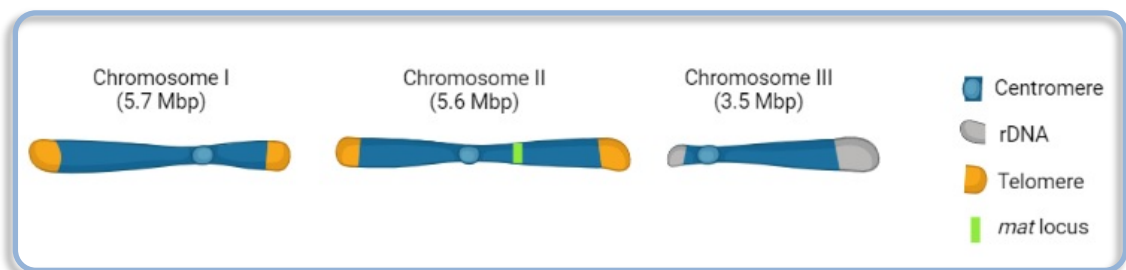


Figure 6. *S. pombe* chromosomal architecture. Figure adapted from (Mizuguchi, et al., 2015).

The rest of the genome assembly include: 1,522 non-coding RNAs, short introns of ~100 bp, only present for 46% of the genes, an average gene density of 1 gene

per every 2,528 bp, and centromeric and telomeric sequence gaps of 20 kbp and 40-100 kb, respectively (Lock, et al., 2019; Wood, et al., 2002).

The genome of this model is reported to have a low degree of gene redundancy, with only 41% of the protein-coding genes being duplicated (Kim, et al., 2010; Wood, et al., 2002). Recent work based on the Markov model to identify transposon insertions across the non-coding/unannotated genome which include sequences such as non-essential coding regions, non-coding RNAs, and untranslated regions (UTRs), showed that those sections of the genome sustain depleted transposon insertion, revealing robust mechanisms to control duplications, and suggesting that ~91% of the non-coding genome contain functional regulatory elements (Grech, et al., 2019).

In terms of evolution, the preservation of gene functions in this species led to over three-quarters of the protein-coding genes to be non-paralogue genes, with approximately two-thirds of them showing human orthologues (Lock, et al., 2019). Several genomic elements of this model organism highly resemble those observed in higher eukaryotes. These features include its chromosomal organisation, the large number of molecular mechanisms shared with mammalian cells [RNAi, TOR signalling, etc.] (Chen & Runge, 2009; Egel, 2004), the conserved telomeric proteins, and large replication origins among other aspects (Wood, et al., 2002), which together with the extensive collection of molecular tools available for its study, make *S. pombe* an ideal model for studies in the field of functional genomics (Hoffman, et al., 2015).

1.5. The GATA transcription factor Gaf1

The GATA family of transcription factors have a wide array of functions in nature, ranging from terminal differentiation in vertebrates, to siderophore biosynthesis, nitrogen metabolism, photoinduction, and mating type switching in fungi, generally showing conservation in their mechanisms of action across species (Scazzocchio, 2000).

In *S. pombe*, the GATA factors bind to a consensus sequence of six base-pairs, 5'-HGATAR-3' (where H can be A/C/T and R can be A/G), embedded in the promoters of their transcriptional target genes (Kim, et al., 2012). The current annotations for this species report five GATA transcription factors, they are: Gaf1, Gaf2/Fep1, Ams2 (Laor, et al., 2015), Sfh1 (Ma, et al., 2015), and Fil1 (Duncan, et al., 2018).

Gaf1 was the first GATA transcription factor identified in *S. pombe* (Hoe, et al., 1998). This protein has a molecular weight of 91.78 kDa consisting of 855 residues encoded by the intronless gene *gaf1* [4,256 nucleotides] (Lock, et al., 2019). Much of the current research into this transcription factor has been focused on the characterisation of both its mechanism of action and functional role in the transcriptional regulation of stress responses triggered by nutritional cues (Kim, et al., 2012; Laor, et al., 2015; Ma, et al., 2015; Rodríguez-López, et al., 2020).

Under normal nutritional conditions Gaf1 is reported to be retained in the cytoplasm by the activity of TORC1, which promotes its phosphorylation by

inhibiting the PP2A-like phosphatase Ppe1 (Laor, et al., 2015). Glucose depletion does not affect Gaf1 activity (Kim, et al., 2012; Laor, et al., 2015) but upon nitrogen stress, the inactivation of TORC1 de-represses Ppe1 phosphatase, leading to the dephosphorylation of Gaf1 and nuclear translocation to exert its complete function as a transcription factor [figure 7] (Otsubo, et al., 2017).

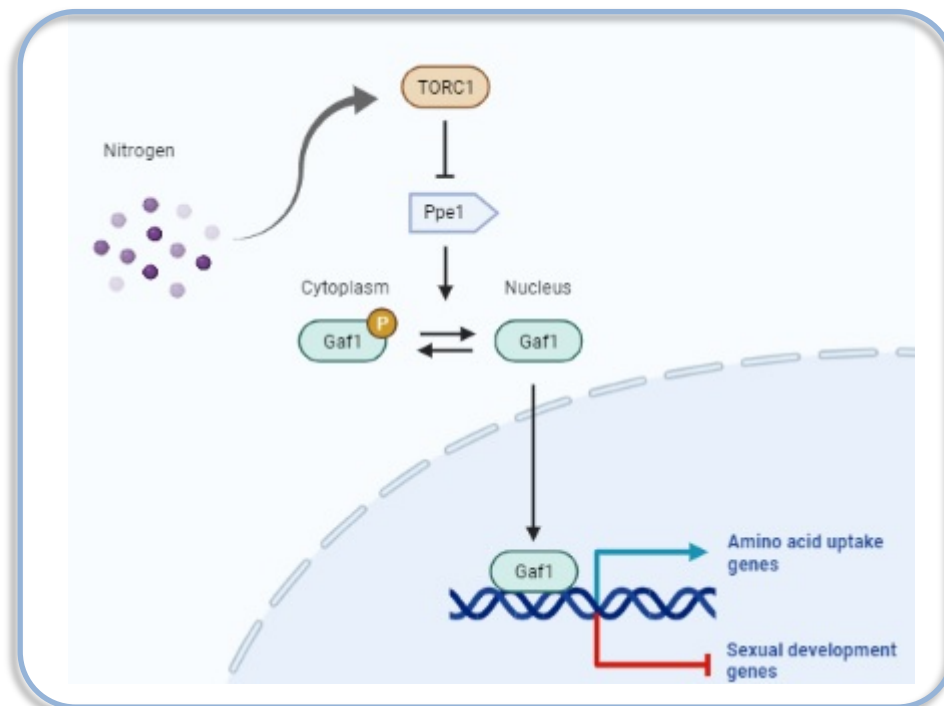


Figure 7. Regulation of nitrogen starvation response by TORC1 via nuclear translocation of Gaf1. Under nitrogen abundance, TORC1 is active and Gaf1 is phosphorylated and retained in the cytoplasm. During nitrogen stress conditions, TORC1 is inactive and de-represses phosphatase Ppe1, leading to Gaf1 dephosphorylation which allows its relocation to the nucleus to act as a transcription factor. Gaf1 induces early nitrogen stress-induced genes, and represses sexual development. Figure adapted from (Laor, et al., 2015).

Tor2 regulates Gaf1 in a different manner than Tor1, since the loss of Tor1 does not affect neither phosphorylation or nuclear localisation of Gaf1 (Ma, et al., 2015). This mechanistic regulation of GATA transcription factors, in which they are retained in the cytoplasm by active TORC1 and translocated to the nucleus upon its inhibition, is conserved in budding yeast Gln3 and Gat1 (Georis, et al.,

2011; Kulkarni, et al., 2006) and other mammalian GATA transcription factors (Xie, et al., 2015; Zhao, et al., 2008).

The nuclear translocation of Gaf1 triggers remarkable transcriptional events in the cell. On one side, it promotes the transcription of early nitrogen starvation-response genes such as *isp7* and *isp5*, encoding permeases for amino acid uptake (Laor, et al., 2015; Ma, et al., 2015). On the other side, it delays other stress responses such as sexual development by directly repressing the transcription of *ste11* (via direct interaction with its promoter), responsible for the activation of more than 80 genes required for mating (Kim, et al., 2012).

The current body of data indicate that Gaf1 operates through a complex network of positive and negative transcriptional control of its target genes, specifically in response to nitrogen limitation. Similarly, there is thorough documentation about the upstream regulators of TOR signalling, as well as downstream at the post-translational stage, however, the analogous transcriptional regulatory network controlled by this fundamental pathway through transcription factors such as Gaf1 is less understood. This represent an interesting niche for the exploration of potential therapeutic interventions of the TOR signalling pathway.

1.6. Aims of the project and contribution

The enhanced complexity of the biochemical mechanisms used by the cell to auto-regulate its physiology in response to nutritional status, could be significantly narrowed by studying the functional role of the TOR pathway, as this is a

conserved master regulator that couples cellular fate with environmental stimuli (Weisman & Choder, 2001).

This dissertation aims to elucidate the role of the evolutionarily conserved GATA transcription factor Gaf1 in nutrient responses coordinated by the TOR signalling pathway, focusing on the characterisation of both novel phenotypic features of growth and survival, as well as the transcriptional and functional profiles exerted by this unique transcription factor, intending to contribute to the understanding of mechanisms involved in cellular ageing.

Through the use of mutagenesis and chemical genetics, the project also aims to contribute to the development of comprehensive omics-datasets for data mining, gathering information about candidate genes conferring resistance to TOR signalling inhibition, relevant to understand molecular mechanisms involved in the resistance to the anticancer-drug torin1 used in the study to globally screen the Gaf1-dependent transcriptome, and the network of synthetic genetic interactions between *gaf1* and all the non-essential genes present in the genome of the robust model organism *S. pombe*, currently validated for these applications due to its similarities with higher eukaryotic cells.

A more comprehensive understanding of the functional role of Gaf1 will provide insights into the molecular mechanisms controlling cellular survival and chronological lifespan, contributing to decipher the physiology of cellular ageing.

The project is divided in three parts and aims to answer the following questions:

1.- To what extent Gaf1 transcription factor controls chronological lifespan, in particular during the inhibition of the rheostat for cellular energy sensing, the TOR pathway?

2.- What are the direct and indirect transcriptional targets of the GATA transcription factor Gaf1?

3.- What is the global genetic interaction network of *gaf1* in fission yeast and what is its relevance in response to TOR inhibition?

Chapter 2. Materials and methods

2.1. *In-silico analyses of Gaf1 transcription factor*

2.1.1. *Screening for orthologues*

- The search for orthologues of Gaf1 was executed using the PomBase database (Lock, et al., 2019).
- The protein sequences were obtained from the Universal Protein Resource (The UniProt Consortium, 2019).
- The multiple sequence alignments were performed with the software Clustal Omega to identify evolutionarily and structurally related residues (Sievers, et al., 2011).
- Conservation across species was assessed with the Basic Local Alignment Search Tool [BLAST] (Altschul, et al., 1997).

2.1.2. *Transcriptional responses of gaf1*

- The global transcriptome of fission yeast was assessed with the Pombe Transcriptome Viewer (*pombeTV*) tool (The Bähler Lab, 2016). This tool provides strand-specific information on the expression of *gaf1* during rapid proliferation in different experimental conditions independently from reported gene annotations.
- The assessment of the 5' Untranslated Regions (UTRs) in *S. pombe* genes was performed using the PomBase database (Lock, et al., 2019).

2.1.3. Protein interactions network of Gaf1

- The assessment of the protein-to-protein interactions (PPI) network was performed using the tools: Pombe Interactome (*Plnt*) that predicts interactions (Pancaldi, et al., 2012), and the String Consortium that contains reported interactions in *S. pombe* (Szklarczyk, et al., 2015).
- The gene list generated was analysed with the tool Analysis of Gene Lists (*AnGeLi*) to systematically detect functional enrichments among multiple sources of comprehensive reference information, allowing to define Gene Ontology (GO) categories (Bitton, et al., 2015).

2.2. General techniques

2.2.1. Fission yeast strains, media and treatments

This study has been conducted using *S. pombe* as an experimental model. The cells were grown in liquid or solid media, using either rich Yeast Extract with supplements (YES) also called rich media, and Edinburgh Minimal Medium (EMM2) supplemented with ammonium chloride as the nitrogen source, also called minimal media. Both media were acquired from the provider Formedium, and the ammonium chloride from Sigma-Aldrich.

The composition of the rich media is 5 g/l yeast extract, 30 g/l dextrose, supplemented with 0.05 g/l of adenine, L-histidine, L-leucine, L-lysine hydrochloride, uracil. The minimal media contained 20 g/l dextrose, 3 g/l phthalic Acid K⁺, 2.2 g/l disodium phosphate Na₂HPO₄, 1.05 g/l magnesium chloride hexahydrate MgCl₂.6H₂O, 14.7 mg/l calcium chloride dihydrate CaCl₂.2H₂O, 1 g/l

potassium chloride KCl, 40 g/l sodium sulphate Na₂SO₄, 1mg/l pantothenic acid, 10 mg/l nicotinic acid, 10 mg/l inositol, 1mg/l biotin, supplemented with trace elements and 5 g/l ammonium chloride (NH₄Cl).

Treatment and supplementation of the media were performed using several compounds (table 1).

Compound name	Supplier
Torin1	Tocris Cat. No. 4247
Rapamycin	LC laboratories Cat. No. R-5000
Compound 991 (C991)	Aobious, Inc. Cat No: AOB8150
Caffeine	Sigma Cat. No. C0750-500G
Arginine	Sigma Cat. No. A5006-100G
Nourseothricin (clonNAT)	Werner BioAgents Cat. No. 5
Geneticin (G418)	ThermoFisher Scientific Cat. No. 11811023

Table 1: Details of media supplement, stressors and antibiotics used in this research project.

The heterothallic 972 *h*- strain was the wild type used throughout the study as the control. For growth, toxicity, lifespan assays and expression profiling the mutant strains were obtained from the *S. pombe* genome-wide non-essential haploid deletion library from Bioneer v5.0, kindly provided by Prof. Jürg Bähler from the Institute of Healthy Ageing at University College London.

These experiments were conducted using prototroph strains carrying deletions in specific genes, including: *ade6*Δ depleted of the phosphoribosylaminoimidazole carboxylase Ade6, *car1*Δ disrupted in the plasma membrane high-affinity import

carrier for pyridoxine, pyridoxal, and pyridoxamine Bsu1, *car2* Δ deficient in ornithine aminotransferase Car2, *aru1* Δ lacking the arginase Aru1, *fil1* Δ depleted of the transcription factor Fil1, which is a master transcriptional regulator during amino acid starvation that activates genes required for amino acid biosynthesis, *aca1* Δ dysfunctional in the N-acetyltransferase involved in oxidative stress resistance, *gaf1* Δ disrupted on the gene encoding the transcription factor Gaf1, *tor1* Δ depleted of a core component essential for TORC2 activity, *tco89* Δ depleted of a non-essential core component of TORC1, *ssp2* Δ depleted of the AMP-activated protein serine/threonine kinase alpha subunit, and *amk2* Δ depleted of the AMP-activated protein kinase beta subunit (Ikai, et al., 2011; Lock, et al., 2019).

Other auxotroph strains were used in the lifespan assays, including 7 subtypes of the mutant *rps23* Δ , in which the disruptions in the ribosomal protein S23 that is a component of the small ribosomal subunit 40S, carried several restriction sites and punctual mutations. These mutants were kindly provided by Dr. Ivana Bjedov from the Cancer Institute at University College London.

For the synthetic genetic array (SGA) experiments, the deletion strain *gaf1* Δ resistant to nourseothricin was generated via transformation using PCR products with homologous recombination as previously described (Bähler, et al., 1998) adding a final step of electroporation adapting a published protocol (Forsburg & Rhind, 2006). The SGAs were performed using the Bioneer v5.0 haploid (*h+*) library as previously described (Kim, et al., 2010), kindly provided by Prof. Jürg Bähler from the Institute of Healthy Ageing at University College London.

The yeast strains used in this work are detailed below, including a description of their genotype and source (table 2).

Strain name	Genotype	Source
<i>aca1</i> Δ	<i>aca1::natMX6, h⁺</i>	Jürg Bähler, UCL, London
<i>ade6</i> Δ	<i>ade6::natMX6, h⁻</i>	Jürg Bähler, UCL, London
<i>amk2</i> Δ	<i>amk2::kanMX4, h⁺</i>	Bioneer collection
<i>aru1</i> Δ	<i>aru1::kanMX4, h⁺</i>	Bioneer collection
<i>car1</i> Δ	<i>car1::kanMX4, h⁺</i>	Bioneer collection
<i>car2</i> Δ	<i>car2::kanMX4, h⁺</i>	Bioneer collection
ED666	<i>ade6-M210 ura4-D18 leu1-32, h⁺</i>	Bioneer collection
ED668	<i>ade6-M216 ura4-D18 leu1-32, h⁺</i>	Bioneer collection
<i>fil1</i> Δ	<i>fil1::kanMX4, h⁺</i>	Bioneer collection
<i>gaf1</i> Δ	<i>gaf1::kanMX6, h⁻</i>	Jürg Bähler, UCL, London
<i>gaf1</i> Δ (SGA)	<i>gaf1::natMX6, h⁻</i>	This work
<i>tco89</i> Δ	<i>tco89::kanMX4, h⁺</i>	Bioneer collection
<i>tor1</i> Δ	<i>tor1::kanMX4, h⁺</i>	Bioneer collection
<i>rps23</i> Δ	<i>rps23::kanMX6, h⁻</i>	Ivana Bjedov, UCL, London
<i>rps23+::kanMX6</i> (4373-WT)	<i>rps23+::kanMX6, h⁻</i>	Ivana Bjedov, UCL, London
<i>rps23-SnaBI::kanMX6</i> (4376-SnaBI)	<i>rps23-SnaBI::kanMX6, h⁻</i>	Ivana Bjedov, UCL, London
<i>rps23-K60R-SnaBI::kanMX6</i> (4377-cgc)	<i>rps23-K60R-SnaBI::kanMX6 (cgc), h⁻</i>	Ivana Bjedov, UCL, London
<i>rps23-K60N-SnaBI::kanMX6</i> (4380-aat)	<i>rps23-K60N-SnaBI::kanMX6 (aat), h⁻</i>	Ivana Bjedov, UCL, London
<i>rps23-K60Q-SnaBI::kanMX6</i> (4383-cao)	<i>rps23-K60Q-SnaBI::kanMX6 (cao), h⁻</i>	Ivana Bjedov, UCL, London
<i>rps23-K60T-SnaBI::kanMX6</i> (4386-aac)	<i>rps23-K60T-SnaBI::kanMX6 (aac), h⁻</i>	Ivana Bjedov, UCL, London
<i>ssp2</i> Δ	<i>ssp2::kanMX4 h⁺</i>	Bioneer collection
Wild type	972, <i>h⁻</i>	Laboratory strain

Table 2: *S. pombe* strains used in this research project.

2.2.2. Collection and storage of *S. pombe* cells

Cell stocks were prepared according to the duration of the storage. Long term storage involved the generation of glycerol stocks as follows: inoculation of 0.8 ml YES medium and incubation at 30°C for 2 days at 250 rpm, addition of 0.8 ml of YES containing 50% glycerol (yellow freezing mix) to the culture and transfer into sterile, screw cap, round bottom, 2.0 ml cryotube (*Ratiolab*). The stocks were kept at -80°C where the cells remain viable for several years. Short term storage involved: inoculation of YES agar plates and incubation at 30°C for 2 days, the agar plates containing colonies were sealed with parafilm to prevent drying out and stored at 4°C for maximum of 2 months (Forsburg & Rhind, 2006).

The re-isolation of frozen cultures stored in YES + glycerol included: briefly thawing the required glycerol stock on ice, scraping off a small quantity of biomass from the frozen glycerol stock with a sterile inoculation loop, inoculation onto 10 cm petri dishes containing solid YES agar (each plate containing a single strain to avoid cross-contamination), and keeping the stock frozen. The plates were incubated at 30°C for 1-4 days (depending on the strain) to obtain fresh colonies. When growth was visible, single colonies were streak out onto fresh YES agar plates and incubated at 30°C for 2-3 days.

Pre-cultures in liquid media were prepared from fresh cell colonies and were grown overnight at 30°C with shaking at 250 revolutions per minute (rpm) in a rotating/shaker incubator at 250 rpm (*New Brunswick™*) suspended in 10 ml of media. The Bioneer haploid deletion library strains used were independently

validated by PCR of the genomic-marker junctions created by the gene deletions (Bähler, et al., 1998).

The cells from pre-cultures were used to inoculate the main cultures consisting of 10 ml liquid media. The required optical density (OD) was recorded at a wavelength of 600nm (*WPA S800 spectrophotometer from Biochrom*), to detect light scattering and estimate the concentration of cells in the culture. For physiological experiments, the main cultures were synchronised at mid exponential phase between 2×10^6 and 1×10^7 cells/ml at the beginning of the experiments, where an $OD_{600} = 0.1$ is approximately equivalent to 2×10^6 cells/ml (Forsburg & Rhind, 2006). Liquid cultures were grown at 30°C with shaking at 250 rpm.

2.2.3. Genomic DNA extraction

Cultures at stationary phase were centrifuged for 5 min at 3,000 rpm (*Labnet Prism from Corning Incorporated*). Cell pellets were resuspended in 1 ml ice-cold 1X PBS (137 mM NaCl, 2.7 mM KCl, 10 mM Na₂HPO₄, 1.8 mM K₂PO₄, pH 7.4) and transferred into 1.5 ml microtubes (*Eppendorf*) for another round of centrifugation for 5 mins at 3,000 rpm. The pellets were processed for genomic DNA (gDNA) extraction using the QIAamp DNA Mini Kit (*Qiagen*) according to the following protocol (figure 8).

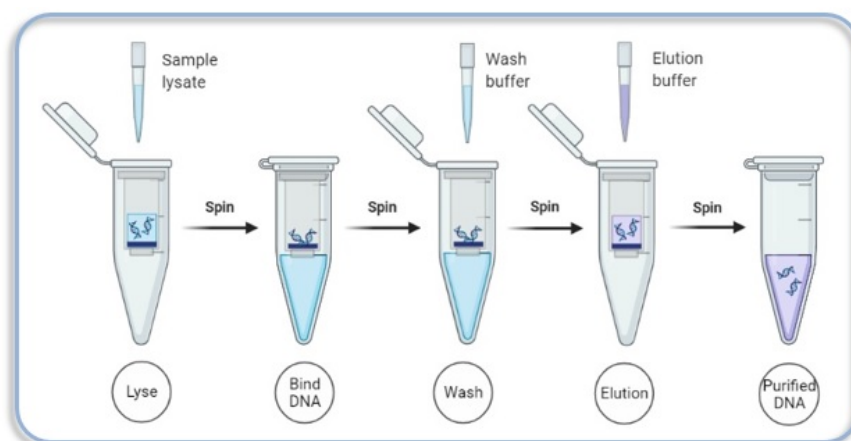


Figure 8: Summary of the steps followed for the extraction of DNA. Adapted from Qiagen.

The cell pellets were resuspended in 100 μ l Buffer ATL equilibrated at room temperature (15–25°C). 10 μ l of proteinase K were added to the lysate, which was mixed by pulse-vortexing for 15 s and subsequently incubated for 10 min at 56°C. 50 μ l of ethanol (96–100%) were added and the lysate was pulse-vortexed for 15 s. After incubating at room temperature for 3 min, the lysate was transferred to the QIAamp MinElute column (in a 2 ml collection tube), and centrifuged at 6,000 x g (8,000 rpm) for 1 min.

The column was transferred to a new 2 ml collection tube and washed with 500 μ l of buffer AW1 first, and 500 μ l of buffer AW2 afterwards. In each step, the centrifugation was performed at 6,000 x g (8,000 rpm) for 1 min, with a final centrifugation in a clean 2 ml collection tube at full speed (20,000 x g; 14,000 rpm) for 3 min to dry the membrane. The column was transferred to a clean 1.5 ml microtube and 50 μ l of buffer AE were added to the centre of the membrane and incubated for 1 min. This was centrifuged at full speed (20,000 x g; 14,000 rpm) for 1 min. The DNA was stored at -20°C until required for further processing.

2.2.4. RNA extraction

All the materials and equipment used for this procedure (work top surfaces, racks, pipettes, etc.) were cleaned with RNase-ZAP (*Sigma*) before starting. The cells from 10 ml liquid cultures at OD_{600nm} ~0.2 were harvested and centrifuged for 2 min at 2000 rpm. The pellet was snap-frozen in liquid nitrogen. The cells were thaw on ice for ~5 min, afterwards 1 ml of pre-chilled DEPC water (*ThermoFisher Scientific*) was used to resuspend the cells to transfer them into 2 ml tubes (*Eppendorf*), the cells were spin for 10 s at 5000 rpm. The pellet was resuspended in 750 µl of TES (10 mM Tris pH 7.5, 10 mM EDTA pH 8, 0.5% SDS), and immediately after 750 µl acidic phenol-chloroform (*Sigma*) were added. The samples were vortexed and incubated at 65°C in a heat block (*ThermoFisher Scientific*) for 1 h vortexed 10 s every 10 min.

The samples were then placed on ice for 1 min, vortexed for 20 s, and centrifuged for 15 min at 20,000 rcf at 4°C. The 2 ml yellow phase-lock tubes (*Qiagen*) were pre-spun for 10 s, and 700 µl of acidic phenol-chloroform were added. 700 µl of the water phase from the lysate were transferred to the phase-lock tubes thoroughly mixed by inverting (not vortexing), and centrifuged for 5 min at 20,000 rcf at 4°C. Another set of 2 ml phase-lock tubes were pre-spun for 10 s and 700 µl of chloroform:isoamyl alcohol [24:1] (*Sigma*) were added, to which 700 µl of the water phase obtained from the flow-through of the yellow phase-lock tubes were added and mixed thoroughly by inverting (not vortexing), this was centrifuged once for 5 min at 20,000 rcf at 4°C. 500 µl of the water phase were transferred to 2 ml tubes pre-prepared with 1.5 ml of 100% EtOH (-20°C) and 50 µl of 3 M NaAc pH 5.2.

This fraction was vortexed for 10 s and left at -20°C overnight to precipitate. The samples were then centrifuged for 10 min at 20,000 rcf at room temperature to collect the pellet. 500 µl of 70% EtOH (4°C) were added without mixing and spin for 1 min, the supernatant was aspirated and the samples were spin for another 5 s and allowed to air dry for 5 min at room temperature. The pellet was resuspended in 100 µl of DEPC water, and incubated 1 min at 65°C, the pellet was gently dissolved by pipetting up and down (~30x) until no particles were present, then vortexed for 10 s.

The RNA was quantified (*Nanodrop from ThermoFisher Scientific*) and 100 µg were purified using the RNeasy mini spin columns (*Qiagen*) as described by the company. ~500 µl were transferred to an RNeasy spin column placed in a 2 ml collection tube and centrifuged for 15 s at $\geq 8,000 \times g$ ($\geq 10,000$ rpm). The column was washed with 700 µl of buffer RW1 first and then with 500 µl of buffer RPE twice, in all cases the column was centrifuged for 15 s at $\geq 8,000 \times g$ ($\geq 10,000$ rpm). A final centrifugation was performed in a clean 2 ml collection tube at full speed (20,000 x g; 14,000 rpm) for 3 min to dry the membrane. The column was transferred to a clean 1.5 ml microtube and 30 µl of RNase-free water were added to the centre of the membrane and centrifuged at full speed (20,000 x g; 14,000 rpm) for 1 min. The RNA was stored at -80°C until required for further processing.

2.2.5. Polymerase chain reaction (PCR)

The amplification of the DNA was performed by collecting a small fraction of a single yeast colony with a micropipette tip from a YES agar plate. The DNA extraction was performed as described in 2.2.3., and the DNA was quantified

using the NanoDrop™ (*ThermoFisher Scientific*). The master mix for the PCR was prepared using MyTaq™ (*BioLine*), 1 μM of each custom-made primers (*Eurofins*), 10 ng/μl of linearized plasmid DNA and 50 ng/μl for gDNA to a final volume of 25 μl per tube.

PCR reactions were performed according to the cycling conditions recommended by the master mix manufacturers, annealing temperature and extension time were adjusted according to the size/composition of the primers and the size of the amplicon, respectively. The standard 3-step cycling profile was used, with 95°C for 1 min, followed by 35 cycles of 95°C for 15 s, annealing ranging from 57°C to 80°C for 15 s and 72°C for 10 s. Subsequently, 5 μl of the final product was differentiated by size using gel electrophoresis as described in 2.2.6.

The samples were tested in duplicate using positive and negative controls in each experiment. The amplifications were performed in a T100 PCR Thermal Cycler (*Bio-Rad*). The list of primer sequences and their (*S. pombe*) genomic coordinates are provided below in 2.2.7.

2.2.6. Gel electrophoresis for DNA visualisation

UltraPure™ agarose (*Invitrogen™*) was used to prepare agarose gels at the required concentrations (1-2% w/v depending on the size of the DNA) following the manufacturer's instructions. 0.01% of SYBRSafe (*ThermoFisher Scientific*) were added to the dissolved agarose prior to the polymerisation of the gel to allow band visualisation. The agarose was dissolved in UltraPure™ 1X TAE buffer [40

mM Tris-acetate and 1 mM EDTA pH 8.3] (*Invitrogen*TM). 1X TAE buffer was also used in the tank for the electrophoresis (*Invitrogen*TM).

Samples were loaded into the gel using 1X Gel Loading Dye (*New England BioLabs*) and compared to the molecular weight size markers Quick-Load[®] purple 100 bp and 1 kb DNA ladders (*New England BioLabs*) depending on the expected amplicon size to identify their approximate molecular weight.

The gels were run for 30-60 min at 80-100 volts (V) or until the bands separated clearly. The product sizes were observed against the pre-loaded marker using a UV light transilluminator (*ChemiDoc XRS+ from Bio-Rad*). Pictures of the gels were attained with the inbuilt camera of the gel photo documentation system.

2.2.7. Generation of the *gaf1* Δ query strain

The generation of the query strain *gaf1::natMX6* for this project required the preparation of a construct derived from the plasmid pFA6a (3,704 bp) containing the yeast selectable marker *natMX6* (1,123 bp), which confers nourseothricin resistance. This was kindly provided by Dr. Maria Rodriguez-Lopez from the Institute of Healthy Ageing at University College London. The *natMX6* deletion-cassette was isolated from the plasmid by means of PCR/linearization using 100 nt long custom primers, designed using the Pombe PCR Primer Programs (PPPP) from the Bähler Lab resources (Bähler, et al., 1998). The sequences were further validated with the NCBI-BLAST tool, and requested as HPLC purified after synthesisation (*Eurofins*).

The primers consisted of 80 nt flanking the sequences used for homologous genomic integration either immediately upstream of the *gaf1* start codon (sense oligonucleotide) or immediately downstream of the *gaf1* stop codon (anti-sense oligonucleotide), and 20 nt complementary to the *natMX6* module. Consequently, the resulting PCR amplicon contains the *NatMX6* cassette nested between terminal ends corresponding to homologous sequences that flank the *gaf1* ORF. These terminal ends allow the integration of the *NatMX6* cassette into the *gaf1* locus by homologous recombination, removing the *gaf1* ORF in a single step disruption process [figure 9] (Bähler, et al., 1998).

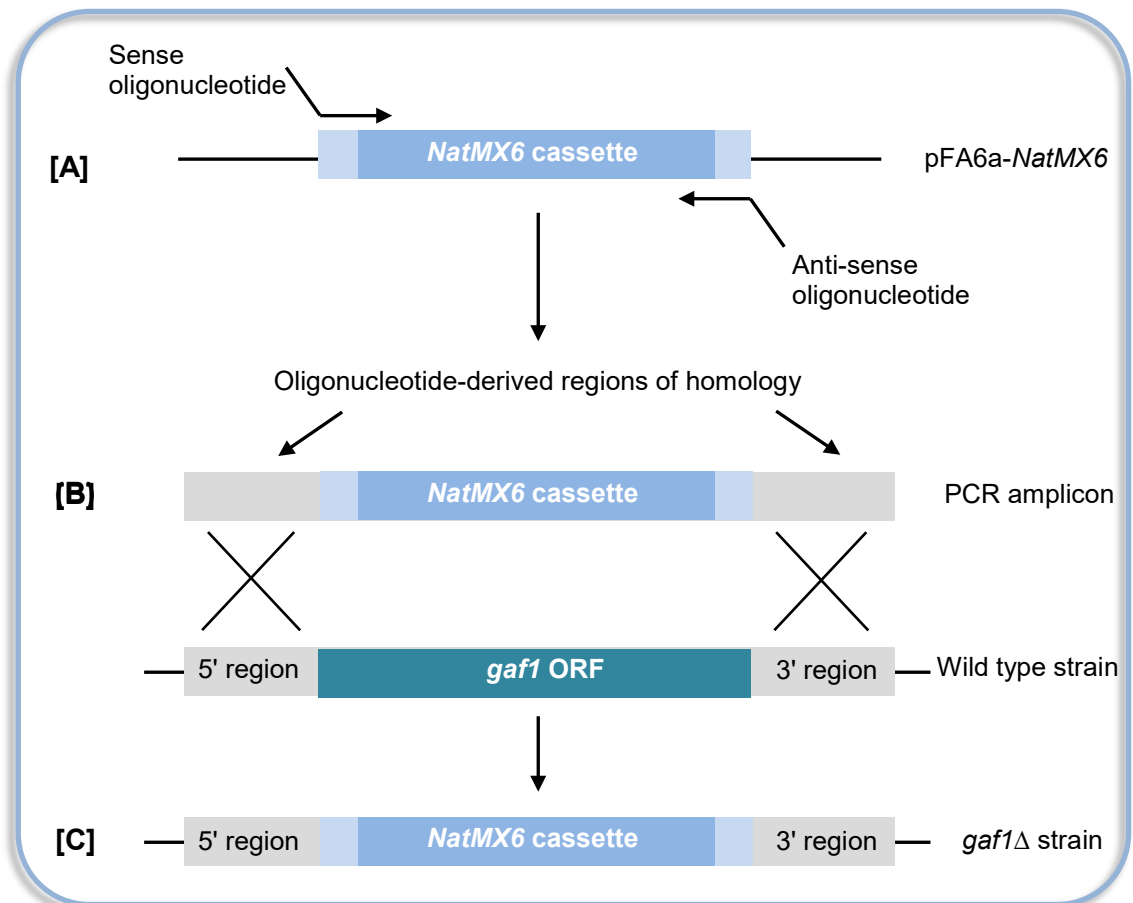


Figure 9: PCR-mediated gene deletion technique used to construct *gaf1*Δ yeast strains. **[A]** The *NatMX6* cassette was amplified from a pFA6a construct using primers designed to introduce 80 bp of sequence homologous to genomic regions that flank the *gaf1* ORF. **[B]** The purified PCR amplicon was transformed into wild type yeast strains. The PCR fragment is integrated into the yeast chromosome by homologous recombination directed by the regions of homology at the terminal ends of the amplicon. **[C]** The resulting strain has the *NatMX6* cassette disrupting the *gaf1* ORF in the endogenous *gaf1* locus. Stable transformants were selected in the presence of 100 mg/ml nourseothricin and confirmed by PCR screens.

Two sets of primers were successful for the genomic integration of the selectable marker and disruption of the *gaf1* gene (table 3).

Oligo name	Sequence
Forward primer N° 2	5'-AACTTCCCTTTTTCTTTCTTATCCACATTTCAAGCTGGCTGAAGTTAC TGA TTTTTGGGTATCATTTTTGGATATATCC - CCGATCCCCGGGTTAATTAA-3'
Reverse primer N° 2	5'-TCCGACAAGAAAAAATTCAAGTCGAAAATATACTATCTACCGAAAAT GATGATCAACGCATTGTGTTTTATATAAAAAA - GAATTCGAGCTCGTTTAAAC-3'
Forward primer N° 5	5'-ACCTTATATTATTATTTTTTTGTGATTTTTTACTACAACTTTTTTTTTGT TTAACGTTTGAGAGGCGATCTCTTTCGTTT - CCGATCCCCGGGTTAATTAA-3'
Reverse primer N° 5	5'-GCAGAAAACTCCCATCAAATTTAAATTAATTTGTGGGAACAAGGAG CCAAATAGTGATGAAGCCATACTTCGTCCATCA - GAATTCGAGCTCGTTTAAAC-3'

Table 3: List of primers used for the amplification of the deletion cassette and generation of the query strain *gaf1::natMX6*. The last 20 nt include the linking sequence to the cassette (blue). The primer increment (adjacency to the ORF) for primers N° 2 and N° 5 were 40 bp, and 160 bp, respectively.

The correct integration of the deletion cassette into the desired genomic site for *gaf1* gene disruption in the transformants, was confirmed with both phenotypic assessment in selective media (YES + nourseothricin agar) as well as torin1 resistance (YES agar). Additionally, positive transformants were confirmed with molecular characterisation of their gDNA by PCR and subsequent gel electrophoresis, following the procedures described in 2.2.5. and 2.2.6, respectively. The confirmatory primers were designed with the PPPP tool from the Bähler Lab resources [table 4] (Bähler, et al., 1998).

Confirmation oligo name	Sequence
Left primer N° 2	5'-CGTTGTTGGTGTGTCTTGGTAT-3'
Right primer N° 2	5'-AGCCAAATAGTGATGAAGCCAT-3'
Left primer N° 5	5'-GTGTGGTTTGCACAATCATTTC-3'
Right primer N° 5	5'-CGAACTAACCAAACACACCAAA-3'

Table 4: List of primers used to confirm the correct genomic insertion of the selectable marker and successful deletion of the *gaf1* gene for the generation of the query strain *gaf1::natMX6*.

The query strain *gaf1::natMX6* selected for the subsequent experiments was generated with the primers N° 2. The genomic coordinates of the *gaf1* gene and the binding sites of primers N° 2 are summarised below (table 5).

Primer name	Chromosome III		Gene position	
	Forward	Reverse	Forward	Reverse
Transformation primers N° 2	1,666,150	1,669,037	3,639	752
Check primers N° 2	1,666,115	1,669,215	3,674	574
<i>gaf1</i> gene genomic coordinates	1,665,533	1,669,788	1	4,256

Table 5: List of genomic location of *gaf1* gene and primers used for the generation / confirmation of *gaf1::natMX6* query strain. Coordinates according the National Center for Biotechnology Information (NCBI).

2.2.8. Transformation of *S. pombe* cells into *gaf1*Δ query strain

The transformation of *S. pombe* cells with linear DNA was performed following an electroporation method (Prentice, 1992) successfully adapted and applied in this study. The wild type strain was used to inoculate 10 ml of YES culture grown overnight as described in 2.2.1., until reaching an OD₆₀₀ ~0.7 equivalent to a

density of 1×10^7 cells/ml. At this point, the cells were incubated on ice for 15 min and centrifuged for 5 min at 4°C.

After discarding the supernatant, the pellet was kept on ice (at all time) and was resuspended and washed three times with 5ml of ice-cold filter-sterilised 1.2 M sorbitol (*Sigma*), centrifuging for 5 min at 4°C each time. The cell pellet was resuspended in ice-cold 1.2M sorbitol to a cell concentration of $\sim 1 \times 10^9$ cells/ml. 200 μ l of the cell suspension was transferred into clean 1.5 ml tubes containing 1 μ g of linear DNA, and then immediately transferred into ice-cold 0.2 cm electroporation cuvettes to be processed.

The cuvette was placed in the chamber slide and introduced in the electrode gap of the MicroPulser™ (*BioRad*) used for the electroporation, the cells were pulsed with settings for *S. pombe* cells following the manufacturer's instructions. Immediately after the pulse, 800 μ l of ice cold 1.2 M sorbitol was added to the cuvette and the suspension was gently transferred to a sterile tube incubated at room temperature for 60 min. After that, the electroporated cells were plated on minimal agar plates containing 1.2 M sorbitol and incubated for five days at 30°C. The colonies were replica plated on YES agar plates containing 1X of antibiotic nourseothricin for selection of positive transformants.

2.3. Specific techniques

2.3.1. Growth assays for fitness assessment

Spot tests were performed following the standard protocol (Rallis, et al., 2013) to assess the ability of wild type and *gaf1* Δ cells to form colonies when transferred from exponentially growing liquid cultures to rich solid media in the presence and absence of torin1 (20 μ M), rapamycin (100 ng/ml) combined with a titration of caffeine (1 mM, 5 mM, 10 mM) treatments.

These treatments were also used to assess growth of the strains wild type, *gaf1* Δ , *car1* Δ , *car2* Δ , *aru1* Δ , *fil1* Δ , *aca1* Δ , *tco89* Δ , *tor1* Δ on solid minimal media supplemented with ammonium as the nitrogen source, and a titration of the basic amino acid arginine, to assess if it reverses the effects of torin1 and rapamycin. The concentrations of arginine were 2 mM, 5 mM, 10 mM, for torin1 were 5 μ M, 10 μ M, and for rapamycin was 100 ng/ml.

The cells were grown for 24 hours in 10 ml of liquid media (rich and/or minimal) at 30°C at 250 rpm. The cultures were synchronised to an OD = 0.5 equivalent to 1×10^7 cells/ml, before performing six-steps of ten-fold serial dilutions. The diluted cells were spot-plated using a 48-well replica plater with prongs of 0.125 inches in diameter (*Sigma*). The cultures were spotted onto YES and/or EMM agar plates supplemented with the different treatments. Plates were incubated at 30°C and growth was monitored every 24 hours for 7 days.

2.3.2. Toxicity tests for torin1 sensitivity

The *S. pombe* strains wild type, *gaf1* Δ , *tco89* Δ , *tor1* Δ , were assessed within the framework of chemical genetics, in order to identify the level of sensitivity to torin1 produced by the deletion of those genes, specially dissecting TOR complex 1 from complex 2. This assessment was also required to standardise the threshold level of cytotoxicity produced by the compound to be administered to the cells in the subsequent experiments (chronological lifespan assays, transcriptomics, global genetic interaction network).

The growth curve of the strains was established by means of OD_{600nm}, collecting aliquots of 100 μ l from the liquid cultures at different time points during a period of 24 hours, measuring 1:10 dilutions. The liquid cultures were incubated at 30°C with 250 rpm.

The rapidly growing cultures at OD = 0.5 were diluted at OD = 0.2 and were treated with a titration of torin1 (0 μ M to 20 μ M). 10 ml of rich and minimal media were used for the wild type and *gaf1* Δ strains, whereas 10 ml of minimal media supplemented with nitrogen was used in the liquid cultures for *tco89* Δ and *tor1* Δ , to increase the specificity of the treatment by ruling out potential interferences produced by complex nutrients present in rich media (amino acids, higher glucose, etc.). The results from these experiments were tabulated and plotted using Prims version 9.2.0 (*GraphPad*).

2.3.3. Chronological lifespan assays

The revivability assays were performed using the wild type strain as a control and the prototroph mutant cells *amk2Δ*, *gaf1Δ*, *ssp2Δ*, *tco89Δ*, *tor1Δ*, together with seven subtypes of the auxotrophic strain *rps23Δ*. The strains were obtained from collaborating groups at University College London as described in 2.2.1. (table 2).

The strains were revived from frozen storage as described in 2.2.2. Single colonies were grown in 10 ml pre-cultures for 24 hours. The experiments were started inoculating 10 ml of liquid media of either YES or EMM supplemented with nitrogen (EMM+N), synchronised to an initial OD₆₀₀ = 0.5 equivalent to 1 x 10⁷ cells/ml in conical centrifuge tubes with a capacity of 50 ml (*Corning™ Falcon*). The lids were loosened to allow aeration and were incubated at 30°C rotating at 250 rpm.

When the cultures reached cell saturation density 2 days post-inoculation and no further changes in the OD of the culture were detected, the Colony Forming Units (CFUs) were used to estimate cell viability within a culture population. CFUs viability was assessed from the point at which the first measurements were taken (day 0), this is assigned as 100% viability (figure 10).

CFUs were prepared by serially diluting ten-folds culture aliquots of 50 µl in 150 µl of fresh media at specific time points, and plating 100 µl of the final dilution on solid YES media in technical duplicates, in order to obtain 20-300 colonies. The cells were evenly spread using 2 mm (diameter) sterile glass beads.

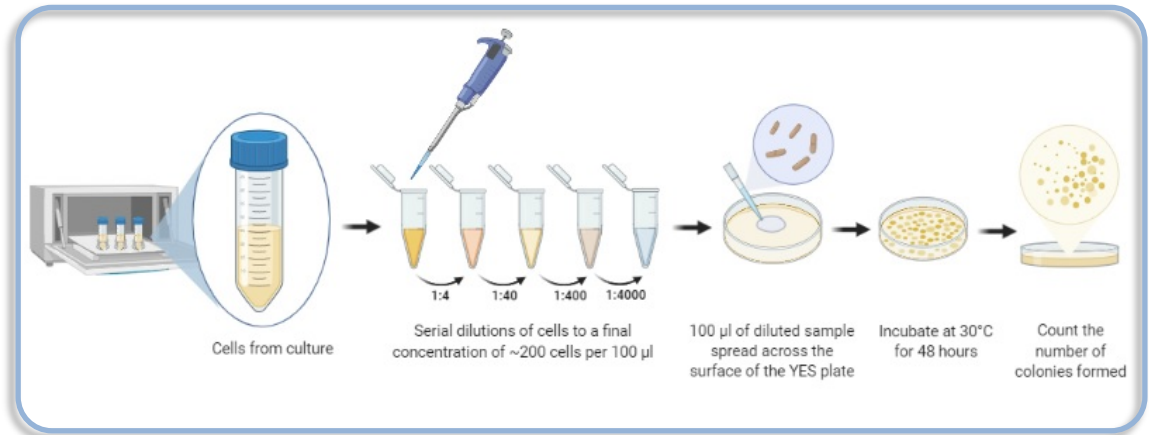


Figure 10. Growth curve of fission yeast showing the onset of chronological lifespan at the beginning of the stationary phase where a constant OD is reached. From that point, the decrease in clonogenic ability is recorded using a revivability assays.

The plates containing an even layer of cells were incubated at 30°C for 2-3 days or until colonies appeared. The number of colonies were counted manually with a digital colony counter (*Stuart*) and with the software Open CFU (Geissmann, 2013) after recording the plate in a transilluminator (*ChemiDoc XRS+ from Bio-Rad*).

This allowed to generate a viability curve until the cultures reached 0.1 % survival used to estimate cell survival within a culture population over time (figure 11). The results from these experiments were gathered in Microsoft Excel (2016) and the data was plotted using Prims version 9.2.0 (*GraphPad*).

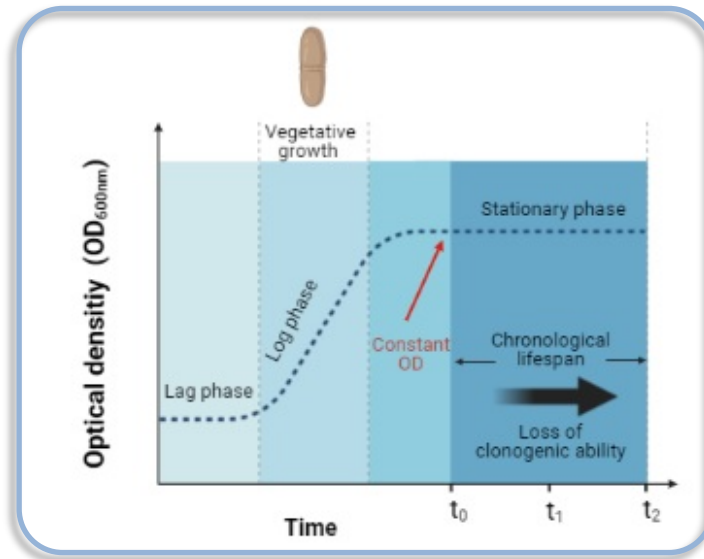


Figure 11. Revivability assay used to estimate the proportion of viable cells present in a non-proliferative liquid culture that are able to grow when transferred to a nutrient rich environment. Adapted from Graeme Smith (unpublished).

The Chronological Lifespan assays (CLS) were used to determine the maximal lifespan of wild type and mutant cells in rich and restricted nutritional contexts. These experiments assessed the survival *S. pombe* cells after treatment with several compounds that inhibit the TOR signalling pathway directly [rapamycin and torin1] (Atkin, et al., 2014; Weisman, 2010), and indirectly [compound 991] (Xu, et al., 2018) via the induction of alternative nutrient sensing pathways controlled by the adenosine monophosphate (AMP) activated protein kinase (AMPK) that inhibit TOR signalling (Kim, et al., 2016).

2.3.4. Transcriptome analysis

Expression microarrays were used to study gene expression changes in the whole genome of fission yeast of wild type and *gaf1*Δ cells in the presence or absence of torin1, aiming to identify Gaf1-dependent transcribed genes during TOR active and inactive states.

The microarray slides included probes (180–500 bp) printed in duplicate onto different regions with random control elements for a total of ~13,000 spots per slide. The coverage involves 5,269 fission yeast genes (known and predicted), including oligos for open reading frames, 11 mitochondrial genes, 19 pseudogenes, few different RNA genes (ribosomal RNA genes, tRNAs, small nuclear RNAs, and 68 larger genes for miscellaneous RNAs), 33 large introns, autonomously replicating sequences, centromeric repeats, 22 *S. cerevisiae* genes and 5 *Bacillus subtilis* genes as cross-hybridization controls (Lyne, et al., 2003). More detailed information containing all the primer sequences and parameters for data processing have been previously published (Penkett, et al., 2006).

For these experiments, samples from independent biological repeats combined with dye swapping were used to prevent signal bias during hybridisations (Lyne, et al., 2003). The strains wild type and *gaf1*Δ were treated with 20 μM torin1 for 1 hour at the exponentially growing phase in YES liquid media (OD₆₀₀ 0.5 = 1×10⁷ cells/ml), the analyses also involved an untreated control of the strains (figure 12).

The cells were harvested by centrifugation at 2,000 rpm for 3 min at 4°C. The RNA was isolated following the procedure in described in 2.2.4. Subsequently, 2 μg of purified RNA were reverse-transcribed into cDNA using the RevertAid reverse transcription kit (*ThermoFisher Scientific*) following manufacturer's instructions. The cDNA from each strain (wild type = 1 and *gaf1*Δ = 2) was purified using the PureLink PCR purification system (*Invitrogen*) and fluorescently

labelled with distinguishable dyes as previously described (Lyne, et al., 2003). Untreated cells (controls 1 and 2 respectively) were marked with green Alexa Fluor 555, whereas torin1-treated cells (experiments 1 and 2 respectively) were labelled with far-red Alexa Fluor 647.

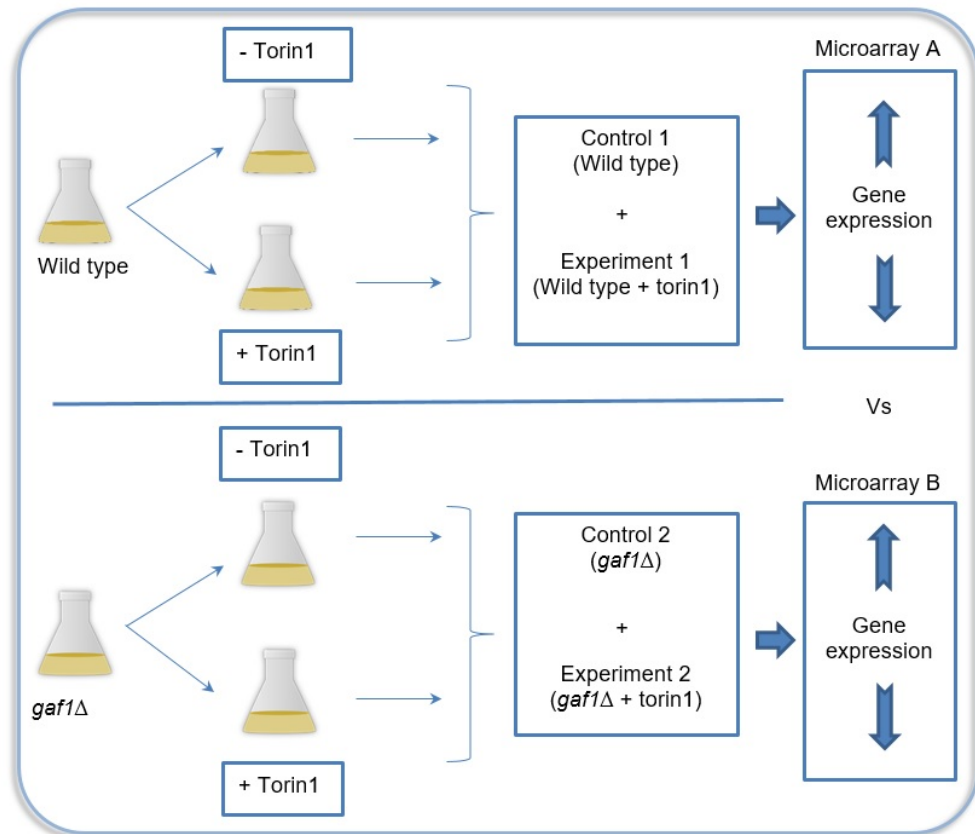


Figure 12. Diagram of sample preparation for expression microarrays using the strains wild type and *gaf1Δ* mutant grown in YES liquid medium in the presence and absence of 20 μ M torin1.

Agilent 8 \times 15K custom-made *S. pombe* expression microarrays were used, and the hybridizations and subsequent washes were performed according to the manufacturer's protocol. Briefly, the labelled cDNAs were hybridised by adding 40 μ l of sample into each chamber on the cover slip, 45 μ l of sterile 2X hybridisation buffer containing 48% formamide, 10X SSC and 0.2% SDS. The microarrays were sealed using LifterSlip® microarray coverslips (*Erie Scientific*) and were left in the hybridisation oven with humid chamber (*Boeckel Scientific*) incubating at 67°C for 17 hours.

After incubation, the slides were washed three times at room temperature in warm 100 ml of 0.1X SSC and 0.2% SDS, with a final in 100 ml 0.1X SSC. Incubated for 4 min at room temperature, and scanned (with the active side facing down) using the Agilent G2565AA DNA microarray scanner. The data was extracted using GenePix, processed with R scripts for quality control and normalisation (Lyne, et al., 2003), and analysed using GeneSpring GX3 (*Agilent Technologies*).

The values represent gene expression levels for each experimental condition (torin1 treatment) relative to the expression levels of the untreated controls from the same experiment. Differentially expressed genes (DEGs) were based on a conservative fixed cut-off of 1.5-fold change compared to the control, where genes with consistent changes across biological repeats were the ones considered.

The results obtained were the input data for the software *AnGeLi* (Bitton, et al., 2015), used to systematically generate GO enrichments (see 2.1.3.) and explore the biological processes controlled by those genes. Additionally, the g:GOST module from the g:Profiler platform (Raudvere, et al., 2019) was used to corroborate the enrichments and visualise the significance of the GOs categories. In both cases, the data sets were compared against all known *S. pombe* genes, the multiple testing was adjusted by using the False Discovery Rate (FDR), with $p < 0.01$ considered as significant. The role of individual genes was manually accessed using the web-based platforms PomBase database (Lock, et al., 2019) and the Universal Protein Resource (The UniProt Consortium, 2019).

Multiple comparisons of the gene lists were performed using Venn diagrams, generated with the software GeneVenn and Venny version 2.1. These data sets comprise the integrations of coding/non-coding regions against introns/exons observed in the genes transcriptionally regulated by Gaf1. The comparisons also include integrations of the transcriptional profile controlled directly and indirectly by Gaf1 and its direct target genes before and after activation previously published by the group (Rodríguez-López, et al., 2020).

2.3.5. Genetic interactome analysis

The *gaf1*-dependent genetic interaction network was studied applying Synthetic Genetic Arrays (SGAs). These experiments were performed following the protocol previously described (Baryshnikova, et al., 2010; Dixon, et al., 2008).

The query strain *gaf1*Δ resistant to nourseothricin (see genotype in 2.2.1., table 2) was generated for this study following an optimised version of the standard method (Bähler, et al., 1998) described in 2.2.7. Briefly, the *natMX6* cassette confers antibiotic resistance which was used for spore selection, the genetic integration was performed with transformation by electroporation that results in homologous recombination and substitution of the *gaf1* open reading frame with the cassette.

The query strain was systematically mated with the *S. pombe* genome-wide haploid deletion library from Bioneer v5.0 containing 3,420 non-essential genes covering ~95% of the genome. This was performed using the benchtop robot RoToR HDA (*Singer*) following manufacturer's instructions. This approach

allowed to screen synthetic genetic interactions across the genome through the construction of double deletion mutants, combining *gaf1*Δ with the single-gene mutant strains from the library. The fitness of the single and double mutant strains was assessed in rich nutritional contexts with and without 10 μM of torin1 (Baryshnikova, et al., 2010).

The SGA experiments included the control strain *ade6*Δ resistant to nourseothricin (see genotype in 2.2.1., table 2) as a control query, which was used to simultaneously to compare spot sizes. The *ade6*Δ mutant does not affect the fitness of the deletion library when used to generate double mutants, and is used as a reference to determine the fitness of the library for colony size normalisation purposes (Baryshnikova, et al., 2010; Rallis, et al., 2017).

The following steps were completed in the present study for the efficient isolation of double mutant haploids (figure 13).

The resulting single and double mutant colonies distributed in arrays of 384 spots per plate -12 plates in total containing the entire library-, were imaged using the MultiDoc-It imaging system (*UVP*). Colony size measures of the single and double mutants in the presence and absence of TOR signalling were used as a proxy for fitness.

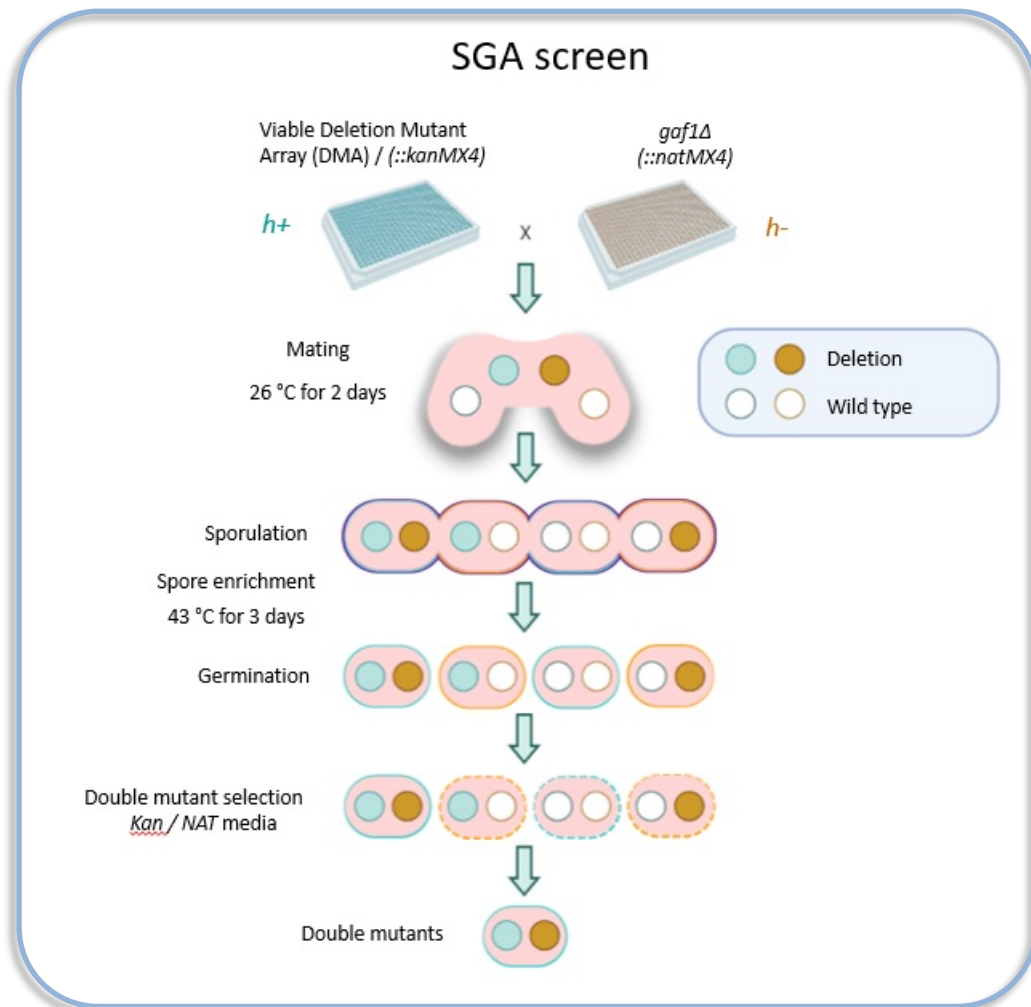


Figure 13. Schematic illustrating the SGA method. Cells of opposite mating type (*h+*, *h-*) are mated on minimal media and allowed to sporulate for 3 days at 26 °C. Subsequently, the mating plates are heat treated for 3 days at 42 °C for spore enrichment and to eliminate unmated haploid cells. Lastly, cells are transferred to rich medium for germination (no antibiotics), followed by selection of recombinant double-mutant progeny using double-drug (G418 and nourseothricin) rich medium. Adapted from (Baryshnikova, et al., 2010).

They were obtained using the gitter package in R (Wagih & Parts, 2014). This software applies systematic normalisations for the correction of experimental effects to calculate the interaction values. They include: normalisation of colony sizes with respect to the plate median in order to control for the effect of the query mutation and different growth rate between plates, differences in colony sizes due to nutrient availability (row/column location), gradients in media thickness (spatial), neighbouring mutant strains (competition), and batch effects (Baryshnikova, et al., 2010).

The parameters used to exclude interactions included: high variability between replicates, dubious interaction values as a result of linkage involving library mutants located within 100 kb distance of the *gaf1* gene, library mutants showing reduced colony size in the *ade6* Δ double mutants (less than 100 pixels). Mutants within these criteria were not considered as accurate to calculate interaction values and were excluded from the dataset as previously described (Rallis, et al., 2017).

Medians of colony sizes from two independent biological repeats of *gaf1* Δ -double mutants, were normalised against the control strain *ade6* Δ -double mutants (reflecting fitness of the single mutant library) to calculate the value of the genetic interactions. The logarithms in base 10 of the interaction were used for interaction scores. The cut-offs in interaction scores for defining increased or decreased fitness in the single mutant, and positive and negative interactions with *gaf1* in the double mutants (in the different conditions) were established as +0.15 and -0.15, respectively (Rallis, et al., 2017). The quantified measures of fitness were then exported to Microsoft Excel (2016) and the data was plotted using Prims version 9.2.0 (*GraphPad*).

The SGA experiments comprised data gathered from four groups: the single mutants from the library, the negative and positive interactions of the double mutants, and the resistance and sensitivity to torin1 observed in the single and double mutants. All of them grown in rich nutritional contexts.

The gene lists generated in this section of the study were assessed for GO enrichments using the *AnGeLi* tool (Bitton, et al., 2015), used to elucidate the biological processes controlled by those genes. The data sets were compared to all known *S. pombe* genes, and the multiple testing was adjusted by using the False Discovery Rate (FDR), with $p < 0.01$ considered as significant. The role of individual genes was explored manually using the web-based platforms PomBase database (Lock, et al., 2019) and the Universal Protein Resource (The UniProt Consortium, 2019).

Further examinations across data sets were performed using the web-based tools for gene lists comparisons GeneVenn, Venny version 2.1, and Molbiotools. All the SGA hits were integrated to generate a matrix compiling the prevalence of genes in 28 different categories. The matrix combined the transcriptional profile of Gaf1 described in chapter 5 (up- and down-regulated genes transcriptionally controlled by Gaf1, and target genes before and after activation of Gaf1), with the global fitness of *S. pombe* non-essential single mutants, and the network of synthetic genetic interactions of *gaf1* in the presence and absence of torin1 described in chapter 6 (single mutants decreasing and increasing fitness, single and double mutants conferring sensitivity and resistance to torin1, and the positive and negative interactors with *gaf1*).

Chapter 3. GATA transcription factor Gaf1 as a relevant model:

In silico analyses

3.1. *Introduction*

Transcription factors have been found to be grouped in highly related multifactorial families that share similar DNA-binding motifs but differentially recognise specific sites from a variety of regions with similar sequences to perform their respective functions (Ko & Engel, 1993). Within them, the transcriptional regulators GATA factors are highly conserved throughout evolution being present among plants, fungi and metazoans. They have an extensive range of functions from nitrogen source utilisation and mating-type shift in fungi to development and differentiation in mammals (Scazzocchio, 2000).

In this chapter, the GATA transcription factor Gaf1 from *S. pombe* was studied using several bioinformatics tools aiming to validate it as a relevant model with the capability to extrapolate the results to other species. This body of work includes the assessment of three main elements of Gaf1: its conservation among different species with a screen for orthologues and comparison of their primary structures with the human form; its level of expression in different growth conditions resembling nitrogen/nutrient-deprived environments to identify parameters inducing or repressing its transcript; and the predicted/established Protein-to-Protein Interactions (PPIs) annotated until the present day for this transcription factor.

3.2. Screening for orthologues of *Gaf1* transcription factor

This search was executed using the PomBase database (Lock, et al., 2019) which provided a general systematic description of the protein in *S. pombe*. The screening detected two matches with: *Saccharomyces cerevisiae* Gat1 transcriptional activator of nitrogen catabolite repression genes, and *Homo sapiens* GATA binding protein 6 (GATA6). Their sequences were obtained from the UniProt Consortium (Gaf1: Q10280; GATA6: Q92908; Gat1: P43574) and used to perform multiple sequence alignment with the program Clustal Omega to identify evolutionarily and structurally related residues (figure 14).

This standard bioinformatics technique allowed the visualisation of relationships between equivalent residues to infer similar functional roles, establish comparisons with the human/mammalian type and elaborate phylograms to assess conservation throughout evolution (The UniProt Consortium, 2019). The multiple sequence alignment revealed that the protein is highly conserved, with 41 identical positions (out of ~855 amino acids in *S. pombe*) between the three orthologues. The majority of the conserved residues (21 of them) were located within/near a loop-like structure described as GATA type zinc-binding motif characterised by the general sequence C-X(2)-C-X(17)-C-X(2)-C which is used to classify them depending on its length and the number of loops, elements that are always followed by a highly alkaline terminal domain (McDowall, 2007).

Identical positions	41
Identity	4.205%
Similar positions	93
Program	CLUSTALO

<input type="checkbox"/>	Entry	Entry name	Protein names	Organism
<input type="checkbox"/>	Q10280	GAF1_SCHPO	Transcription factor gaf1	Schizosaccharomyces pombe (strain 972 / ATCC 24843)
<input type="checkbox"/>	Q92908	GATA6_HUMAN	Transcription factor GATA-6	Homo sapiens (Human)
<input type="checkbox"/>	P43574	GAT1_YEAST	Transcriptional regulatory protein ...	Saccharomyces cerevisiae (strain ATCC 204508 / S288c)

Figure 14. Output data of the multiple sequence alignment comparing Gaf1 with orthologs. Source: (The UniProt Consortium, 2019).

The conserved structure of this specific type of zinc fingers comprise two irregular antiparallel β -sheets and one α -helix that is followed by a prolonged loop with amino acids on the surface. The α -helix and loop connect the two β -sheets and bind to the major groove of the target DNA to recognise a variety sequences (2 to 6 base pairs per finger) by making tandem contacts (Wolfe, et al., 2000). The recognition of the consensus sequence A/C/T GATA A/G by this domain defines a GATA factor (Kim, et al., 2012).

These compact DNA-binding motifs are stabilised by a zinc ion coordinated by four cysteines in a tetrahedral manner that preserve the conformational shape of the protein, being one of the most common features among eukaryotic transcription factors, with over hundred proteins known to possess several of them in the human genome (Persikov, et al., 2009). They originated near the root of the eukaryotic lineage and represent the ancestral state of the gene family, being absent in the entire bacterial and archaeal protein set, with low frequency among plants and fungi (Scazzocchio, 2000). Proteins containing these domains are involved in different cellular processes such as replication, repair,

transcription/translation, metabolism, cell proliferation and apoptosis, which is achieved through interactions and binding to small molecules, proteins and nucleic acids (Krishna, et al., 2003).

Fungal GATA transcription factors typically contain a single zinc finger that consist of a 19 to 20-residue loop that is uncommon in other species (McDowall, 2007). Exceptions of fungal proteins with double-zinc fingers are limited including the *S. pombe* iron-sensing transcription factor Fep1 (PomBase accession number SPAC23E2.01) and the *S. cerevisiae* nitrogen regulatory protein Dal80 [UniProt accession number P26343] (Teakle & Gilmartin, 1998).

In plants, these factors have a single binding domain of 18-residue loop (Scazzocchio, 2000). The results obtained in this study are consistent with the literature showing that Gaf1 and Gat1 (yeast) present a single zinc finger, however, they belonged to the category IVa (17-residue loop) that is attributed to vertebrates (Teakle & Gilmartin, 1998), and reported as the canonical metazoan class of single-finger GATA factors observed in ascomycetes involved in nitrogen metabolism (Scazzocchio, 2000). This *animal* type could be present with either one or two copies of this domain separated by few residues (Emerson & Thomas, 2009) as is the case of the double loop detected in mammalian GATA6 (Zhao, et al., 2008). The roles and structural similarity between these three transcription factors highlight the relevant functional divergence of an early eukaryotic motif for DNA-protein recognition/interaction which conserved its ancestral configuration beyond speciation throughout evolution.

This was supported by the phylogram plot (figure 15) which revealed the presence of two major clusters, the first one containing multicellular organisms and the second one gathering unicellular organisms. In this case, the values closer to zero (0) indicate that the species are closely related to a common ancestor, whereas higher numbers closer to one (1) show a more diverse evolution of the protein with respect to the common ancestor (The UniProt Consortium, 2019).

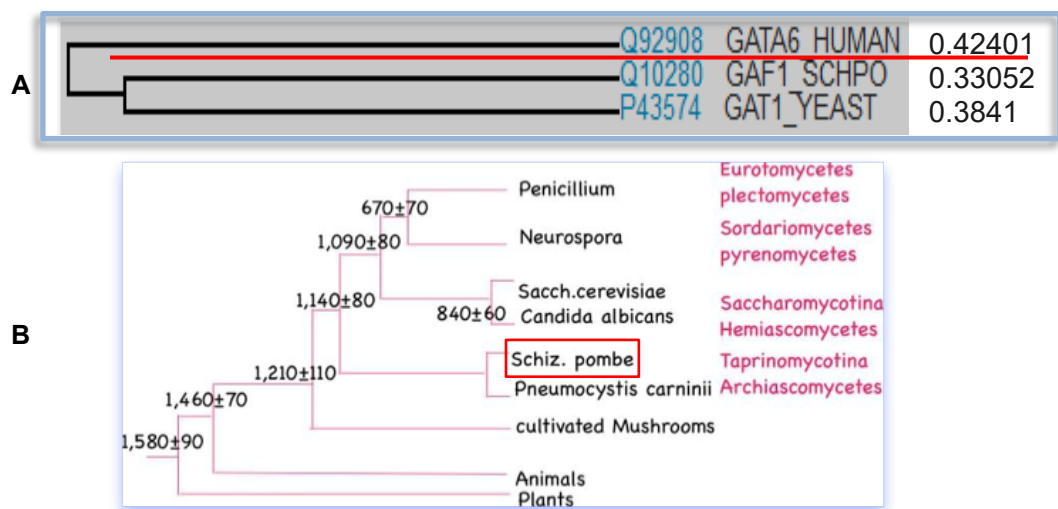


Figure 15. [A] Phylogram of different orthologs of Gaf1 (The UniProt Consortium, 2019).
[B] Phylogeny of life in millions of years. Adapted from (Hedges, 2002).

Considering that the evolutionary relationships represented in this tree are based on orthologue sequences (Arnaoudova, et al., 2010) the similar values closer to one (1) observed amongst human, fission and budding yeast (0.424, 0.330, 0.384 respectively) confirm the similarity between the three forms of the protein and the proximity to a common ancestor, suggesting that this molecule plays important and similar biological functions across species, also confirmed by the lethal effect caused by the lack of expression of the *GATA6* gene during the embryonic stage in humans (Zhao, et al., 2008), which subsequently is not holistically expressed in the human body (Papatheodorou, et al., 2018).

Further investigation of GATA6 prevalence across species was performed with the Basic Local Alignment Search Tool (BLAST), used to detect similarities between sequences and identify functional and evolutionary relationships (Altschul, et al., 1997). The results obtained for this dissertation revealed >90% identity in the protein sequence with at least 65 different species.

These *in silico* analyses of the transcription factor Gaf1 from *S. pombe* confirmed the evolutionary conservation of the protein between species, validating its selection as a relevant biological model to study its role in nutrient signalling pathways and cellular ageing, with the possibility to extrapolate meaningful conclusions to its human orthologue *GATA6* and overall human cell physiology. This is because of the several molecular and cellular biology features shared between them (chromosomes with large/complex centromeres and replication origins, similar heterochromatin, and the presence of RNA interference system, among others), elements that are missing in other models such as the budding yeast (Hoffman, et al., 2015).

3.3. Transcriptional response of *gaf1* under multiple conditions

Another computational analysis was performed using the Pombe Transcriptome Viewer (*pombeTV*) tool (The Bähler Lab, 2016), to globally evaluate the transcriptome of the fission yeast with strand-specific information focusing on the expression of *gaf1* during rapid proliferation in ten different experimental conditions independently from reported gene annotations (figure 16). The data was captured with high-density tiling arrays using complementary DNA (cDNA)

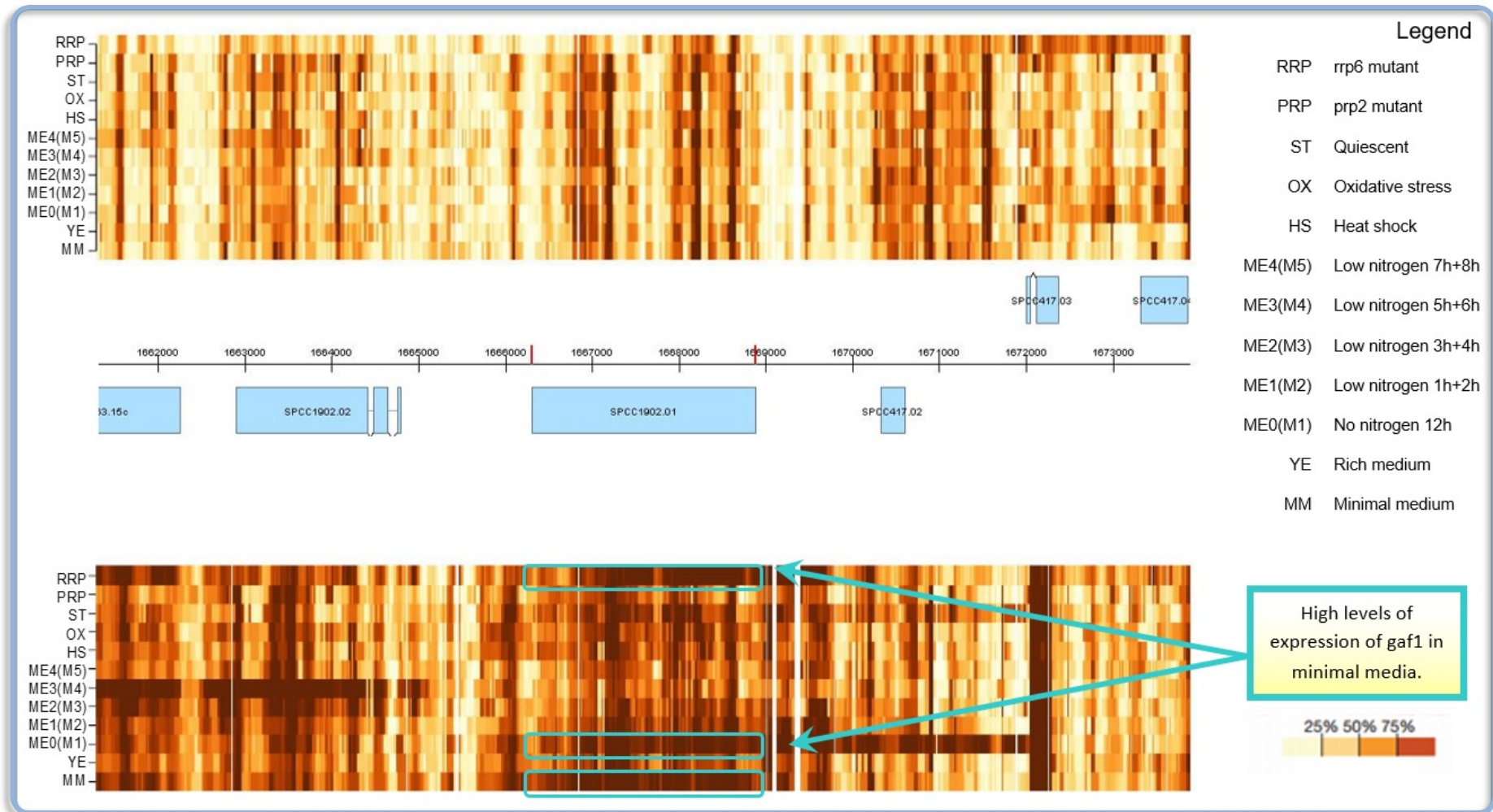


Figure 16. Tiling-chip array profile of *gaf1* gene (SPCC417.01c) in *S. pombe* chromosome 3. Hybridization signals (in which the strength of colour reflects the signal distribution quartile) across the genomic region shown in the centre for forward (top) and reverse (bottom) strands, with rows reflecting different experimental conditions. Rapid proliferation was sampled in rich (YE) and minimal (EMM2) media. Source: *PombeTV* from the Bähler Lab (Wilhelm, et al., 2008).

synthesised from RNA with reverse transcription [RT-PCR] (Wilhelm, et al., 2008). The results obtained from this analysis showed the dynamic plasticity in the expression of *gaf1*, with enriched transcripts when cells were exposed to nitrogen depletion in minimal media (EMM2) -containing restricted amount of nutrients- compared to rich media (YES). This is consistent with the reduced TOR activity described in *S. pombe* when nutrients are limited, specifically nitrogen (Rallis, et al., 2013), and suggests that *gaf1* might be indirectly induced at the transcriptional level by TOR activity.

The results obtained for this dissertation with this analysis also showed an increased transcription of *gaf1* in *rrp6* mutants -defective in nuclear exosome function (Schuch, et al., 2014)-. This was used as a model to assess if the screened regions reflected cryptic unstable transcripts (sub-set of non-coding RNAs) which are rapidly degraded in the nucleus, raising the possibility that *gaf1* is transcribed during fast growth in normal environmental conditions but rapidly degraded by different surveillance systems. This is in contrast to the majority of the novel transcripts identified by (Wilhelm, et al., 2008), that were not strongly expressed in proliferating cells, which suggest a relevant role for the inhibition of *gaf1* transcripts at that stage.

Aside from the reported cytoplasmic retention of Gaf1 -for its inactivation- which is positively regulated by active TORC1 in normal nitrogen conditions (Laor, et al., 2015), there is a possible alternative mechanism for its inactivation that is more efficient at the metabolic level. In *S. pombe*, the mean combined length of the Untranslated Regions (UTRs) is ~465 nucleotides, where short 5' UTRs

confer stability, whereas long 5' and 3' UTRs make mRNA less stable (Wilhelm, et al., 2008). Further evaluation of *gaf1* transcripts carried out for the present study, detected that *gaf1* gene encodes long 5' and 3' UTRs (910 and 776 nucleotides respectively). This supports the hypothesis that such configuration of the *gaf1* transcripts allows their rapid degradation due to the presence of regulatory signals for RNA turnover before translation.

This represent a novel mechanistic regulation for the inactivation of Gaf1 as a transcription factor before translation not previously described in the literature, in addition to the reported cytoplasmic retention positively regulated by active TORC1 in normal nitrogen conditions (Laor, et al., 2015) and shed lights of its role at the logarithmic growing phase when is not needed. Additionally, the high levels of *gaf1* detected with nitrogen starvation, are concordant with previous data that indicates that the suppression of Tor2p (TORC1) in the absence of nitrogen sources, triggers a survival response (Matsuo, et al., 2007). Therefore, this *in silico* characterisation of *gaf1* transcripts contribute to further understand the aforementioned scenario that *gaf1* is also controlled by TOR at the transcriptional level.

3.4. Protein interactions network of Gaf1

The assessment of the protein-to-protein interactions (PPI) network allows the exploration of essential mechanisms to understand how proteins perform their biological functions. This is achieved by means of computational tools that combine molecular characteristics for the prediction of sites that direct such interactions (Li, et al., 2019). These analyses were performed using three

different programs. The initial module consisted of the Pombe Interactome [*PInt*] (Pancaldi, et al., 2012) and the String Consortium (Szklarczyk, et al., 2015), where the first one predicts and the second one contains reported protein interactions in *S. pombe* (figures 17 and 18). They were used to generate a list of candidate genes with more than 102 hits with interconnected functions (appendix I).

This gene list represented the input data analysed with the tool Analysis of Gene Lists [*AnGeL*] (Bitton, et al., 2015), to systematically detect functional enrichments among multiple sources of comprehensive reference information including gene and phenotype ontologies, genetic and protein interactions, transcripts, translation, chromosomal location, genetic diversity, conservation, co-regulation, and many other variables, providing an extensive exploration of the connections between the query genes to detect statistically significant common features among them that uncover protein complexes, enrichment of specific pathways and several additional interactions (Bitton, et al., 2015).

The software allows the analysis of Gene Ontology (GO) categories, defined as a description of common features of the biology of a gene product to establish comparisons based on their annotations. The objective is to provide a classification of all gene products under three unifying principles describing biological processes, molecular functions and cellular components (The Gene Ontology Consortium, 2015).

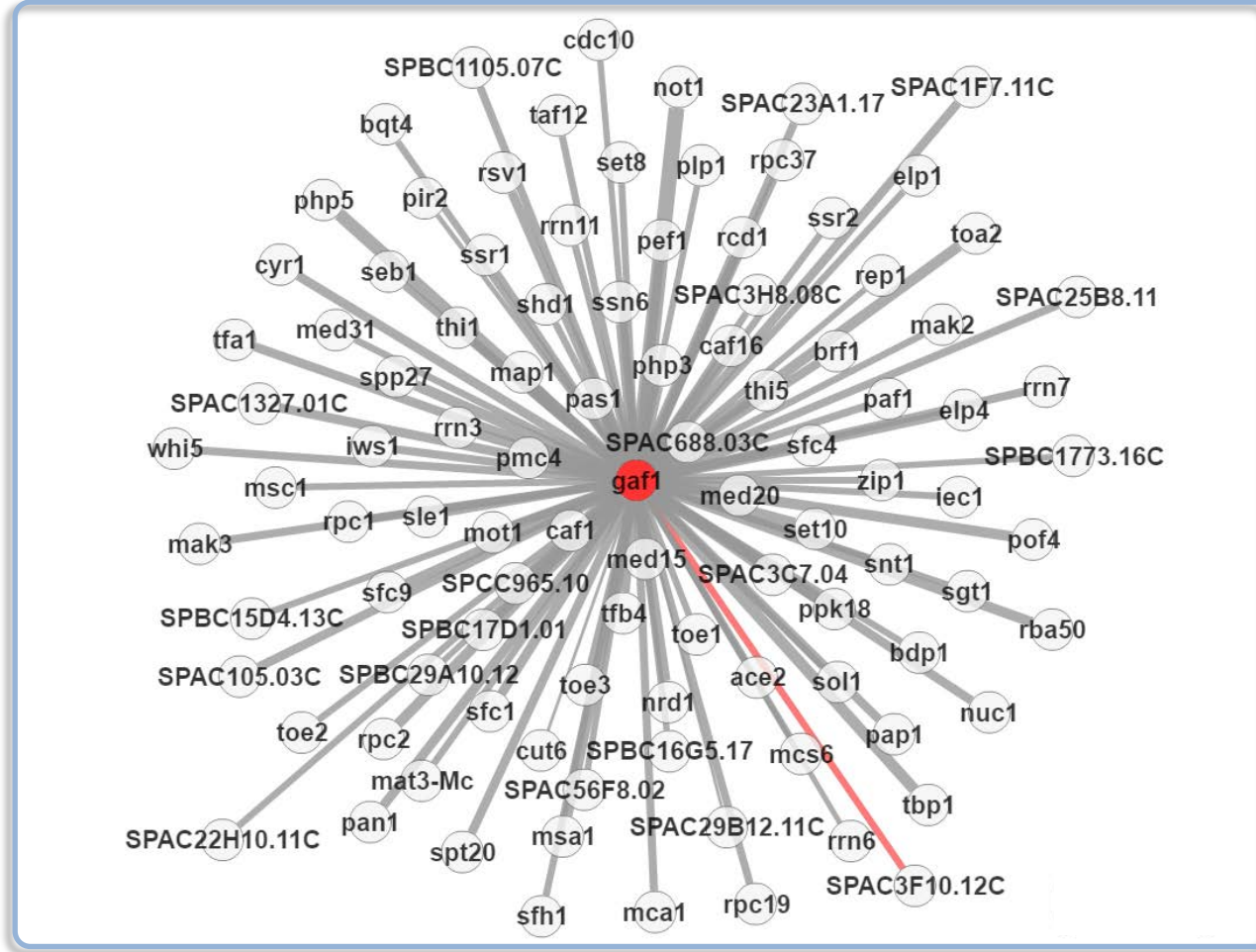


Figure 17. Predicted and known PPI network of the transcription factor Gaf1 in fission/budding yeast represented as a red node. The link thickness with other nodes is proportional to the confidence of the prediction. Source: *Plnt* by the Bähler Lab (Pancaldi, et al., 2012).

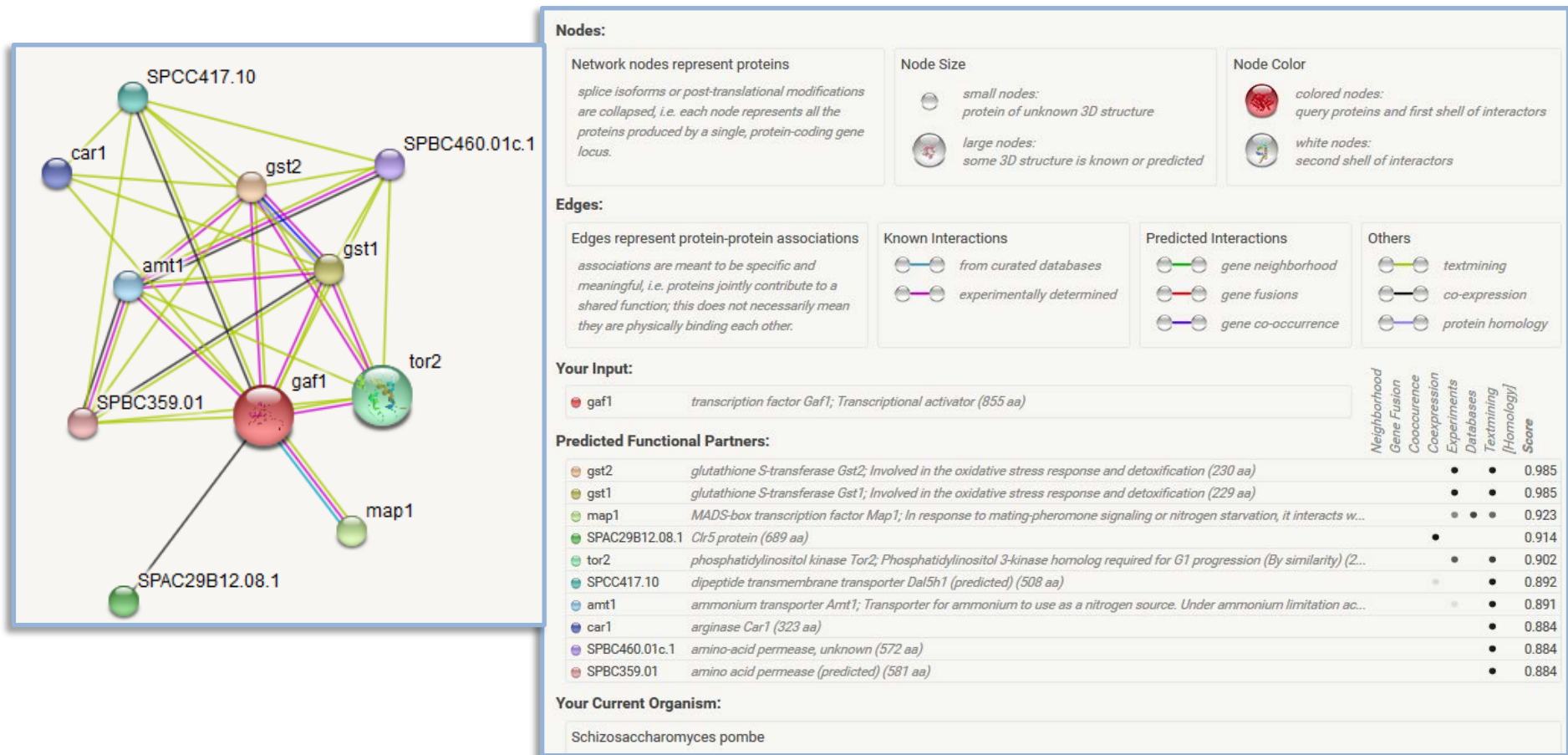


Figure 18. PPI network of the transcription factor Gaf1 in *S. pombe*. Source: The String Consortium (Szklarczyk, et al., 2015).

The output data of *AnGeLi* was classified in clusters of genes that are not mutually exclusive, this is because the product of a single gene could have more than one molecular function, be associated with different cellular components and be involved in several biological processes (figure 19).

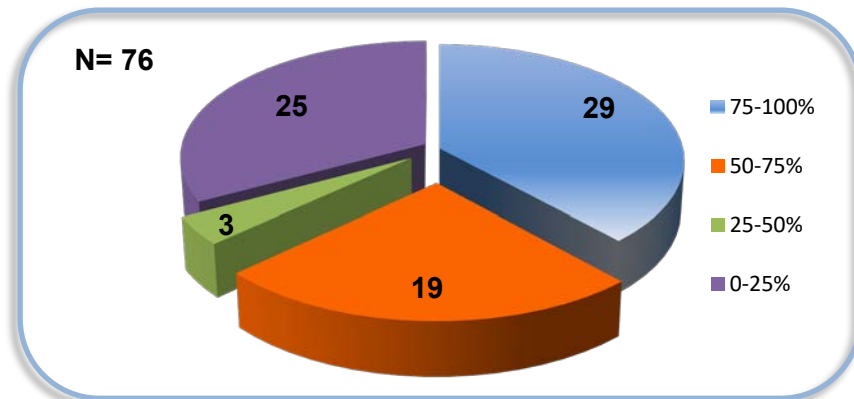


Figure 19. Distribution of interacting genes from the list grouped by their frequency among 76 general processes.

The first cluster of GO enrichments was made by grouping the genes that presented a frequency between 75-100%, this means that ~80 genes of the list (out of 102) were involved in 29 different processes mainly metabolic, some examples are: general cellular metabolic process, organic substance/compound metabolic process, cellular aromatic compound metabolic process, cellular nitrogen compound metabolic process, nucleic acid metabolic process, gene expression, transcription, cellular macromolecule biosynthetic process.

The following group with a frequency of 50-75% was made by ~56 genes of the list generally involved in 19 regulatory processes, such as: regulation of cellular/biological process, regulation of transcription, regulation of gene expression, regulation of cellular macromolecule biosynthetic process, transcription from RNA polymerase II promoter.

The cluster of 25-50% frequency was formed by ~35 genes related to 3 single-organism cellular processes. The last group of 0-25% included ~8 genes belonging to 25 miscellaneous processes such as: positive regulation of cellular biosynthetic process, positive regulation of transcription/gene expression, positive regulation of RNA metabolic process, elongation, negative regulation of conjugation with cellular fusion, negative regulation of reproductive process, regulation of transcription involved in G1/S transition of mitotic cell cycle.

Considering the overlap of processes within each cluster, a general overview indicates a significant enrichment of genes involved in nitrogen metabolism that may be induced or repressed under various stress conditions such as nitrogen starvation which is the case of *gaf1*. Interestingly, the cluster 0-25% showed four enriched genes for the regulation of transcription during the transition in G1/S of mitotic cell cycle, which could be related to the phenotypes described previously of wild type cells deprived of nitrogen that leads to an arrest of the cell cycle in G1 phase with small-rounded cells that are de-repressed for sexual development (Matsuo, et al., 2007).

This association of genes according to categories of processes facilitated the overview of the interactions, tailoring the subsequent analyses to the biological context of the query gene list and providing valuable insights with testable hypotheses for the development of the experiments.

Taken together this *in silico* study of the transcription factor Gaf1 from *S. pombe* validated its selection as a relevant biological model to study its role in nutrient

signalling pathways and cellular ageing with the possibility to extrapolate meaningful conclusions to human cells due to the many molecular and cellular biology features shared between them (chromosomes with large/complex centromeres and replication origins, similar heterochromatin, the presence of RNA interference systems, symmetrical mode of cell division, among others). These features are missing in other models such as the budding yeast, which since their divergence ~350 million years ago, *S. pombe* appears to have evolved less rapidly than *S. cerevisiae* retaining more characteristics of the ancient common ancestor between humans and fungi, making this biological model more similar to higher eukaryotic cells due to shared cytological and growth characteristics (Hoffman, et al., 2015).

Chapter 4. Growth patterns of *S. pombe* mediated by Gaf1 transcription factor

4.1. Introduction

The scientific field during the last 50 years has consolidated yeasts as valuable systems for the elucidation of eukaryotic biology (Egel, 2004; Fantes & Hoffman, 2016; Hoffman, et al., 2015). This has been achieved by producing significant insights into a variety of molecular and cellular processes including cancer biology, vesicular trafficking and cell cycle regulation among others (Lin & Austriaco, 2014). In particular, cell proliferation of the *S. pombe* represent a reliable model to decipher the influence of the extracellular environment over a myriad of cellular responses. Vegetative growth in this unicellular organism consists of an increase in biomass by distal elongation of each edge of the cell until it reaches a critical length at which point extension finishes to initiate mitosis (Ikai, et al., 2011; Petersen & Russell, 2016).

This process requires the integration of a variety of extrinsic signals that inform about the availability of essential elements and energy to either engage in anabolic programs that allow high levels of protein synthesis required to promote cell growth and division, or whether to exit cell cycle progression and sexually differentiate (Gonzalez & Rallis, 2017). Failure to sense the changing environment has negative implications in the overall cellular fitness, thus the signalling pathways conveying this status are highly conserved through evolution (Bar-Peled & Sabatini, 2014).

For the last two decades, the connection between nutritional conditions and the molecular machinery that control cellular and organismal growth has been attributed to the central signalling pathway TOR (Saxton & Sabatini, 2017). In *S. pombe*, this network is operated by two TOR complexes with distinct catalytic subunits, Tor2 in TORC1 and Tor1 in TORC2 (Atkin, et al., 2014; Hartmuth & Petersen, 2009), which bind to a specific set of proteins that differentiate them, playing antagonistic roles between them regarding mitosis (Ikai, et al., 2011) and longevity (Rallis, et al., 2013).

These complexes allow the metabolic plasticity predominantly through global regulatory systems that enable preferential utilisation of nitrogen and carbon sources that are easily assimilated. This is achieved by the (negative) transcriptional and post-transcriptional regulation of genes synthesising catabolic enzymes and permeases -which belong to a family of proteins that mediate cellular amino acid flux with different substrate specificity and subcellular localisation (Ljungdahl & Daignan-Fornier, 2012)-, which are required for the utilisation of alternative sources of both nitrogen and carbon, preventing their consumption in the presence of optimum sources (Wiame, et al., 1985). Such transcriptional/metabolic stages in yeasts are named nitrogen catabolite repression [NCR] (Sun, et al., 2016; Wiame, et al., 1985) and carbon catabolite repression [CCR] (Simpson-Lavy & Kupiec, 2019).

The uptake of poor nitrogen sources such as arginine (Hofman-Bang, 1999), branched-chain amino acids (Sun, et al., 2016), urea and proline is repressed in the presence of good sources such as asparagine, glutamine or ammonia (ter

Schure, et al., 2000). The latter triggers intracellular responses that activate TORC1 to promote anabolism -ribosome biogenesis, protein translation, transcription, etc.- (Ma, et al., 2013; Panchaud, et al., 2013) and inhibit catabolism -autophagy, amino acid uptake, etc.- (Kamada, et al., 2010). Nitrogen starvation response advance mitosis at a reduced cell size, resulting in small-sized rounded stationary cells accumulated at the G1 phase of the cell cycle (Weisman, 2010).

In the case of glucose, it is the preferred carbon source (Simpson-Lavy & Kupiec, 2019) and is detected at the plasma membrane (Sabina J, 2009). In *S. pombe*, its availability regulates the activity of TORC2 [but not nitrogen] (Ikai, et al., 2011), a complex that is involved in survival under stress conditions (osmotic, oxidative and temperature stress), initiation of sexual development during starvation, acquisition of stationary phase physiology (Cohen, et al., 2014; Kawai, et al., 2001; Weisman & Choder, 2001), amino acid uptake (Weisman, et al., 2005), DNA damage response, remodelling of chromatin structure for gene silencing and telomere stability (Schonbrun, et al., 2009), but is not essential for growth under normal conditions (Gonzalez & Rallis, 2017; Laor, et al., 2014; Martín, et al., 2017; Weisman, 2010). Carbon depletion also arrests mitosis but at the G2 phase of the cell cycle (Su, et al., 1996).

Considering that this nutrient-sensing network is orchestrated by the TOR kinases via phosphorylation status of different substrates, including the negative regulation of the nuclear localisation of several GATA transcription factors including Gaf1 (Georis, et al., 2011; Laor, et al., 2015), this chapter is focused on the study of different growth parameters of *S. pombe* controlled by TOR kinases

and Gaf1, aiming to understand their role in the response to nutritional status. Several environmental settings resembling normal and starvation conditions were tested with different growth media, applying pharmacological interventions and mutagenic analyses using haploid, heterothallic, prototrophic strains obtained from the *S. pombe* genome-wide deletion mutant library v5.0 from Bioneer and collaborators. The characterisation of the variations in growth and survival were performed by measuring relevant growth kinetic parameters such as growth rates, pharmacological toxicity/activity and chronological lifespans (CLS).

4.2. Growth assays

4.2.1. Spot tests for fitness assessment

4.2.1.1. Viability of *gaf1* Δ cells

The viability of *S. pombe* cells was explored in different conditions by testing the ability of wild type and *gaf1* Δ mutant cells to form colonies on solid rich media transferred from exponentially growing liquid cultures (figure 20). This is particularly informative to assess gene functions and their interaction with the environment by identifying subtle differences in growth rate and viability (Petersen & Russell, 2016).

These results showed that pharmacological interventions using the global inhibitor of TOR kinases torin1 (Atkin, et al., 2014) in wild type cells completely abrogated cellular growth (figure 20B) compared to caffeine + rapamycin treatment, where the inhibition of growth was not as drastic but increased in a

caffeine concentration-dependent manner (figures 20C, 20D, 20E). Previous reports described that the combination of the last two compounds reduced growth by differentially targeting various cellular processes controlled by TORC1 (Rallis, et al., 2013), eliciting similar responses to those observed after shifts to poor nitrogen sources without both the G1 cell-cycle arrest and the morphology of quiescent cell (Rallis, et al., 2013; Takahara & Maeda, 2012).

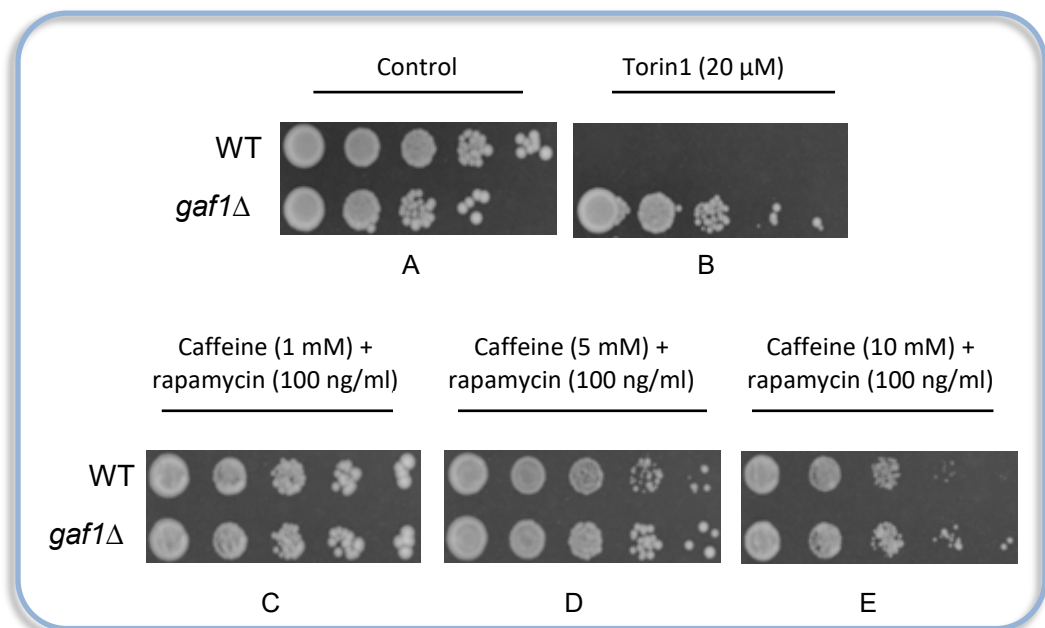


Figure 20: Tenfold serial dilutions of wild type and *gaf1* Δ cells spotted on rich media (YES) agar plates: **[A]** without treatment (control), **[B]** with torin1, and **[C]** rapamycin combined with a titration of caffeine as indicated. Cultures grown in identical physiological conditions. Cell colonies are shown after 3 days of incubation.

The results obtained in these experiments (figures 20C, 20D, 20E) confirmed that in contrast to *S. cerevisiae*, rapamycin does not completely inhibit cell growth in *S. pombe* wild type cells *in vivo* (Takahara & Maeda, 2012). It partially disrupts some physiological processes such as sexual development, amino acid uptake (Weisman, et al., 2005; Weisman & Choder, 2001), and reduce protein synthesis by dephosphorylation of the ribosomal proteins S6 [Rps6] (Nakashima, et al., 2010), which is not sufficient to cause growth defects but induce the onset of

mitosis producing a slight reduction in cell size at division resembling nitrogen starvation (Petersen & Nurse, 2007; Takahara & Maeda, 2012).

Caffeine as an ATP-competitor (Takahara & Maeda, 2012), inhibits in varying degrees the phosphatidylinositol 3-kinase-related kinase family (PIKK) to which TOR proteins belong (Sarkaria, et al., 1999). In *S. pombe*, treatment with this drug mainly targets TORC1 activity but it also affects Tor1 functions. It triggers the induction of stress response genes and the repression of ribosomal and other growth-related genes (Rallis, et al., 2013). Therefore, the combined effects of caffeine + rapamycin sensitise critical effector(s) indiscriminately that escape single-compound treatment, producing TORC1 inhibition which enhances the resulting phenotypes (Rallis, et al., 2013; Takahara & Maeda, 2012). The combination of caffeine + rapamycin treatment allows to obtain systematic insights into fundamental processes regulating cellular growth differentially controlled by either TORC1 or TORC2 when combined with mutagenic analyses.

In this sense, the two treatments (torin1 and caffeine + rapamycin) did not affect to the same extent the proliferation of wild type and *gaf1* Δ cells (figures 20B, 20E). The heightened impact of torin1 on wild type cells observed in the present study (figure 20B), could be produced by the complete inhibition of TORC1 signalling including the rapamycin-resistant elements not affected by caffeine + rapamycin (required for cap-dependent translation and suppression of autophagy), rather than the additive effect of both TORC1 and TORC2 inhibition, consistent with reports for mammalian cells (Thoreen, et al., 2009).

Alternatively, the inhibition of TORC2 produced by torin1 could increase cell sensitivity to environmental signals which combined with TORC1 inhibition may resemble severe starvation that ultimately obstructs cell cycle progression even at the logarithmic growing phase. This data is consistent with the mechanisms of action previously described for torin1 and caffeine + rapamycin, stating that they affect cell growth in different degrees, the latter mildly reducing cell growth without slowing cell division or generation times (Rallis, et al., 2013), whereas torin1 decreased both cell growth and division (Atkin, et al., 2014).

The growth rate of *gaf1* Δ strain in normal conditions was slower than the wild types cells (figure 20A), indicating that the deletion of this non-essential gene has an impact on cell fitness. The high concentration of torin1 used in these experiments was not cytotoxic for this mutant confirmed by their growth (figure 20B), showing resistance to the profound TOR signalling inhibition consistent with previously reported data (Lie, et al., 2018).

Considering that nitrogen starvation arrests cell cycle progression and induce the expression of NCR-sensitive genes to allow the utilisation of alternative sources (Gonzalez & Rallis, 2017; Sun, et al., 2016; Weisman & Choder, 2001), the resistance of *gaf1* Δ to torin1 is remarkably different to its sensitivity to several conditions including poor nitrogen sources such as proline (Laor, et al., 2015), and limited amino acids availability, not being affected by low-glucose in the medium (Kim, et al., 2012).

This suggests that Gaf1 is involved in several signalling systems that sense different nitrogen sources to reprogram patterns of gene expression accordingly. Additionally, the nucleo-translocation of this transcription factor (negatively regulated by TORC1) rapidly occurs in response to nitrogen stress (Laor, et al., 2015) and torin1 treatment (Rodríguez-López, et al., 2020), being insensitive to glucose depletion or rapamycin addition (Laor, et al., 2015), contrasting with its orthologue Gat1 from *S. cerevisiae* that its translocation to the nucleus is induced by rapamycin treatment (Georis, et al., 2011; Kulkarni, et al., 2006).

Therefore, the torin1-resistant phenotype of *gaf1*Δ cells unveils the existence of a complex genetic network (further analysed in chapter 6 through interactome) tightly controlled directly or indirectly by this transcription factor that enables cells to either continue proliferating with inactive TOR signalling in the absence of Gaf1, or completely interrupt cell cycle progression when is present in the cell and TOR activity is inhibited. This information is particularly relevant to understand the mechanisms that confer resistance to therapies for the treatment of cancer and other pathologies caused by dysregulations of the TOR pathway.

Overall, this data validated the use of torin1 as a strategy for studying TOR functions in *S. pombe* and provided additional information about the relevant role of Gaf1 as a critical regulator of probably redundant pathways that induce both transcriptional and physiological changes that together support growth under nitrogen stress conditions through TOR signalling.

4.2.1.2. Viability of relevant strains

From this rationale, the viability of additional *S. pombe* strains was evaluated using this experimental setting to explore the complex dynamic regulating amino acid biosynthesis, metabolism and sensing during TOR inhibition (figure 21). To this aim, growth was assessed on minimal solid media supplemented with both ammonium as a nitrogen source and a titration of the basic amino acid arginine to counteract and reverse the effects of torin1 and rapamycin treatments, due to its reported capability to induce cell growth via activation of the TOR signalling pathway (Sancak, et al., 2008; Sancak, et al., 2010; Yuan, et al., 2015; Wang, et al., 2018).

The results below were sectioned according to the strains used, they could be classified as: controls, amino acid biosynthesis and metabolism, and amino acid sensing and uptake.

4.2.1.2.1. Viability of control cells

Regarding the controls, the data showed that wild type cells grew slower in minimal solid media supplemented with ammonia (figure 21A) compared to rich media (figure 20A) in consistency with previous reports (Petersen & Russell, 2016). The growth of this strain in solid media was slightly reduced by the addition of rapamycin (figure 21M) and it was not induced by the different concentrations of arginine when treated individually (figures 21D, 21G, 21J). The treatments using rapamycin combined with different concentrations of arginine were able to marginally rescue growth of wild type cells (figures 21N, 21O, 21P) to a similar rate as the one observed in the (non-treated) control plate (figure 21A).

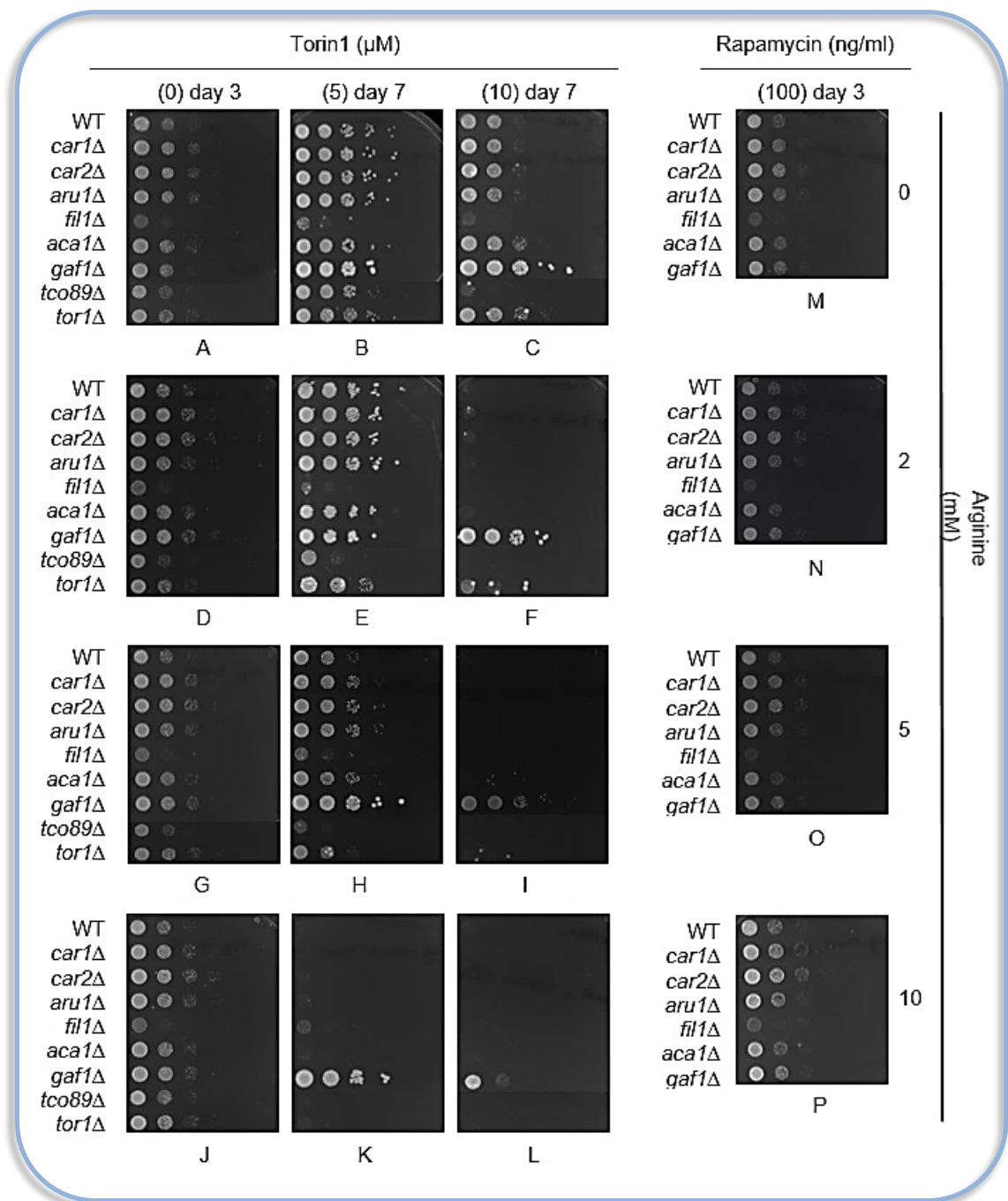


Figure 21: Tenfold serial dilutions of wild type, *car1* Δ , *car2* Δ , *aru1* Δ , *fil1* Δ , *aca1* Δ , *gaf1* Δ (in rapamycin), with additional *tco89* Δ and *tor1* Δ (in torin1) spotted on minimal media (EMM+N) agar plates with or without arginine at the indicated concentrations, grown for 3 and 7 days at 30 °C. **[A]** strains without treatment (control) at day 3, **[B]** strains treated with 5 μ M torin1 at day 7, **[C]** strains treated with 10 μ M torin1 at day 7, **[D]** strains treated with 2 mM arginine at day 3, **[E]** strains treated with 5 μ M torin1 and 2 mM arginine at day 7, **[F]** strains treated with 10 μ M torin1 and 2 mM arginine at day 7, **[G]** strains treated with 5 mM arginine at day 3, **[H]** strains treated with 5 μ M torin1 and 5 mM arginine at day 7, **[I]** strains treated with 10 μ M torin1 and 5 mM arginine at day 7, **[J]** strains treated with 10 mM arginine at day 3, **[K]** strains treated with 5 μ M torin1 and 10 mM arginine at day 7, **[L]** strains treated with 10 μ M torin1 and 10 mM arginine at day 7, **[M]** strains treated with 100 ng/ml rapamycin at day 3, **[N]** strains treated with 100 ng/ml rapamycin and 2 mM arginine at day 3, **[O]** strains treated with 100 ng/ml rapamycin and 5 mM arginine at day 3, **[P]** strains treated with 100 ng/ml rapamycin and 10 mM arginine at day 3.

It is of interest that the wild type cells experienced a drastic reduction in growth only by increasing the arginine concentration from 2 mM (figure 21E) to 5 mM (figure 21H) in the presence of equal amounts of torin1 at 5 μ M, indicating a cytotoxic effect triggered by the increase in arginine in the control cells.

Considering that torin1 at 20 μ M in rich solid media completely inhibited growth of wild type cells during the first 3 days of incubation (figure 20B), single treatments with lower concentrations of the drug were used in these experiments. The torin1 treatments (5 μ M and 10 μ M) delayed overall growth of all the strains without stopping cell proliferation (figures 21B, 21C), a phenotype that was enhanced in different degrees by the combinations of arginine and torin1 at different concentrations except for *gaf1* Δ (figures 21F, 21H, 21I, 21K) and with a lesser extent *tor1* Δ (figures 21C, 21E, 21F), which showed resistance to the treatments compared to the other strains, but were also sensitive at higher concentrations (figure 21L).

At low titrations of arginine (2 mM) + torin1 (5 μ M), growth resembled torin1 at 5 μ M individual treatment (figures 21B, 21E), whereas at higher concentrations (10 μ M), proliferation was severely compromised by completely arresting cell cycle progression in the majority of the strains (figures 21F, 21I, 21L). This effect that was not achieved with the highest concentration of torin1 at 10 μ M individually (figure 21C).

This is in partial agreement with previous studies indicating that increases in the concentrations of arginine combined with torin1 treatment elevated the pH of the

cultures and delayed growth (Hillson, 2018), however, the same study reported that at a lower-linear concentration of arginine, the combined treatment was able to rescue both the delays in generation times in wild type, *tco89* Δ and *tor1* Δ , but not in *gaf1* Δ cells, as well as the reduction in cell size (biomass) experienced by wild type and *gaf1* Δ strains (Hillson, 2018).

It is relevant to mention that the results from (Hillson, 2018) are based on optical density (OD) measurements performed in liquid cultures of rich media with cells at the lag phase of growth. In contrast, the results obtained in the present study showed that arginine supplementation did not bypass the delay in growth produced by *torin1* in solid minimal media, which could be attributed to the different experimental conditions used in each case, including the distinct technical platform of solid minimal media supplemented with ammonia [preferred for physiological studies] (Bicho, et al., 2010), the measurement of growth as a colony effect in agar plates instead of ODs from liquid cultures that could be more sensitive to small changes in cell numbers, and the varied stages in growth of the cells in the colonies rather than the liquid culture at the lag phase.

The *gaf1* Δ mutant was slow grower compared to the wild type in rich media (figure 20A), whereas in minimal media and in rapamycin treatment they both grew at similar rates (figures 21A, 21M). This suggests a potential role of Gaf1 in temporal development controlled by nutrient availability and uptake, different from nitrogen abundance which was present in both types of media.

4.2.1.2.2. Viability of mutants disrupted in amino acid biosynthesis and metabolism

In terms of amino acid biosynthesis and metabolism, yeast cells are able to synthesise all 20 amino acids including arginine (Saxton & Sabatini, 2017). This amino acid is engaged in several metabolic pathways within the cell, being extensively catabolised *in vivo* in the fission yeast (Borek, et al., 2015). It has considerable physiological significance since it is one of the most versatile amino acids that is used as a precursor for the synthesis of proteins, urea, nitric oxide, polyamines, agmatine and creatine (Morris, 2006; Song, et al., 2008), involving high levels of catabolic conversion to other amino acids mainly proline but also significantly to lysine, glutamine and glutamate (Borek, et al., 2015).

In contrast, mammalian cells are able to reduce conversion when exogenous arginine concentrations are low (Bicho, et al., 2010). Its homeostasis depends on environmental intake, protein turnover, biosynthesis and catabolism, being dispensable for healthy adults but essential for young growing animals due to the stimulation of hormone secretion such as insulin, growth hormone, glucagon and prolactin (Wu & Morris, 1998). Given this importance of arginine in several metabolic pathways, the effects of the titration of exogenous arginine supplementation were further explored to understand its outcome on cellular growth during pharmacological inhibition of TOR signalling.

The growth patterns of cells with reduced arginine conversion were studied by using mutants containing disruptions in enzymes involved in arginine catabolism and biosynthesis in the fission yeast. They included the strains *car1*Δ and *aru1*Δ

impaired in the two arginase genes that hydrolyse arginine to ornithine and urea, and *car2* Δ depleted of the ornithine transaminase gene (Lock, et al., 2019). Previous reports indicated that nearly all arginine conversion is avoided in these strains, with only low levels of proline detected as its outcome (<10% of the proline pool), with Aru1 being the major arginase in fission yeast (Bicho, et al., 2010). An additional mutant, *aca1* Δ that lacks the L-azetidine-2-carboxylic acid acetyltransferase gene was included due to its role in arginine biosynthesis (Lock, et al., 2019).

These four single mutants were able to grow slightly faster than the wild type in minimal media (figure 21A) but did not show major differences with either rapamycin treatment independently (figure 21M), the titration of arginine on their own (figures 21D, 21G, 21J), or the combination of these two compounds, growing in similar rates to the wild type (figures 21N, 21O, 21P). Torin1 treatments delayed their growth (figures 21B, 21C) and none of the combinations with arginine were able to rescue this feature, on the contrary it only sensitised them (figures 21F, 21H, 21I, 21K, 21L). However, comparing the sensitivity at a constant concentration of torin1 at 5 μ M with an increase of arginine from 2 mM (figure 21E) to 5 mM (figure 21H) the three mutants *car1* Δ , *aru1* Δ and *car2* Δ with reduced arginine conversion showed more resistance than the wild type and *aca1* Δ .

This suggests that increased production of specific derivatives generated during arginine metabolism such as nitric oxide, urea, or ornithine which leads to putrescine among others (Borek, et al., 2015) -suggested to be responsible for

the ammonia-induced cell death in *S. cerevisiae* (Santos, et al., 2012)-, could be the cause of the sensitivity observed in the wild type, *aca1* Δ and the rest of the mutants apart from the resistance observed in *gaf1* Δ and slightly in *tor1* Δ . Another possibility is that intracellular accumulation of (unmetabolized) arginine in *car1* Δ , *aru1* Δ and *car2* Δ might be conferring an advantage for survival in the presence of the drug.

In line with this second hypothesis, previous studies indicated that addition of arginine to the medium, overexpression of genes for arginine biosynthesis, and downregulation of arginases conferred tolerance to general stress conditions in several unicellular organisms including the budding yeast (Cheng, et al., 2016). In particular, intracellular accumulation of arginine inhibited heat-induced aggregation of unfolded protein intermediates, protected against cryogenic and ethanol stress (Cheng, et al., 2016), osmotic stress (Xu, et al., 2011) and hydrogen peroxide-induced oxidative stress (Bearson, et al., 2009).

In *S. cerevisiae*, more than 90% of the free arginine in the cell is reported to be located in the vacuoles to maintain intracellular acidic pH (Abdel-Sater, et al., 2004; Cooper, et al., 2010). In this model organism, medium supplemented with arginine exerts the upregulation of *CAR1* and *CAR2* genes, expressing arginase and ornithine transaminase respectively, controlling the arginine catabolic pathway (Hofman-Bang, 1999), while represses genes encoding enzymes involved in arginine anabolism (*ARG1*, *ARG3*, *ARG4*, and *ARG8*), with no other genes displaying arginine-dependent transcriptional variation in this context (Godard, et al., 2007). This is consistent with the mechanisms of mutual exclusion

between anabolism and catabolism described for this amino acid (Dubois, et al., 1978). Similarly, the arginase gene *CAR1* is induced during nitrogen depletion and under the nitrogen sources ornithine, leucine, isoleucine, threonine, methionine, tyrosine, and tryptophan, not being involved in their catabolism (Godard, et al., 2007).

4.2.1.2.3. Viability of mutants disrupted in amino acid sensing and uptake

The present study followed the conventional concentration of ammonium chloride (96 mM) as the nitrogen source in minimal growth medium for *S. pombe*, which inhibits arginine uptake (Bicho, et al., 2010). Previous reports documented the existence of at least two systems for arginine uptake in fission yeast, system I is generic for basic amino acids and operates whether the nitrogen source is ammonium or glutamate (Fantes & Creanor, 1984). This appears to be competitively inhibited by the uptake of basic amino acids such as lysine or ornithine, but not significantly by tryptophan.

The system II is specific for arginine uptake and is strongly inhibited or repressed by ammonium but not by glutamate (Fantes & Creanor, 1984). This has been attributed to the repression of ammonia-sensitive permeases that reduce amino acid uptake (Weisman, et al., 2005), and could be related to the reduced amino acid import described during hyperactivation of Tor2 (Weisman, 2010) and its downregulation, which in both scenarios conferred canavanine resistance -a toxic analogue of arginine- (Murai, et al., 2009) suggesting reduced arginine uptake, opposite to the sensitivity reported in *tor1Δ* (Weisman, et al., 2007).

This inhibition of the second system for arginine uptake in the presence of ammonium is consistent with the results obtained in this study, where even the highest concentration of arginine supplementation on its own (10 mM) did not show major effects in growth (enhancement or reduction) in any of the strains apart from advanced proliferation in *gaf1* Δ (figures 21A, 21D, 21G, 21J) and in a lesser extent in *tco89* Δ (figures 21A, 21J), also reflecting that the pH was not detrimental in this environment. Previous publications indicated that in wild type cells arginine uptake reach saturation at a concentration of 100 μ M in ammonium (Fantes & Creanor, 1984).

Conversely, lower amounts of ammonium in minimal medium (6–9 mM) promote higher arginine absorption and robust growth in wild type cells (Bicho, et al., 2010; Borek, et al., 2015) and auxotrophic strains supplemented with amino acids, suggesting that the conventional amount of ammonium chloride used in the original formulation of minimal media could be considerable higher than necessary (Bicho, et al., 2010). Furthermore, the precise molecular mechanisms triggering the hyperammonemia-induced cytotoxicity in yeast are not completely understood (Santos, et al., 2012).

Thus, the effect of torin1 mimicking nitrogen-deprived conditions (Atkin, et al., 2014), could be allowing uptake and accumulation of arginine leading to the slight resistance observed in this study in the mutants depleted of genes involved in arginine metabolism (figures 21E, 21H). This resembles the phenotype previously described in arginase-defective strains of *S. cerevisiae* that accumulated higher levels of arginine and showed increased physiological

activity after cryogenic processes (Shima, et al., 2003) and resistance to ethanol stress (Cheng, et al., 2016).

Another component of this section, is the mutant *fil1* Δ which lacks a GATA transcription factor that is a master regulator of genes for amino acid biosynthesis in response to amino acid starvation (Duncan, et al., 2018). This strain was slow grower with and without arginine, rapamycin or torin1 either in separate treatments or with the aforementioned combinations (figures 21A-P).

Those results are consistent with previous reports documenting poor growth of this mutant in minimal media with ammonia or proline, but with similar rate to the wild type in either rich media or minimal media supplemented with different amino acids (Duncan, et al., 2018; Laor, et al., 2015), suggesting a considerate burden on this transcription factor for both the production of *de novo* amino acids required for cell viability, and a possible involvement in the transcriptional regulation of mechanism(s) for amino acid trafficking, where the presence ammonia as described before, might be inhibiting the recognition or absorption of the additional arginine which is not sufficient to promote growth when *de novo* amino acids are not being synthesised. This is not the case in rich media that supports growth of this mutant as amino acids could be obtained from the environment (Duncan, et al., 2018; Laor, et al., 2015).

To study amino acid sensing and uptake, mutants of the TOR pathway were selected because of its relevance as a crucial regulator of nutrient status (Gonzalez & Rallis, 2017). The role of TORC1 signalling in these scenarios was

assessed using the strain *tco89Δ*, depleted of a non-essential core component of this complex. The function of TORC2 was assessed through the mutant *tor1Δ*, which lacks the gene encoding the catalytic subunit of this complex (Ikai, et al., 2011).

The growth of *tco89Δ* was slow relative to the wild type, whereas *tor1Δ* showed similar rate to the latter (figure 21A), confirming their roles in vegetative growth where TORC1 is essential for growth but not TORC2 (Ikai, et al., 2011). Supplementation with arginine 10 mM slightly accelerated growth only in *tco89Δ* (figures 21G, 21J) with the rest of the concentrations not producing major effects among these two strains (figures 21D, 21G). This could be the outcome of having a functional TORC2 that positively regulates amino acid uptake (Gonzalez & Rallis, 2017).

The effects of rapamycin on *tco89Δ* cells have been previously studied, they showed that the biochemical profile of TORC1 (carrying the *tco89* deletion) is resistant to the drug (Nakashima, et al., 2012). Conversely to wild type cells, treatment with this compound in this mutant does not inhibit the phosphorylation of downstream targets of TORC1 such as the AGC kinase Psk1 (high homology with the human S6K) vastly phosphorylated in rich nitrogen conditions, and its direct substrate Rps6, a component of the 40S ribosomal subunit involved in regulation of protein translation, which is used as readout of TORC1 activity (Nakashima, et al., 2010; Nakashima, et al., 2012). A different effect occurs with the disruption of *pop3* gene, controlling another non-essential core component of

TORC1 that is involved in the interaction between Tor2 and the rapamycin–FKBP12 complex (fission yeast homolog Fkh1).

The mutants lacking this gene show sensitivity to rapamycin by inhibiting phosphorylation of Psk1 and subsequently Rps6 (Nakashima, et al., 2012). Similarly, the loss of Tco89 in the budding yeast rendered cells sensitive to rapamycin, being required for the TORC1-mediated phosphorylation of Sch9 [homolog of S6K] (Binda, et al., 2009).

Regarding torin1 treatments in *tco89Δ*, the data obtained in the present study revealed that higher concentrations of the drug had stronger effects delaying growth (figures 21B, 21C), even more in combination with arginine (figures 21E, 21F, 21H, 21I, 21K, 21L), resembling the strong inhibition of growth reported in this mutant when treated with caffeine and rapamycin (Rallis, et al., 2013).

The sensitivity of *tor1Δ* cells to rapamycin was also previously described (Kawai, et al., 2001; Weisman, et al., 2007). The disruption of this gene reduces the expression of amino acid permeases, the same effect is produced by the drug in this mutant, restricting amino acid uptake (leucine particularly) as the result of the enhanced downregulation of general amino acid permeases (*isp5*, *per1* and *put4*), a phenotype also observed in rapamycin-treated wild type cells (Weisman, et al., 2005), and in mutants depleted of *gaf1* (Laor, et al., 2015), *tsc1* and *tsc2* (Weisman, et al., 2007). The last two genes encode hamartin and tuberin respectively that physically interact with each other and are the orthologs of the human *TSC1–TSC2* genes -absent in the budding yeast- (Weisman, et al., 2007).

Mutations in those two genes cause the human syndrome tuberous sclerosis complex, characterised by benign tumours (hamartomas) and severe neurological defects among other symptoms (Matsumoto, et al., 2002).

Tsc2 contain a GTPase-activating protein (GAP) domain which in complex with Tsc1 catalyse the GTP hydrolysis of Rhb1 (GTPase Rheb in humans) into its GDP-bound inactive form (Mach, et al., 2000; van Slegtenhorst, et al., 2004), leading to the inhibition of TORC1 (Chia, et al., 2017) via direct interaction and negative regulation of Tor2 (Urano, et al., 2005; Urano, et al., 2007). Ultimately, this cascade of events induces amino acid uptake by lowering TORC1 signalling (Matsumoto, et al., 2002; van Slegtenhorst, et al., 2004). In fission yeast, loss of Tsc function leads to canavanine resistance and decreased arginine uptake (van Slegtenhorst, et al., 2004), opposite to *tor1Δ* mutants that present defects in the uptake of leucine, histidine, and uracil but are sensitive to canavanine and thialysine -toxic analogue of lysine- (Weisman, et al., 2005).

Therefore, Tor1 and Tsc1/2 apart from being required for sexual development (Weisman, et al., 2007; Weisman & Choder, 2001), they positively regulate amino acid uptake through separate mechanisms (Weisman, et al., 2007) via induction of transcription, translation, and post-translational processing including membrane integration and localisation of amino acid permeases upon nitrogen starvation (Matsumoto, et al., 2002; van Slegtenhorst, et al., 2004). They have been extensively used as models to explore amino acid sensing and transportation, especially to elucidate mechanism(s) that confer resistance to rapamycin during growth in *S. pombe* (Weisman, 2010).

Rapamycin in ammonia-containing minimal medium differentially affects amino acid trafficking, conferring canavanine resistance in wild type cells (Weisman, et al., 2007), and leading to growth inhibition of auxotrophic strains for leucine (rely on single amino acid import for survival), due to the disruption of TORC1 signalling. This compound reduces growth of auxotrophs for uracil and histidine, but not affecting auxotrophs for adenine (Weisman, et al., 2005), indicating the existence of different mechanisms for signalling amino acid levels to TORC1 (Saxton & Sabatini, 2017).

Interestingly, the sensitivity to rapamycin of leucine auxotrophs only occurs when they grow in minimal media containing ammonia as the nitrogen source, as mentioned above, this condition diminishes the capacity of several mechanisms for amino acid uptake as the result of reduced expression of ammonia-sensitive permeases, a phenotype that is also enhanced by rapamycin (Weisman, et al., 2005).

Leucine auxotrophs are resistant to rapamycin in rich media and in minimal media with either low concentrations of ammonia or non-repressing poor nitrogen sources such as proline, which triggers the induction of amino acid permeases (Matsumoto, et al., 2002; van Slegtenhorst, et al., 2004; Weisman, et al., 2005). The shift from rich nitrogen sources in the medium (ammonia) to poor ones (proline) also suppresses the amino acid uptake defect described in rapamycin-treated wild type cells, auxotrophic strains of *tor1Δ* (Weisman, et al., 2005), *tsc1Δ* and *tsc2Δ* (Weisman, et al., 2007).

In contrast, prototrophic *tsc1Δ* and *tsc2Δ* mutants are sensitive to rapamycin on proline via inhibition of TORC1 (and not TORC2), but not in ammonia possibly by the inability to metabolise proline, rather than defects in amino acids uptake (Laor, et al., 2014; Weisman, et al., 2007). Also, the sensitivity to rapamycin reported in prototrophic *tor1Δ* occurred in rich (Weisman, et al., 2005) and minimal media with proline as the nitrogen source (Weisman, et al., 2007). This complex regulation of amino acid uptake under rapamycin treatment could bring insights to understand the resistance to torin1 observed in the present study, particularly in *gaf1Δ* (figures 21C, 21F, 21H, 21I, 21K, 21L) and slightly in *tor1Δ* mutants (figures 21C, 21E, 21F). Among all the strains evaluated, these two mutants share common features in their disrupted ability to import amino acids (Laor, et al., 2014; Ma, et al., 2015).

4.2.1.2.4. Involvement of amino acid uptake and metabolism in *torin1* resistance

In the case of *gaf1Δ*, the downregulation of *isp7*, a putative 2-oxoglutarate-Fe(II)-dependent oxygenase gene which product controls amino acid uptake through either positive or negative transcriptional regulation of half of the 30 (general and specific) amino acid permeases predicted in the fission yeast genome (Laor, et al., 2015). This gene operates in a similar manner to TORC1 and opposite to TORC2 (Laor, et al., 2014; Laor, et al., 2015; Lie, et al., 2018; Weisman, et al., 2007), including the induction of the main transporter for arginine Cat1 (Aspuria & Tamanoi, 2008).

Among the four non-essential GATA transcription factors reported in *S. pombe* [Gaf1, Fil1, Gaf2/Fep1, Ams2] (Lock, et al., 2019) Gaf1 is the sole responsible for the transcription of *isp7* (Laor, et al., 2015), it is also essential for growth in proline as the nitrogen source in an *Isp7*-independent fashion (Laor, et al., 2014), exhibiting growth defects when amino acids are limited (Kim, et al., 2012). Interestingly, negative/lethal genetic interactions were reported during growth in proline in double mutants carrying a combination of either *isp7* Δ (Laor, et al., 2014), *tor1* Δ (Weisman, et al., 2007), disruptions in the components of TORC2, or Gad8 (downstream target of TORC2), in the background of *tsc1* Δ or *tsc2* Δ (Laor, et al., 2014; Weisman, et al., 2007), indicating that they act independently to regulate growth in the presence of poor nitrogen sources, and suggesting that Gaf1 directly or indirectly operates in different redundant pathways that together sustain growth under nitrogen stress conditions. This topic is further explored at the transcriptional level in chapter 5.

Moreover, resistance to canavanine was described in the strains *isp7* Δ (Laor, et al., 2014), *tsc1* Δ , *tsc2* Δ (van Slegtenhorst, et al., 2004), with synthetic lethality as an additive effect in the double mutants *isp7* Δ *tsc2* Δ when grown on arginine as the sole nitrogen source (Laor, et al., 2014), indicating that they regulate arginine uptake independently.

In the present study, arginine supplementation slightly increased growth of the *gaf1* Δ mutant (figures 21A, 21J). This is consistent with previous findings showing basal levels of *cat1* transcripts in the absence of Gaf1 (Ma, et al., 2015), which unveils the presence of alternative mechanisms for its transcription apart from

Isp7, and implying that arginine uptake occurs in *gaf1Δ* cells. Hence, it could stimulate their growth through the activation of TORC1 signalling (Yuan, et al., 2015). Conversely, *gaf1Δ* mutants did not show differences in growth under rapamycin treatment alone or in combination with the arginine titration (figures 21M, 21N, 21O, 21P), demonstrating that the compound either reduces arginine uptake or inhibits the activation of TORC1 by this amino acid in *gaf1Δ*.

Therefore, the reduced amino acid uptake of *tor1Δ* (Kawai, et al., 2001) and *gaf1Δ* cells (Ma, et al., 2015), as a result of the downregulation of the nitrogen starvation-induced permease genes *isp5*, *per1* and *put4* (Ma, et al., 2015; Weisman, et al., 2005), which leads to decreased amino acid uptake (Weisman, et al., 2007), could be contributing to the mild resistance to torin1 treatment alone (figure 21C) and in combination with arginine (figure 21F).

Rapamycin reduces the expression of *isp5* (Ma, et al., 2013) in ammonia or proline media (Weisman, et al., 2005), only producing significant transcriptional changes in poor nitrogen sources (Rallis, et al., 2013). This drug does not resemble an environment of poor- or high-quality nitrogen sources (Weisman, et al., 2005). In contrast to rapamycin treatment, the transcriptional activity of *isp5* is induced during nitrogen depletion and by mutagenic inhibition of Tor2 (Ma, et al., 2015), similar to the effect of torin1 in wild type cells, but different to the *tor2*-temperature sensitive mutants, where torin1 downregulates *isp5*, revealing that this inhibitory effect depends on Tor1 (Ma, et al., 2013).

This model is supported by the downregulation of *cat1* and canavanine resistance reported in *tor2*-temperature sensitive mutants (Ma, et al., 2015), which in combination with *isp7Δ* as double mutants almost completely abrogated arginine uptake (Laor, et al., 2014). This could be the outcome of torin1 treatment in *tor1Δ* and *gaf1Δ* cells, possibly signalling conditions equivalent to nutrient/nitrogen depletion that lead to reduced arginine import, as reflected by the shrinking phenotype reported during treatment in wild type cells (Atkin, et al., 2014).

This regulation of transmembrane transporters reveals that the TOR-dependent transcriptional regulation of amino acid permeases is differentially affected by torin1 and rapamycin. In this respect, contrasting literature indicate that these two drugs promote canavanine resistance in wild type cells in *S. Pombe* (Ma, et al., 2013), while others argue that rapamycin and other TOR inhibitors such as aminoimidazole carboxamide riboside (AICAR) increase arginine influx in human endothelial cells (Visigalli, et al., 2007).

Moreover, comparing the phenotypes of the two mutants *tor1Δ* and *tco89Δ*, the higher sensitivity of TORC1-disrupted cells (*tco89Δ*) to those treatments could be the result of Tor1 inhibition. Since Tor1 lies downstream of Isp7 (Laor, et al., 2014), cells lacking this kinase show normal levels of *cat1* transcripts as a single mutant (Ma, et al., 2015) and in the background of *isp7Δ* (Laor, et al., 2014).

This induction of *cat1* in *tor1Δ* (Laor, et al., 2014) and its normal levels in *gaf1Δ* mutants (Ma, et al., 2015) that allow arginine uptake, could be affected by torin1 treatment through the inhibition of Tor2-dependent activities that abolish the

negative feedback loop and interdependent regulation of amino acid uptake reported between the two TOR complexes (Ikai, et al., 2011; Weisman, et al., 2007), resulting in either downregulation of *cat1*, aberrant subcellular localisation of its product and/or protein degradation that overall reduces arginine uptake via disruption of the system II for arginine uptake (Aspuria & Tamanoi, 2008) in both mutants, allowing their resistance to the combination of arginine + torin1 that sensitised the rest of the strains tested in the present study (figures 21M, 21N, 21O, 21P).

This indicates that both the resistance and sensitivity is determined by the nutritional context. Consistently, previous reports indicated that mutants of the gene encoding Ppk32 (a SCYL family pseudo-kinase), were resistant to torin1 only as auxotrophic for leucine grown on solid rich media but not on minimal media, with no resistance of prototrophic *ppk32Δ* grown on rich media (Kowalczyk & Petersen, 2016).

This potential interference in arginine uptake in the two mutants *tor1Δ* and *gaf1Δ*, is possibly extended to an additional permease that is localised to the Golgi apparatus under rich nitrogen conditions but translocated to the plasma membrane following a shift to poor nitrogen sources (Nakase, et al., 2013), it is named Aat1 -homolog of the general amino acid permease Gap1 from *S. Cerevisiae*- (Nakase, et al., 2013), which is responsible for arginine import as part of system II in fission yeast (Aspuria & Tamanoi, 2008), and is a direct/specific transcriptional target of activated Gaf1 (Rodríguez-López, et al., 2020).

Such interruption could affect the traffic between the Golgi apparatus and endoplasmic reticulum in the sensitive strains, which is proven to compromise viability in the fission yeast (Kowalczyk & Petersen, 2016). Both permeases Cat1 and Aat1 are reported to be enriched towards the growing ends of fission yeast during vegetative growth (Aspuria & Tamanoi, 2008; Matsumoto, et al., 2002), with Tsc/Rheb signalling altering their intracellular distribution (Aspuria & Tamanoi, 2008). This data supports the idea that Tor1 and Gaf1 functions might be interconnected in *S. pombe*, proving their relevant role in the regulation of amino acid sensing and uptake to coordinate growth in this organism.

The negative correlation between increasing the concentration of arginine (combined with torin1) and survival, suggests that the sensitive strains present normal levels of arginine uptake. Recent concerns raised against supplementation with this amino acid are mainly focused at the cytotoxicity of increased nitric oxide production (Luiking, et al., 2005).

Arginine is the only substrate for the synthesis of this gaseous radical which in low concentration operates as a signalling molecule controlling numerous physiological processes, but at higher concentrations is toxic to mammalian cells and unicellular organisms including the fission yeast (Kig & Temizkan, 2009; Lewinska, et al., 2011). Even though *S. pombe* lacks orthologues of the mammalian nitric oxide synthases in its genome, there is evidence of nitric oxide synthase-like enzymatic activity in its physiology (Nishimura, et al., 2013).

Another factor that could be contributing to the enhanced sensitivity described in the present study is hyperammonemia, which is involved in different human disorders and is toxic for mammalian and yeast cells (Hofman-Bang, 1999). In *S. cerevisiae*, is especially harmful in non-arrested cells in the context of amino acids limitation. This is caused by the overactivation of the growth-inducer pathways TOR and protein kinase A (PKA), and the inhibition of the protein kinase Sch9 also involved in growth control (Santos, et al., 2012).

Additionally, considering that high pH levels reduce leucine uptake by lowering the primary electrochemical gradient across the membrane (Karagiannis, et al., 1999), and that arginine transport into the vacuole is regulated by vacuolar ATPase to maintain acidic pH (Abdel-Sater, et al., 2004; Cooper, et al., 2010), it will be relevant to examine whether torin1 treatment affects amino acid transport by mechanisms involving regulation of membrane potential and transcription of genes involved in vacuole organisation.

Overall, the results obtained in these experiments supports the idea that the slight resistance to arginine + torin1 treatments observed in the mutants *car1* Δ , *aru1* Δ and *car2* Δ carrying disruptions in enzymes involved in arginine catabolism (Lock, et al., 2019), could be attributed to the absence of excessive arginine by-products that might be present in the sensitive strains. Nevertheless, even though this is a novel hypothesis, it is highly speculative at present and awaits further studies to ascertain this possibility.

Since some amino acid permeases have their own substrate specificity and subcellular localisation (Ma, et al., 2015), this analysis brings insights into potential patterns of amino acid import and metabolism to control cell growth during nutritional limitation, particularly induced by pharmacological interventions of the TOR pathway.

The results from this section demonstrate for the first time that arginine supplementation in minimal media combined with torin1 treatment in the presence of ammonium, enhanced the inhibition in cell growth, suggesting that this drug instead of reducing amino acid uptake, as is the case of rapamycin (Weisman, et al., 2005), might be increasing it leading to cytotoxic effects when combined with arginine.

Future studies will clarify the effects of ammonium on arginine uptake during torin1 treatment and ammonium/arginine-induced cell death assessing canavanine resistance, transcription/localisation of permeases, and their interplay with downstream effectors that regulate amino acid transport in the fission yeast.

4.2.2. Toxicity tests for torin1 treatments

Beyond the original use of torin1 as an inhibitor of cell cycle progression (Atkin, et al., 2014), the present study also explores several additional downstream applications derived from its capability to inactivate both TOR complexes (Thoreen, et al., 2009), especially when combined with mutagenic analyses, also called chemical genetics (Doi, et al., 2015).

The use of this approach allows to target independently TOR complex 1 from 2. To achieve this, a consensus was established for the optimum concentration(s) of the compound that could trigger physiological responses without inducing cell death in the fission yeast. The majority of the literature using torin1 treatments in this model organism includes a standard range from 0.2 μ M (Ma, et al., 2013) to 25 μ M (Atkin, et al., 2014; Chica, et al., 2016; Martín, et al., 2017; Oya, et al., 2019), with some studies reporting the use of 50 μ M (Madrid, et al., 2016).

In order to determine the minimum and maximum concentrations of torin1 to be used in the subsequent experiments -chronological lifespan assays, transcriptome, interactome- without completely inhibiting cell growth, the proliferation of wild type cells and the mutants *gaf1* Δ was examined in liquid cultures of rich (YES) and minimal (EMM+N) media supplemented with nitrogen. This was complemented with the strains *tor1* Δ and *tco89* Δ in minimal media with a titration of torin1 applied at the vegetative growing phase (figure 22).

Altogether, the results obtained from these growth fitness experiments showed a strongest inhibition of growth during the first 24 hours of incubation caused by torin1 on wild type cells in solid media -either in rich (figure 20A) or minimal (figures 21B, 21C)- compared to liquid cultures (figures 22A, 22C), reflecting the differences in timelines (days in solid agar against hours in liquid cultures) and physiological conditions in terms of cell densities in the two types of platforms.

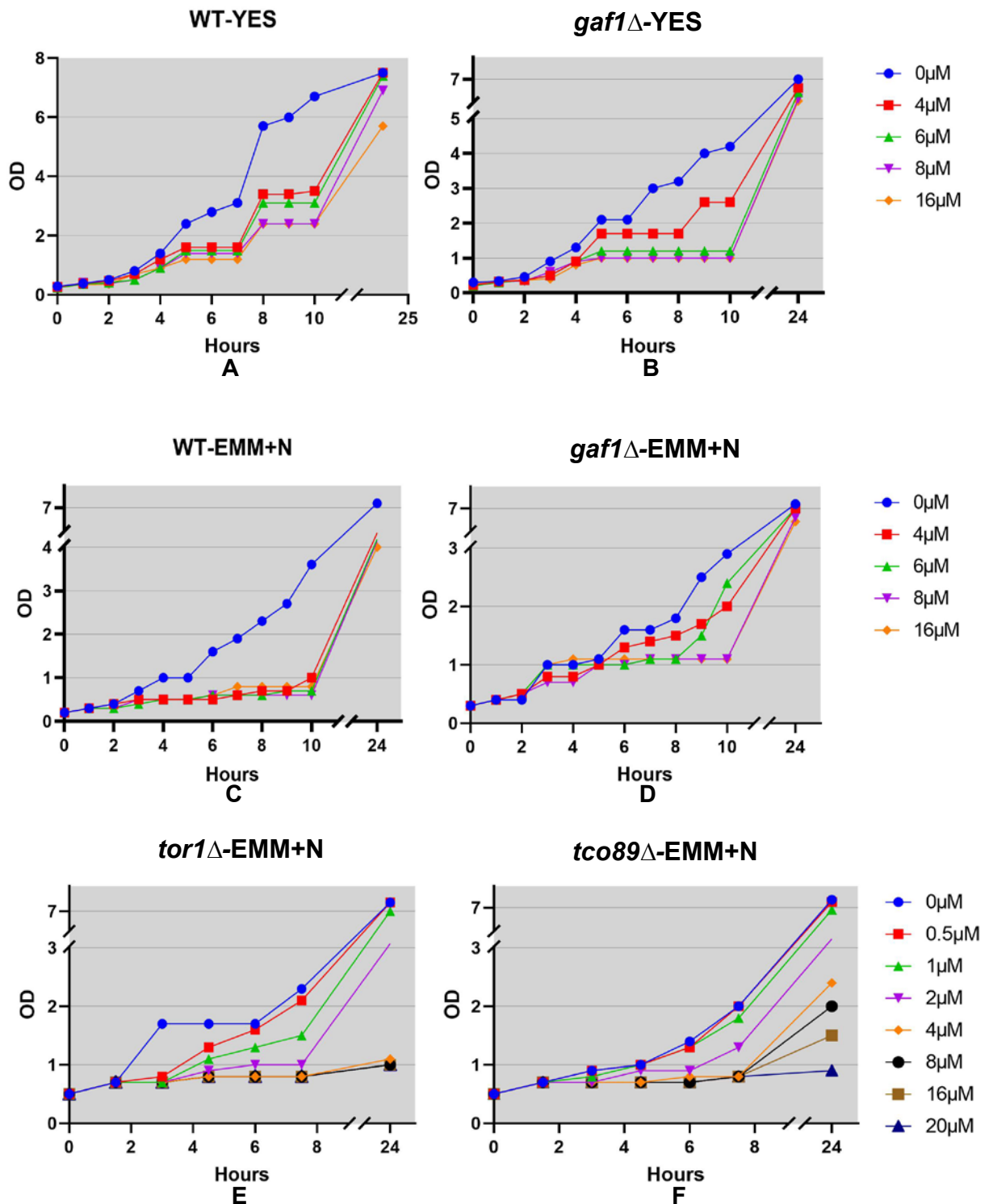


Figure 22: Proliferation of cells in liquid cultures with or without (control) torin1 in rich and minimal media at different concentrations as indicated. **[A]** wild type cells in rich media, **[B]** *gaf1*Δ cells in rich media, **[C]** wild type cells in minimal media supplemented with nitrogen, **[D]** *gaf1*Δ cells in minimal media supplemented with nitrogen, **[E]** *tor1*Δ cells in minimal media supplemented with nitrogen, **[F]** *tco89*Δ cells in minimal media supplemented with nitrogen.

The results also revealed that the liquid cultures of wild type and *gaf1* Δ cells grew slower in minimal media (figures 22C, 22D) compared to rich media (figures 22A, 22B), consistent with previous reports in fission yeast due to the effect of caloric restriction (Rallis, et al., 2013). The literature indicates that torin1 at 0.2 μ M induce transcriptional activity that resembles TOR inhibition by nitrogen depletion in *S. pombe* (Ma, et al., 2013).

The wild type cells at torin1 concentrations above 4 μ M showed strongest growth inhibition in minimal liquid media (figure 22C) than in rich conditions (figure 22A), most probably because of the diversity of nutrients present in rich media that could be recognised by alternative mechanisms, which may reduce the pharmacological inhibition of TOR signalling or parallelly induce its activation. Similarly, *gaf1* Δ mutants treated with torin1 at 4 μ M were able to proliferate faster in rich media (figure 22B), compared to minimal (figure 22D), suggesting that cells lacking this transcription factor are able to sense the presence of nutrients in the extracellular environment.

Those observations together with previous reports supporting the use of minimal media as the preferred option for physiological studies (Bicho, et al., 2010), were the basis for the selection of this media in the subsequent experiments. In this context, torin1 concentrations from 4 μ M to 20 μ M arrested proliferation for ~10 hours in wild type, *tor1* Δ and *tco89* Δ strains (figures 22C, 22E, 22F).

The mutant *tco89* Δ was slow grower compared to the rest of the strains (figure 22F) consistent with the disruption of TORC1. This mutant was able to resume

growth at 2 μM after 6 hours of incubation (figure 22F), in contrast to *tor1* Δ and wild type cells, indicating that in *tco89* Δ the pharmacological inhibition of TORC2 might be de-repressing some TORC1 activities that allow growth. Only the *gaf1* Δ mutant slightly grew at 4 μM and 6 μM after 8 hours of incubation (figure 22B), confirming its resistance to torin1 and involvement in the TOR signalling pathway as described before (Rallis, et al., 2014), where it has the potential to (directly or indirectly) cease proliferation when is present in the cell.

The maximal cell densities of the strains were differentially affected by the treatments and type of media. The stationary phase of wild type cells in minimal media was not achieved after 24 hours of incubation at all concentrations of torin1 (figure 22C). During this period in rich media, the maximal densities were reached at concentrations $\leq 8 \mu\text{M}$, which did not occur at $\geq 16 \mu\text{M}$ (figure 22A), resembling the enhanced toxicity of the drug when combined with arginine supplementation as observed in the results described in the previous section of experiments in solid media that overall increased sensitivity.

The mutant *gaf1* Δ was resistant to the treatments at all the concentrations in both types of media after 24 hours of incubation (figures 22B, 22D), in contrast to the wild type cells that were not able to growth in this period when treated at 16 μM in rich media or with concentrations $> 4 \mu\text{M}$ in minimal media. This is similar to the results observed when *gaf1* Δ was treated on solid media (figures 20B, 21C) in which this strain was able to growth.

The mutants *tco89* Δ and *tor1* Δ were not able to reach stationary phase at concentrations $\geq 1\mu\text{M}$ after 24 hours of incubation in minimal media (figures 22E, 22F), indicating that the pharmacological inhibition of TORC1 and TORC2 respectively, requires more than 24 hours for the cells to reengage in proliferation as observed in solid minimal media at 10 μM concentration (figure 21C).

Taken together, these results suggest that torin1 affects growth by delaying cell cycle duration as observed in the extended generation times, caused by TORC1 inhibition, consistent with a reduction in cell size at division with reversible growth arrest that does not lead to apoptosis (Atkin, et al., 2014). In fission yeast, inhibition of TOR activity with either rapamycin or starvation, arrests cell proliferation in G1 to undergo sexual differentiation and mating (Egel, 2004; Petersen & Nurse, 2007). During torin1 treatment mating of wild type cells is completely prevented and the cell cycle arrest does not occur in G1 phase -in contrast to mammalian cells (Thoreen, et al., 2009)-, this is indicative of TORC2 inactivation as this complex is essential for the G1 arrest (Atkin, et al., 2014).

The double mutant *tor1* Δ *tor2* Δ -temperature sensitive- present a similar phenotype, they are sterile, not viable and arrest growth at the G2 phase with an intermediate cell-size, suggesting that Tor2 requires Tor1 for divisions at smaller sizes (Weisman, et al., 2007). This is in contrast with the mild effect on cell division produced by rapamycin, which slightly reduces cell growth in a TORC1-dependent manner but does not affect cell division (Weisman, 2010), producing smaller cells without affecting generation times (Rallis, et al., 2013; Weisman, 2010). This data provided the bases to establish the titration of torin1 applied

during the subsequent experiments, providing significant insights into the effects of high and low dosages of this compound on cell viability to further explore the overall architecture and control of TOR signalling.

4.2.3. Chronological Lifespan assays

The entire length of time that multicellular organisms stay alive is commonly measured chronologically, this relies on both the replicative lifespans (RLS) and chronological lifespans (CLS) of several cell types (Chen & Runge, 2009). RLS is the number of divisions a cell achieves before proliferation ceases, this is the case of stem cells such as the ones repopulating the human immune and haematopoietic systems (Brummendorf & Balabanov, 2006). CLS is the length of time a cell survives without dividing, this is applicable to post-mitotic cells such as skeletal muscle and neurons (Lodish, et al., 2004).

Non-mammalian model systems used to study ageing confer advantages compared to human populations such as shorter lifespans, smaller size and thoroughly characterised genetics (Chen & Runge, 2009). In yeast, the theoretical framework behind CLS assays is based on the environmental niche of (wild) saprophytic fungi. They have evolved under selective pressure to survive in non-dividing states depending on the availability of carbon and nitrogen sources, with the cellular machinery that regulates lifespan adapted to rapidly resume growth when food is reintroduced in order to compete with other prokaryotic and eukaryotic microorganisms (Chen & Runge, 2009).

Haploid cells of fission yeast respond to limiting nutrients by either undergoing conjugation between cells of opposite mating types or by entering a stationary phase with no further increase in cell numbers (Fantes & Nurse, 1977). When such stationary phase is induced by carbon depletion or saturation in cell numbers (which leads to carbon depletion), cells arrest growth at the G2 phase of the mitotic cycle with a 2N DNA content, experiencing a slight reduction in cell size compared to actively growing cells and a metabolic shift from fermentation to oxidative carbon metabolism (Costello, et al., 1986; Dimitrov & Sazer, 1998; Roux, et al., 2009).

Conversely, nitrogen starvation halts cell cycle progression at the G1 phase with a 1N DNA content, producing significant smaller cells (Costello, et al., 1986; Fantes & Nurse, 1977). Mating is less frequent during carbon withdrawal than when nitrogen is depleted (Mach, et al., 2000), nevertheless, under both stress conditions cells maintain similar long-term viability, are able to re-enter the cell cycle in the presence of complete medium regardless of the G1 or G2 arrest (Costello, et al., 1986), and show relative resistance to heat shock compared to the sensitivity reported on actively growing cells, such resistance is enhanced by longer periods of nitrogen starvation (> 7 days), similarly to spores but differing from them in their requirement of glucose for viability (Egel, 2004; Su, et al., 1996).

An additional non-dividing stage is triggered at either the G1 or G2 phases of the vegetative cell cycle. This occurs by the combination of limited nitrogen, the absence of partners for mating, and the presence of carbon sources (such as

glucose). Those conditions induce haploid cells to enter a dormant G0 state that show increased survival to metabolic/environmental traumas and maintain viability for longer periods (Costello, et al., 1986; Fantes & Nurse, 1977; Su, et al., 1996).

Therefore, the objective of the CLS assays in the present study is to monitor the entire length of time that fission yeast cells survive in stationary phase in the culture (arrested in G0), from the moment they reach maximal density until they die, defined as the point in which they fail to form colonies when plated on fresh medium, producing a survival curve that reflects the decline in viable cells until they decrease to 0.1 % - 1 % of their original numbers (Chen & Runge, 2009).

This quantification of cell viability has been proven to be more reliable than flow cytometry as this last technique is useful to differentiate G1 (1N) from G2 (2N), but compared to CLS, it underestimates the percentage of dead cells (lower DNA content than living cells) because of the time DNA degradation takes after apoptosis (Costello, et al., 1986). Furthermore, CLS assays allows to understand evolutionarily conserved signalling pathways that regulate lifespan, acting as a post-mitotic model to study molecular mechanisms controlling cellular ageing of differentiated non-dividing somatic cells in higher organisms including humans (Chen & Runge, 2009; Fontana, et al., 2010).

Although the general morphological and physiological characteristics of *S. pombe* cells in response to starvation have been described (Dimitrov & Sazer, 1998; Kawai, et al., 2001; Mach, et al., 2000; Weisman, et al., 2007), further information

is needed about the mechanisms controlling longevity in this context. Thus, the following section aims to elucidate the involvement of TOR kinases and Gaf1 in the regulation of lifespan in this model organism in response to nutrient availability and pharmacological interventions of the TOR signalling pathway, by applying mutagenesis to CLS assays. The availability of defined mutant libraries incorporated to these experiments have been previously used for the systematic identification of genes whose mutations actively modulate longevity (Chen & Runge, 2009; Rallis, et al., 2014).

The subsequent experiments were performed using different strains to identify differences in their lifespan. The first stage involved the standardisation of the conditions for the assessment of the maximum lifespan of wild type and *gaf1* Δ cells, using several volumes of rich and minimal liquid media to grow the cultures, their aeration and rotation requirements, revealing significant differences in their CLS depending on those variables. This initial validation provided evidence to establish the conditions for the subsequent experiments assuring high levels of reproducibility and accuracy being consistent with the literature (Chen & Runge, 2009; Rallis, et al., 2013; Rallis, et al., 2014).

These CLS experiments confirmed that *gaf1* Δ mutants grow slower and experience shortened CLS compared to the wild type, indicating its relevance in chronological longevity in fission yeast (figure 23). These findings are concordant with previous results reporting that the hyper-function of TOR signalling causes ageing in a conserved manner (Gonzalez & Rallis, 2017; Ikai, et al., 2011; Rallis, et al., 2013).

TORC1 positively regulates the cytoplasmic retention of Gaf1 (through its phosphorylation) in normal nitrogen conditions avoiding its translocation into the nucleus resulting in inhibition of the transcription of nitrogen starvation-response genes and allowing the expression of sexual development genes required for mating, otherwise repressed by Gaf1 (Kim, et al., 2012; Laor, et al., 2015; Rodríguez-López, et al., 2020). In this regard, relevant genes expressed during nitrogen starvation such as *ecf1* -its product is localised in the nucleus and is probably involved in chromosome maintenance- that have been reported as responsible for CLS extension (Miwa, et al., 2011), are potential additional targets of Gaf1.

4.2.3.1. Survival of *gaf1* Δ and wild type cells with rapamycin treatment in minimal media

To further study the growth patterns and viability of wild type and *gaf1* Δ during TORC1 inhibition, the cultures were treated with rapamycin to assess the resulting CLS (figure 23).

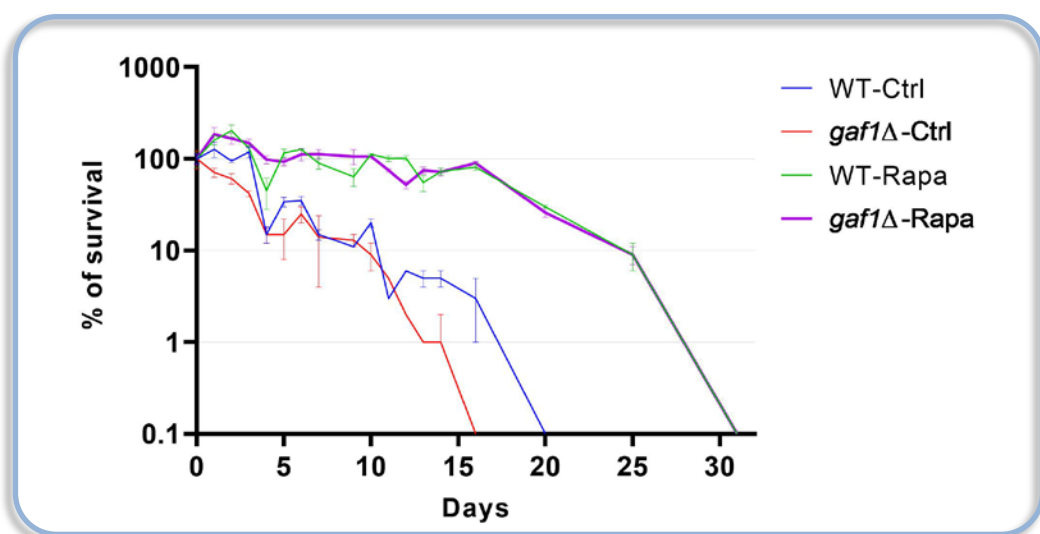


Figure 23. Survival curves of wild type and *gaf1* Δ mutant cells in minimal media with or without rapamycin (100ng/ml) treatment during growth phase as indicated.

The two strains showed significant lifespan extension after treatment compared to the untreated control due to the inhibition of TORC1 signalling at the beginning of the exponential growth phase when the complex is active.

These results indicate that the increase in lifespan is not driven by the *gaf1* gene, and confirm that the inhibition of growth caused by rapamycin during cell proliferation subsequently prolongs lifespan of non-dividing cells via interference of TORC1 signalling during vegetative cell growth, providing additional information about the pro-ageing effects of this conserved complex, also described to increase lifespan when inhibited by rapamycin in budding yeast (Powers, et al., 2006), worms, flies, and mice (Laplante & Sabatini, 2012), indicating that this drug represent a potential candidate to prolong lifespan in multiple species (Rallis, et al., 2013). Nevertheless, previous reports proved that when this compound is administered at the stationary phase when TORC1 is inactive (Ikai, et al., 2011; Weisman, 2010), it does not increase CLS in fission yeast (Rallis, et al., 2013) nor budding yeast (Powers, et al., 2006).

Considering the variability within the rapamycin-sensitive and rapamycin-resistant functions of TOR signalling, the subsequent CLS experiments in the present study, intended to further asses the TOR signalling pathway by differentiating the effects that TORC1 and TORC2 inhibition have on lifespan (independently and together), by means of mutagenic and chemical genetics analyses in the context of minimal and rich liquid media. In addition to *gaf1* Δ and wild type cells, the mutant strains *tco89* Δ and *tor1* Δ were included using a titration

of torin1 for the pharmacological inhibition of Tor1 and Tor2 kinases, applying the compound to the cultures at different growth stages.

4.2.3.2. Survival of *gaf1* Δ , *tco89* Δ , *tor1* Δ and wild type cells in rich and minimal media

The comparisons started with the assessment of the maximal lifespans of the strains without torin1 treatment for validation purposes (figure 24).

All the strains showed longer CLS in minimal (figure 24B) compared to rich liquid media (figure 24A) by the effect of caloric restriction, presenting similar patterns of longevity in both conditions and being consistent with previous reports (Chen & Runge, 2009).

This confirmed that nutrient availability is detected by all the strains, especially *tco89* Δ and *tor1* Δ which even though carry disruptions in TORC1 and TORC2 respectively, they preserve active gene expression programs that allow cell cycle progression that rely on environmental cues (Laboucarié, et al., 2017).

This essential integration between proliferation and environment has significant implications in cell fate, as is exemplified by the case of cancer pathogenesis, which is related to deficient differentiation and abnormal fast growth that is dissociated from the nutritional context (Martín, et al., 2017).

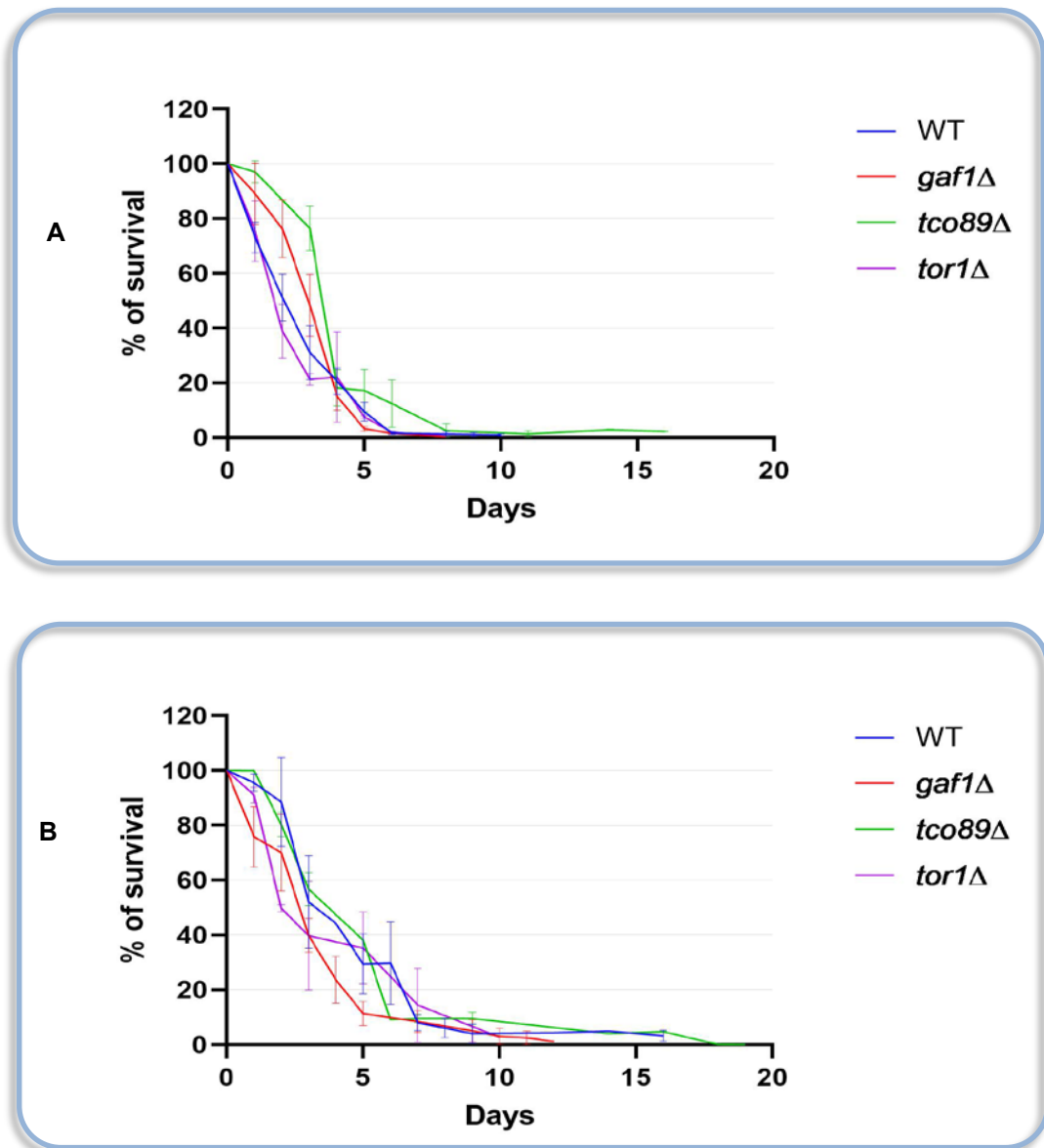


Figure 24. Maximal lifespan and survival curves of strains in **[A]** rich and **[B]** minimal media, estimated as the day in which the cultures reached 0.1 % survival.

The mutant *tco89Δ* showed extended CLS in contrast to *tor1Δ* and *gaf1Δ* that were short-lived compared to the wild type cells in minimal and rich media (figure 24A, 24B). This is consistent with the literature (Rallis, et al., 2013; Rallis, et al., 2014), and reflects the opposite roles of TORC1 and TORC2 regulating longevity (Ikai, et al., 2011) in both contexts. This increase in lifespan on this model organism (figure 24A, 24B) could be attributed to both caloric restriction and reduced TORC1 activity, via acquisition of the dormant G0 state previously

described during nitrogen starvation (Costello, et al., 1986; Su, et al., 1996), combined with the expression of survival genes triggered by the de-repression TORC2 signalling (Matsuo, et al., 2007; Rallis, et al., 2013).

After establishing the maximal lifespan of the strains in different media, it was possible to decipher the individual contribution of TORC1 and TORC2 to lifespan regulation by combining mutagenic analyses (gene disruptions in the complexes) and global inhibition of the TOR kinases via both nutrient restrictions in the liquid media and pharmacological interventions.

The minimal media used in these experiments contained reduced amount of nutrients, this was supplemented with the standard concentration of ammonium chloride (96 mM) as the nitrogen source described in the literature for fission yeast (Forsburg & Rhind, 2006; Petersen & Russell, 2016), which at the onset of the stationary phase leads to the inactivation of TORC1 and induction of TORC2 signalling (Weisman, et al., 2007).

Conversely, other reports indicate that lower amounts of ammonium (6–9 mM) allow normal growth of wild type cells (Bicho, et al., 2010), suggesting that former standard concentration might be excessive (Borek, et al., 2015). Therefore, the use of the drug torin1 in rich and minimal media at different concentrations and time points, intended to simulate physiological conditions analogous to nitrogen-depleted environments through decreased TOR signalling (Atkin, et al., 2014).

4.2.3.3. Survival of wild type cells with torin1 treatment in rich and minimal media

The results indicate that the median lifespan of the wild type cells was extended in rich media only when treated at the exponential growth phase with 0.5 μM and 8 μM torin1 (figure 25). This phenotype was not achieved using the same concentrations of the drug at either the onset of the stationary phase and after 3 days of that point (figure 25).

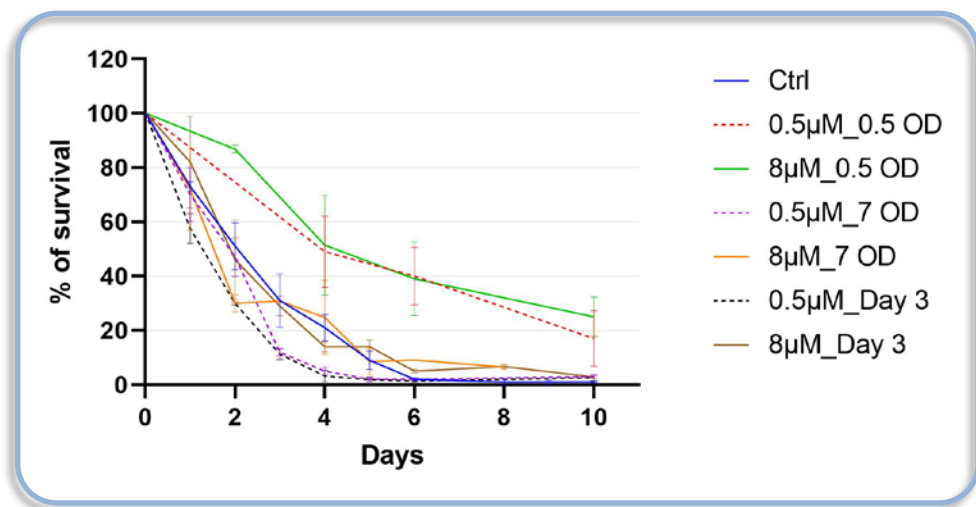


Figure 25. Survival curves of wild type cells in rich media with or without torin1. Treatments with 0.5 μM and 8 μM at the fast-growing phase (OD 0.5), onset of stationary phase (OD 7), and after 3 days in the stationary phase as indicated.

The CLS of the wild type cells was also assessed in minimal media at the same concentrations of torin1. Lifespan extension in this strain was achieved with all the treatments (0.5 μM and 8 μM) applied during vegetative growth, the onset of the stationary phase and 6 days after that point (figure 26).

Apart from the time points of the treatments, these differences could be attributed to the presence and absence of nutrients in the rich and minimal media respectively. In the context of nutrient abundance, the global TOR inhibition

caused by torin1 at the logarithmic growth phase reduces TORC1 activity when is essential for cell proliferation, which has been proven to subsequently extend lifespan of stationary cells under rapamycin or low glucose treatment (Rallis, et al., 2013).

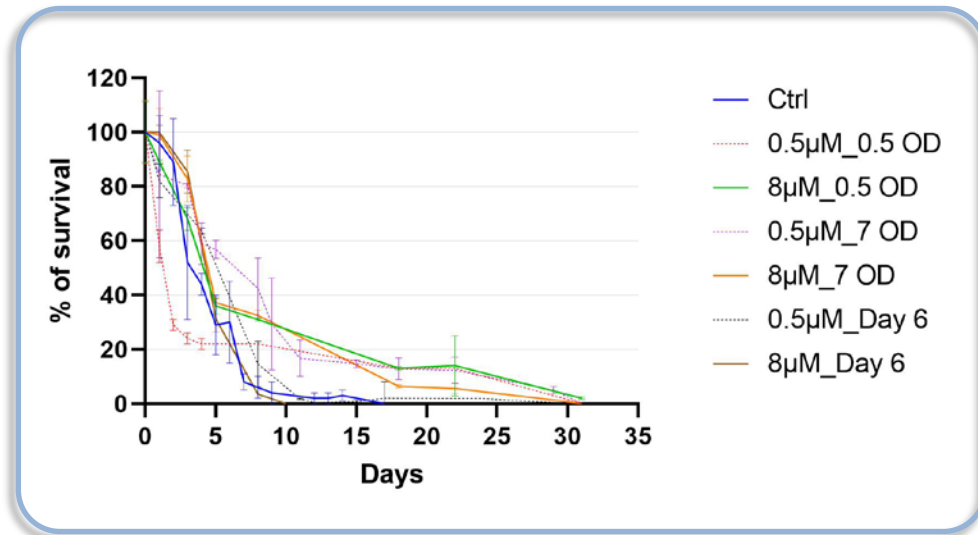


Figure 26. Survival curves of wild type cells in minimal media with or without torin1. Treatments with 0.5 µM and 8 µM at the fast-growing phase (OD 0.5), onset of stationary phase (OD 7), and after 6 days in the stationary phase as indicated.

Such event combined with the disruption of TORC2 -not essential for growth but required to reach stationary phase and promote longevity at that stage (Weisman, 2010; Weisman & Choder, 2001)-, debilitated cell viability when the treatment was added at the onset of the stationary phase and beyond that point, possibly produced by the impairment of TORC2 at those periods combined with active metabolic functions triggered by the presence of other nutrients in the media, mainly amino acids. This is consistent with the lack of CLS extension of wild type cells reported for rapamycin treatment after cells entered stationary phase in rich media (Rallis, et al., 2013).

Conversely, reduced amount of nutrients in the environment extended lifespan regardless of the time point of the treatments and their concentration, suggesting the existence of alternative mechanisms for the recognition of nutrients that influence overall cell fate and/or a potential transient pan-TOR inhibition by torin1 in liquid media which allows subsequent TORC2 activity and TORC1 inactivation caused by reduced amount of nutrients in the media.

4.2.3.4. Survival of *gaf1*Δ cells with torin1 treatment in rich and minimal media

The growth of *gaf1*Δ cells in rich and minimal liquid media showed resistance to the growth inhibition at the exponential growth phase induced by torin1 in wild type cells, similarly to the results described before obtained on solid media. All the growth experiments of this mutant showed this particular phenotype in this project, being consistent with previous reports (Hillson, 2018; Lie, et al., 2018).

The treatments in rich media produced extension of maximal lifespan, in particular when applied at the logarithmic phase. Using 8 μM at this point reduced survival on day 1 but produced the longest extension of lifespan (figure 27).

The torin1 treatments in minimal media showed differential effects on *gaf1*Δ depending on the stage of the cell growth when they were applied. Regardless of the concentration of the drug, CLS extension was only achieved when treated at the exponential growth phase (figure 28). The addition of torin1 at the onset of the stationary phase and after 6 days of this point were detrimental at all the concentrations (figure 28).

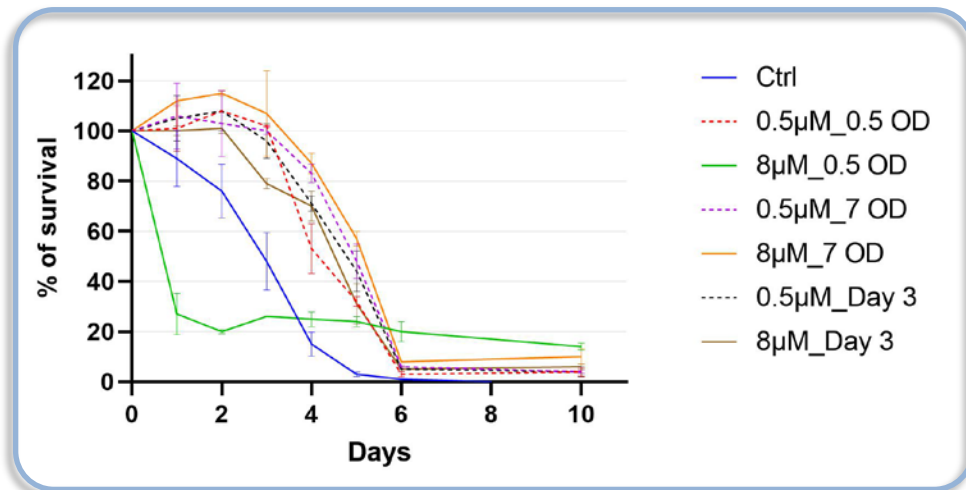


Figure 27. Survival curves of *gaf1*Δ cells in rich media with or without torin1. Treatments with 0.5 μM and 8 μM at the fast-growing phase (OD 0.5), onset of stationary phase (OD 7), and after 3 days in the stationary phase as indicated.

After the onset of the stationary phase, the CLS of *gaf1*Δ in rich media did not present the deleterious (figure 27) effects observed with the treatments in minimal media (figure 28). In this regard, recent studies conducted in mammalian cell lines in nutrient deprived environments reported that extended disruption (>24 hours) of the mTOR signalling with 0.5 μM torin1, resulted in attenuated autophagy with pro-apoptotic effects (Zhang, et al., 2017).

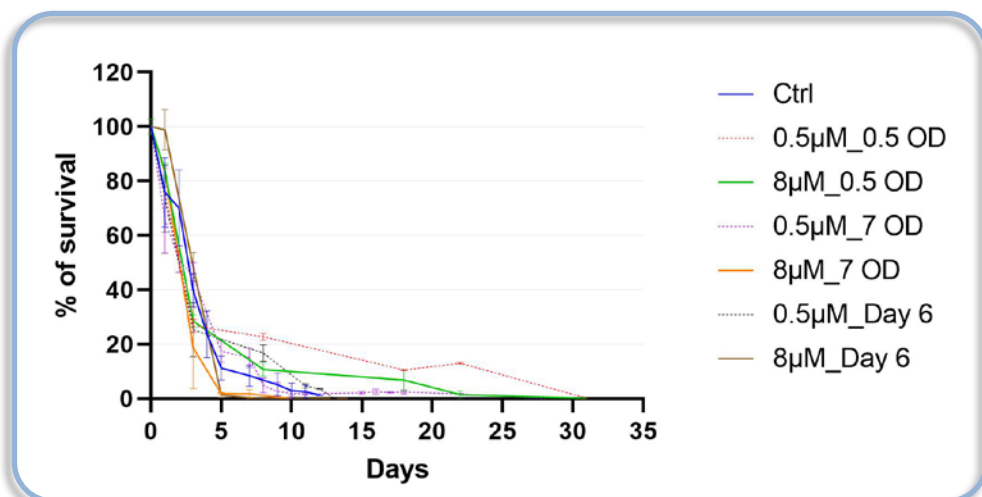


Figure 28. Survival curves of *gaf1*Δ cells in minimal media with or without torin1. Treatments with 0.5 μM and 8 μM at the fast-growing phase (OD 0.5), onset of stationary phase (OD 7), and after 6 days in the stationary phase as indicated.

This could be the case of fission yeast, where the absence of Gaf1-transcriptional targets during starvation may be affecting cell viability which was not observed in the wild type cells, probably by reducing TORC2 activity and impairing the traditionally described pro-survival autophagic action induced by moderate inhibition of the pathway which diminishes cell apoptosis (Mason, et al., 2018; Zhang, et al., 2017).

It has been documented that rapamycin and torin1 increase the degradation of long-lived proteins -but not short-lived ones- by means of proteolysis and autophagy, in order to provide essential amino acids and other molecules to the cell, leading to slow growth and extended survival when nutrients are limited (Zhao, et al., 2015). The results obtained in the present study for Gaf1 revealed a potential role for this transcription factor in the interplay between autophagy and apoptosis subjected to nutrient availability.

4.2.3.5. Survival of *tco89*Δ cells with torin1 treatment in rich and minimal media

The subsequent CLS assays aimed to explore the role of TORC1 in extending lifespan under torin1 treatments. This was studied using the strain *tco89*Δ that lack a non-essential core component of TORC1 (Ikai, et al., 2011). In rich media, only 8 μM of torin1 treatment was used to ensure the complete inhibition of the Tor2 (TORC1) and Tor1 (TORC2) kinases.

Similar to minimal media, the addition of the drug in this nutrient rich context at the three stages of cell growth (fast growth, onset of the stationary phase and 3

days after that point) did not produce increase in lifespan of *tco89Δ* cells (figure 29), on the contrary, the treatments in both types of media were detrimental in all cases.

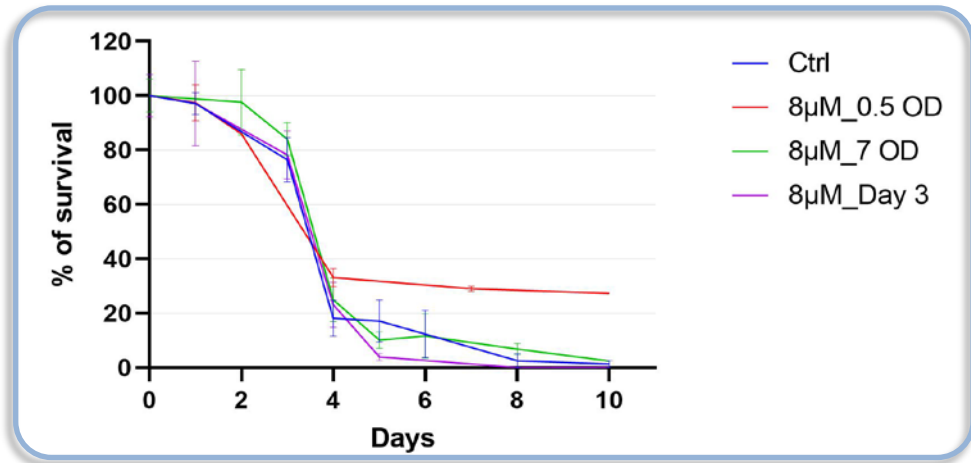


Figure 29. Survival curves of *tco89Δ* cells in rich media with or without torin1. Treatment with 8 μM at the fast-growing phase (OD 0.5), onset of stationary phase (OD 7), and after 3 days in the stationary phase as indicated.

In minimal media, the global TOR inhibition produced by torin1 (0.5 μM and 8 μM) during all stages of the cell growth (fast growth, beginning of the stationary phase and 6 days after that point) did not show extension of lifespan on *tco89Δ*(figure 30).

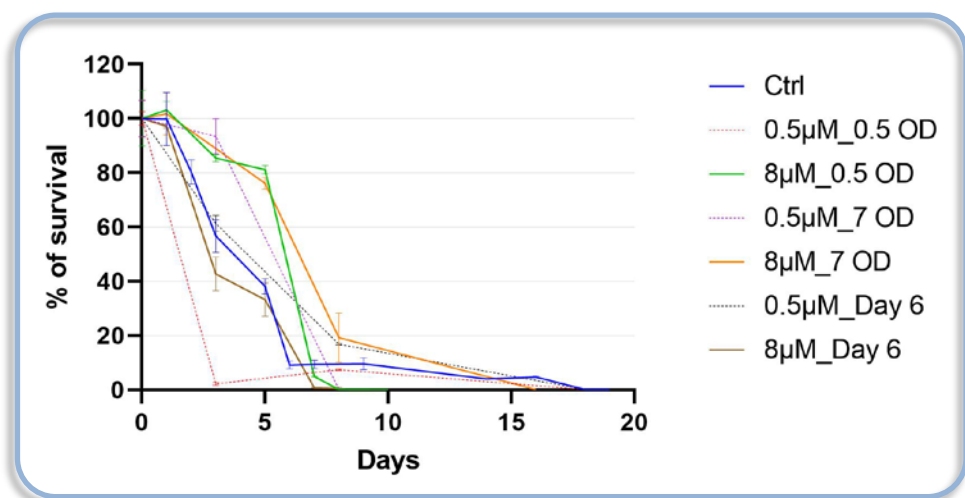


Figure 30. Survival curves of *tco89Δ* cells in minimal media with or without torin1. Treatment with 8 μM at the fast-growing phase (OD 0.5), onset of stationary phase (OD 7), and after 6 days in the stationary phase as indicated.

This is consistent with previous studies reporting that treatment with rapamycin at both the exponential growing and stationary phase did not increase CLS of *tco89Δ* cells (Rallis, et al., 2013). In this strain TORC1 is disrupted, therefore, the results obtained in the present study with torin1 treatments introduce the possibility that CLS could also be modulated by TORC2 after the beginning of the stationary phase, as this complex is important for survival at that point (Weisman, et al., 2007), suggesting a novel contribution of this complex regulating the increase in cellular longevity.

4.2.3.6. Survival of *tor1Δ* cells with torin1 treatment in rich and minimal media

The role of TORC2 activity in the regulation of lifespan was evaluated independently from TORC1 using the mutant *tor1Δ*, which lack the non-essential Tor1 core component of TORC2 (Ikai, et al., 2011).

Torin1 treatment (8 μ M) in rich media at the exponential growth stage produced lifespan extension of *tor1Δ* cells, which was not observed when the treatment was applied either at the onset of the stationary phase or 3 days after that point, being detrimental for cell viability (figure 31).

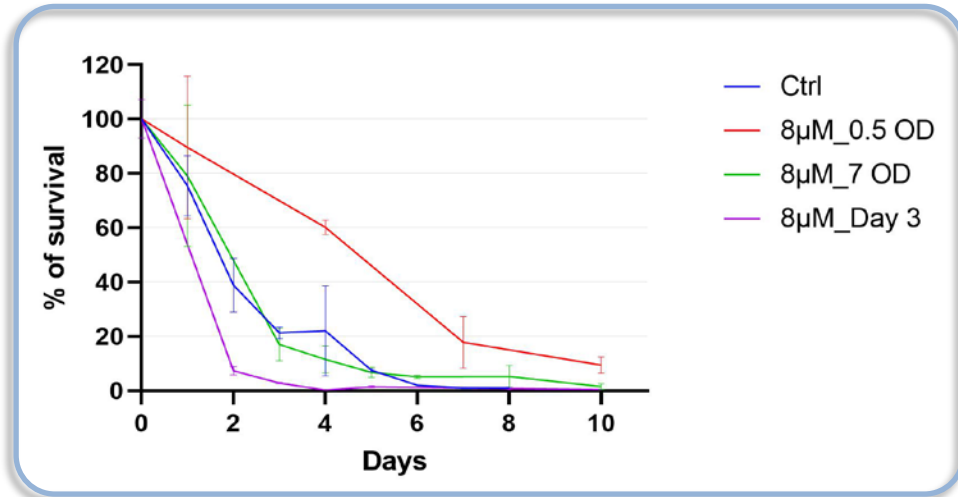


Figure 31. Survival curves of *tor1Δ* cells in rich media with or without torin1. Treatment with 8 μM at the fast-growing phase (OD 0.5), onset of stationary phase (OD 7), and after 3 days in the stationary phase as indicated.

In minimal media, none of the treatments with torin1 (0.5 μM and 8 μM) at the three stages of the cell growth (fast growth, beginning of the stationary phase and 6 days after that point) produced lifespan extension in *tor1Δ*(figure 32), however, lifespan was extended without treatments in this media compared to rich media (figure 31) due to limited nutrient availability, consistent with an overall reduction of TORC1 activity (Gonzalez & Rallis, 2017).

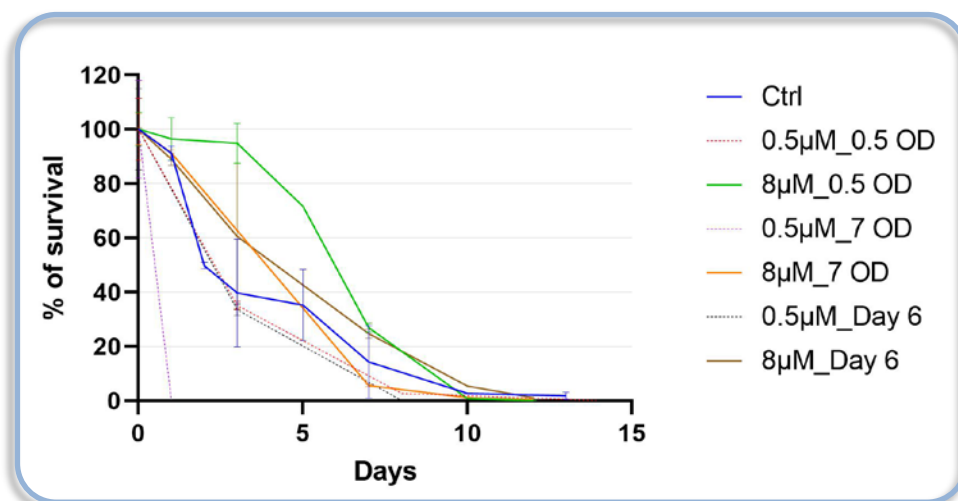


Figure 32. Survival curves of *tor1Δ* cells in minimal media with or without torin1. Treatment with 8 μM at the fast-growing phase (OD 0.5), onset of stationary phase (OD 7), and after 6 days in the stationary phase as indicated.

In contrast to the wild type, *tor1* Δ cells showed reduced lifespan in minimal and rich media. This could be attributed to two main elements, either because of the absence of the negative regulation of Tor1 over Tor2, which leads to hyperactivation of Tor2 that signals nitrogen availability even in its absence, an element that has been classically described as detrimental for viability (Weisman, et al., 2007); or because of the lack of TORC2 signalling -required for stress responses and long-term survival in stationary phase (Weisman, et al., 2014).

These findings resemble the unfavourable phenotype observed in the wild type (figures 25, 26) and *tco89* Δ (figures 29, 30) under treatments with torin1 after the onset of the stationary phase in rich and minimal media that were detrimental for survival, most probably due to TORC2 inhibition at the stationary phase.

Comparing the results obtained for this mutant in the contexts of minimal against rich media, the abundance of nutrients in the media (but not their depletion) combined with the inhibition of TORC1 at an early stage of the cell growth -when the complex is active and essential (Weisman, 2010)-, promoted extension of lifespan, also previously reported in this mutant using rapamycin treatment in rich media (Rallis, et al., 2013).

Considering that TORC2 is not active in *tor1* Δ , the data from the present study suggests a paradoxical behaviour where nutrient availability in rich media reduces lifespan in normal conditions (figure 31), but when TOR signalling is pharmacologically inhibited with torin1 at the exponential growing phase in the background of *tor1* Δ , it induces alternative mechanisms that enhance cellular

survival, not occurring when nutrients are scarce (minimal media). Probably by downstream effects caused by the potential re-activation of TORC1 signalling (after the drug is metabolised) in a manner that triggers benefits for longevity that are still unknown.

These types of negative feedback loops are common in the regulation of the TOR pathway (Gonzalez & Rallis, 2017; Ikai, et al., 2011), where this particular case could be linked to the activity of genes controlling nutrient homeostasis (amino acids) such as the 2-oxoglutarate-Fe(II) dependent oxygenase (*isp7*), which is a target of Gaf1 induced by TORC2 when TORC1 is inactive, but its product (*Isp7*) negatively regulates its own expression, inhibits TORC2, and its overexpression activates TORC1 under nitrogen stress conditions (Laor, et al., 2014; Laor, et al., 2015).

Even though the entire network of mechanisms underlying TORC2 activity are not completely understood in all model systems (Schonbrun, et al., 2013), in fission yeast its activity is controlled by glucose levels -but not nitrogen- (Cohen, et al., 2014). This complex induces the translocation to the cell surface of the high-affinity glucose transporter Ght5 (Takeda, et al., 2015), relevant for proliferation under limited glucose, similarly to the human glucose transporters GLUT (Saitoh, et al., 2015).

In this sense, the carbon source used in the present experiments in both rich and minimal media was dextrose at similar concentrations of 30 % and 20 % respectively, with fission yeast cells reported to survive in glucose levels as low

as 0.2–0.1 % (Takeda, et al., 2015). This suggest that the difference in CLS caused by the media in this mutant probably are not related to the amount of glucose in the media, instead was mediated by other nutrients such as amino acids, present in rich but no in minimal media, which could be triggering alternative mechanisms for survival that bypass TORC2 functions, and even supporting the idea of a negative feedback loop where genes such as *Isp7* could be inducing the re-activation of TORC1 with beneficial effects.

It has been established that TORC2 is not essential for normal growth but is crucial for survival under stress conditions (Weisman, et al., 2014). Disruptions in this complex result in pleiotropic defects in different species such as failure to sense starvation, inability to grow in limited glucose (Ikai, et al., 2011; Kawai, et al., 2001), reduced amino acid uptake (Weisman, et al., 2005), enhanced sensitivity to stresses [osmotic, oxidative, temperature] (Weisman & Choder, 2001), inability to initiate sexual development or acquire stationary phase physiology (Kawai, et al., 2001; Weisman & Choder, 2001), delayed entry into mitosis (Petersen & Nurse, 2007; Schonbrun, et al., 2009) and inability to induce gene silencing, tolerate DNA damaging environments, or maintain telomere lengths (Schonbrun, et al., 2009).

4.2.3.7. TOR signalling and cellular nutritional context

Taken together, the findings obtained in this section of the study bring novel insights into the regulation of TOR signalling, especially the complex interaction between starvation in combination with pharmacological inhibition of the pathway, reopening and challenging the classic discussion about the antagonistic roles of

the two complexes regarding longevity, traditionally described as TORC1 activity shortening lifespan, in contrast to TORC2 signalling that increases it (Rallis, et al., 2013).

Overall, the CLS of the untreated strains (wild type vs mutant cells) showed no significant differences between them in minimal or rich media. To present, this is the first study of lifespan in fission yeast using treatments with torin1 at different stages of the cell growth in different nutritional contexts. This revealed that the extension in lifespan relied on the type of media, time of the treatment and the dosage, where higher concentrations during both the logarithmic phase in rich media and stationary phase in minimal media were correlated to an increase in CLS only in the mutants containing TORC1 activity.

This is in agreement with previous studies that showed evidence of a concentration-response effect of torin1 on lifespan extension via induction of autophagy (Mason, et al., 2018), attributed to inactivation of TORC1 which is a suppressor of autophagy (Ben-Sahra & Manning, 2017). The data presented in this section highlights the usefulness of this approach, in which the drug in different nutritional contexts combined with mutagenesis analyses were used to differentiate the contribution of TORC1 and TORC2 activity in cellular ageing. Altogether, this set of assays provided information about the effects of the TOR signalling inhibitors rapamycin and torin1 in the CLS of fission yeast cells, where each drug target the same conserved nutrient-sensing pathway but differentially affect it.

4.2.3.8. Survival of *ssp2* Δ , *amk2* Δ and wild type cells with compound

991 treatment in rich media

In order to further explore additional molecular mechanisms used by the cell to recognise energy levels in the extra-cellular environment, another compound recently identified named compound 991 (C991) was used in this study. This is a potent direct activator of the highly-conserved adenosine monophosphate (AMP) activated protein kinase [AMPK] (Lai, et al., 2014). AMPK is a rheostat of energy homeostasis that regulates metabolic pathways to balance nutrient inputs such as glucose and fatty acid uptake with energy expenditure via sensing levels of its allosteric activator AMP. AMPK ensures survival during cellular metabolic stress, interacting with the TOR pathway to limit its functions and induce catabolism among other survival mechanisms (Kim, et al., 2016).

The fission yeast ortholog of AMPK consists of the α (catalytic) subunit Ssp2, and the $\beta\gamma$ (regulatory) subunits Amk2 and Cbs2 to which AMP binds providing a target for the unique stress-responsive kinase Ssp1, which phosphorylates Ssp2 to activate AMPK, promoting catabolic processes and inhibiting anabolic pathways (TORC1) in response to nutritional stress, leading to a global inhibition of translation (Schutt & Moseley, 2017; Viollet, et al., 2010).

Activation of AMPK has been linked to favourable physiological outcomes, making it a novel therapeutic target for controlling diseases such as metabolic syndrome and cancer. C991 is a small molecule that resembles cellular AMP. It is a novel and highly-efficient AMPK activator, as it triggers conformational

changes in that allow increased phosphorylation of the α subunit blocking its dephosphorylation (Kim, et al., 2016; Xu, et al., 2018).

In this study, CLS experiments were performed using a titration of the compound in rich media assessing the wild type and mutants depleted of AMPK α subunit and the AMPK β subunit [*ssp2* Δ and *amk2* Δ respectively] (figure 33).

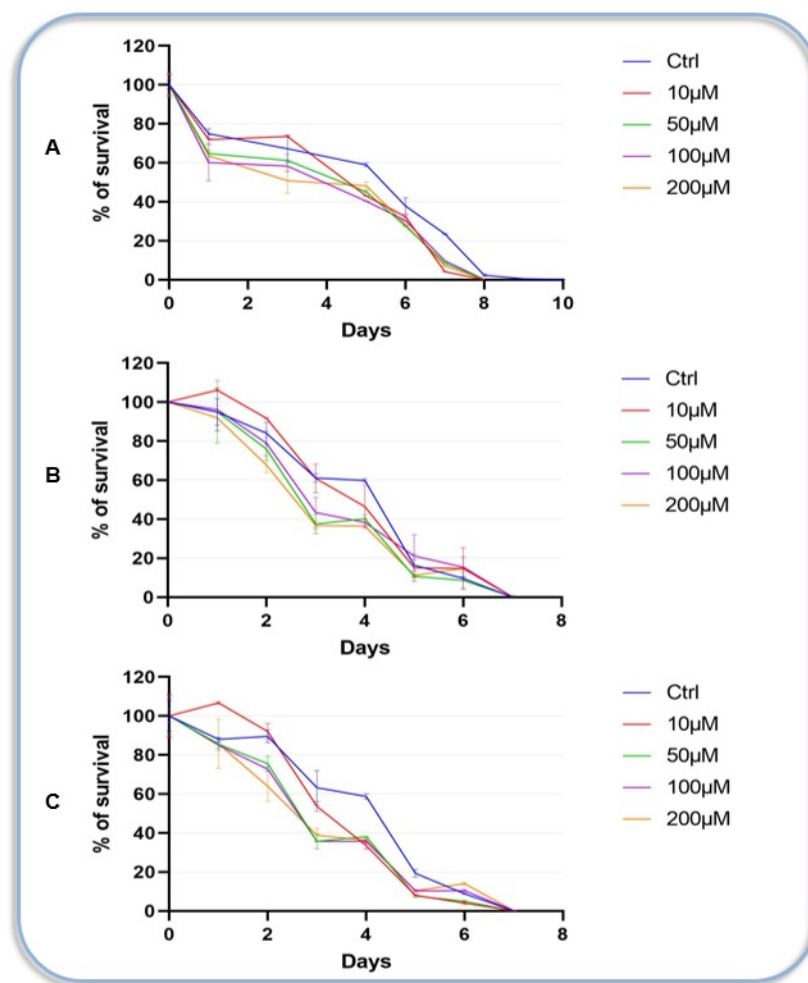


Figure 33. Survival curves of **[A]** wild type, **[B]** *ssp2* Δ and **[C]** *amk2* Δ cells in rich media with or without C991. Treatment with 10 μ M, 50 μ M, 100 μ M and 200 μ M at the fast-growing phase (OD 0.5) as indicated.

The CLS assays showed similar lifespans of *ssp2* Δ and *amk2* Δ compared to the wild type in rich media, being consistent with previous reports for *amk2* Δ (Rallis,

et al., 2017). No significant effects were observed with any of the treatments added to the strains at the fast-growing phase. These results could be revealing either the lack of interaction between the compound and the two AMPK subunits of the fission yeast tested here, or an inefficient -indirect- inhibition of the TOR signalling pathway theoretically triggered by activation of AMPK, which leads to autophagy and reduced protein biosynthesis to preserve energy under stress conditions (Rallis, et al., 2017).

Even though the mechanisms involved in the inhibition of AMPK are still elusive, the conserved Glycogen Synthase Kinase (Gsk3) inhibits AMPK activity (Suzuki, et al., 2013). Here, it was hypothesised that the activation of AMPK by the C991 compound could reduce TOR activity and increase lifespan, however the observed phenotypes resembled those reported for *gsk3Δ* mutant cells, which disruption promotes high AMPK activity without an increase in lifespan since TORC1 signalling is not interfered (Rallis, et al., 2017).

4.2.3.9. Protein translation accuracy and CLS in the fission yeast

Protein translation accuracy and efficiency constitute an additional factor involved in the control of lifespan (Filer, et al., 2017). In order to explore this, another set of CLS experiments were designed using a series of mutants with alterations in the ribosomal protein S23 [rps23] (figure 34), a component of the small ribosomal subunit 40S (The UniProt Consortium, 2019). Specifically, at residue Lysine-60 located near a conserved catalytic site for ribosome hydroxylation which is implicated in several cellular functions ranging from oxygen-dependent regulation

of sterol response genes to translation termination/mRNA polyadenylation (Singleton, et al., 2014).

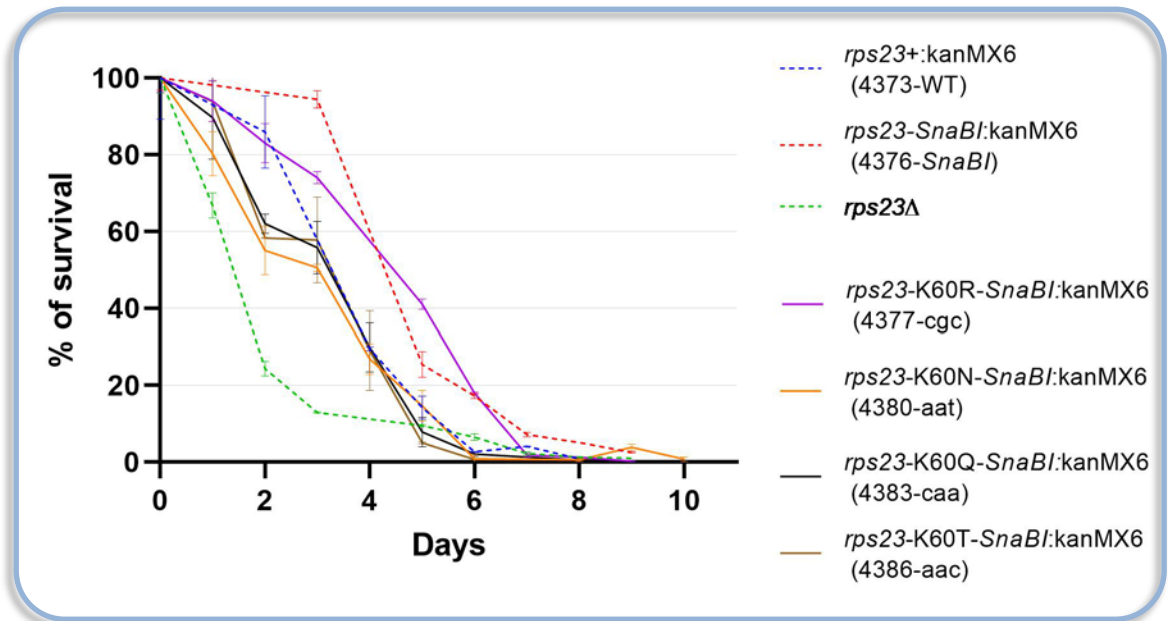


Figure 34. Survival curves of *rps23* mutant cells in rich media. Control strains (dotted lines) and mutants at Lys-60 (solid lines) as indicated.

The results revealed that depletion of *rps23* drastically reduced median lifespan compared to the other control strains where the kanamycin cassette *MX6* and the restriction site *SnaBI* were added to *rps23*. As expected, the rest of the strains containing modifications in the Lys-60 showed reduced CLS, only the mutant Lys60Arg presented similar lifespan to the control *rps23-SnaBI:kanMX6*_(4376). These mutations increase or decrease the accuracy to recognise stop codons, confirming that *rps23* plays a pivotal role in quality control during translation, where even minor posttranslational modification such as addition of a single oxygen atom impacts translation (Ishiguro, et al., 2000). Therefore, not only the rate of translation, but its accuracy are fundamental for the regulation of lifespan, suggesting that modulation of ribosomal conformation could also be considered as a target for therapeutic interventions (Loenarz, et al., 2014).

The CLS assays performed in this study followed the entire curve of the lifespan of fission yeast until the majority of the cells were dead (Chen & Runge, 2009). They recapitulated features of ageing that are conserved throughout eukaryotes including lifespan shortening by excess of nutrients, lifespan extension by caloric restriction, regulation of lifespan by TORC1/TORC2 and translation efficiency (Filer, et al., 2017; Fontana, et al., 2010; Mair & Dillin, 2008).

The analysis of the cells exposed to normal and nutrient-deprived conditions revealed that nutrient availability is detected by all the strains assessed here, including *tco89Δ* and *tor1Δ* which carry disruptions in TORC1 and TORC2 respectively, confirming that additional mechanisms recognising the presence of nutrients also regulate cellular fate independently of TOR signalling.

The increased survival of *tco89Δ* reported here could be attributed to caloric restriction, reduced TORC1 activity (Costello, et al., 1986; Su, et al., 1996), and the expression of survival genes triggered by the de-repression TORC2 signalling (Matsuo, et al., 2007; Rallis, et al., 2013) after torin1 is metabolised in the stationary phase, indicating both a possible transient pan-TOR inhibition induced by the drug in liquid media which allows subsequent TORC2 activation in *tco89Δ*, and suggesting a novel contribution of TORC2 in the regulation of lifespan after the onset of the stationary phase.

This notion is supported by the short lifespan observed in *tor1Δ* mutants, probably by either the lack of TORC2, or the overactivation of TORC1. The treatments with torin1 at the exponential growing phase in this strain revealed that nutrient

availability increased survival which did not happen during starvation, suggesting a possible beneficial re-activation of TORC1 signalling triggered by amino acids (not present in minimal media) or genes such as *isp7* that extended lifespan.

The global TOR inhibition caused by the drug at the stationary phase and beyond that stage reduced cell viability in *tor1Δ* mutants, being consistent with the detrimental phenotype observed in this study in wild type cells and *tco89Δ* under treatments with torin1 in minimal and rich media during the stationary phase, as well as with previous reports using rapamycin at that point in rich media (Rallis, et al., 2013). This is probably due to TORC2 inhibition at the stationary phase even with rapamycin, reported to inhibit this complex under specific nutritional contexts or when TORC1 is disrupted (Weisman, 2010), as it occurs in certain human cell lines upon prolonged treatment (Sarbasov, et al., 2006).

In the case of *gaf1Δ*, even though this strain show resistance to torin1, the treatments with the drug at the logarithmic phase extended CLS regardless of the nutritional contexts. Nevertheless, after the onset of the stationary phase nutrient abundance allowed torin1 treatments to extend lifespan, a phenotype not present during starvation (minimal media), possibly due to sustained inhibition of TOR by the combination of torin1 with limited nutrients, described in mammalian cells to reduce autophagy leading to pro-apoptotic effects (Zhang, et al., 2017).

The absence of Gaf1-target genes during starvation may also affect cell viability probably by reducing TORC2 activity, impairing its pro-survival autophagic action that diminishes apoptosis (Mason, et al., 2018; Zhang, et al., 2009). These results

suggest that Gaf1 is involved in the regulation of autophagy and apoptosis depending on nutrient availability and highlight the relevant role of amino acid availability during the stationary phase, which contributed to extend lifespan in the background of *gaf1* Δ , *tco89* Δ and *tor1* Δ .

Regarding alternative mechanisms for homeostasis in cellular energy, the highly efficient AMPK activator C991 showed either a lack of interaction between this molecule, the wild type and the mutants containing disruptions in two AMPK subunits of the fission yeast, or an inefficient indirect-inhibition of the TOR signalling pathway that does not lead to lifespan extension.

Finally, the influence of translation accuracy in lifespan assessed through a set of mutants carrying disruptions in *rps23*, revealed the fundamental role of this protein sustaining longevity, where depletion of the protein produced severe reductions in CLS compared to milder mutations involved in the recognition of stop codons, confirming the fundamental role of *rps23* in quality control for accurate translation, and supporting the idea that ribosomal configuration could be a potential target for therapeutic interventions for lifespan extension (Filer, et al., 2017; Loenarz, et al., 2014).

Altogether, the results demonstrate the value of these different types of growth assays to elucidate the influence of nutritional contexts and genetic networks controlling cellular ageing in *S. pombe*. Although the detailed molecular mechanism by which nutrient depletion extend lifespan remain unknown (Powers, et al., 2006), the data confirmed that nutrient availability, specifically

amino acids, control common cellular responses among model organisms such as lifespan and resistance to stress, reinforcing the existence of broadly evolutionarily conserved properties of ageing present in both unicellular and multicellular eukaryotes (Chen & Runge, 2009; Partridge, 2010). Therefore, genetic, pharmacological and environmental interventions that decrease activity of conserved nutrient-sensing pathways are promising strategies to be further explored in mammalian systems with the aim of improving human health.

Chapter 5. Gaf1-dependent expression profile and transcriptional network

5.1. Introduction

One of the main challenges in modern biology is to understand the relationship between genomic diversity and phenotypic variation of quantitative or complex traits (Jeffares, et al., 2015). The latter are orchestrated not only by protein-coding genes, but by numerous elements that regulate their expression by mechanisms that remain vastly unknown (David, et al., 2014). The use of simple model unicellular organisms such as yeast has provided significant information for the identification of conserved molecular pathways controlling multifactorial phenotypes in eukaryotes including stress-resistance, lifespan and ageing (Fabrizio, et al., 2005).

Evidence from the fission yeast confirmed the link between nutrient signalling with lifespan (Gonzalez & Rallis, 2017; Rallis, et al., 2013; Roux, et al., 2010), indicating that nutritional status in general produces changes in transcriptional activity, particularly nitrogen availability is of interest in the present study because it induces fast and drastic transcriptional responses in *S. pombe*, making it a relevant model for whole-genome studies of gene regulation and transcription (Kristell, et al., 2010; Rallis, et al., 2013), especially due to its compact genome of ~5,000 protein-coding genes (Lock, et al., 2019). Furthermore, the ability of cell-permeable chemical inhibitors to block specific cellular functions within minutes (even seconds), is a strategy that has been used in the fission yeast to

examine underlying patterns of gene expression (Kawashima, et al., 2012; Ma, et al., 2015).

Recent developments in genomics platforms involving high-throughput measurement of gene expression such as (cDNA) microarrays and sequencing have allowed the systematic screening of the level of expression of thousands of genes in different environments, providing significant insights about the molecular basis of the abovementioned multifactorial phenotypes (Rallis, et al., 2013). Such data combined with the additional technology of chromatin immunoprecipitation followed by high-throughput sequencing (ChIP-seq), constitute a powerful tool for the characterisation of the transcriptome in yeast (Lefrançois, et al., 2014).

Even though computational analyses could predict putative binding regions containing consensus motifs, it has been experimentally proven that in some occasions transcription factors remain either unbound to these regions or bound to other non-specific sequences, requiring experimental confirmation for validation after producing *in-silico* results (Borneman, et al., 2007).

Framed in functional genomics, this chapter is focused in the analysis of large-scale datasets obtained with microarray technology. This was used to quantify the level of transcription of ~5,000 genes simultaneously, identifying sets of genes which expression is controlled by Gaf1. In order to understand direct and indirect regulation of such genes, the results from this section were compared against datasets published by collaborators using ChIP-seq, which provided the binding sites of Gaf1 throughout the genome of the fission yeast (Rodríguez-

López, et al., 2020). In both cases the results were produced under equal experimental conditions applying the same treatment with the ATP analogue torin1 to pharmacologically inhibit TOR kinases (Thoreen, et al., 2009) to mimic nitrogen starvation (Atkin, et al., 2014).

The results provide a comprehensive characterisation of the functional role of Gaf1 by mapping changes detected in the transcriptional network governed by this transcription factor in response to the nutritional context and the implication of its target genes in pathways regulating ageing and survival. Overall, the data contributes to better understand the organisation of yeast genome and regulatory mechanisms of gene expression under different experimental conditions.

5.2. Global expression profile controlled by Gaf1

The conserved TOR signalling pathway is of interest for this study as it is a rheostat of cellular growth and metabolism in response to nutrient availability, proven to be involved in the regulation of lifespan and ageing in all organisms tested (Blagosklonny, 2013; Gonzalez & Rallis, 2017; Weisman, 2010). In *S. pombe*, TOR operates via two multi-protein complexes, TORC2 which senses carbon sources and is required for sexual differentiation, actin function and stress response (Matsuo, et al., 2007; Weisman & Choder, 2001), and TORC1 that functions on lysosomes (vacuoles in yeast), in response to growth signals controlling growth through the inhibition of autophagy and activation of protein synthesis which promotes ageing (Binda, et al., 2009; Chia, et al., 2017; Valbuena, et al., 2012; Valvezan & Manning, 2019).

Peptide production is controlled by TORC1 at the transcriptional and post-transcriptional levels via phosphorylation of different components of the translational machinery including transcription factors (Ma, et al., 2015), ribosomal S6 kinase (S6K) and the translation factors eIF2 α and 4E-BP (Ma & Blenis, 2009). Additionally, transcription of ribosomal RNAs is promoted by TORC1 via RNA polymerases I and III (RNA Pol I and III) by mechanisms still not completely understood (Iadevaia, et al., 2014). The highly abundant 5S ribosomal RNAs and transfer RNAs (tRNAs) -essential for translation- are transcribed by RNA Pol III (Arimbasseri & Maraia, 2016). It has been proven that disruptions in translation by inhibition of S6K prolongs lifespan in several model organisms (Bjedov, et al., 2010; Rallis, et al., 2014; Roux, et al., 2006; Selman, et al., 2009), as well as decreased RNA Pol III activity downstream of TORC1 (Filer, et al., 2017).

Even though these findings indicate that TORC1-dependent regulation of RNA Pol III transcription is relevant for translation and therefore ageing, at present there are no specific transcription factors identified that bind to RNA Pol III-dependent promoters to mediate translation (Rodríguez-López, et al., 2020).

The conserved *S. pombe* GATA transcription factor Gaf1 positively and negatively regulates gene expression specifically in response to nitrogen limitation downstream of TORC1, being insensitive to glucose depletion (Kim, et al., 2012; Laor, et al., 2015). Gaf1 is mainly retained in the cytoplasm by the activity of TORC1, which promotes its phosphorylation by inhibiting the PP2A-like phosphatase Ppe1 (Laor, et al., 2015). Inactivation of TORC1, allows the

activation of Ppe1 phosphatase, leading to the dephosphorylation of Gaf1 and nuclear translocation to exert its complete function as a transcription factor (Otsubo, et al., 2017). Therefore, Tor2 regulates Gaf1 in a different manner than Tor1, since the loss of Tor1 does not affect neither phosphorylation or nuclear localisation of Gaf1 (Ma, et al., 2015). This mechanistic regulation of GATA transcription factors being retained in the cytoplasm by active TORC1 and translocated to the nucleus upon its inhibition is conserved in budding yeast Gln3 and Gat1 (Georis, et al., 2011; Kulkarni, et al., 2006) and other mammalian GATA transcription factors (Xie, et al., 2015; Zhao, et al., 2008).

Torin1 inhibits the activity of TORC1 and TORC2 in *S. pombe* (Atkin, et al., 2014; Thoreen, et al., 2009), obstructing cell cycle progression and reducing the size of both vacuoles and cells (Rodríguez-López, et al., 2020). Such phenotypes have also been described during treatment with caffeine and rapamycin proven to block TORC1 functions (but not TORC2) which induce Gaf1 nuclear translocation (Rallis, et al., 2013; Rodríguez-López, et al., 2020).

Previous studies using low concentrations of torin1 (5 μ M) to assess growth of thousands of mutants under reduced TOR signalling, identified *gaf1* Δ as resistant (Lie, et al., 2018). Multi-drug resistance analyses revealed that *gaf1* Δ cells effectively uptake torin1, excluding the possibility that the resistance occurs by the lack intake of the compound (Rodríguez-López, et al., 2020). This mutant shows phenotypes of TORC1 inhibition after torin1 treatment, including limited ribosomal S6 protein phosphorylation and reduced cell size (Rodríguez-López, et al., 2020). The drug resistance was also confirmed in the present study with

growth assays and toxicity tests (chapter 4, section 4.2.2.), proving that Gaf1 is essential for the growth inhibition induced by torin1.

The translocation to the nucleus/activation of this transcription factor was induced via pharmacological inhibition of TOR kinases using torin1 (Ma, et al., 2015). A high dosage of this compound (20 μ M) was applied at the exponentially growing phase in rich media for 1 hour. These analyses were performed using the strains wild type and *gaf1* Δ , to identify genes controlled directly or indirectly by Gaf1 and elucidate functions of its transcriptional role.

To understand the transcriptional network controlling the growth inhibition produced by Gaf1 in the presence of torin1, custom-made microarrays for fission yeast were used in the present study (Lyne, et al., 2003). This technology allowed to simultaneously screen genome-wide the level of expression of genes and other global DNA-dependent processes controlled by Gaf1. The microarrays involved strand-specific probes printed in distinct regions of the slide, with genes represented by two or more array elements. It also contained inter-species sequences used as negative and specificity controls, with a total of ~13,000 spots per slide, covering 5,269 different genes and additional genomic features of the fission yeast (Lyne, et al., 2003; Penkett, et al., 2006).

The microarray technology was selected over other platforms such as RNA sequencing, due to the availability of a framework of experimental procedures and protocols for improved array performance, as well as customised scripts developed to discard unreliable data (normalisation of artefacts), providing

optimised interpretation of array data (Lyne, et al., 2003). These elements ultimately reduced the financial impact of the project.

The microarrays involved two independent biological repeats of treated and untreated control cells for each strain, the standard two-colour dye swapping was used to fluorescently label the samples prepared from RNA obtained from the two different cell populations per strain (Shalon, et al., 1996). The samples were co-hybridised onto microarrays to measure gene expression levels for each experimental condition relative to the expression levels of the untreated wild type controls (Lyne, et al., 2003). Differentially expressed genes (DEGs) were established on a conservative fixed cut-off of 1.5-fold change compared to the control, where genes with consistent changes across biological repeats were the ones considered (Rodríguez-López, et al., 2020).

The systematic identification of Gaf1-dependent transcripts revealed that before torin1 treatment, the wild type and *gaf1Δ* cells display similar expression profiles, with only 3 genes downregulated in *gaf1Δ* compared to wild type cells [figure 32] (Rodríguez-López, et al., 2020). This is consistent with the TORC1 activity in proliferating cells, which inhibits most of the Gaf1 transcriptional functions (Laor, et al., 2015; Rodríguez-López, et al., 2020), apart from the reported basal expression of *isp5* (Ma, et al., 2015).

Treatment with torin1 induced drastic transcriptional changes in both the wild type and *gaf1Δ* cells, with a marked contrast in the expression profile between the two strains (figure 35). There were 90 and 108 genes that consistently showed ≥ 1.5 -

fold higher or lower expression respectively, in *gaf1Δ* compared to wild type cells after the treatment (see full list of genes in appendices II and III, respectively). The expression profile of wild type cells under torin1 treatment was similar to previous reports that induced TORC1 inhibition, but not TORC2, by using caffeine and rapamycin (Rallis, et al., 2013; Rodríguez-López, et al., 2020), and nitrogen starvation in diploid cells (Mata, et al., 2002), validating that the torin1-mediated expression profile obtained in the present study reflects TORC1 inhibition. The results indicate that Gaf1 -either positively or negatively- affects the expression of ~200 genes after TORC1 inhibition.

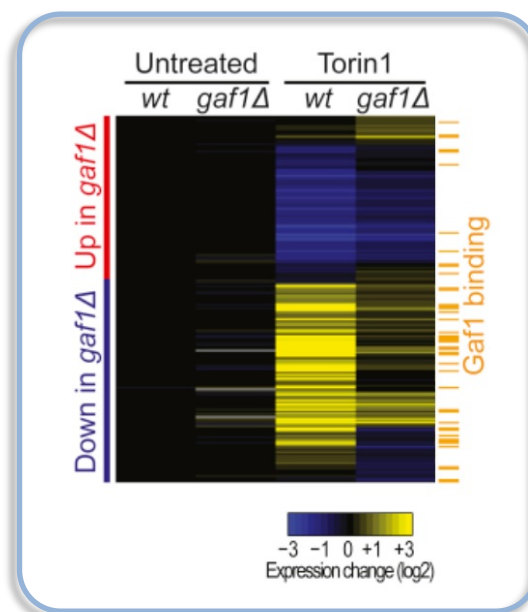


Figure 35. Hierarchical clustering of microarray data. Columns indicate wild type or *gaf1Δ* before and after 1 h of treatment with 20 μ M of torin1 in rich media. Rows represent the 198 genes which expression changed ≥ 1.5 -fold in torin1-treated *gaf1Δ* compared to wild type cells. Red bar indicates 90 genes upregulated and blue bar shows 108 genes downregulated in *gaf1Δ* relative to wild type cells. Untreated cells showing 3 genes with ≥ 1.5 -fold expression changes in *gaf1Δ*. Average RNA expression changes (from 2 independent repeats) are colour coded as shown. The orange bars indicate 43 genes whose promoters were bound by Gaf1 after 60 min with torin1. Adapted from (Rodríguez-López, et al., 2020).

These Gaf1-dependent set of genes were the input data to perform functional enrichment analyses applying the tools Analysis of Gene Lists [*AnGeLi*] (Bitton, et al., 2015) and g:Profiler (Raudvere, et al., 2019), used to systematically

generate Gene Ontology (GO) enrichments to identify biological processes in which those genes are involved. In this regard, the gene clusters generated by the software are not mutually exclusive between each other due to the different biological processes that a product of a single gene could have (The Gene Ontology Consortium, 2015).

There were more downregulated (DR) genes than upregulated (UR) in *gaf1Δ* cells with respect to the wild type after torin1 treatment. Interestingly, the 90 genes UR in the mutant were DR in wild type cells after treatment, indicating that in normal conditions they are repressed by Gaf1 upon TORC1 inhibition (figure 32).

This fraction of genes was predominantly enriched in processes related to anabolism, including: biosynthesis (61 genes, $p = 9.4 \times 10^{-10}$), cytoplasmic translation (31 genes, $p = 1.6 \times 10^{-15}$), and ribosome biogenesis (19 genes, $p = 1.9 \times 10^{-3}$), together with 25 genes encoding ribosomal proteins (figure 36). The list also includes genes that are repressed during stress responses [43 genes, $p = 1.4 \times 10^{-20}$] (Chen, et al., 2003). 78% of these genes have an ortholog in Humans [70 genes $p = 2.2 \times 10^{-14}$] (Lock, et al., 2019).

The eukaryotic genome comprises 10% of genes and 90% of intergenic regions (Shabalina, et al., 2001). In fission yeast ~46% of the genes have introns (Wood, et al., 2002). The frequency of essential genes for cell viability that contain ≥ 1 intron(s) is significantly higher than essential genes without introns [33% vs. 21% respectively, $p = 1 \times 10^{-14}$] (Kim, et al., 2010). This is because essential genes

are less likely to be rapidly regulated in contrast to genes that contain less introns, which are rapidly regulated and are involved in stress responses, cell proliferation, differentiation or development (Jeffares, et al., 2008).

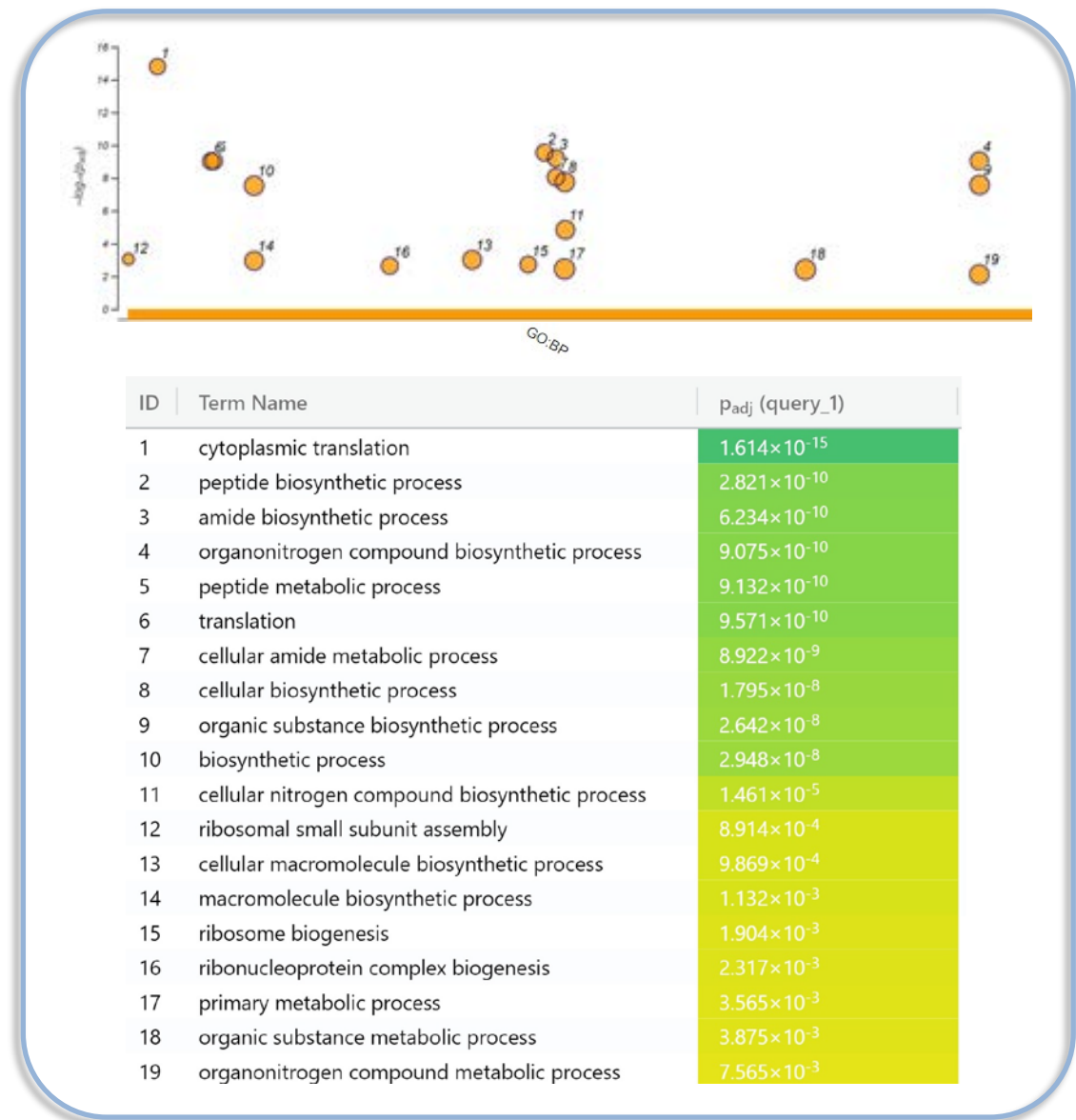


Figure 36. Functional enrichments among differentially expressed genes using g:Profiler. Visualisation of GO Biological Processes enriched among the 90 genes upregulated in *gaf1Δ* cells with respect to the wild type after torin1 treatment in rich media. The size of the circles represents the ratio between the number of genes in the gene list and the total number of genes in the GO category.

Further scrutiny of the 90 genes UR in torin1-treated *gaf1Δ* cells, revealed that regarding cell viability 31% were essential (28 genes, $p = 1.3 \times 10^{-67}$), and 60%

were not essential (54 genes, $p = 2.7 \times 10^{-104}$), no data was available for the other 9% [8 genes] (Lock, et al., 2019). In terms of intronic regions, a fraction of 40% contained one or more introns (36 genes, $p = 2.3 \times 10^{-71}$), and 60% did not have introns [54 genes, $p = 2.7 \times 10^{-104}$] (Lock, et al., 2019).

From the group of intron-containing genes, only 33% were essential (12/36 genes, $p = 5.3 \times 10^{-20}$), and 61% were not essential (22/36 genes, $p = 8.0 \times 10^{-37}$). Among the intron-less genes, a similar fraction of 30% were essential (16/54 genes, $p = 5.7 \times 10^{-26}$), and 59% were not essential (32/54 genes, $p = 3.3 \times 10^{-54}$), no data was available for the remaining 11% (8 genes) [figure 37] (Lock, et al., 2019).

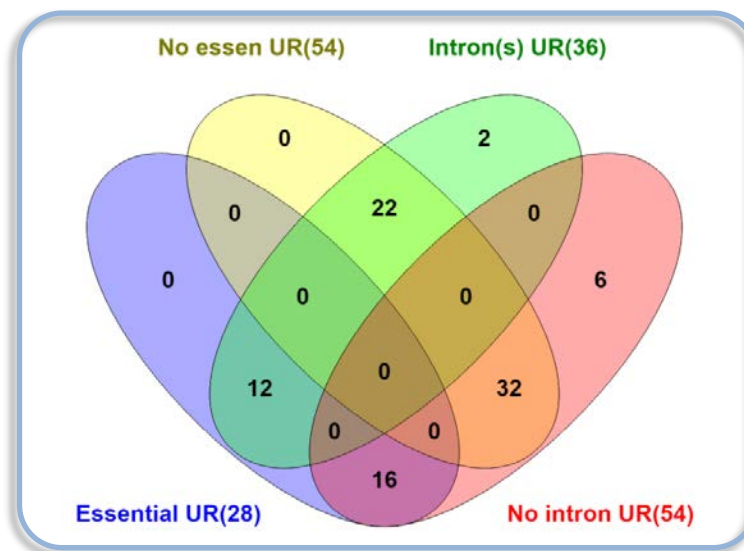


Figure 37. Venn diagram using Venny 2.1 showing overlaps between upregulated genes essential (purple) / non-essential (yellow) vs genes with intron[s] (green) / intron-less (pink) in *gaf1Δ* cells with respect to the wild type after torin1 treatment in rich media.

Following this classification, the UR genes in torin1-treated *gaf1Δ* cells revealed that the essential genes with and without intronic regions showed similar enrichments, where the entire set of genes of each category were related to cell viability (Bitton, et al., 2015).

In contrast, the non-essential genes with and without intron(s) contained the fraction of genes predominantly enriched in processes related to anabolism, involving: cellular biosynthetic process (17/22 genes with introns, $p = 5.1 \times 10^{-4}$, and 23/32 intron-less genes, $p = 6.5 \times 10^{-5}$), and cytoplasmic translation (13/22 genes with introns, $p = 1.4 \times 10^{-7}$, and 11/32 intron-less genes, $p = 1.0 \times 10^{-3}$), among other processes (Bitton, et al., 2015). Interestingly, within the non-essential group, only the genes containing introns were enriched in ribosome biogenesis (4/22 genes, $p = 2.9 \times 10^{-4}$), macromolecule biosynthetic process (15/22 genes, $p = 7.0 \times 10^{-4}$), and protein metabolic process (15/22 genes, $p = 1.2 \times 10^{-3}$), whereas the intron-less genes were exclusive for cellular amino acid metabolism [8/32 genes, $p = 8.3 \times 10^{-4}$] (Bitton, et al., 2015).

These results indicate that during TORC1 inhibition, Gaf1 represses highly expressed genes used for protein synthesis, which may be rapidly regulated to adjust for survival to environmental challenges. In this sense, conserved pathways controlling stress resistance have been intrinsically linked to longevity in yeast, worms, fruit flies and mammals as they prevent damage and ensure survival during periods of starvation (Fabrizio & Longo, 2003).

The 108 genes that were DR in *gaf1Δ* with respect to the wild type cells after torin1 treatment, were typically UR in wild type cells after treatment, indicating that in normal conditions they are induced by Gaf1 upon TORC1 inhibition. These genes were enriched in different metabolic processes of small molecules, involving: organonitrogen compounds (43 genes, $p = 4.6 \times 10^{-14}$), organic acids (20 genes, $p = 0.001$), amino acids (18 genes, $p = 4.1 \times 10^{-5}$), and urea [6 genes,

$p = 7.3 \times 10^{-5}$] (figure 38). A total of 57% of these DR genes have an ortholog in Humans [62 genes $p = 3.7 \times 10^{-114}$] (Lock, et al., 2019).

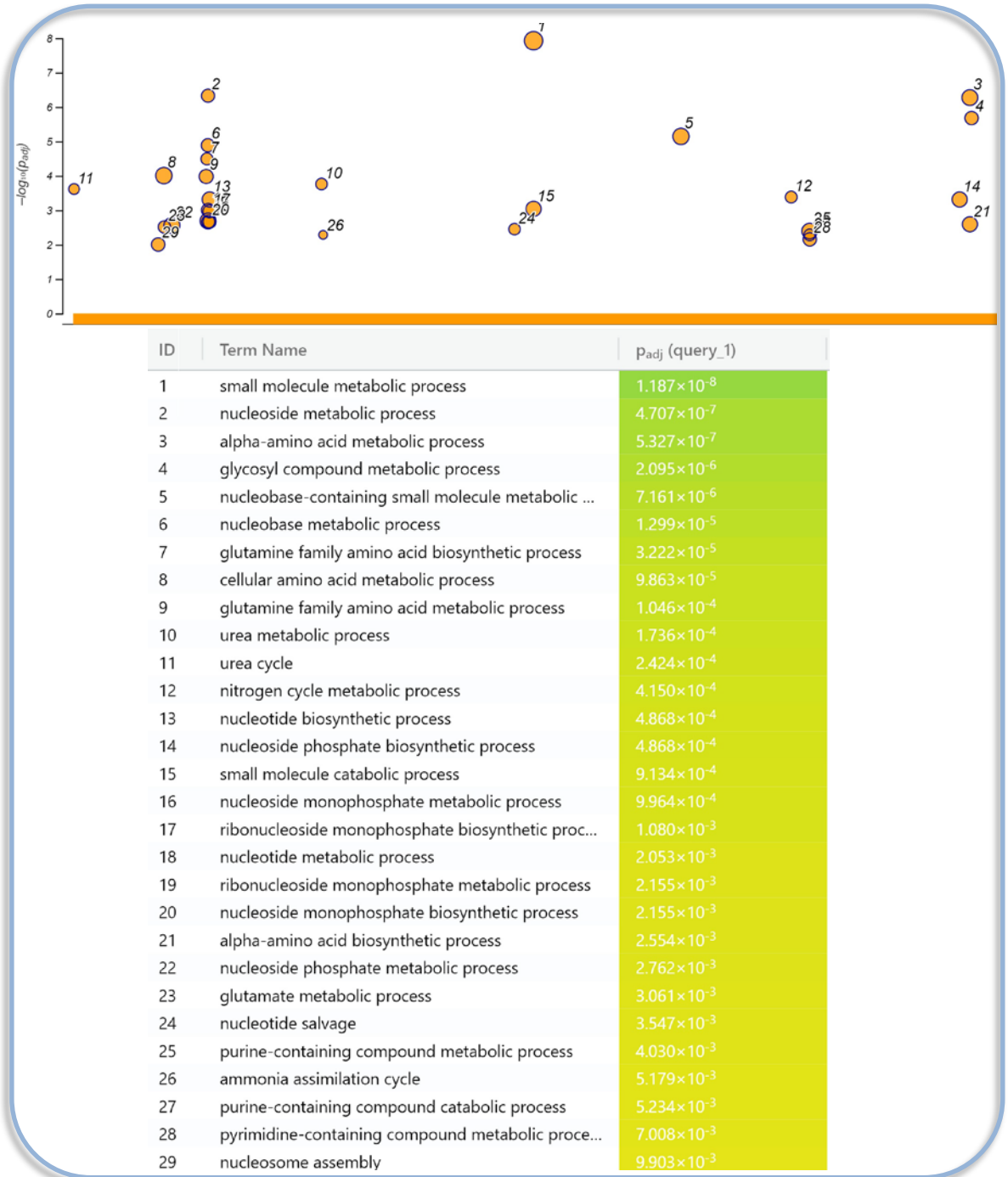


Figure 38. Functional enrichments among differentially expressed genes using g:Profiler. Visualisation of GO Biological Processes enriched among the 108 genes downregulated in *gaf1Δ* cells with respect to the wild type after torin1 treatment in rich media. The size of the circles represents the ratio between the number of genes in the gene list and the total number of genes in the GO category.

There was a considerable overlap between these DR genes and genes that are routinely expressed during the cell cycle [41 genes, $p = 1.6 \times 10^{-12}$] (Marguerat, et al., 2006), including 9 histone genes. Consistently, many of these DR genes have been reported to be induced by nitrogen starvation [42 genes, $p = 1.0 \times 10^{-25}$] (Mata, et al., 2002).

The list contains 8% of essential genes (9 genes, $p = 5.9 \times 10^{-16}$), and 84% of non-essential genes (91 genes, $p = 2.4 \times 10^{-178}$), no data was available for the remaining 8% [8 genes] (Lock, et al., 2019). Regarding intronic regions, a fraction of 22% had one or more introns (24 genes, $p = 8.7 \times 10^{-6}$), and 78% did not have introns [84 genes, $p = 1.1 \times 10^{-161}$] (Lock, et al., 2019).

From the group of intron-containing genes, only 21% were essential (5/24 genes, $p = 1.8 \times 10^{-10}$), and 75% were not essential (18/24 genes, $p = 1.7 \times 10^{-49}$), no data was available for the other 4% (1 gene). Among the intron-less genes, 5% were essential (4/84 genes, $p = 4.8 \times 10^{-2}$), and 87% were not essential (73/84 genes, $p = 2.3 \times 10^{-152}$), no data was available for the remaining 8% (7 genes) [figure 39] (Lock, et al., 2019).

In torin1-treated *gaf1Δ* cells the DR essential genes with intron(s) were enriched in processes required for DNA synthesis including: nucleoside monophosphate metabolic processes (3/5 genes, $p = 5.4 \times 10^{-4}$), ribose phosphate biosynthetic process (3/5 genes, $p = 3.0 \times 10^{-3}$), nucleotide biosynthetic process (3/5 genes, $p = 7.7 \times 10^{-3}$), nucleoside phosphate biosynthetic process [3/5 genes, $p = 7.7 \times$

10⁻³] (Raudvere, et al., 2019). The essential genes without intron(s) were not enriched in any biological process (Bitton, et al., 2015; Raudvere, et al., 2019).

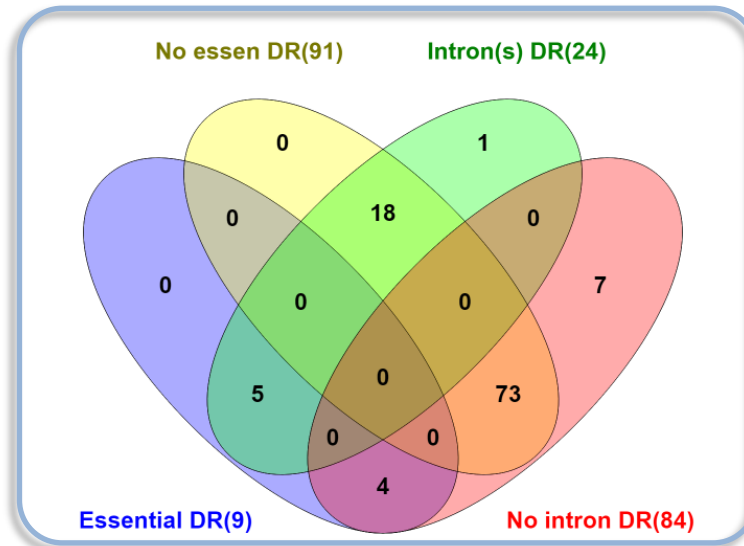


Figure 39. Venn diagram using Venny 2.1 showing overlaps between downregulated genes essential (purple) / non-essential (yellow) vs genes with intron[s] (green) / intron-less (pink) in *gaf1Δ* cells with respect to the wild type after torin1 treatment in rich media.

The DR non-essential genes with intron[s] (18 genes) did not show significant enrichments (Bitton, et al., 2015; Raudvere, et al., 2019). In contrast, the largest group of DR genes were non-essential with no introns. They were enriched in several biological processes including: organonitrogen compound metabolic- (26/73 genes, $p = 1.5 \times 10^{-9}$) and catabolic processes (13/73 genes, $p = 1.0 \times 10^{-9}$), amino acid metabolic process (14/73 genes, $p = 1.1 \times 10^{-7}$), nitrogen cycle metabolic process (6/73 genes, $p = 3.1 \times 10^{-6}$), arginine metabolic (5/73 genes, $p = 1.1 \times 10^{-4}$) and biosynthetic processes (4/73 genes, $p = 5.0 \times 10^{-4}$), catabolic processes [cellular amino acid, small molecule, organic acid] (22/73 genes, $p = 1.4 \times 10^{-4}$), cellular amino acid biosynthetic process (9/73 genes, $p = 4.8 \times 10^{-4}$), DNA packaging (8/73 genes, $p = 2.4 \times 10^{-3}$), and nitrogen compound metabolic process [36/73 genes, $p = 6.3 \times 10^{-3}$] (Bitton, et al., 2015).

Characteristically, the most abundant genes with GO enrichments within the UR and DR genes were the non-essential without intronic regions (32/90 and 73/108 respectively). The UR genes were exclusive for processes involved in anabolism, whereas the DR genes were unique for several catabolic processes, which are upregulated in torin1-treated wild type cells when Gaf1 is present. This set of genes include genes previously described as Gaf1-targets responsible for survival responses when TORC1 is not active, including nitrogen stress response and amino acid permeases genes (Laor, et al., 2015; Ma, et al., 2015).

This fraction of genes contained relevant candidates that could be dictating the growth arrest produced by torin1 treatment in wild type cells, which does not occur in *gaf1Δ* mutants as shown in chapter 4. The genetic basis of the torin1-resistance phenotype of *gaf1Δ* cells will be further explored in chapter 6 through the analysis of genetic interactions.

Additionally, the fact that only the non-essential genes without introns showed the most diverse range of GO enrichments, suggests that this could be a mechanism to enhance resistance to stress and survival avoiding selection against them, in comparison to the more “exposed” essential genes subjected to stringier controls from natural selection (Chorev & Carmel, 2012).

These results are consistent with reports showing that most of the stress-response genes with rapid changes in expression levels, contain significantly less intronic regions in a conserved manner (Jeffares, et al., 2008). Nevertheless, emerging data from a range of organisms revealed that for a specific set of highly-

expressed ubiquitous genes, the most important regulatory sequences controlling their expression are situated within their introns rather than in the promoters. Such expression-controlling introns strongly stimulate accumulation of mRNA downstream of the transcription start site, even in the absence of promoters. Conversely, they could also repress genes through heterochromatin structures (Rose, 2019; Rose, et al., 2011).

Even though the diversity of mechanisms by which introns regulate gene expression remain to be explored, their study could go beyond the classical model describing the delay in regulatory responses produced by introns (Jeffares, et al., 2008; McKnight & Miller, 1976), conferring alternative regulatory roles for intronic regions. Thus, understanding these mechanisms could provide novel approaches particularly useful in clinical studies of genetic diseases and for therapeutic applications including protein production in biotechnology. These types of introns affect gene expression by either reducing it (Gromak, 2012) or enhancing it, only controlling the transcription unit in which they are located (Rose, 2019; Rose, et al., 2011).

Overall, these results suggest that Gaf1 control transcriptional programs that balance the metabolism of amino acids and other molecules, possibly by recycling nutrients under detrimental conditions that do not allow rapid proliferation. A similar pattern of gene expression has been described in the budding yeast controlled by the GATA transcription factors Gln3 and Gat1 during TORC1 inhibition (Georis, et al., 2011; Kulkarni, et al., 2006).

This is consistent with the reported role of Gaf1 as a regulatory element for the TOR-mediated transcription of amino acid permeases upon nitrogen depletion to control amino acid homeostasis. Previous studies indicate that inhibition of TORC1 by rapamycin treatment did not increase transcriptional activity of Isp5 [amino acid permease] (Ma, et al., 2015), however treatments with caffeine & rapamycin (Rallis, et al., 2013), and torin1 (Ma, et al., 2015) induced *isp5* in wild type cells. This is in agreement with the downregulation of *isp5* in torin1-treated *gaf1Δ* cells detected in the present study.

Nevertheless, reports indicate that torin1 treatment in *tor2*-temperature sensitive mutants (TORC1 defective) downregulates *isp5*, revealing that the precise role of Tor1 (core component of TORC2) in this process is not completely understood, one possibility is that this inhibitory effect on *isp5* depends on Tor1 activity (Ma, et al., 2013; Ma, et al., 2015). However, nuclear translocation of Gaf1 is not significantly induced in *tor1Δ* mutants in minimal medium, as well as its dephosphorylation (required for the translocation) which is insensitive to glucose depletion, and is specifically triggered in response to nitrogen stress (Laor, et al., 2015). Future studies will clarify if such repression could be due to the effectiveness of the compound rather than the roles of TORC1 and TORC2 over Gaf1 transcriptional activity.

Additionally, when nutrients are abundant, TORC1 phosphorylates Atg13 (autophagy associated protein kinase) to repress its association with Atg1 (autophagy serine/threonine protein kinase) to block autophagy (Kamada, et al., 2010). In the present study, the expression of *atg1* was downregulated in *gaf1Δ*

mutant after torin1 treatment, but this gene was normally expressed in wild type cells (where Gaf1 is present), and it was not detected among the Gaf1 target genes, revealing an indirect positive-regulation of autophagy mediated by Gaf1 activity.

This notion is further supported by the downregulation of *isp6* in torin1-treated *gaf1* Δ cells observed in the present study, and the direct binding of Gaf1 (upon its activation) to its promoter (Rodríguez-López, et al., 2020). This gene encodes Isp6, a vacuolar serine protease with the ortholog Prb1 in the budding yeast (Kohda, et al., 2007). This protein is specifically expressed during nitrogen depletion to induce bulk protein degradation to provide nitrogen through autophagy (Nakashima, et al., 2006).

Taken together, these findings indicate that Gaf1 regulates physiological changes that support the cell cycle arrest caused by TORC1 inhibition (Laor, et al., 2015; Rodríguez-López, et al., 2020). They also open the discussion for future studies focused on the effects of TORC2 over Gaf1 activity to complement the classically described and established TORC1-dependent regulation of this transcription factor.

5.3. *Transcriptional network controlled by Gaf1*

The gene lists obtained in the present study with microarray analyses that identified Gaf1-dependant gene expression profiles, were further explored by integrating them with the gene lists from ChIP-seq experiments conducted by collaborators, which detected the Gaf1-binding sites across the genome of *S.*

pombe under equal experimental conditions (Rodríguez-López, et al., 2020). This approach allowed to evaluate the level of expression of the transcriptional targets of Gaf1, and interpret the direct and indirect regulation of the Gaf1-transcriptional profile.

There was an increase in the number of Gaf1-bound promoters from 165 before torin1 treatment to 454 after the treatment in rich media (Rodríguez-López, et al., 2020). These two datasets were compared to differentiate basally-bound sites by Gaf1, from those specifically bound after TORC1 inhibition. This revealed that Gaf1 binds to 93 genes before and after torin1 treatment (figure 40).

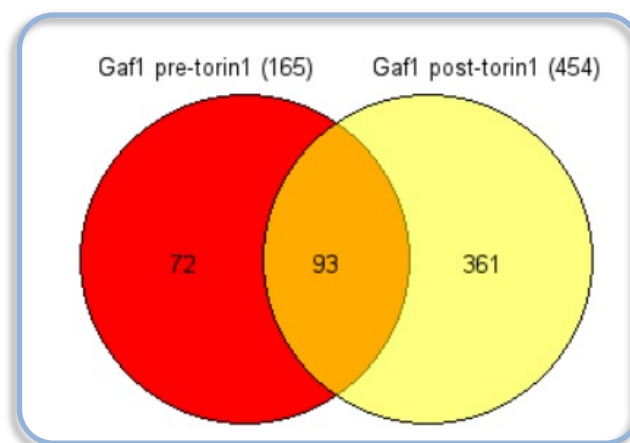


Figure 40. Venn diagram using Gene Venn showing overlaps between Gaf1-binding sites detected before (red) and after torin1 treatment (yellow) in rich media.

The GO enrichments for this fraction of 93 genes indicated that they are involved in translational elongation (14/93 genes, $p = 3.0 \times 10^{-4}$), glucose metabolic process (6/93 genes, $p = 2.4 \times 10^{-3}$), glycolysis (4/93 genes, $p = 6.8 \times 10^{-3}$), and NADH regeneration [4/93 genes, $p = 8.4 \times 10^{-3}$] (Bitton, et al., 2015).

The enrichment of glucose-related metabolic processes may be reflecting a possible influence of TORC2 activity over Gaf1 transcriptional function under

normal conditions as mentioned above. Furthermore, this group of 93 genes includes *isp7*, a putative 2-oxoglutarate (2OG)-Fe(II)-dependent oxygenase gene that was not differentially expressed in torin1-treated *gaf1Δ* cells. *Isp7* is a regulator of starvation-induced amino acid permease gene transcription that requires TORC2 for its expression (Laor, et al., 2014; Laor, et al., 2015). This is consistent with evidence indicating that a sub-population of Gaf1 resides in the nucleus under nitrogen-rich conditions, demonstrated by the transcription of this gene (Laor, et al., 2015).

From the 93 genes constantly targeted by Gaf1 independently of TORC1 activity, only 8% were essential for cell viability (7/93 genes, $p = 1.0 \times 10^{-3}$), and 40% were non-essential (37/93 genes, $p = 6.8 \times 10^{-43}$), no information was available for the remaining 52% [49 genes] (Lock, et al., 2019). Regarding the presence of introns, 10% of these genes contained introns (9/93 genes, $p = 4.0 \times 10^{-5}$), and 90% were intron-less [84/93 genes, $p = 1.6 \times 10^{-161}$] (Bitton, et al., 2015). Even though this suggests that the majority of these genes may be involved in rapid responses for survival, a mere 7% were downregulated (7/93 genes, $p = 3.0 \times 10^{-3}$), and 4% were upregulated (4/93 genes, $p = 8.0 \times 10^{-2}$) in torin1-treated *gaf1Δ* cells. From this gene list, 17% have an ortholog in Humans [16/93 genes, $p = 4.6 \times 10^{-12}$] (Lock, et al., 2019).

In this sense, the comparison between the genes targeted by Gaf1 before and after its activation, against the genes that showed differential expression (higher or lower) in torin1-treated *gaf1Δ* mutants, revealed that there are 19 genes which transcription is not Gaf1-specific, as they are indirectly downregulated (12 genes, $p = 1.6 \times 10^{-5}$) and upregulated (7 genes, $p = 2.5 \times 10^{-3}$) in the mutant (where

Gaf1 is absent). There are 146 Gaf1-target genes that were not differentially expressed in torin1-treated *gaf1Δ* mutants (figure 41).

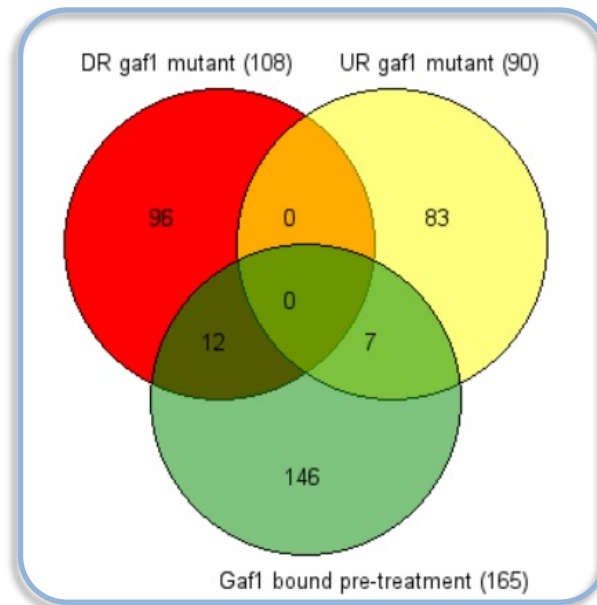


Figure 41. Venn diagram using Gene Venn showing overlaps between Gaf1-specific targeted genes before torin1 treatment (green) and downregulated (red) / upregulated (yellow) genes in torin1-treated *gaf1Δ* mutants with respect to wild type cells in rich media.

The comparison between the 146 Gaf1-specific target genes before torin1 treatment with the 93 genes to which Gaf1 binds before and after treatment, produced a fraction of 64 genes bound by Gaf1 before its complete translocation to the nucleus. In consistency with a mechanism of basal expression, these genes were significantly enriched only in cytoplasmic translational elongation (14/64 genes, $p = 2.0 \times 10^{-6}$), and single-organism process [11/64 genes, $p = 7.1 \times 10^{-3}$] (Bitton, et al., 2015).

The 146 Gaf1-specific target genes contained 7% of essential genes (10/146 genes, $p = 2.6 \times 10^{-16}$), and 32% of non-essential genes (47/146 genes, $p = 4.9 \times 10^{-39}$), no information was available for the remaining 61% [89 genes] (Lock, et

al., 2019). Regarding intronic regions, 15% contained introns (22/146 genes, $p = 3.7 \times 10^{-6}$), and 85% were intron-less [124/146 genes, $p = 3.7 \times 10^{-6}$] (Bitton, et al., 2015).

The integration between these gene lists showed a similar distribution as described above, where intron-less non-essential genes were the most abundant (31/47 genes) compared to the other groups (figure 42). Interestingly, the comparison also revealed that 91% of the intron-less genes (79/87 genes) were related to RNA processes, including 25 tRNAs genes for 15 amino acids out of the 20 available in nature (excluding lysine, methionine, phenylalanine, serine, and tryptophan).

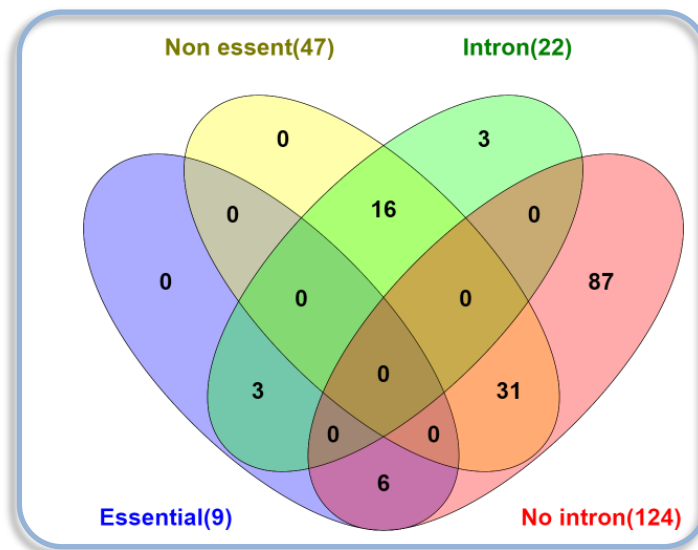


Figure 42. Venn diagram using Venny 2.1 showing overlaps between essential (purple) / non-essential (yellow) genes vs genes with intron[s] (green) / intron-less (pink) from 146 Gaf1-specific target genes before its nuclear translocation induced by torin1 treatment in rich media.

This highlights the importance of dissecting gene lists to assess genes individually as a complement to GO enrichments which rely on previously curated records included in the data bases. This is because some of the genes from the lists are not annotated as belonging to any specific gene ontology

categories even though they perform relevant functions or are involved in important physiological processes such as contributing towards protein translation.

The comparison between the genes bound by Gaf1 after torin1 treatment with the genes that showed differential expression (higher or lower) in *gaf1Δ* compared to wild type cells after treatment, uncovered 43 non-specific Gaf1 target genes that are indirectly downregulated (32 genes, $p = 3.4 \times 10^{-10}$) and upregulated (11 genes, $p = 1.7 \times 10^{-2}$) in the absence of Gaf1 (figure 43).

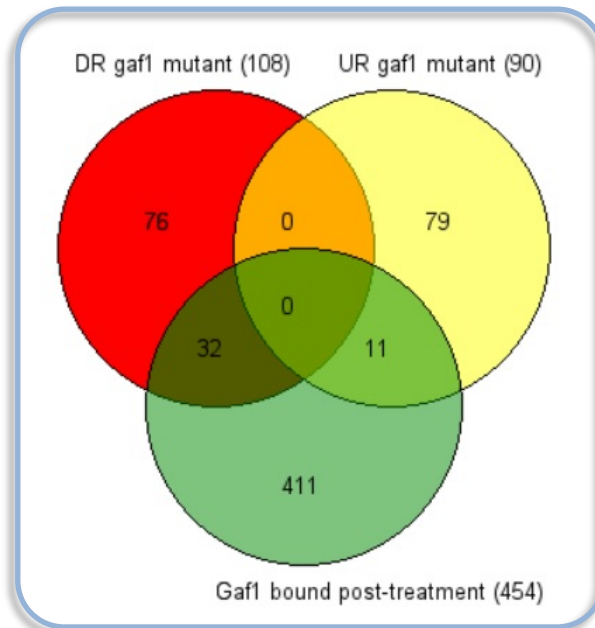


Figure 43. Venn diagram using Gene Venn showing overlaps between Gaf1-specific target genes after torin1 treatment (green) and downregulated (red) / upregulated (yellow) genes in *gaf1Δ* mutants with respect to wild type cells in rich media.

The 411 Gaf1-specific target genes after torin1 treatment, showed several GO enrichments including: cytoplasmic translational elongation (81/411 genes, $p = 1.7 \times 10^{-47}$), cellular component organisation or biogenesis (43/411 genes, $p = 3.7 \times 10^{-17}$), RNA processing (4/411 genes, $p = 1.6 \times 10^{-8}$), ribonucleoprotein complex biogenesis (5/411 genes, $p = 2.5 \times 10^{-5}$), cellular nitrogen compound

metabolic process (65/411 genes, $p = 2.4 \times 10^{-4}$), ribosome biogenesis (5/411 genes, $p = 1.2 \times 10^{-3}$), and cellular catabolic process (16/411 genes, $p = 7.5 \times 10^{-3}$), among others. From this gene list, 22% have an ortholog in Humans [92/411 genes, $p = 2.1 \times 10^{-29}$] (Lock, et al., 2019).

This fraction of 411 genes contained 8% of essential genes (32/411 genes, $p = 2.8 \times 10^{-36}$), and 36% were not essential (150/411 genes, $p = 3.5 \times 10^{-68}$), no information was available for 56% [229 genes] (Lock, et al., 2019). Regarding the presence of introns, 16% contained one or more introns (66/411 genes, $p = 6.8 \times 10^{-18}$), and 84% were intron-less [345/411 genes, $p = 6.8 \times 10^{-18}$] (Bitton, et al., 2015).

The integration between these gene lists showed a similar pattern as described above, with intron-less non-essential genes being more abundant (116/150 genes) than the other groups (figure 44).

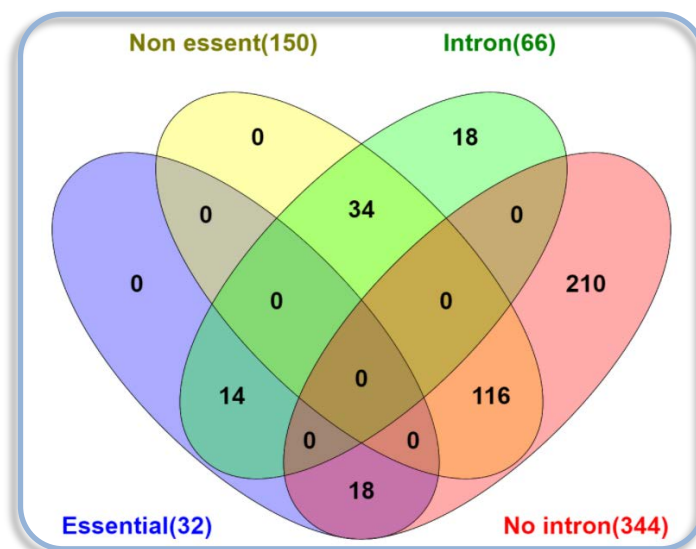


Figure 44. Venn diagram using Venny 2.1 showing overlaps between essential (purple) / non-essential (yellow) genes vs genes with intron[s] (green) / intron-less (pink) from 411 Gaf1-specific target genes after its nuclear translocation induced by torin1 treatment in rich media.

The comparison uncovered that 61% of the intron-less genes (210/344 genes) are undetermined regarding essentiality for cell viability (Lock, et al., 2019). Interestingly, within the 411 Gaf1-specific target genes after its activation, the latter fraction of 210 genes contained GO enrichments for processes mainly related to translation (75/210 genes, $p = 8.5 \times 10^{-25}$) and protein metabolic process (75/210 genes, $p = 2.4 \times 10^{-4}$), whereas the remaining group of 201 genes were mostly enriched in small molecule metabolic process (40/201 genes, $p = 2.0 \times 10^{-4}$) and transmembrane transport [23/201 genes, $p = 6.5 \times 10^{-3}$] (Lock, et al., 2019).

The binding sites of Gaf1 after torin1 treatment consisted of 244 protein-coding genes and 210 non-coding genes. The 244 protein-coding genes were significantly enriched in genes induced by nitrogen limitation (40 genes, $p = 1.6 \times 10^{-11}$), periodically expressed during the cell cycle (53 genes, $p = 4.5 \times 10^{-6}$), metabolic processes of organonitrogen compounds (55 genes, $p = 1.4 \times 10^{-6}$), including nucleotides (24 genes, $p = 9.0 \times 10^{-6}$) and organic acids (34 genes, $p = 3.0 \times 10^{-5}$) [figure 45] (Bitton, et al., 2015).

Consistently, these Gaf1-target genes presented similar functional enrichments to the gene expression profile induced by Gaf1 (downregulated in *gaf1* Δ cells), indicating that most of the protein-coding genes from this section are upregulated by Gaf1 during TORC1 inhibition.

It was detected that Gaf1 binds to the promoters of 20 genes encoding transcription factors (Rodríguez-López, et al., 2020). In the present study, these

factors were induced in wild type cells after TORC1 inhibition in contrast to torin1-treated *gaf1Δ* cells, where some of them were downregulated. The function of the majority of these factors is related to stress responses and regulation of the cell-cycle (Lock, et al., 2019).

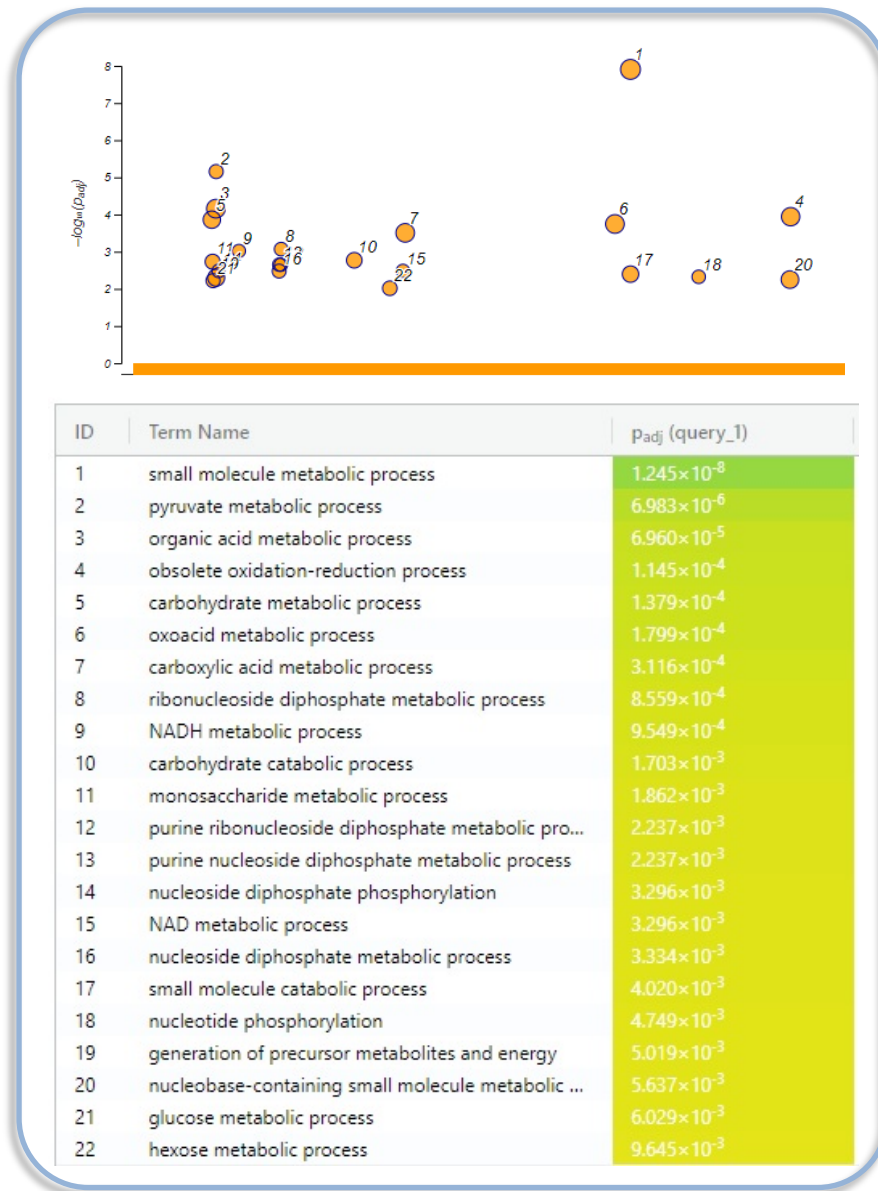


Figure 45. Functional enrichments using g:Profiler. Visualisation of GO Biological Processes enriched among 244 protein-coding genes targeted by Gaf1 after torin1 treatment in rich media. The size of the circles represents the ratio between the number of genes in the gene list and the total number of genes in the GO category.

These genes were classified in three categories, some of them were part of the 37 protein-coding genes bound by Gaf1 before and after torin1 treatment that were not differentially expressed in torin1-treated *gaf1Δ* mutant. They included several genes encoding: Atf1 which represses genes that induce translation during stress (Chen, et al., 2008; Wilkinson, et al., 1996), the positive regulator of cell adhesion during stationary phase Cbf12 (Prevorovský , et al., 2009), the repressor Fep1, which controls genes involved in the reductive/non-reductive iron transport system (Pelletier, et al., 2003), the inducer Hsr1, which supports gene expression in response to oxidative stress (Chen, et al., 2008), and Isp7, a negative regulator of nitrogen starvation-induced amino acid permease genes (Laor, et al., 2014).

The binding to these transcription factors supports the idea that Gaf1 may indirectly control some Gaf1-dependent genes through other transcription factors. This was illustrated above with the integration between expression profile of torin1-treated *gaf1Δ* cells, compared to the Gaf1 binding sites before and after torin1 treatment. Additionally, such comparison provided relevant information about the Gaf1 function as a repressor of non-coding sequences relevant for stress resistance and survival.

Even though it has been reported that Gaf1 inhibits the expression of several genes that promote translation and differentiation, including the main transcription factor *ste11*, responsible for the regulation of the switch from cellular proliferation to sexual/meiotic differentiation (Kim, et al., 2012; Mata & Bähler , 2006), this gene was absent in both the direct Gaf1-binding targets (Rodríguez-

López, et al., 2020), and amongst the differentially expressed genes observed in torin1-treated *gaf1Δ* mutant in the present study, suggesting that there are alternative mechanisms to indirectly regulate Gaf1-target genes.

An example of this indirect regulation may occur through the binding of Gaf1 to *atf1*, which encodes a co-factor in the Atf1-Pcr1 heterodimeric transcription factor, also required for the expression of *ste11* (Kim, et al., 2012). Interestingly, Gaf1 may be regulating this gene downstream of TORC2, which is required for sexual differentiation (Kawai, et al., 2001; Weisman & Choder, 2001). Previous reports suggested that this complex may positively regulates the expression of *ste11* (Otsubo & Yamamoto, 2012).

Consistently, the transmembrane transporter *isp4* and two of the negatively regulated target genes of Isp7, the amino acid transmembrane transporters *per1* and *isp5*, were not bound by Gaf1 but were downregulated in torin1-treated *gaf1Δ* mutant, however, *isp7* was not affected, revealing the Gaf1-induced indirect regulation.

Another category of relevant transcription factors bound by Gaf1 only after its activation but not differentially expressed in torin1-treated *gaf1Δ* mutant includes: Klf1 involved in survival during stationary phase by enhancing the differentiation signal and repressing metabolism for growth (Shimanuki, et al., 2013), the transcriptional repressor Loz1, which controls zinc homeostasis (Corkins, et al., 2013), Php3 involved in iron homeostasis (Mercier, et al., 2006), and Sep1 that regulates periodic expression of mitotic genes (Rustici, et al., 2004).

The last group included genes that were downregulated in torin1-treated *gaf1Δ* mutant but showed miscellaneous binding. Some examples include the gene encoding Pap1, involved in the regulation of oxidative stress responses, drug and heavy metal resistance (Chen, et al., 2008), which is bound by Gaf1 only after its induction. Similarly, the amino acid transmembrane transporters *fur4* for uracil (Lock, et al., 2019), and SPAC1039.01 [generic] (Lock, et al., 2019) follow the same pattern. In contrast, the transcription factor Fil1, required for transcriptional responses to amino acid starvation (Duncan, et al., 2018), which is bound by Gaf1 before and after its induction.

This complex network of Gaf1-indirect transcriptional regulation of starvation genes and transcription factors demonstrate the extensive rewiring occurred during the evolution for these key responses to provide survival, highlighting the plasticity of the transcriptional network controlled by Gaf1. Future studies focusing on further classification of such target genes, their mechanism of expression (direct/indirect regulation), and their genetic interactions, will provide matrixes of information for the establishment of genetic clusters or categories based on their characteristic patterns of expression, which could help to classify and predict the function of specific genetic pathways and their modulation.

From the 210 non-coding genes targeted by Gaf1 after its induction, 93% of these genes were shared with the 210 intron-less genes that do not contain annotations regarding essentiality for cell viability described above (195/210 genes, $p = 5.4 \times 10^{-314}$). The GO enrichments for biological processes between these two groups were highly similar (Bitton, et al., 2015). Both gene lists shared large non-coding

RNAs, small nucleolar RNA (snoRNA) involved in tRNA regulation, and remarkably 82 tRNA genes for 18 amino acids out of 20 available, excluding cysteine and phenylalanine which were present in the tRNA gene pool bound by Gaf1 before torin1 treatment. The total count of tRNA genes in *S. pombe* is 174, which are needed to decode all codons present in this model organism (Wood, et al., 2002).

Similar to the pattern of gene expression described during major biological events such as meiosis and sporulation, which require hundreds of neighbouring genes (close to telomeres) to be globally regulated in successive waves of transcription (Mata, et al., 2002), the induction of Gaf1 by torin1 produces its binding near the transcription start sites of all tRNA genes that are clustered in the centromere of chromosome II in *S. pombe*, indicating that the binding occurs in genes transcribed by both RNA Polymerase II and tRNA genes transcribed by RNA Polymerase III (Rodríguez-López, et al., 2020). Previous studies reported the absence of protein-coding genes in the centromeres of this model organism, where tRNA genes are found (Wood, et al., 2002). Conversely, the function of the Gaf1 orthologs in the budding yeast Gln3 and Gat1 exclude the regulation of tRNAs genes (Kuroda , et al., 2019; Scherens, et al., 2006).

This could be a potential mechanism used by Gaf1 to reduce translation during TORC1 inhibition, via binding to tRNA genes in order to repress their expression (Rodríguez-López, et al., 2020). This is consistent with the upregulation of genes involved in translation identified in torin1-treated *gaf1Δ* mutant in the present study, they include: the translation initiation factors eIF4A, eIF1A, eIF3b, the

translation elongation factor EF-1 (β & γ subunits), and 25 ribosomal proteins. This set of genes would be otherwise repressed in the presence of active Gaf1 when TORC1 is inactive.

Previous reports described that the downregulation of precursor tRNAs is required for TORC1 inhibition in *S. pombe*, suggesting that tRNAs could act upstream of TORC1 (Otsubo Y, 2018). Conversely, the data integration performed in this section uncovered a mechanism controlled by Gaf1 to bind the promoters of tRNA genes downstream of TORC1, indicating a regulatory feedback that involves precursor tRNAs, TORC1, and Gaf1, to balance the expression of tRNAs depending on physiological requirements (Rodríguez-López, et al., 2020).

The results revealed a novel transcriptional role of Gaf1 which after TORC1 inactivation, inhibits the expression of RNA Pol II-subjected genes functioning in processes related to translation and metabolism, and uncovered the binding to the promoters of RNA Pol III-mediated tRNA genes to represses their expression (Rodríguez-López, et al., 2020), conferring Gaf1 its essentiality for growth suppression upon TORC1 inactivation and providing a mechanism for transcriptional control of global protein translation that prolongs lifespan (figure 46).

Altogether, Gaf1 elicit direct and indirect inhibition of genes functioning in protein translation (present study) as well as tRNA genes by direct binding (Rodríguez-López, et al., 2020). A possible mechanism used by this transcription factor to

repress tRNA genes activity, is by the recruitment of the conserved histone deacetylase Clr6 (orthologue of human HDAC1/2 and budding yeast Rpd3) responsible for providing epigenetic tags for the repression of transcription (Rodríguez-López, et al., 2020). This notion is based on previous studies that identified potential loading sites for the components of the Clr6 multiprotein complexes at tRNA loci (Zilio, et al., 2014). Parallely, Gaf1 also induces genes functioning in metabolic pathways for nitrogen-containing molecules to allow survival during reduced global protein translation, which is proven to be a phenotype beneficial for longevity in all organisms tested (Filer, et al., 2017; Kaeberlein & Kennedy, 2011; Rallis, et al., 2013).

The repression exerted by Gaf1 over different translation-inducing genes, may contribute to the lifespan extension observed when translation is downregulated upon TORC1 inhibition. This finding confers Gaf1 a novel transcriptional-based control of translation and metabolism downstream of TORC1 that is essential to achieve the growth inhibition triggered by reduced TORC1 activity. It is relevant to mention that this Gaf1-transcriptional branch operates in addition to other translational regulators such as S6K [figure 46] (Ma & Blenis, 2009; Nakashima, et al., 2010).

It has been proven that the downregulation of RNA Pol III extends lifespan in several models (yeast, worms, flies), and is required for the lifespan extension mediated by TORC1 inactivation (Filer, et al., 2017). Considering that there is a limited number of general transcription factors that indirectly control RNA Pol III transcription including TFIIB, TFIIC, and TBP (Hummel , et al., 2019), the

coactivators PNC, MYC, and its repressor Maf1 (Campbell & White, 2014; Graczyk, et al., 2018; Zhou, et al., 2007), the novel role of Gaf1 as a specific transcription factor controlled by TORC1 activity that globally binds to tRNA genes to repress them (Rodríguez-López, et al., 2020), constitutes a significant finding that could be involved in the ageing-associated function of RNA Pol III.

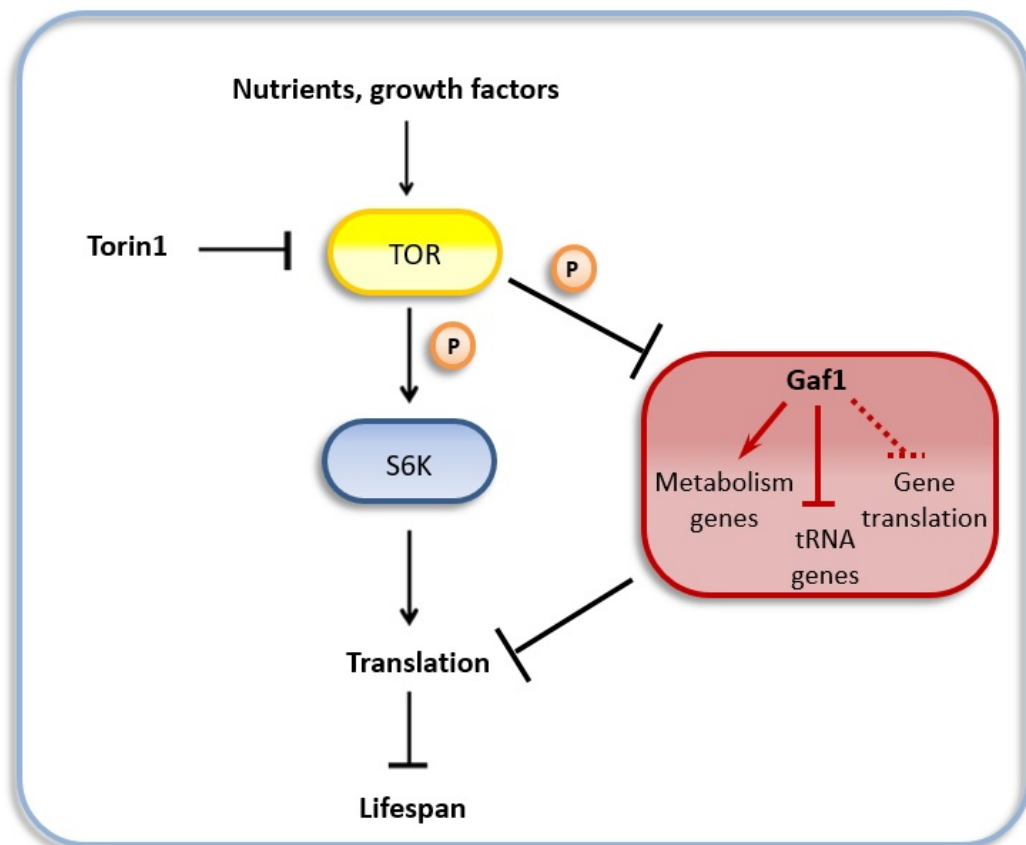


Figure 46. Model for Gaf1-mediated transcriptional repression of translation downstream of TORC1. After TORC1 inhibition, dephosphorylated Gaf1 activates the transcription of genes for small-molecule metabolic pathways, directly represses the transcription of tRNAs and indirectly inhibits genes involved in translation (hatched). Together with the S6K-mediated translational control (Ma & Blenis, 2009), this branch promotes longevity.

Overall, these results raise the possibility that the regulation of the ageing-related processes governed by Gaf1 are conserved, suggesting that other GATA transcription factors may perform similar functions downstream of TORC1 (Kim, et al., 2012). Recent evidence from flies revealed that GATA transcription factors

also mediate the effects of dietary restriction on lifespan in this model organism (Dobson, et al., 2018).

This section provides comprehensive details about the expression profile and transcriptional network regulated by Gaf1, laying the foundations for future mechanistic analyses that will clarify if other orthologues GATA transcription factors exert similar functions as those described for Gaf1 following TOR inhibition, including the repression of genes focused on the induction of translation and the suppression of tRNAs to promote survival. These studies will ultimately contribute to the identification of key components of these fundamental processes that regulate cellular ageing and longevity.

Chapter 6. High-throughput screening of genetic interactions and functional analyses of *gaf1* in the context of TOR signalling network

6.1. Introduction

The recent advances in whole-genome sequencing have led to great strides in the annotation of protein-coding genes and overall characterisation of genomic elements, nevertheless, the current challenge still resides in the elucidation of the functional role of individual genes and their interaction with genetic networks to modulate specific cellular processes (Kuzmin, et al., 2016).

The last decade has seen the development of systematic approaches to study the function of individual genes via introduction of single-gene modifications and subsequent assessment of phenotypic outcomes in eukaryotic cells (Costanzo, et al., 2019). Relevant examples of these platforms include reverse genetics (Hardy, et al., 2010), and synthetic genetic arrays [SGA] (Baryshnikova, et al., 2010). The latter is focused on the analysis of genetic networks and the interactions between genes that comprise them, aiming to understand both their individual function and the genetic basis underlying the relationship between genotype (different alleles and combination of polymorphisms) and phenotype (Baryshnikova, et al., 2010).

The technical difficulty of obtaining genetic interaction data from metazoans could be overcome with the use of experimentally tractable model systems such as yeast (Hartwell, et al., 1997). Large-scale studies mapping genetic interactions

were pioneered in the budding yeast *Saccharomyces cerevisiae*. They are based on a multiplicative model which suggests that corresponding gene products have a functional relationship (St Onge, et al., 2007). These genetic interactions are established by comparing the size of the colonies of double mutants against single mutants to define fitness scores (Baryshnikova, et al., 2010; Ryan, et al., 2012; St Onge, et al., 2007). The quantitation of genetic interactions is then established by the deviation between the quantitative measure of a double mutant phenotype, and its predicted neutral phenotype while carrying two non-interacting mutations (Mani, et al., 2008).

These studies were focused on the detection of a specific type of interaction named aggravating-sick interactions/negative epistasis or synthetic lethality. They occur when the combination of two defective-mutant genes that neither by itself affect phenotype, results in reduced fitness or cell death, respectively (Tong, et al., 2001). These interactions arise among genes acting in two different pathways that functionally compensate or buffer the defects in each other, highlighting genes whose products compensate one another and impinge on the same essential biological process (Hartman, et al., 2001).

The other category is defined as neutral synthetic relationships, alleviating interactions, or positive epistasis (Costanzo, et al., 2010; St Onge, et al., 2007). They occur when the fitness of double-mutants is greater than expected, revealing genes functioning in a single biochemical pathway, where a mutation in one gene impairs the function of a whole pathway masking the deleterious effects of other mutations in that pathway (Tong, et al., 2001).

The SGA approach has been extensively applied in several model organisms including *S. pombe*, *E. coli*, *C. elegans*, and human cancer cell lines, creating functional wiring diagrams that contribute to the understanding of the complex relationship between genotype and phenotype (Baryshnikova, et al., 2010; Costanzo, et al., 2019; Dixon, et al., 2008; Kuzmin, et al., 2016).

The sequencing of the fission yeast genome (Wood, et al., 2002), together with several recent developments in technologies including: genetic mapping using the genome-wide deletion collection (Kim, et al., 2010; Kuzmin, et al., 2016), the availability of quantitative phenotypic analyses based on quantification of colony size for the assessment of cellular fitness (Narayanan, et al., 2015), and robotic procedures for replica plate production (pinning steps on solid agar media), used for the construction of haploid double mutants through mating and meiotic recombination (Baryshnikova, et al., 2010; Harris, et al., 2013), have enabled the systematic construction of double mutants for the high-throughput screening of synthetic genetic interactions (Costanzo, et al., 2016; Tong & et al, 2004).

The SGA technique provides a powerful tool for genome-wide screening of several relevant biological aspects including the roles of individual genes *in vivo*, the order of gene functions, and the identification of new components of specific biochemical pathways/molecular mechanisms (Fay, et al., 2002; Hartman, et al., 2001; St Onge, et al., 2007; Tong, et al., 2001). Ultimately revealing targets amenable for therapeutic interventions, also allowing the improvement of diagnosis and elucidation of processes involved in complex human diseases (Boone, et al., 2007; Kuzmin, et al., 2016).

This chapter is focused on the analysis of high-throughput screenings of genetic interactions of *gaf1* in an optimal nutritional context and during the pharmacological inhibition of TOR signalling in *S. pombe*. This was performed by using the haploid deletion library available from the commercial company Bioneer, in which the open reading frame of 3,420 non-essential genes are depleted through targeted mutagenesis, and replaced with a drug-resistance cassette (*kanMX4*), containing molecular tags or barcodes -unique 20-bp DNA sequence- that function as a mutant strain identifier (Bioneer, n.d.).

The library provides 95.3% coverage of the genome and includes several human cancer genes with over 30% of homology (Bioneer, n.d.). The generation of double mutants was performed by crossing haploid cells from the library (mating type *h+*) with the query haploid strain *gaf1*Δ (mating type *h-*) containing a second selectable marker (usually *natMX6*) to generate the double mutants resistant to two drugs for strain selection (Baryshnikova, et al., 2010). The procedure followed a series of selective steps diagrammed in the methods in section 2.3.5. (figure 13).

The versatility of the SGA methodology was further exploited in this section by introducing chemical genomics, using the compound torin1 to inhibit the TOR signalling pathway (Atkin, et al., 2014; Rodríguez-López, et al., 2020). This approach was applied to explore several functional factors of the fission yeast genome including: screening for non-essential genes that provide resistance or sensitise cells to torin1 treatment, elucidate the *gaf1*-dependent interactome in the context of TOR inhibition, and detect the genetic interactions within this

network that either reduce or enhance the resistance of *gaf1*Δ mutants to high concentrations of the drug. These experiments also allowed to explore additional genes involved in the same biological processes that may be indirectly targeted by the compound (Arita, et al., 2011; Baryshnikova, et al., 2010).

Altogether, the SGA analyses produced in this study generated genetic networks linked to *gaf1* in the presence and absence of global TOR inhibition, that provide comprehensive information about individual functional roles of key genes involved in survival and cell cycle regulation, contributing to elucidate the complex relationship between genotype and phenotype (Kuzmin, et al., 2016), and uncovering conserved candidate genes that could be responsible for the torin1-resistance potentially applicable to cancer cells (Lie, et al., 2018). The present chapter also provides further insight into the functions of TOR signalling, which is essential for both the elucidation of TORC1 control of cellular ageing and for the design of therapeutic interventions that target specific functions of the network (Rallis, et al., 2014).

6.2. Screening of *gaf1*-dependent genetic interaction network during global TOR inhibition.

Evidence from the present study demonstrated that *gaf1* depletion in *S. pombe* confers resistance to TOR signalling inhibition by treatment with torin1 (Rodríguez-López, et al., 2020). In the present chapter, the functional relationships of Gaf1 were examined through the study of genetic interactions. Particularly, synthetic lethality was of interest to identify proteins that impinge on common essential functions within the TOR signalling network (Baryshnikova, et

al., 2010; Dixon , et al., 2009). The drug-resistance of *gaf1*Δ cells allowed to explore both functional relationships within the cellular processes targeted by compound, and to decipher candidate genes controlling the phenotypic outcome of *gaf1*Δ-double mutants when TOR signalling is pharmacologically disrupted (Baryshnikova, et al., 2010).

The SGA experiments started with the construction of the haploid heterothallic (*h*-) query strain *gaf1*Δ by means of targeted mutagenesis using PCR-mediated gene deletion (ORF) and transformation following standard procedures [see chapter 2, section 2.2.7] (Baryshnikova, et al., 2010). This query strain was crossed with the haploid heterothallic (*h*+) non-essential mutants from the genome-wide deletion collection of *S. pombe* (Bioneer Corporation v5.0) using pinning robotics, each interaction was examined in quadruplicate as described previously (Baryshnikova, et al., 2010; Kim, et al., 2010).

The single mutant library and the double mutant (selected progeny) were grown in solid rich media, as well as in the context of global TOR inhibition using 10 μM of torin1 in rich media to block both TORC1 and TORC2 (Atkin, et al., 2014). The resistance and sensitivity of the single and double mutants were assessed after 48 hours of growth in the presence of the compound. All the experiments were performed as independent biological duplicates. The fitness of individual strains was established in each condition based on biological duplicates spotted in a format of 384 colonies per plate.

The quantitative measure of fitness in the present study was established by applying the relative-growth-rate fitness of double mutants with respect to the

single mutants as the control (Jasnos & Korona, 2007; Young & Loewen, 2013). Library mutants with colony sizes smaller than the threshold filter (100 pixels) were deemed as inaccurate to calculate interaction values and hence excluded from the dataset (Rallis, et al., 2017).

Colony size measures were used as a proxy for fitness, they were obtained using the gitter package in R which applies systematic normalisations of experimental effects to ensure accurate genetic interaction measurements [see chapter 2, section 2.3.5] (Wagih & Parts, 2014). The corrections of several effects included: different growth rate between plates (plate-specific median), differences in colony sizes due to nutrient availability (row/column location), gradients in media thickness (spatial), neighbouring mutant strains (competition), and batch effects (Baryshnikova, et al., 2010).

The quantitative measure of the interactions or SGA scores, were obtained using the multiplicative model for independent genes, which states that mutations in non-interacting genes often combine in a multiplicative manner (Mani, et al., 2008). The resulting double mutant phenotype is expected to be equivalent to the product of the two individual mutations, therefore the quantitative measure of the interactions follows the equation $SGA\ score = f_{ab} - (f_a \times f_b)$, which is the deviation of the fitness of the double mutants with respect to the expected phenotype observed in each single (progenitor) mutant (Baryshnikova, et al., 2010).

The quantitative extent of the genetic interaction is measured depending on the distribution of the values, where numbers close to zero indicate low dispersion.

Thus, negative genetic interactions ($\epsilon < 0$) refer to double mutants that show a more severe fitness defect than expected, and in extreme cases synthetic lethality, whereas positive genetic interactions ($\epsilon > 0$) refer to double mutants with a less severe fitness defect than expected, and involve interactions such as epistasis and suppression (Dixon , et al., 2009; Mani, et al., 2008).

The cut-offs for positive and negative interactions with *gaf1* in the different conditions were established as +0.15 and -0.15, respectively (Rallis, et al., 2017). The biological role of the genes interacting was established with GO enrichments performed with the *AnGeLi* tool, for which *p*-values were corrected for multiple tests according to the false discovery rate (FDR) method (Bitton, et al., 2015).

The comparisons were established by defining four groups within the dataset, all of them grown on solid rich media: the first one comprised the untreated single mutants from the library used as the growth reference for fitness scores. The second group involved single mutants from the library spotted in the context of TOR inhibition using plates treated with torin1, this group revealed genes resistant to the treatment. The third group included double mutants (*gaf1* Δ + library) without treatment, which detected genetic interactions in convergent pathways with *gaf1*. The fourth group was made of double mutants (*gaf1* Δ + library) in torin1 treatment, which revealed genes involved in the resistance to torin1 observed in *gaf1* Δ cells (figure 47).

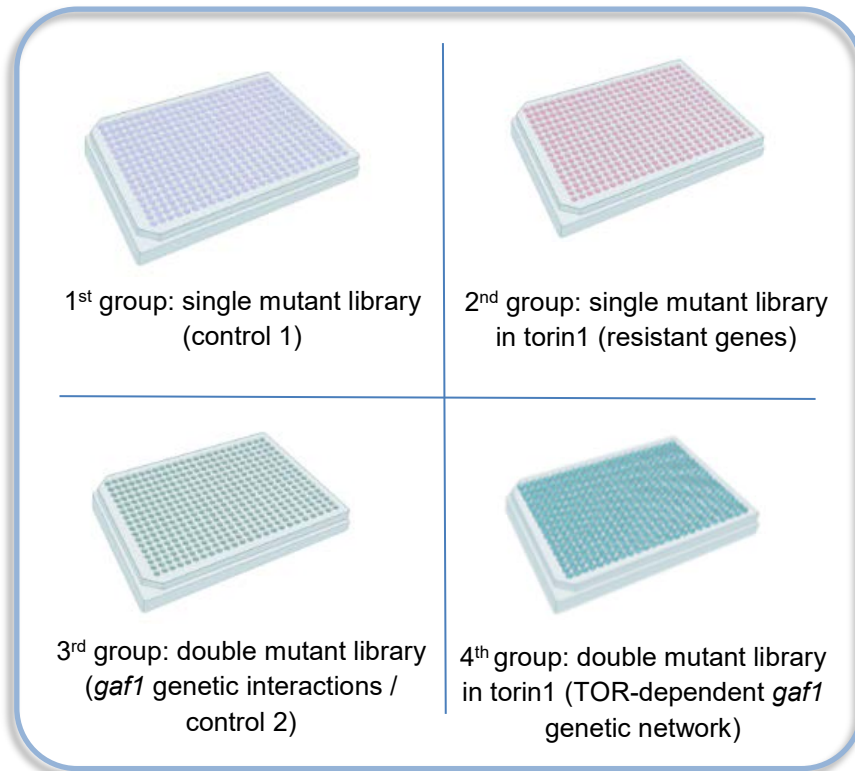


Figure 47. Classification of SGA experiments per group used for the comparisons and data analyses.

The first group contained a total of 2,956 deletion mutants providing coverage of ~87% of all *S. pombe* non-essential genes. Among these group, depletion of 215 genes produced fitness deficiencies that delayed growth in the optimal nutritional conditions of rich media, whereas 182 deletions contributed to fast growth [see full list of genes in appendices IV and V, respectively] (figure 48).

The GO enrichments for the 215 genes that reduced fitness when depleted included a broad range of biological processes, the most abundant categories involved: biosynthetic processes (119 genes, $p = 3.5 \times 10^{-16}$), metabolic processes (164 genes, $p = 8.7 \times 10^{-14}$), transcription (50 genes, $p = 2.7 \times 10^{-11}$), gene expression (101 genes, $p = 5.4 \times 10^{-11}$), and stress response (10 genes, $p = 6.4 \times 10^{-4}$), among others (Bitton, et al., 2015). All these processes have been

described to be regulated by nutrients (Gonzalez & Rallis, 2017) and will be discussed later.

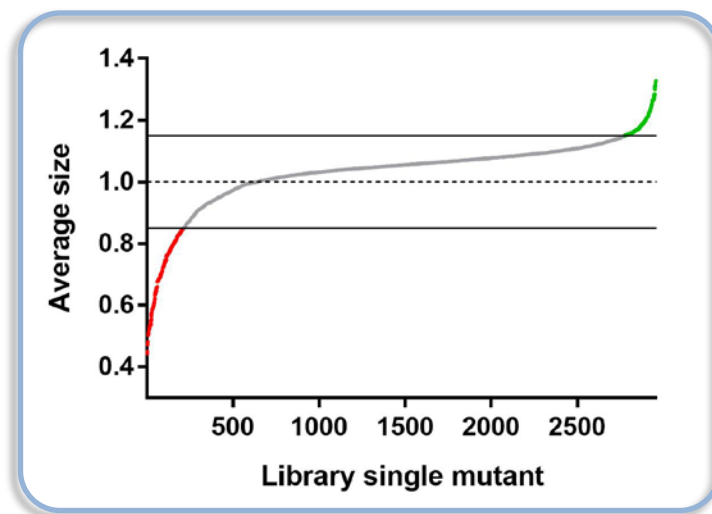


Figure 48. Single mutant library fitness in rich media used as a control for SGA experiments. Strains with growth defect represented in red, and fast grower mutants in green. Solid lines indicate cut-off. Colony sizes measured by pixel count and converted to circularity values, where 1 represents perfectly circular objects (dotted line) as per *ade6Δ* control.

Conversely, most of the GO enrichments for the 182 genes that increased growth when mutated included genes focused on the negative regulation of several processes involving: gene expression (19 genes, $p = 2.7 \times 10^{-4}$), macromolecule biosynthesis (19 genes, $p = 8.5 \times 10^{-4}$), transcription (16 genes, $p = 2.4 \times 10^{-3}$), RNA biosynthesis and metabolism (16 genes, $p = 2.4 \times 10^{-3}$), among others (Bitton, et al., 2015). These processes are related to stress responses (Gonzalez & Rallis, 2017), fitting a model in which their absence allow the cells to grow faster.

Previous studies screened the same *S. pombe* deletion library searching for strains sensitive to the inhibition of TOR signalling using several treatments to target different components of the pathway including: assessment of sensitivity to TORC1 inhibition using rapamycin on rich media (Doi, et al., 2015), and a

combination of rapamycin and caffeine on rich media (Rallis, et al., 2013; Rallis, et al., 2014), another study evaluated the fitness of the library using several nitrogen sources in minimal media and treatment with torin1 in minimal media supplemented with ammonium chloride as the nitrogen source (Lie, et al., 2018).

Considering that TORC1 acts alongside TORC2 to regulate cell growth and metabolism depending on nutritional status (Weisman, et al., 2007), the present study used a combination of rich media and a higher concentration of torin1 compared to previous reports (Lie, et al., 2018), to mimic natural physiological conditions with enhanced reduction in the signal of both complexes (Atkin, et al., 2014). In this regard, the second group involving single mutants from the library, allowed to identify genes that when depleted confer resistance or sensitivity to torin1 in rich media. The fitness of the treated strains was compared to the untreated cells and was plotted against the significance as volcano plot (figure 49).

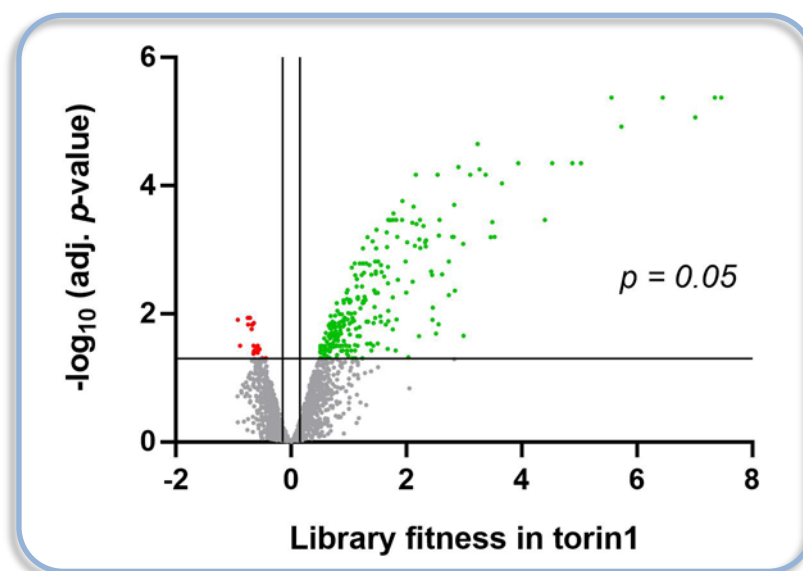


Figure 49. Cell fitness of single mutant library in rich media treated with torin1 against the untreated single mutant library. Adjusted significance ($\alpha = 0.05$) equivalent to $-\log_{10} = 1.3$ indicated by horizontal line. Vertical lines show cut-off values of $+0.15 / -0.15$. Red dots indicate 22 mutant strains with reduced fitness. Green dots represent 264 mutant strains with increased growth in the context of rich media treated with torin1.

In this group, there were 286 gene deletions that significantly altered ($\alpha = 0.05$) cell fitness when torin1 was present in rich solid media. The screen revealed that 22 strains were hypersensitive to the treatment, while 264 mutants showed certain level of resistance (see full list of genes in appendices VI and VII, respectively). This latter phenotype requires thoughtful interpretation as torin1 induced overall drastic reductions in growth of all the strains including controls, meaning that slight increases in growth may be potentially enhanced by the software during normalisations (Baryshnikova, et al., 2010).

The GO enrichments for the 22 depleted genes that produced sensitivity to the compound, were mainly focused on the regulation of phenotypes controlling cell viability/morphology (22 genes, $p = 1.5 \times 10^{-3}$), and mating efficiency (10 genes, $p = 4.9 \times 10^{-3}$), among others (Bitton, et al., 2015). The genes that produced this sensitive cluster have 17 orthologs in budding yeast and 16 in humans (Lock, et al., 2019).

The deletion of these genes did not reduce fitness of the strains grown in rich media, conversely, the absence of a specific subset of genes (*whi5*, *vcx1*, *msn5*) encoding: the cell cycle transcriptional repressor Whi5, the vacuolar exchanger (proton/calcium) Vcx1, and the nuclear signal receptor Msn5, allowed cells to proliferate faster in rich media but produced sensitivity when TOR signalling was inhibited, revealing that they are required for fitness during limited TOR activity, and suggesting a conserved involvement in this pathway.

Previous studies reported 241 gene deletions that conferred sensitivity to torin1 in minimal media (Lie, et al., 2018), this is in contrast to the 22 gene deletions that sensitised to the treatment in rich media in the present study, with an overlap of *msn5* and *wdr44* (encoding WD repeat protein) between the two gene lists. These differences could be attributed to the abundance of amino acids and complex nitrogen sources included in rich media which are absent in minimal media, where alternative nutrient-sensing mechanisms recognising those elements may allow survival when TOR signalling is inhibited.

Interestingly, out of the 21 autophagy genes reported in fission yeast (Sun, et al., 2013), depletion of several conserved autophagy genes (*atg10*, *atg9*, *atg1801*, *ire1*) involved in membrane formation (Wood, et al., 2002), produced sensitivity only in rich media. This is consistent with their essential role supplying nitrogen in *S. pombe*, which is activated in the absence of exogenous nitrogen and required to maintain viability under those conditions (Kohda, et al., 2007; Nakashima, et al., 2006), an environment mimicked in the present study by the addition of torin1 (Atkin, et al., 2014).

Considering that TOR coordinates the nuclear localisation of certain nutrient-regulated transcription factors in yeast (Beck & Hall, 1999; Laor, et al., 2015; Rodríguez-López, et al., 2020) and in mammalian cells (Yang, et al., 2008), future studies will elucidate the involvement of TOR signalling in the localisation or activation of nucleocytoplasmic transports such as Msn5 detected in this section, which revealed that depletion of the *msn5* gene is tolerated by the cell while TOR is active, potentially due to interactions with alternative buffering mechanisms,

but this normal functioning is lost during TOR inhibition observed in the single mutant treated with torin1.

In budding yeast, the phosphorylation of Whi5 (functionally related to mammalian retinoblastoma protein RB) that leads to its inactivation downstream of TORC1, have been described as a major event regulating the interface between nutritional signalling pathways and the cell cycle machinery, as it allows the activation of the SBF transcription complex required for the G1/S transition of the cell cycle (Pérez-Hidalgo & Moreno, 2017). In *S. pombe*, Vcx1 is essential for the delay in transition from monopolar to bipolar growth termed NETO (new end take off), during the G2 phase of the cell cycle upon perturbations of DNA replication, being relevant for cell viability (Kume, et al., 2017) and intracellular calcium homeostasis (Tisi, et al., 2016).

Disruptions of this Vcx1 protein may affect fungal vacuole function as they contain > 95% of the total cellular calcium (Dunn, et al., 1994). Since the membrane of the vacuoles is the residing place for TORC1 to exert its activity (Valbuena, et al., 2012), the sensitivity produced by the deletion of *vcx1* described in this section could be uncovering possible buffering functions for survival related to TOR activity. This revealed potential novel implications (direct or indirect) of Vcx1 and Whi5 as critical cell cycle-regulator proteins relevant for survival during reduced TOR signalling.

The GO enrichments for the remaining 264 genes that produced resistance to torin1 when depleted, showed a remarkable 96% of biological processes (50 out

of 52 categories) responsible directly and indirectly for cellular catabolism, some of them are: vacuolar transport (26 genes, $p = 4.8 \times 10^{-14}$), protein localisation to vacuole (14 genes, $p = 1.4 \times 10^{-7}$), protein catabolism (31 genes, $p = 4.9 \times 10^{-6}$), endocytosis (13 genes, $p = 6.8 \times 10^{-4}$), Golgi to vacuole transport (6 genes, $p = 5.5 \times 10^{-3}$), among others. The additional 4% were processes related to metabolism of amide (12 genes, $p = 4.5 \times 10^{-3}$) and urea [5 genes, $p = 9.4 \times 10^{-3}$] (Bitton, et al., 2015). The cluster of 264 genes that produced such resistant included 206 orthologs in budding yeast and 184 in humans (Lock, et al., 2019).

Among this group of depleted genes that produced resistance to TOR inhibition in rich media, there were 10 genes that reduced fitness of the strains in rich media [*atd1*, *atp11*, *dhm1*, *hhp1*, *hit1*, *idh1*, *rpp103*, *sec28*, *tif308*, *SPBC365.16*]. On the other side, there were 12 genes that increased fitness under the same conditions [*atg6*, *cki2*, *map1*, *plp1*, *pub3*, *sin1*, *sst4*, *vps1*, *zrg17*, *SPAC12B10.01c*, *SPAC17A2.10c*, *SPAC1952.09c*] (figure 50).

Even though none of those genes lists presented significant GO enrichments, there was a significant overlap between the 264 genes that produced resistance to torin1 in the present study and previous reports of mutants resistant to this compound, including an overlap of 27 genes ($p = 3.0 \times 10^{-13}$) with 100 gene deletions reported to confer resistance in minimal media (Lie, et al., 2018), and with 12 genes ($p = 1.0 \times 10^{-11}$) out of 19 gene deletions that produce resistance in rich media [figure 51] (Rodríguez-López, et al., 2020).

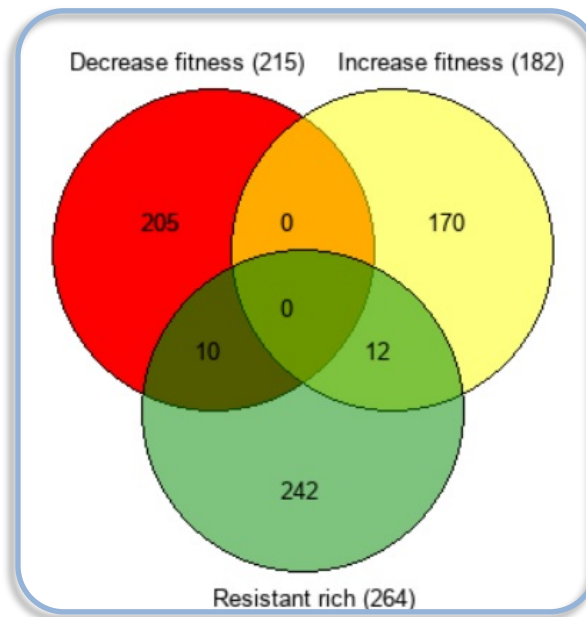


Figure 50. Venn diagram using Gene Venn showing overlaps between single gene deletions that confer resistance to torin1 (green), gene deletions that decrease fitness (red), and gene deletions that increase fitness (yellow). All of them grown in rich media.

Remarkably, the entire fraction of these 33 common genes were enriched in vacuolar trafficking and catabolism (Bitton, et al., 2015).

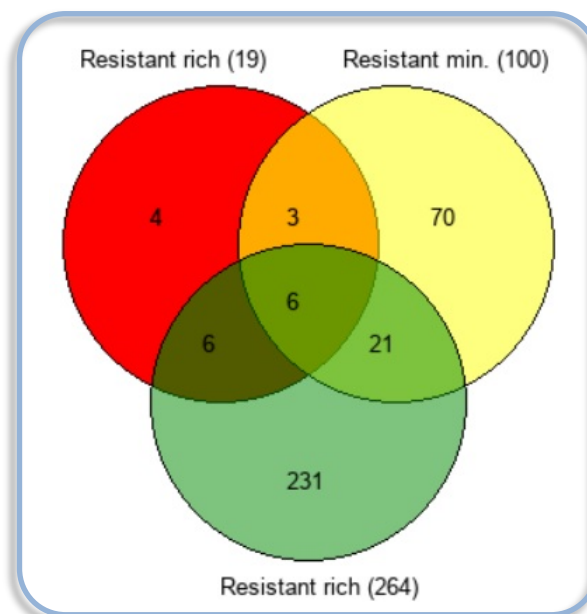


Figure 51. Venn diagram using Gene Venn showing overlaps between single gene deletions that confer resistance to torin1 in rich media detected in this study (green), previously reported gene deletions conferring resistance to torin1 in rich media [red] (Rodríguez-López, et al., 2020), and previously reported gene deletions conferring resistance to torin1 in minimal media [yellow] (Lie, et al., 2018).

Consistent with the resistance of *gaf1* Δ cells to torin1 treatment due the lack of repression of tRNA genes exerted by Gaf1 (Rodríguez-López, et al., 2020), the deletion of the mitochondrial peptidyl-tRNA hydrolase Pth1, involved in aminoacyl-tRNA hydrolase activity, and the wybutosine biosynthesis protein Tyw3, implicated in tRNA methylation, also promoted resistance to the compound in the present study. Additionally, the results showed that depletion of *gsk3*, which encodes the glycogen synthase kinase-3 Gsk3, also conferred resistance. Previous studies reported that *gsk3* Δ mutants are resistant to TORC1 inhibition by caffeine and rapamycin (Rallis, et al., 2014) and feature enlarged cell size (Rallis, et al., 2017).

The classification of the mutants as resistant to torin1 due to increased colony size growth, could have an alternative interpretation derived from the remarkable enrichment of vacuolar processes controlled by the 264 genes integrating this group, where increased cell size or biomass may be responsible for the colony size effect recognised by the software rather than increases in cell numbers.

Cellular homeostasis in eukaryotic cells requires the coordinated response of different organelles to intra- and extra-cellular signals. The yeast vacuole (analogous to the mammalian lysosome) is the degradative compartment of the cell responsible for both proteolysis and for the catabolic process of autophagy (Mukaiyama, et al., 2010).

In the fission yeast, autophagy is triggered by nitrogen depletion whereby damaged portions of the cytoplasm and long-lived proteins are enclosed within

isolated membranes called autophagosomes or autophagic bodies that are transferred to the vacuole for turnover (Kohda, et al., 2007). In this organism, the vacuoles are small under normal growth conditions, but rapidly fuse in response to stress conditions (Bone, et al., 1998). This process provides cytoplasmic detoxification, maintenance of cellular pH, survival to osmotic shock/nutrient limitation, and storage of metabolites and ions (Li & Kane, 2009).

The morphology of this multi-copy organelle is intimately linked to its function as the size and numbers depend on environmental stimuli (Mukaiyama, et al., 2010). This dynamic conformation is achieved through the processes of fusion and fission in response to stress, where components of the TOR signalling network are involved (Stauffer & Powers, 2017). During nutrient limitation or hypotonic conditions, both vacuoles and lysosomes become enlarged and their copy number reduced. Conversely, under hyperosmotic or acid stress, vacuoles undergo asymmetric fragmentation resulting in smaller and more numerous organelles (Stauffer & Powers, 2017).

While the steps and molecular mechanisms responsible for vacuolar fusion have been well described, the molecular drivers of vacuolar fission remain poorly understood (Stauffer & Powers, 2017). To this respect, TORC1 activity negatively regulates autophagy, its localisation at the vacuolar membrane is not affected by nutritional status but is strategic for nutrient control (Binda, et al., 2009), being responsible for vacuolar fragmentation or fission (Stauffer & Powers, 2017).

Previous studies in *S. cerevisiae* proved that acute inhibition of TORC1 with high concentrations of rapamycin block both hyperosmotic, and Endoplasmic Reticulum (ER) stress-induced vacuolar fragmentation, suggesting that operative TORC1 at the vacuolar membrane may convey information regarding ER stress to the vacuolar membrane to facilitate fragmentation (Stauffer & Powers, 2015). Other study using rapamycin treatment reported a paradoxical increase in cell size produced by the swelling of the vacuole as a consequence of increased autophagy in *S. cerevisiae* (Loewith & Hall, 2011).

In *S. pombe*, treatment with torin1 in wild type cells reduced the size of both cells and vacuoles (Rodríguez-López, et al., 2020), similar to the phenotype produced by caffeine and rapamycin that block TORC1 function (Rai, et al., 2013). Nevertheless, there are reports describing that in the context of nitrogen depletion, specific mutants with impaired functions in autophagy-dependent proteolysis showed significantly enlarged vacuoles, due to the accumulation of autophagic bodies (Sawada, et al., 2021; Takeshige, et al., 1992).

Consistently, the present genetic screening identified that those same mutants showed significantly increased (single) colony sizes when grown in torin1, which is not the case of torin1-treated wild type cells (Rodríguez-López, et al., 2020), suggesting that the increased colony size of the mutants in this context, could be the result of impaired vacuolar function that are unable to complete proteolysis and overall organelle digestion.

Some examples of mutant strains with previously described enlarged vacuoles that were also detected in the present study include genes encoding for: The SPX-RING-type ubiquitin ligase Pqr1 that restricts phosphate uptake into the cell through the ubiquitination and subsequent degradation of phosphate transporters on the plasma membranes (essential for vacuolar proteolysis). Deletion of this gene produce hyperaccumulation of intracellular phosphate and polyphosphate that interfere with proteolysis in vacuoles during nitrogen starvation (Sawada, et al., 2021); the GTPases Ypt7 and Ypt71 localised in the vacuolar membrane involved in trafficking from the endosome to the vacuole and in homotypic vacuolar fusion (Mukaiyama, et al., 2010); and the 1-phosphatidylinositol-3-phosphate 5-kinase Fab1 (Morishita & Shimoda, 2000).

Considering that the deletion of stress-response genes such as *gaf1* produce resistance to torin1 (Rodríguez-López, et al., 2020), future studies will clarify if the increased colony/spot size detected in SGA screenings of TOR inhibitors, particularly in mutants disrupted in vacuolar functions, is either because of vacuolar enlargement, or due to the capacity of the cells to bypass the restrictive effect of the drugs in proliferation.

Altogether, the results from this second group provide additional information regarding the relationship between TOR signalling and vacuolar morphology, introducing new insights into potential candidate genes responsible for vacuolar fragmentation, and suggesting that mutant strains with disruptions in vacuolar functions may present enlarged vacoules and cell size due to their inability to undergo vacuolar fission in response to TOR inhibition. Further characterisation

of the precise role of TORC1 localised at the vacuoles, will clarify additional roles of the TOR pathway particularly in the context of its association with membranes.

Ultimately, the elucidation of the mechanisms involved in cellular maintenance during TOR inhibition -including differentiated post-mitotic quiescent cells- will provide both comprehensive description of normal cellular physiology, and insights into the regulatory mechanisms governing several human disorders that involve the loss of adequate lysosomal function, including cancer and neurodegenerative diseases (Kirkegaard & Jäättelä, 2009; Zhang, et al., 2009).

The third group involving double mutants grown in rich media, allowed to identify genetic interactions between *gaf1* (query strain) and the library of non-essential single mutants. The fitness of the double mutant strains was compared to the single mutants and was plotted against the significance as volcano plot (figure 52).

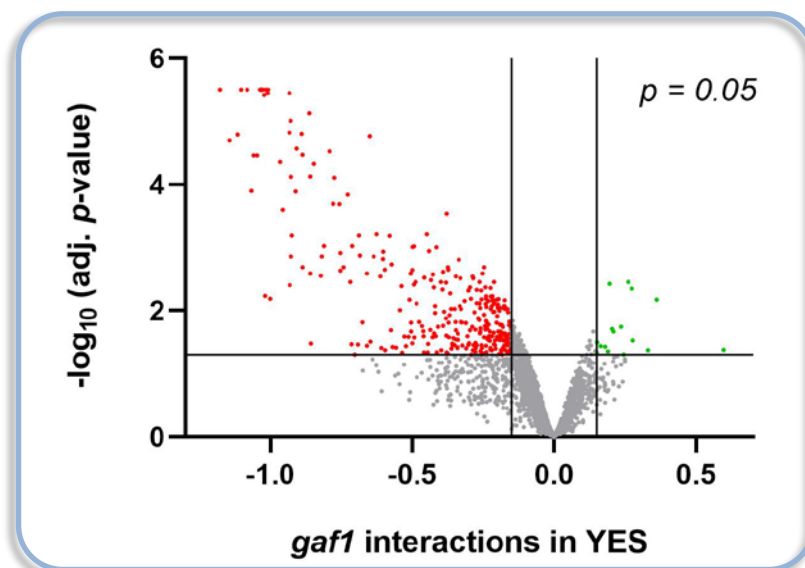


Figure 52. Cell fitness of double mutants in rich media against the untreated single mutant library. Adjusted significance ($\alpha = 0.05$) equivalent to $-\log_{10} = 1.3$ indicated by horizontal line. Vertical lines show cut-off values of $+0.15 / -0.15$. Red dots indicate 307 double mutant strains with reduced fitness. Green dots represent 16 double mutant strains with increased growth in the context of rich media.

In this group, there were 323 synthetic genetic interactions in which fitness was significantly altered ($\alpha = 0.05$) when double mutants were grown in rich solid media. The screen revealed that 16 strains showed positive genetic interactions, while 307 strains presented negative genetic interactions (see full list of genes in appendices VIII and IX, respectively). This is consistent with previous reports describing that on average, negative interactions are more prevalent than positive interactions (Baryshnikova, et al., 2010; Costanzo, et al., 2010).

There were no significant GO enrichments for the 16 deleted genes that presented positive interactions when combined with *gaf1* Δ (Bitton, et al., 2015). This sub-cluster has 15 orthologs in budding yeast and 11 in humans (Lock, et al., 2019).

The comparison of these 16 double mutants with positive interactions against the single mutants in *torin1* in rich media, revealed an overlap of 1 gene (*mtg1*) only with the resistant fraction, but not with the sensitive group. This gene encodes the mitochondrial translation factor GTPase Mtg1, which is involved in expression of the mitochondrial translational machinery (Lock, et al., 2019).

Interestingly, the deletion of these genes did not increase fitness of the single mutants grown in rich media, on the contrary, the depletion of 10 genes reduced fitness of the single strains grown in rich media. They include genes implicated in arginine biosynthesis (*arg5*, *arg12*), chromatin organisation (*pcf3*), meiotic nuclear division (*nab3*), membrane organisation (*mic60*), mitochondrial gene

expression (*cbp3*), catabolism (*hul5*), transcription (*res2*), and small molecule metabolism [*yfh7*] (Lock, et al., 2019).

These positive interactions indicate that these genes function in the same biochemical linear pathways as *gaf1*, where the mutation in one gene impairs the function of the entire pathway (Tong, et al., 2001) masking the deleterious effects caused by the absence of Gaf1. These results revealed the presence of a complex network of indirect interactions controlling fitness governed by those genes, where their mutations reduced viability in optimal conditional but when combined with *gaf1* depletion, their individual deleterious effects were ameliorated. Potentially, this could be attributed to the cell cycle-restrictive properties such as the ones described for Gaf1 during nitrogen stress responses (Laor, et al., 2015; Rodríguez-López, et al., 2020).

The GO enrichments for the remaining 307 mutant strains that showed negative interactions with *gaf1*, involved genes responsible for: metabolic processes (214 genes, $p = 9.2 \times 10^{-11}$), RNA biosynthesis (51 genes, $p = 1.6 \times 10^{-8}$), regulation of gene expression (57 genes, $p = 7.2 \times 10^{-8}$), nitrogen metabolism (132 genes, $p = 1.3 \times 10^{-7}$), macromolecule biosynthesis (56 genes, $p = 1.5 \times 10^{-7}$), cell communication (46 genes, $p = 2.1 \times 10^{-7}$), reproduction (36 genes, $p = 1.4 \times 10^{-4}$), among others (Bitton, et al., 2015). From this group, 255 genes have orthologs in budding yeast and 224 in humans (Lock, et al., 2019).

The comparison of the profiles obtained from the chemical-genetic screening of the single mutants treated with torin1 in rich media, against the 307 double

mutants that showed negative interactions with *gaf1*, produced a compendium of genetic interactions that allowed to identify pathways and genes targeted by the drug. There were 3 genes (*whi5*, *msn5*, *tef101*) overlapping with the sensitive single mutants (figure 53), they encode: the cell cycle transcriptional repressor Whi5, the nuclear signal receptor Msn5, and the translation elongation factor EF-1 alpha Ef1a-a (Lock, et al., 2019).

Regarding the comparison with the single mutants resistant to torin1, the overlap showed 24 genes that are shared between the two groups [*atd1*, *asl1*, *blt1*, *cwf12*, *dhm1*, *erp5*, *gcd1*, *map1*, *mpc1*, *php5*, *reb1*, *rpl1902*, *sdh3*, *shd1*, *sin1*, *SPBC12C2.04*, *SPBC16H5.08c*, *SPBC776.03*, *SPCC1393.12*, *SPCC320.05*, *SPCC757.05c*, *vht1*, *vps1*, *ubc6*] (figure 53). No significant GO enrichments were detected amongst these genes.

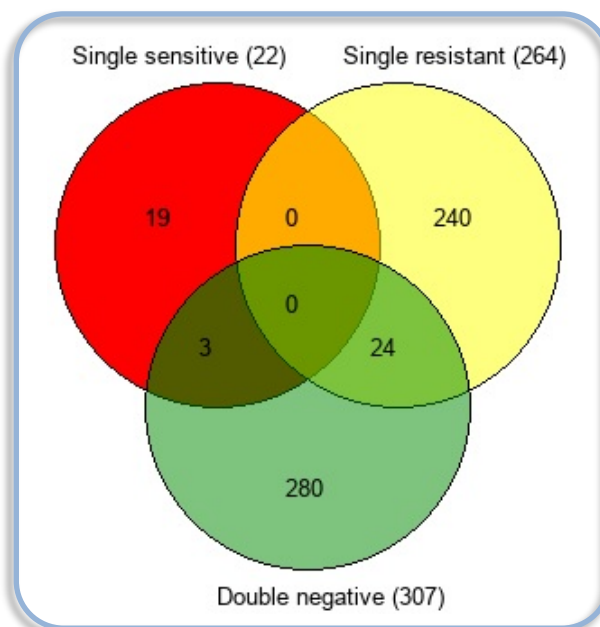


Figure 53. Venn diagram using Gene Venn showing overlaps between double mutants containing genes negatively interacting with *gaf1* (green), single mutants sensitive to torin1 (red), and single mutants resistant to torin1 (yellow). All of them grown in rich media.

Some of their functions were related to: actin cytoskeleton organisation (*shd1*), carbohydrate metabolic process (*asl1*, *gcd1*), cellular amino acid metabolic process (*SPBC776.03*), conjugation with cellular fusion (*map1*, *sin1*), transcription/translation (*map1*, *php5*, *reb1*, *rpl1902*), glutathione catabolism (*SPCC757.05c*), generation of precursor metabolites and energy (*atd1*, *gcd1*, *php5*, *sdh3*), nucleocytoplasmic transport (*SPBC16H5.08c*), protein catabolic process (*ubc6*), ribosome biogenesis (*SPBC16H5.08c*), transmembrane transport (*mpc1*, *SPCC320.05*, *vht1*), vesicle-mediated transport (*erp5*, *shd1*, *vps1*), among others (Lock, et al., 2019).

Considering that the chemical perturbations of torin1 mimic genetic perturbations that inhibit the TOR signalling pathway (Atkin, et al., 2014; Thoreen, et al., 2009), the comparison of these gene lists provided information about the involvement of the 24 genes described above, which are implicated in pathways that buffer the activity of Gaf1. The results also suggest that they are novel candidate genes regulated directly or indirectly by the TOR signalling pathway.

Among this group of 307 depleted genes that showed negative interactions with *gaf1*, there were 33 gene deletions that reduced fitness of the single mutant strains in rich media (figure 54).

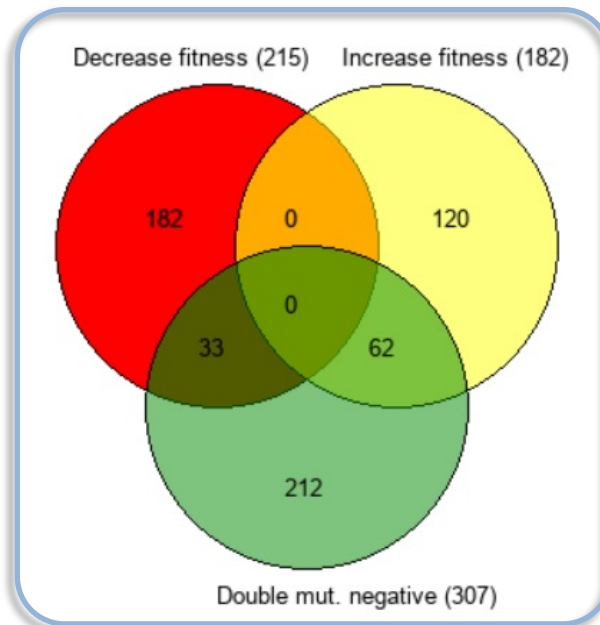


Figure 54. Venn diagram using Gene Venn showing overlaps between double mutants containing genes negatively interacting with *gaf1* (green), gene deletions in single mutants that reduced fitness (red), and gene deletions in single mutants that increased fitness (yellow). All of them grown in rich media.

All the GO enrichments for these genes were focused on the biosynthesis and metabolism of branched-chain essential amino acids, including: valine (3/33 genes, $p = 3.3 \times 10^{-4}$), leucine (3/33 genes, $p = 1.2 \times 10^{-3}$), and isoleucine [3/33 genes, $p = 1.2 \times 10^{-3}$] (Lock, et al., 2019).

The integration of the depleted genes that produced negative interactions, against the genes detected to decrease and increase fitness of the mutant strains from the library, revealed more specific functions of Gaf1 in optimum nutritional conditions. The absence of 33 genes that decreased fitness and negatively interacted with Gaf1, revealed functions related to its contribution in cell viability through the biosynthesis, metabolism and possibly uptake of essential branched-chain amino acids (valine, leucine, isoleucine), potentially related to the role of Gaf1 in the basal transcription of *isp7* (Laor, et al., 2015), encoding a member of the family of 2-oxoglutarate-Fe(II)-dependent oxygenases named Isp7, which

controls amino acid uptake via transcriptional regulation of general and specific amino acid permeases (Laor, et al., 2014).

The results from this group are consistent with the previously reported functions of Gaf1 as a transcription factor implicated in gene expression and protein synthesis regulation, especially in the context of nitrogen stress and subsequently in reproduction (Laor, et al., 2015; Ma, et al., 2015; Rodríguez-López, et al., 2020).

Conversely, this group of 307 negative interactors also shared 62 genes with the single mutant strains that presented increased fitness in rich media (figure 54). All the GO enrichments for these genes were focused on the negative regulation of protein synthesis, including: gene expression (10/62 genes, $p = 2.7 \times 10^{-3}$), macromolecule biosynthesis (10/62 genes, $p = 5.4 \times 10^{-3}$), transcription (10/62 genes, $p = 5.4 \times 10^{-3}$), RNA biosynthesis and metabolism [9/62 genes, $p = 5.5 \times 10^{-3}$] (Lock, et al., 2019).

These 307 genes that showed synthetic negative genetic interaction with *gaf1*, allowed to further understand the functional profile of this query gene. This was achieved through the analysis of the phenotypic signature produced by the parallel pathways that buffer the activities of Gaf1.

The absence of 62 genes responsible of repressing transcription and protein biosynthesis, allowed increased growth of the single mutants, a phenotype that was lost when *gaf1* was depleted, revealing both that Gaf1 activity is required for

the increased growth/fitness in rich media observed amongst those single mutants, and a direct or indirect involvement of Gaf1 in the processes controlled by those genes, probably related to the transient or basal activity described for this transcription factor (Laor, et al., 2015; Rodríguez-López, et al., 2020), as reported for the basal expression of *isp5* (Ma, et al., 2015).

Overall these findings suggest that among the non-essential genes, the vast majority of both positive and negative interactions with *gaf1*, exist between pathways, rather than within pathways, connecting those that presumably work together or buffer one another, respectively (Baryshnikova, et al., 2010). In this sense, while the genetic negative interactions detected in the present study provided more functional information than those obtained from positive interactions, the general profile compiled from both negative and positive interactions integrated with the gene lists obtained from the control experiments, allowed to establish a general profile for Gaf1 activities, and predict novel functions for this transcription factor that will require further examination.

The fourth group involving double mutants grown in rich media treated with torin1, allowed the identification of several functions of the *S. pombe* genome, including non-essential candidate genes involved in the drug-resistant phenotype observed in *gaf1* Δ cells, double mutant combinations that lack growth defects in optimal nutritional environments but present altered phenotypes when TOR signalling is limited, and the genetic network of non-essential genes targeted during the inhibition of the TOR pathway. The fitness of the double mutant strains treated

with torin1 was compared to the double mutant strains without treatment and was plotted against the significance as volcano plot (figure 55).

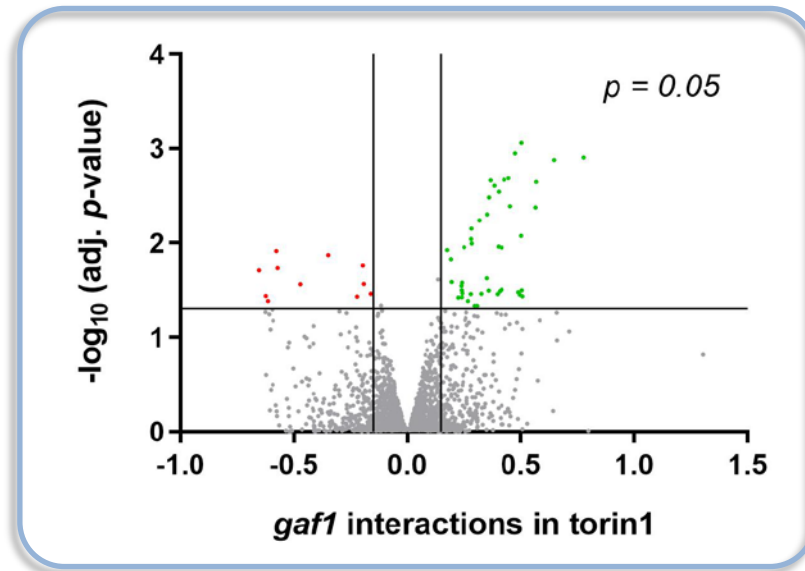


Figure 55. Cell fitness of double mutants in rich media treated with torin1 against the untreated double mutant library in rich media without treatment. Adjusted significance ($\alpha = 0.05$) equivalent to $-\log_{10} = 1.3$ indicated by horizontal line. Vertical lines show cut-off values of $+0.15 / -0.15$. Red dots indicate 11 double mutant strains with reduced fitness. Green dots represent 45 double mutant strains with increased growth in the context of rich media treated with torin1.

In this group, there were 56 synthetic genetic interactions in which fitness was significantly altered ($\alpha = 0.05$) when double mutants were grown in rich solid media treated with torin1. The screen revealed that 11 strains showed negative genetic interactions, while 45 strains presented positive genetic interactions (see full list of genes in appendices X and XI, respectively).

There were no significant GO enrichments for the 11 deleted genes that produced sensitivity to the compound when combined with *gaf1* Δ (Bitton, et al., 2015). This sub-cluster has 8 orthologs in budding yeast and 8 in humans (Lock, et al., 2019).

The deletion of these 11 genes on their own (single mutants) did not increase or decrease fitness of the strains in rich media. The comparison against the double

mutant strains, showed an overlap of 2 genes (*grn1*, *ogm4*) that presented negative interactions with *gaf1*. They encode the GTPase Grn1 and the O-mannosyltransferase Ogm4, which are critical for normal cell growth (Du, et al., 2006) and morphology (Tanaka, et al., 2005), respectively.

Regarding sensitisation to torin1, none of these 11 genes produced sensitivity when disrupted in the single mutants either in rich or minimal media (Lie, et al., 2018). On the contrary, the depletion of 5 genes (*ckb1*, *kap114*, *nap2*, *pds5*, *SPBC56F2.05c*) conferred resistance in the single mutants only in rich media but not in minimal (Lie, et al., 2018), revealing that they operate in buffering pathways that compensate the absence of Gaf1 activity and vice versa.

Interestingly, some of these genes have been implicated in TOR signalling. In *S. cerevisiae*, *ckb1* encodes Ckb1, which is the regulatory subunit of the highly evolutionarily conserved eukaryotic casein kinase II (CK2). This enzyme is phosphorylated during TORC1 inhibition, an event that leads to the repression of transcription via two mechanisms: the reduction in the CK2 occupancy of the tRNA genes that results in repression of RNA polymerase III [pol III] (Otsubo, et al., 2020), and the dephosphorisation/activation of the conserved pol III-repressor Maf1, which phosphorylation by CK2 is required for efficient pol III transcription (Graczyk, et al., 2011).

In *S. pombe*, *nab2* encodes Nab2, a histone H2A-H2B chaperone involved in chromatin organisation, which phosphorylation status is subjected to TOR kinase inhibition with torin1 (Mak, et al., 2021). The other genes are implicated in DNA

integrity (*pds5*), nucleocytoplasmic transport (*kap114*), and regulation of transcription [*SPBC56F2.05c*] (Lock, et al., 2019).

These results suggest that genes with direct or indirect implications in the repression of protein synthesis via regulation of chromatin organisation, transcription and the ribosomal machinery including tRNAs, provide significant resistance to torin1 when they are not present in the cell. Therefore, the negative interactions detected in this chemical-genetic screening of double mutants, revealed novel genes that operate in such functions during TOR inhibition, particularly buffering the activity of Gaf1.

Considering the resistance to torin1 observed in the single mutants in contrast to the sensitivity of the double mutants carrying the same trait, this set of genes constitute an interesting reference group to understand if vacuolar and cell size are increased during TOR inhibition, which will require further characterisation.

In consistence with the single mutants resistant to torin1 detected in the second group of this chapter, the entire GO enrichments for the remaining 45 double mutant strains that showed positive genetic interactions with *gaf1*, were related to biological processes implicated in vacuolar function and catabolism, some categories include: vacuolar transport (15 genes, $p = 3.5 \times 10^{-14}$), protein targeting to vacuole (10 genes, $p = 8.9 \times 10^{-11}$), endosomal transport (12 genes, $p = 9.5 \times 10^{-11}$), proteolysis involved in cellular protein catabolic process (11 genes, $p = 9.6 \times 10^{-5}$), protein catabolism (11 genes, $p = 1.1 \times 10^{-4}$), organelle fusion (6 genes, $p = 1.9 \times 10^{-4}$), and Golgi vesicle transport (7 genes, $p = 4.1 \times$

10^{-3}), among others (Bitton, et al., 2015). From this group, 40 genes have orthologs in budding yeast and 36 in humans (Lock, et al., 2019).

Interestingly, the deletion of these genes did not decrease fitness of the single mutants grown in rich media, on the contrary, the depletion of 4 genes from this group (*atg6*, *pub3*, *SPAC17A2.10c*, *sst4*) increased fitness of the single strains grown in rich media.

These genes have been implicated in autophagy, including: the *atg6* gene encoding Atg6, a subunit of the phosphatidylinositol (PtdIns) 3-kinase complexes I and II and is essential for autophagy (Obara, et al., 2006; Ohsumi, 1999). Other genes are *pub3* encoding Pub3, a ubiquitin-protein ligase E3, and *sst4* encoding Sst4, a receptor for ubiquitinated membrane proteins, both of them involved in ubiquitin-dependent protein catabolic process (Lie, et al., 2018; Lock, et al., 2019). These results suggest that those 4 genes are essential for efficient autophagy even under optimum nutritional environments. Future studies will determine if there is an increase in cellular biomass produced by enlarged vacuolar size.

Within this group of 45 genes, there were no overlapping genes with the double mutants that presented positive genetic interaction with *gaf1*, conversely, there were 5 genes (*erp5*, *rpl1902*, *sdh3*, *SPBC776.03*, *SPBC16H5.08c*) that showed negative interactions with *gaf1* (figure 56). These genes encode proteins involved in cellular amino acid metabolism (*SPBC776.03*), generation of precursor

metabolites and energy (*sdh3*), vesicle-mediated transport (*erp5*), translation, ribosome assembly and nucleocytoplasmic transport (*rpl1902*, *SPBC16H5.08c*).

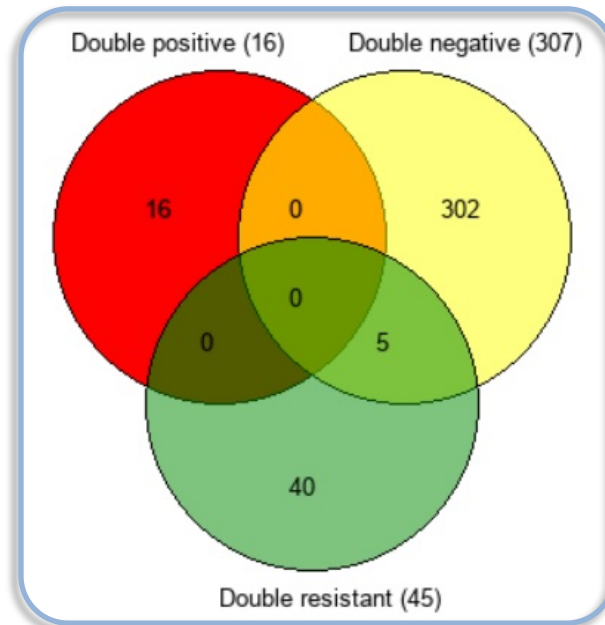


Figure 56. Venn diagram using Gene Venn showing overlaps between double mutants resistant to torin1 (green), double mutants containing genes negatively interacting with *gaf1* (red), double mutants containing genes positively interacting with *gaf1* (yellow). All of them grown in rich media.

These results are consistent with the reported role of Gaf1 in protein synthesis (Laor, et al., 2015; Rodríguez-López, et al., 2020), and provide additional information about the functional profile of this transcription factor in optimum nutritional conditions, revealing its involvement and buffering genes for those processes, as well as the presence of alternative mechanisms only activated during TOR inhibition that improved survival.

Among this group of 45 double mutants resistant to torin1, there were 2 single mutants (*gid5*, *ucp12*) that showed certain level of sensitivity, and 1 single mutant (*atg1801*) that was significantly sensitive to the compound. These genes were involved in autophagy, catabolism (*atg1801*, *gid5*) and carbohydrate metabolism

(*gid5*). This additive resistance to torin1 of the double mutants suggests that these genes operate in parallel to negatively regulate TOR-dependent processes.

Additionally, there were 42 genes that also conferred resistance when they were depleted in the single mutant strains (figure 57). There was a significant overlap of 11 genes ($p = 5.3 \times 10^{-10}$) between this resistant group and 100 gene deletions reported to confer resistance to torin1 in minimal media [figure 57] (Lie, et al., 2018). All the GO enrichments for these fractions were related to vacuolar function and catabolism (Bitton, et al., 2015).

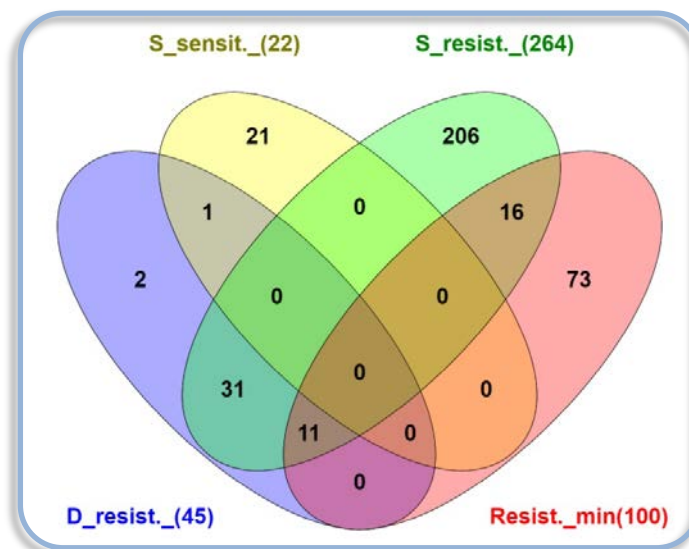


Figure 57. Venn diagram using Venny 2.1 showing overlaps between: double mutants resistant to torin1 in rich media (purple), single mutants sensitive to torin1 in rich media (yellow), single mutants resistant to torin1 in rich media (green), and previously reported single mutants resistant to torin1 in minimal media [pink] (Lie, et al., 2018).

Consistent with the results from the second group, where the majority of the single mutants resistant to torin1 included gene deletions involved in vacuolar function, the entire set of resistant double mutants from the fourth group were also implicated in catabolism, and included mutants reported to have enlarged vacuoles due to impaired in autophagy in the context of nitrogen depletion (Sawada, et al., 2021; Takeshige, et al., 1992).

In fission yeast, there are ~100 vacuoles per cell, they are small in size under normal growth conditions, but rapidly fuse in response to stress conditions in a similar as mammalian cells (Bone, et al., 1998). Future studies will establish if this set of mutants is involved in molecular mechanisms by which TOR signalling control the process of vacuolar fission in response to stress, determining if disruptions in those genes produce enlarged vacuoles and increased cell size (biomass) during TOR inhibition due to their inability to undergo vacuolar fission that lead to increases in colony size.

The considerable representation of positive interactions among double mutants during torin1 treatment, driven by genes enriched in proteolysis, vacuolar function and catabolism, suggest that the examination of their role in other rapamycin-sensitive processes is likely to be fruitful, as the majority of the genes identified in this study are conserved in both budding yeast and humans. This will clarify if the highest levels of resistance to torin1 conferred by mutations in those candidate genes, could be attributed to either increases in cell size or to progression in cell proliferation, as observed in *gaf1*Δ cells (Rodríguez-López, et al., 2020).

The summary of significant hits detected in the present screening of genetic interactions with *gaf1* in the context of TOR signalling (table 6), revealed two relevant clusters of genes that are highly informative.

SGA Phenotype	1st group	2nd group	3rd group	4th group
Reduced fitness	215	22	307	11
Increased fitness	182	264	16	45

Table 6: Number of genes with significant genetic interactions with *gaf1* identified in each group of the SGAs analyses. Highlighted in bold are clusters of relevant genes.

The 11 genes that reduced fitness of the fourth group, allow to further understand the functional profile of *gaf1* and provide additional information to explain the torin1-resistance phenotype of this strain, potentially achieved via disruptions in genes regulating chromatin organisation, transcription and biosynthesis of the ribosomal machinery including tRNAs, the latter proposed to be molecules that transduce nutrient availability to TORC1 (Otsubo, et al., 2020). Consistently, all of those processes have been described to be regulated by TOR signalling (Gonzalez & Rallis, 2017; Weisman, 2010). Future studies focused on molecular mechanisms conferring resistance to torin1, will provide relevant information for the improvement of its therapeutic use as an anti-cancer compound (Thoreen, et al., 2009).

These results identified Gaf1 as a transcription factor that mainly operates between different pathways that buffer each other, rather than within the same pathways. They also revealed novel functions for this transcription factor involving catabolism, and presented novel approaches for the interpretation of SGA data, introducing cellular size of the mutants as variable of interest.

The 264 genes that increased fitness of the second group, represent the first report of a global chemical-genetic screening of non-essential deletion mutants from *S. pombe* that produced altered fitness in the presence of torin1 treatment in rich media *in vivo*. The genes and pathways identified in this group provide valuable insights into the complex relationship between proteolysis, catabolism, vacuolar morphology and TOR signalling. Additionally, these results introduce new insights into potential candidate genes responsible for vacuolar fission, and open new questions regarding the additional roles that TORC1 may have during its association with membranes.

The elucidation of the conserved molecular mechanisms orchestrating the normal physiology of vacuoles during TOR inhibition, including differentiated post-mitotic quiescent cells, is relevant for clinical applications aiming to improve human disorders related to inadequate lysosomal function, including cancer and neurodegenerative diseases (Kirkegaard & Jäättelä, 2009; Zhang, et al., 2009).

Ultimately, the documented central role of amino acid homeostasis and autophagy in maintaining chronological longevity in yeast and higher organisms, have been attributed to the recycling and removal of cellular damage in the nutrient-limited context of non-dividing cells. These notions have prompted dietary nutritional balance as an emerging strategy for increasing healthy lifespan in humans via “dietary interventions” rather than through caloric restriction or pharmacological treatments (Aris, et al., 2012).

6.3. Data integration between *gaf1*-dependent genetic interaction network and *Gaf1* transcriptional profile in the context of TOR inhibition.

The data obtained from the synthetic genetic interactions screenings described above was further compared with the genes identified to be subjected to the direct or indirect transcriptional control of Gaf1 reported in chapter 5. This section provides an overview of the integration between the results from the SGA experiments, the differential gene expression profile controlled by Gaf1 obtained with microarrays, and the transcriptional targets of this transcription factor previously reported obtained with CHIP-seq technology (Rodríguez-López, et al., 2020). These comparisons provide additional insights into the functional profile of Gaf1 in the presence and absence of TOR signalling, produced via pharmacological inhibition of torin1 treatment (Atkin, et al., 2014; Thoreen, et al., 2009).

All the comparisons were focused on the integration of the SGA screenings, with both the genes differentially expressed in *gaf1*Δ cells after torin1 treatment, and the transcriptional targets of Gaf1 before and after torin1 treatment. For that aim, a standard matrix of four gene lists, referred here as Gaf1-dependent transcriptional profile, was juxtaposed to individual gene lists obtained from the SGA screenings.

The matrix included: 90 upregulated (UR) and 108 downregulated (DR) genes, which are typically downregulated and upregulated respectively by Gaf1 during torin1 treatment in wild type cells, and the previously reported 165 transcriptional targets of Gaf1 before torin1 treatment and 454 targets after treatment

(Rodríguez-López, et al., 2020). The GO enrichments of these gene lists were described above in chapters 5.2, 5.3 and 6.2.

The comparison between the gene deletions that decreased the fitness of the single mutant in rich media, with the Gaf1-dependent transcriptional profile, showed an overlap of 21 genes (figure 58).

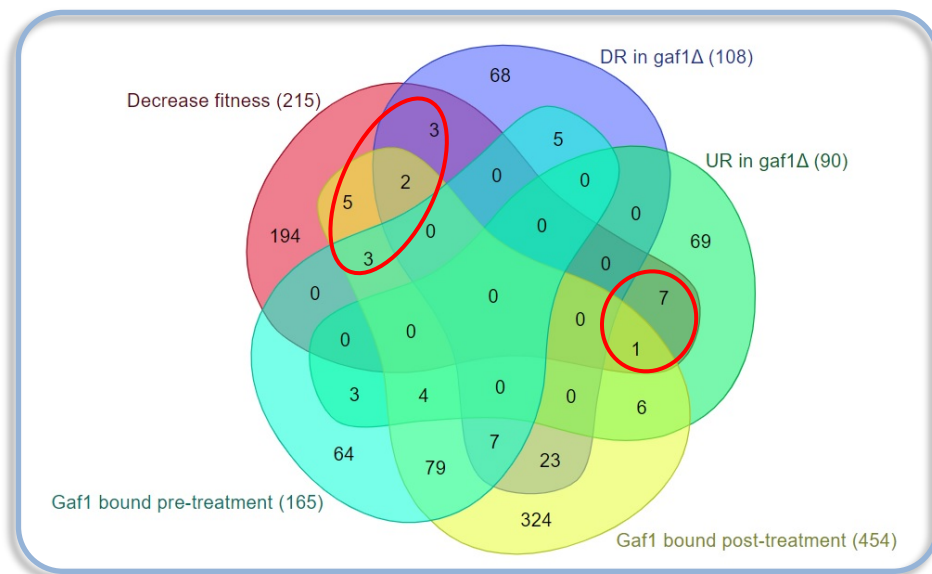


Figure 58. Venn diagram using Molbiotoll showing overlaps between single gene deletions that decrease fitness (red), downregulated genes in *gaf1*Δ after torin1 treatment (purple), upregulated genes in *gaf1*Δ after torin1 treatment (green), transcriptional target genes of Gaf1 before torin1 treatment (yellow), and transcriptional target genes of Gaf1 after 1 hour of torin1 treatment (magenta). The relevant overlaps are circled in red. All of the experiments were performed in rich media.

The integration between these genes lists revealed that among the single gene mutations that decreased fitness, there were 5 DR genes (*arg5*, *arg12*, *pap1*, *SPAC1039.07c*, *SPBC1861.05*), 8 UR genes (*hmt2*, *plb1*, *rps1002*, *rpl1602*, *rps2801*, *rpl3001*, *rpl702*, *rpl801*) in *gaf1*Δ cells treated with torin1, and 3 genes (*hsr1*, *SPAC27E2.11c*, *tdh1*) to which Gaf1 binds before and after its activation, and 11 genes (*dad5*, *gpd1*, *hsr1*, *loz1*, *nde1*, *pap1*, *prz1*, *tdh1*, *plb1*,

SPAC1039.07c, *SPAC27E2.11c*) bound after its activation induced by torin1 treatment.

The GO enrichments for the fraction of DR genes were related to urea cycle (2 genes, $p = 4.1 \times 10^{-3}$), and arginine biosynthesis (2 genes, $p = 6.3 \times 10^{-3}$). The UR genes were focused on translation (6 genes, $p = 9.1 \times 10^{-3}$). This is consistent with the roles reported for Gaf1 in limiting translation during nitrogen stress and scavenging relevant amino acids such as arginine which contributes to the feedback loop for the activation of TORC1 (Laor, et al., 2015; Ma, et al., 2015; Wang, et al., 2018).

The GO enrichments for the Gaf1-target genes (after its activation) were involved in NADH metabolic process (3 genes, $p = 7.7 \times 10^{-3}$), and response to osmotic stress [3 genes, $p = 5.8 \times 10^{-3}$] (Bitton, et al., 2015). Even though there were no significant GO enrichments for the Gaf1-targets before its activation, these genes were involved in the regulation of transcription (*hsr1*), and carbohydrate metabolism and signalling [*tdh1*] (Lock, et al., 2019).

Notably, Gaf1 is constantly bound to the promoter of *hsr1* (Rodríguez-López, et al., 2020) which encodes Hsr1, a transcription factor that globally supports gene expression in response to hydrogen peroxide (Chen, et al., 2008). Activated Gaf1 binds to the promoter of 20 transcription factors (Rodríguez-López, et al., 2020), some of these were present in this group, they are involved in stress responses and cell-cycle regulation, including the genes encoding for Loz1 (Corkins, et al., 2013), Pap1 and Hsr1 (Chen, et al., 2008).

The presence of these transcription factor target genes in this group, particularly Pap1 which is DR in *gaf1*Δ cells after torin1 treatment, confirms that Gaf1 may indirectly control some its target genes via other transcription factors (Rodríguez-López, et al., 2020).

The comparison between the gene deletions that increased the fitness of the single mutant in rich media, with the Gaf1-dependent transcriptional profile, showed an overlap of 20 genes (figure 59).

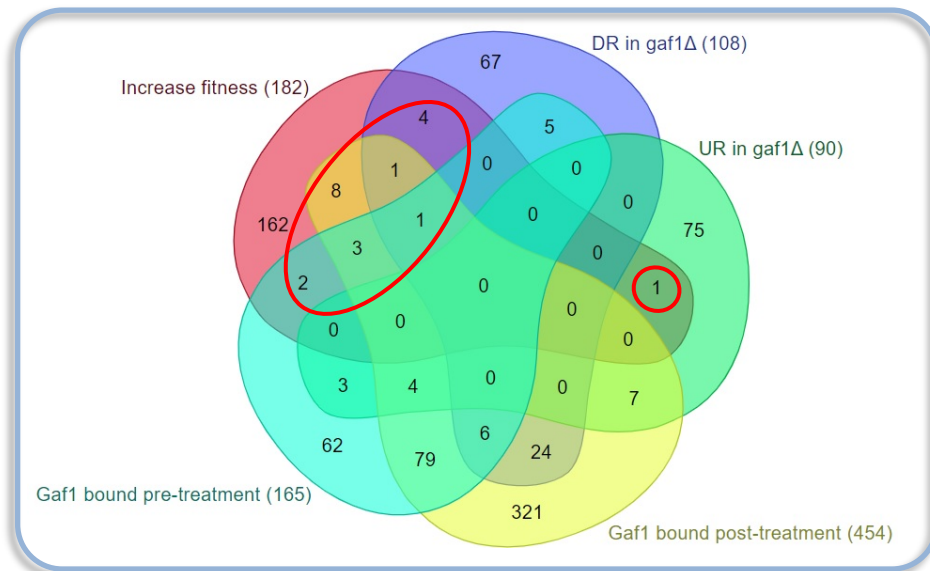


Figure 59. Venn diagram using Molbiotoll showing overlaps between single gene deletions that increase fitness (red), downregulated genes in *gaf1*Δ after torin1 treatment (purple), upregulated genes in *gaf1*Δ after torin1 treatment (green), transcriptional target genes of Gaf1 before torin1 treatment (yellow), and transcriptional target genes of Gaf1 after 1 hour of torin1 treatment (magenta). The relevant overlaps are circled in red. All of the experiments were performed in rich media.

The integration of these gene lists revealed that among the single gene mutations that increased fitness, there were 6 DR genes (*hhf1*, *pmp3*, *ptr2*, *put2*, *sib2*, *xan1*), 1 UR gene (*rps1001*) in *gaf1*Δ cells treated with torin1, and 6 genes (*atg6*, *isp7*, *ptr2*, *SPAC1002.20*, *SPBC12C2.03c*, *SPAC17A2.10c*) to which Gaf1 binds before its activation, and 13 genes (*cbf12*, *cmt1*, *crs1*, *isp7*, *ptr2*, *SPAC1002.20*,

SPAC683.03, *SPBC12C2.03c*, *SPBC1271.07c*, *SPCC330.07c*, *SPCC594.02c*, *sib2*, *srk1*) after its activation induced by torin1 treatment.

Even though there were no significant GO enrichments for the groups overlapping with the Gaf1-dependent transcriptional profile, the function of some of the DR genes was related to cellular amino acid metabolism (*put2*), chromatin organisation (*hhf1*), and transmembrane transport (*ptr2*), whereas the UR gene was involved in translation [*rps1001*] (Lock, et al., 2019).

The Gaf1-targets before its activation were involved in autophagy (*atg6*), and transmembrane transport (*isp7*, *ptr2*), while the Gaf1-targets after its activation were focused on cell adhesion and transcription (*cbf12*), conjugation with cellular fusion and mitotic cell cycle phase transition (*srk1*), meiotic nuclear division (*crs1*), and transmembrane transport [*isp7*, *ptr2*, *SPCC330.07c*] (Lock, et al., 2019).

This group contained a fraction of genes that their depletion from the cell required Gaf1 for the improved fitness phenotype observed in rich media. They encoded the plasma membrane PTR family peptide transmembrane transporter Ptr2, the delta-1-pyrroline-5-carboxylate dehydrogenase Put2, and a putative transmembrane transporter encoded by *SPCC330.07c*, indicating a relevant function of Gaf1 in the uptake of small peptides, in addition to other transmembrane transporters such as *Isp7* which was also present in this group.

The comparison between the gene deletions that conferred resistance to torin1 in single mutants grown in rich media, with the Gaf1-dependent transcriptional profile, showed an overlap of 21 genes (figure 61).

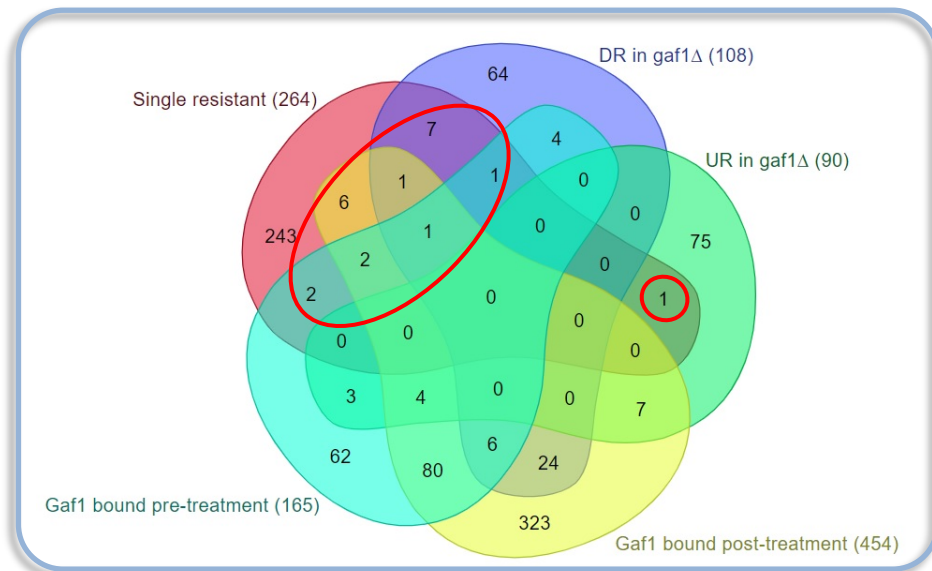


Figure 61. Venn diagram using Molbiotoll showing between single gene deletions that conferred resistance to torin1 (red), downregulated genes in *gaf1*Δ after torin1 treatment (purple), upregulated genes in *gaf1*Δ after torin1 treatment (green), transcriptional target genes of Gaf1 before torin1 treatment (yellow), and transcriptional target genes of Gaf1 after 1 hour of torin1 treatment (magenta). The relevant overlaps are circled in red. All of the experiments were performed in rich media.

The integration of these gene lists revealed that among the single mutants resistant to torin1, there were 10 DR genes (*car1*, *glt1*, *hhf3*, *lcb4*, *pet2*, *pmc1*, *SPAC25B8.10*, *SPAC521.03*, *sro1*, *uck2*), 1 UR gene (*asl1*) in *gaf1*Δ cells treated with torin1, and 6 genes (*atg6*, *mug124*, *SPAC17A2.10c*, *SPAC17A2.11*, *SPAC521.03*, *uck2*) to which Gaf1 binds before its activation, and 10 genes (*fsv1*, *gcd1*, *glt1*, *mrs3*, *mug70*, *mug124*, *SPAC17A2.11*, *SPAC29B12.14c*, *sdh3*, *uck2*) after its activation induced by torin1 treatment.

There were no significant GO enrichments for the groups overlapping with the Gaf1-dependent transcriptional profile. The function of some of the DR genes

was related to cellular amino acid metabolism (*car1*, *glt1*), chromatin organisation (*hhf3*), metal ion homeostasis (*pmc1*), transmembrane transport (*pet2*, *pmc1*). The UR gene was involved in cell wall organisation or biogenesis [*asl1*] (Lock, et al., 2019).

The most relevant Gaf1-target before its activation has a role in autophagy, lipid metabolism, and vesicle-mediated transport (*atg6*). The Gaf1-targets after its activation were focused on carbohydrate metabolism (*gcd1*), cellular amino acid metabolism (*glt1*), generation of precursor metabolites and energy (*gcd1*, *sdh3*), membrane organisation and organelle localisation (*fsv1*), and transmembrane transport [*mrs3*] (Lock, et al., 2019).

The comparison between the gene deletions that showed positive genetic interactions with *gaf1* in rich media, against the Gaf1-dependent transcriptional profile, showed an overlap of 2 genes (figure 62).

The integration of these gene lists revealed that among the double mutants containing genes that positively interacted with *gaf1*, there were only 2 DR genes (*arg5*, *arg12*) in *gaf1* Δ cells treated with torin1. The GO enrichments for these genes revealed that they are involved in the urea cycle (2 genes, $p = 3.6 \times 10^{-4}$), arginine biosynthesis and metabolism [2 genes, $p = 5.5 \times 10^{-4}$] (Bitton, et al., 2015).

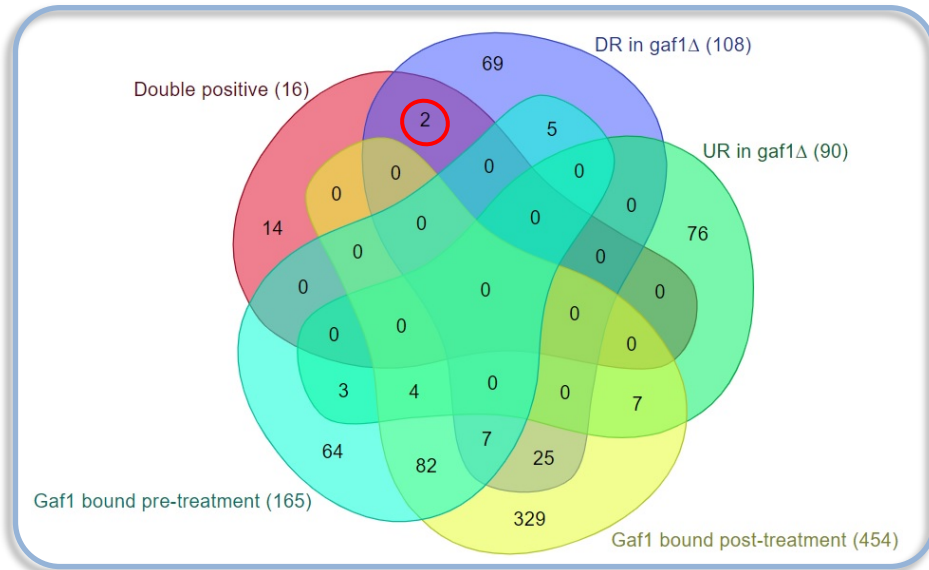


Figure 62. Venn diagram using Molbiotoll showing between double mutants with positive genetic interactions with *gaf1* (red), downregulated genes in *gaf1*Δ after torin1 treatment (purple), upregulated genes in *gaf1*Δ after torin1 treatment (green), transcriptional target genes of Gaf1 before torin1 treatment (yellow), and transcriptional target genes of Gaf1 after 1 hour of torin1 treatment (magenta). The relevant overlaps are circled in red. All of the experiments were performed in rich media.

Interestingly, the deletion of these two genes reduced the fitness of the single mutants grown in rich media, in contrast to the increased growth of the double mutant containing *gaf1* depletion. This revealed two elements, a potential novel involvement of Gaf1 in the indirect regulation of *arg5* and *arg12* to maintain normal cellular fitness, and a Gaf1-dependent restrictive effect on cellular fitness observed in the single mutants but abolished in the double mutants.

The comparison between the gene deletions that showed negative genetic interactions with *gaf1* in rich media, against the Gaf1-dependent transcriptional profile, showed an overlap of 35 genes (figure 63).

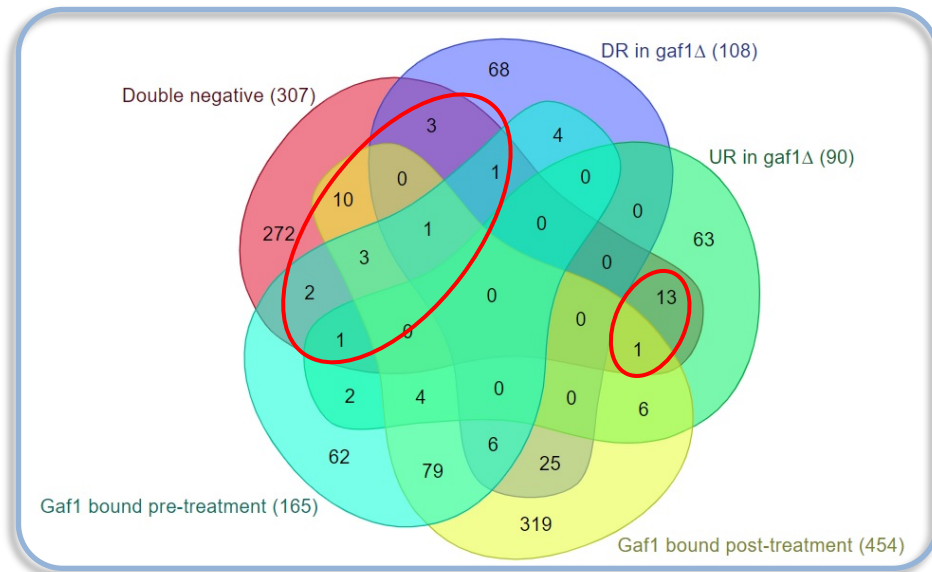


Figure 63. Venn diagram using Molbiotoll showing between double mutants with negative genetic interactions with *gaf1* (red), downregulated genes in *gaf1*Δ after torin1 treatment (purple), upregulated genes in *gaf1*Δ after torin1 treatment (green), transcriptional target genes of Gaf1 before torin1 treatment (yellow), and transcriptional target genes of Gaf1 after 1 hour of torin1 treatment (magenta). The relevant overlaps are circled in red. All of the experiments were performed in rich media.

The integration of these gene lists revealed that among the double mutants containing genes that negatively interacted with *gaf1*, there were 5 DR genes (*cxr1*, *hhf2*, *ptr2*, *put2*, *tsc1*), 15 UR genes (*asc1*, *asl1*, *eki1*, *plb1*, *pof15*, *rad57*, *rps101*, *rps1002*, *rps1102*, *rps1201*, *rps1701*, *rpl1102*, *rpl4302*, *sua1*, *ura1*) in *gaf1*Δ cells treated with torin1, and 8 genes (*elp5*, *hhf2*, *hsr1*, *pho842*, *ptr2*, *SPBC12C2.03c*, *SPAC27E2.11c*, *sua1*) to which Gaf1 binds before its activation, and 15 genes (*aah1*, *gas2*, *gcd1*, *hem3*, *hsr1*, *php3*, *plb1*, *ptr2*, *sdh3*, *SPAC27E2.11c*, *SPBC12C2.03c*, *SPCC594.02c*, *SPCC757.13*, *SPCC330.07c*, *tef101*) after its activation induced by torin1 treatment.

The only GO enrichments were detected among the UR genes, which were involved in translation (8 genes, $p = 1.7 \times 10^{-4}$) and organonitrogen compound biosynthetic process [11 genes, $p = 2.6 \times 10^{-3}$] (Bitton, et al., 2015).

There were no significant GO enrichments for the other groups. However, the DR genes were involved in cellular amino acid metabolic process (*put2*), chromatin organisation (*hhf2*), mitotic cell cycle phase transition (*tsc1*), mRNA metabolic process (*cxr1*), transmembrane transport [*ptr2*, *tsc1*] (Lock, et al., 2019).

The transcriptional targets of Gaf1 before its activation included genes responsible for chromatin organisation (*hhf2*), transcription (*hsr1*), sulphur metabolism (*SPBC12C.03c*, *sua1*), transmembrane transport (*pho842*, *ptr2*), and tRNA metabolic process [*elp5*] (Lock, et al., 2019). whereas the Gaf1-targets after its activation included genes for carbohydrate metabolism (*aah1*, *gas2*, *gcd1*), cell wall organisation/biogenesis (*aah1*, *gas2*), translation (*tef101*), generation of precursor metabolites and energy (*gcd1*, *sdh3*), lipid metabolism (*plb1*), transcription (*php3*, *hsr1*), transmembrane transport [*ptr2*, *SPCC330.07c*, *SPCC757.13j*] (Lock, et al., 2019).

In the single mutant, deletion of *plb1* decreased fitness, this gene encodes the phospholipase B homolog Plb1, which catalyses the release of fatty acids from lysophospholipids and is required for survival under high osmolarity and for the nutrient-mediated repression of sexual differentiation (Yang, et al., 2003). Interestingly, its depletion has been reported to increase chronological lifespan (Sideri, et al., 2015). The double mutant for this gene also presented reduced fitness, indicating that Gaf1 and Plb1 perform buffering functions between each other. In *gaf1* Δ cells, *plb1* was UR and it was detected as a transcriptional target of Gaf1 after its activation (Rodríguez-López, et al., 2020), potentially for the repression of *plb1* for functions that remain to be elucidated.

The deletion of *put2* and *ptr2* increased fitness of the single mutant but decreased fitness of the double mutant, indicating a buffering action between Gaf1, Put2 and Ptr2, related to the amino acid metabolic function predicted for Put2 and the transmembrane transport exerted by Ptr2 (Lock, et al., 2019). Potentially, these proteins are involved in nutrient sufficiency signalling that is compensated by Gaf1 in the single mutant, but missing in the double mutant. Consistently, in *gaf1Δ* cells *ptr2* is DR, this gene was detected to be a continuous transcriptional target of Gaf1 which is bound before and after its activation (Rodríguez-López, et al., 2020).

The comparison between the double mutants resistant to torin1, against the Gaf1-dependent transcriptional profile, showed an overlap of 5 genes (figure 64).

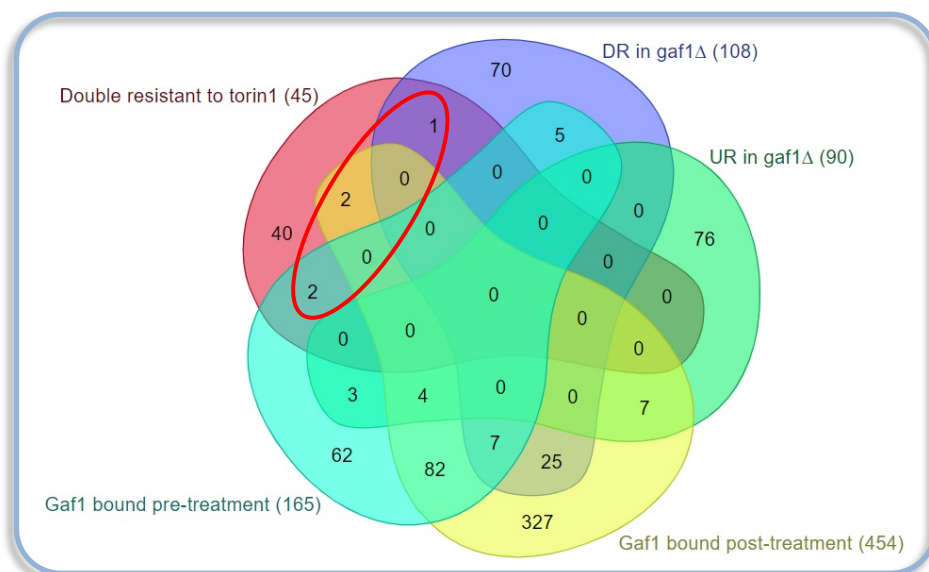


Figure 64. Venn diagram using Molbiotoll showing between double mutants resistant to torin1 (red), downregulated genes in *gaf1Δ* after torin1 treatment (purple), upregulated genes in *gaf1Δ* after torin1 treatment (green), transcriptional target genes of Gaf1 before torin1 treatment (yellow), and transcriptional target genes of Gaf1 after 1 hour of torin1 treatment (magenta). The relevant overlaps are circled in red. All of the experiments were performed in rich media.

The integration of these gene lists revealed that among the double mutants resistant to torin1 there was 1 DR gene (*icb4*) in *gaf1Δ* cells treated with torin1.

This gene encodes the sphingoid long chain base kinase, predicted to be involved in lipid metabolism (Lock, et al., 2019).

Other overlapping genes included 2 genes (*atg6*, *SPAC17A2.10*) to which Gaf1 binds before its activation. As mentioned above *atg6* encodes Atg6, an important regulator of autophagy and lipid metabolism (Lock, et al., 2019). Additionally, there were 2 genes (*fsv1*, *sdh3*) to which Gaf1 binds after its activation induced by torin1. These genes are involved in generation of precursor metabolites and energy (*sdh3*), membrane organisation, organelle localisation and vesicle-mediated transport [*fsv1*] (Lock, et al., 2019).

The comparison between the double mutants sensitive to torin1, against the Gaf1-dependent transcriptional profile, showed no overlaps between the genes (figure 65).

The integration of the Gaf1-transcriptional profile with the Gaf1-genetic interactome across all the non-essential genes of *S. pombe*, allowed to decipher novel additional functions of this transcription factor beyond its reported roles in transcription and amino acid homeostasis in response to nitrogen stress (Laor, et al., 2015; Ma, et al., 2015; Rodríguez-López, et al., 2020).

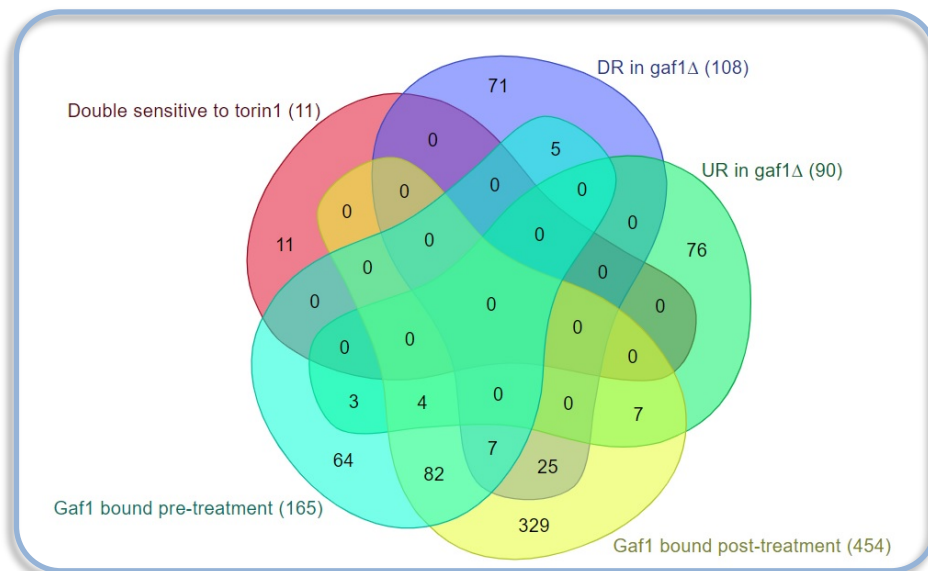


Figure 65. Venn diagram using Molbiotoll showing between double mutants sensitive to torin1 (red), downregulated genes in *gaf1*Δ after torin1 treatment (purple), upregulated genes in *gaf1*Δ after torin1 treatment (green), transcriptional target genes of Gaf1 before torin1 treatment (yellow), and transcriptional target genes of Gaf1 after 1 hour of torin1 treatment (magenta). All of the experiments were performed in rich media.

These results provided a complex matrix of information for both common and specific Gaf1-interactors, allowing to identify the involvement of Gaf1 in a range of biological processes, some of them described for the first time. Some examples include: membrane organisation and biogenesis, lipid metabolism, organelle localisation, chromatin organisation, response to osmotic stress, carbohydrate metabolism, cell signalling, mRNA and tRNA metabolism. Future studies will clarify the mechanisms used by Gaf1 for the direct or indirect regulation of the expression of the genes involved in those processes, elucidating the Gaf1-dependent interplay of that genetic network in the TOR pathway relevant for cell physiology and disease.

Chapter 7. Closing remarks and future work

During the last century, the significant increases in the average age of human populations, have prompted major healthcare and socio-economic challenges to modern societies introduced by a world-wide elderly population. The current scientific perspectives on ageing research aiming to have a future contribution to the improvement of this demographic shift towards population ageing, have focused their efforts not only on increasing lifespan of model organisms, but on enhancing the length of time individuals sustain optimal health without the decay associated with age.

It has been well established that the lifespan of living organisms is determined by environmental and genetic factors that are highly conserved across species and are amenable for interventions. Based on this approach, the principal objective of the current dissertation was to elucidate the functional role of the evolutionarily conserved GATA transcription factor Gaf1 in nutrient responses of the cell coordinated by the TOR signalling pathway. An additional aim of this project was the characterisation of novel phenotypic features of growth and survival, intending to bring insights into molecular mechanisms underlying cellular ageing.

Part of this work also included the development of comprehensive omics-datasets for data mining, gathering information about relevant genes conferring resistance to TOR signalling inhibition, relevant to decipher molecular mechanisms involved in the resistance to the anticancer-drug torin1 used in the present study to globally screen the Gaf1-dependent transcriptome, and the

network of synthetic genetic interactions between *gaf1* gene and all the non-essential genes present in the genome of the model organism *S. pombe*, currently validated for these applications due to its similarities with higher eukaryotic cells.

7.1. *In silico* analyses and growth patterns mediated by Gaf1 transcription factor

The first section of this dissertation was based on the use of bioinformatic tools to validate Gaf1 as a relevant model to extrapolate results to other species, and explore additional aspects of this transcription factor including: the structural organisation of the primary structure of its polypeptide chain, the predicted/established Protein-to-Protein Interactions (PPIs), the mRNA morphology and its transcriptional behaviour in different growth conditions.

These *in silico* analyses demonstrated that Gaf1 transcription factor is a relevant conserved model present from fungi to metazoans, which allows to study the role of other GATA transcriptional regulators involved in nutrient sensing pathways, with implications in survival and cellular ageing downstream of TORC1 signalling.

The orthologues identified were Gat1 in *S. cerevisiae*, and GATA6 in humans. They share 41 identical positions (out of ~855 amino acids in *S. pombe*), from which 21 of them are located within/near the GATA type zinc-binding motif. The zinc finger in these three orthologues belong to the category IVa (17-residue loop) that is a configuration attributed to vertebrates. They are reported to exert similar

functions in those organisms, including nitrogen source utilisation and mating-type shift in fungi, as well as development and differentiation in mammals.

The PPI analyses provided a general overview of the network of proteins interacting with Gaf1, which was used to gain further insights into the functional role of this transcription factor. The genes encoding for proteins interacting with Gaf1 were grouped in Gene Ontologies (GO) categories, the most significant enrichments were observed among genes involved in nitrogen metabolism and transcriptional regulation of gene expression, providing a biological context for the network of PPIs.

Another relevant feature of Gaf1 are the long 5' and 3' UTRs detected in *gaf1* transcripts of 910 and 776 nucleotides respectively, compared to the mean UTR length of ~465 nucleotides in *S. pombe*. These long UTRs in *gaf1* transcripts might confer rapid degradation of its transcripts for RNA turnover when cells are exposed to nitrogen abundance. This represent a novel alternative mechanism for the inactivation of Gaf1 before its translation which has not been previously described in the literature. This could operate in addition to the reported cytoplasmic retention exerted by active TORC1 in normal nitrogen conditions, potentially related to the basal role of Gaf1 before its activation.

Regarding growth patterns mediated by Gaf1, these were studied to decipher the influence of the extracellular environment over a myriad of cellular responses. Several environmental settings resembling normal and starvation conditions were assessed by using different growth media compositions, pharmacological

interventions and mutagenic analyses to characterise cellular growth and survival. The results showed that pharmacological interventions in rich solid media using the global inhibitor of TOR kinases torin1 in wild type cells, completely abrogated cellular growth compared to the mild reduction in growth produced caffeine + rapamycin treatment, which differentially targets various cellular processes controlled by TORC1 that escape single-compound treatment.

This finding suggests that the heightened impact of torin1 on wild type cells could be produced by the complete inhibition of TORC1 signalling including the rapamycin-resistant elements not affected by caffeine + rapamycin, combined with the inhibition of TORC2 that increase cell sensitivity to environmental signals resembling severe starvation that ultimately obstructs cell cycle progression even at the logarithmic growing phase, decreasing both cell growth and division.

The growth rate of *gaf1* Δ strain in rich media was slower than the wild types cells, indicating that the deletion of this non-essential gene has an impact on cell fitness. Nevertheless, high concentration of torin1 are not cytotoxic for this mutant which proved to be resistant to this compound. This is in stark contrast with the sensitivity of this strain to poor nitrogen sources such as proline, revealing that Gaf1 operates in several signalling networks that detect nitrogen sources to reprogram patterns of gene expression accordingly. Depletion of this transcription factor enables cells to proliferate with inactive TOR signalling, but its presence in the cell completely interrupts cell cycle progression when TOR activity is inhibited. This is relevant to understand the mechanisms that confer resistance to cancer therapies and pathologies that involved interference of the TOR pathway.

The complex dynamic regulating amino acid biosynthesis, metabolism and sensing during TOR inhibition, was studied on minimal solid media supplemented with both ammonium as a nitrogen source, and a titration of the basic amino acid arginine -inducer of cell growth via activation of the TOR signalling- to counteract and reverse the effects of torin1 and rapamycin treatments.

The wild type and *gaf1* Δ mutant grew slower in minimal media compared to rich media in both solid and liquid matrixes, with rapamycin treatment producing similar growth rates between these two strains. This suggests a potential role of Gaf1 in temporal development controlled by nutrient availability and uptake, different from nitrogen abundance which was present in both types of media.

Regarding amino acid biosynthesis, metabolism, sensing and uptake, arginine supplementation on its own did not enhanced cell growth or bypassed the inhibitory effect of torin1. Conversely, it enhanced sensitivity in minimal solid media. Nevertheless, disruptions in arginine conversion genes (*car1* Δ , *aru1* Δ , *car2* Δ) conferred slight resistance at high concentrations of arginine, suggesting that either increased production of derivatives generated during arginine metabolism (nitric oxide, urea, ornithine leading to putrescine, etc.) could increase sensitivity, or that intracellular accumulation of unmetabolized arginine could produce resistance to torin1 via TORC1 re-activation.

Considering that arginine uptake is inhibited by the presence of ammonium due to the repression of ammonia-sensitive permeases, future work is needed to elucidate the precise molecular mechanisms controlling the system II specific for

arginine uptake in fission yeast, which will contribute to better understand the hyperammonemia-induced cytotoxicity reported in yeast, particularly at low concentrations of ammonium.

In the present study, enhancements in growth were not observed in all the strains after arginine supplementation on minimal media, apart from *gaf1*Δ and slightly in *tco89*Δ. This could be attributed to the inhibition of the second system for arginine uptake saturated by the standard concentration of ammonium used in the media (96 mM), where the highest concentration of arginine supplementation on its own did not show major effects on growth (enhancement or reduction). This also reflects that the pH was not detrimental in this environment.

Arginine supplementation slightly increased growth of the *gaf1*Δ, consistent with basal levels of *cat1* transcripts in the absence of Gaf1, revealing alternative mechanisms for its transcription apart from *Isp7*. Further studies will clarify both if arginine uptake occurs in *gaf1*Δ cells which activates TORC1, and if rapamycin reduces arginine uptake or inhibits the arginine-dependent activation of TORC1 in this strain.

The reduced amino acid uptake of *tor1*Δ and *gaf1*Δ cells, due to the downregulation of the nitrogen starvation-induced permease genes *isp5*, *per1* and *put4*, may lead to slight torin1 resistance, indicating that resistance and sensitivity is also mediated by the nutritional context. This analysis brings insights into potential patterns of amino acid import and metabolism to control cell growth

during nutritional limitation, particularly induced by pharmacological interventions of the TOR pathway.

The results from this section demonstrate for the first time that arginine supplementation in minimal media combined with torin1 treatment in the presence of ammonium, enhanced the inhibition in cell growth, suggesting that this drug instead of reducing amino acid uptake, might be increasing it leading to cytotoxicity when combined with arginine.

Future studies will clarify the effects of ammonium on arginine uptake during torin1 or rapamycin treatments and the ammonium/arginine-induced cell death, assessing canavanine resistance, transcription/localisation of permeases, and their interplay with downstream effectors that regulate amino acid transport in the fission yeast.

These efforts will also clarify whether torin1 treatment affects amino acid transport by mechanisms involving regulation of membrane potential and transcription of genes involved in vacuole organisation. Additionally, further characterisation of the arginine import permease Aat1 is needed, to understand if this permease is affected in *tor1Δ* and *gaf1Δ*. The present study detected Aat1 amongst the Gaf1 target genes after its activation with no differential expression in *gaf1Δ*, suggesting an interplay between Tor1 and Gaf1 for amino acid sensing and uptake that dictates growth. Future studies will clarify the effects of ammonium on arginine uptake during torin1 treatment and ammonium/arginine-induced cell death.

In this sense, the results from the toxicity assays confirmed that torin1-treated *gaf1* Δ mutants are resistant to the drug and are able to sense/utilise the presence of nutrients in the extracellular environment to proliferate faster. The results also suggest that torin1 affects growth by delaying cell cycle duration as observed in the extended generation times, caused by TORC1 inhibition, consistent with a reduction in cell size at division with reversible growth arrest that does not lead to apoptosis.

This information about torin1 cytotoxicity was used to measure the length of time the fission yeast cells survive without dividing, also called chronological lifespans (CLS). This non-mammalian model system allows to explore evolutionarily conserved signalling pathways that regulate lifespan, acting as a post-mitotic model to study molecular mechanisms controlling cellular ageing of differentiated non-dividing somatic cells in higher organisms including humans.

The aim of these experiments was to elucidate the involvement of TOR kinases and Gaf1 in the regulation of lifespan in the fission yeast, in response to nutrient availability and pharmacological interventions of the TOR signalling pathway. For this purpose, the entire survival curve of fission yeast cells was documented until viability was lost, recapitulating features of ageing conserved throughout eukaryotes involving reduced lifespan by nutrient abundance, lifespan extension by caloric restriction, regulation of lifespan by TORC1/TORC2 and translation efficiency.

The CLS experiments with either rapamycin or torin1, showed that the increase in lifespan produced by TORC1 signalling inhibition is independent from Gaf1. However, Gaf1-induced genes during starvation may contribute to survival by activation of TORC2, impairing its pro-survival autophagic action that diminishes apoptosis. These results suggest that Gaf1 is involved in the regulation of autophagy and apoptosis depending on nutrient availability and highlight the relevant role of amino acid availability during the stationary phase, which contributed to extend lifespan in the background of *gaf1*Δ, *tco89*Δ and *tor1*Δ.

The extension in lifespan produced by TOR inhibition with torin1, depends on the type of media, time of the treatment and dosage, where higher concentrations during both the logarithmic phase in rich media and stationary phase in minimal media were correlated with increased CLS only in the mutants containing TORC1 activity. Torin1 treatment after the log phase is detrimental in the presence of amino acids, whereas the absence of amino acids in the environment allows increases in lifespan regardless of the time point that torin1 treatment is administered and the concentration.

This suggests that alternative nutrient sensing mechanisms influence cell fate, and/or the existence of a transient pan-TOR inhibition by torin1 in liquid media that allows subsequent TORC2 activation and TORC1 inactivation caused by reduced amount of nutrients in the media. These findings represent a novel contribution for TORC2 in the regulation of lifespan after the onset of the stationary phase, additional to its role in survival during stress.

Treatment with the alternative compound C991 which indirectly reduces TOR signalling via induction of the AMPK homeostatic activity for cellular energy, did not produce significant increases in CLS, probably due to the lack of interaction between the compound and the two AMPK subunits of the fission yeast tested in the present study, or an inefficient indirect-inhibition of the TOR signalling that did not trigger lifespan extension.

Additionally, the effect on lifespan of protein translation accuracy and efficiency was explored with another set of CLS experiments. For this purpose, the assessment of several mutants carrying disruptions in the ribosomal protein S23 (*rps23*) -a component of the small ribosomal subunit 40S- affecting translation accuracy, revealed a drastic reduction in median lifespan in *S. pombe*. These mutations increase or decrease the accuracy to recognise stop codons, confirming the pivotal role of *rps23* in quality control during translation. Therefore, the rate of translation and accuracy are fundamental for the regulation of lifespan, and demonstrate that ribosomal conformation has the potential to become a target for therapeutic interventions of cellular ageing.

Altogether the growth assessment in the present study, revealed that nutrient availability, specifically amino acids, control common cellular responses among model organisms such as lifespan and resistance to stress, reinforcing the existence of broadly evolutionarily conserved properties of ageing present in both unicellular and multicellular eukaryotes. Therefore, genetic, pharmacological and environmental interventions that decrease activity of conserved nutrient-sensing

pathways are promising strategies to be further explored in mammalian systems with the aim of improving human health and lifespan.

7.2. Gaf1-dependent transcriptome

One of the greatest challenges in modern biology is to understand the relationship between genomic diversity and phenotypic traits. Recent evidence obtained from the fission yeast confirmed the connection between nutrient signalling and lifespan via a complex network of transcriptional activity, particularly influenced by nitrogen availability.

In this sense, the characterisation of the transcriptional network controlled by Gaf1 revealed that this transcription factor affects either positively or negatively the expression of ~200 genes after TORC1 inhibition. Its functional role involves the repression of highly expressed genes used for protein synthesis, which may be rapidly regulated to adjust for survival to environmental challenges. This is consistent with conserved pathways controlling stress resistance, which have been intrinsically linked to longevity in yeast, worms, fruit flies and mammals as they prevent damage and ensure survival during periods of starvation.

The enrichment of glucose-related metabolic processes during basal Gaf1 binding activity, may be reflecting a possible interplay of TORC2 and Gaf1 transcriptional function under nitrogen-rich conditions. This novel function will require additional scrutiny in future studies.

The results obtained in the present study demonstrated that Gaf1 transcriptional activity reduces the expression of genes involved in anabolism, and induces genes required for catabolism and autophagy. These transcriptional programs are controlled directly and indirectly by Gaf1 to balance the metabolism of amino acids and other molecules, possibly by recycling nutrients under detrimental conditions that do not support rapid proliferation (where amino acid permeases have a relevant role), and regulating physiological changes that support the cell cycle arrest observed during TORC1 inhibition. Similar patterns of gene expression have been described in the budding yeast controlled by the GATA transcription factors Gln3 and Gat1 during TORC1 inhibition.

The thorough characterisation of the Gaf1-dependent transcriptional network prepared for the present study, involved the assessment of gene configuration and gene essentiality for cell viability. This was performed through the comparison between intronic regions and gene essentiality of the Gaf1-transcriptional targets. The aim was to understand the intronic composition of essential genes (less likely to be rapidly regulated, containing more introns) against non-essential genes (likely to be rapidly regulated, containing less introns).

The Gaf1-dependent transcriptional profile revealed that only the non-essential genes without introns, showed the most diverse range of GO enrichments, suggesting that this could be a mechanism to enhance resistance to stress and survival avoiding natural selection against them, in comparison to the more “exposed” essential genes subjected to stringier controls from environmental selection.

Future studies will clarify if the intronic regions detected amongst the genes transcriptionally controlled by Gaf1, operate as regulatory elements for those genes apart from their promoters, also called “expression-controlling introns” that induce or repress their own transcription/translation, which could be clinically relevant for therapeutic interventions in genetic diseases and biotechnology applications including protein production.

The present study revealed a complex network of Gaf1-indirect transcriptional regulation of starvation genes and transcription factors. This is the outcome of the extensive rewiring occurred throughout evolution for crucial responses required for survival, and demonstrate the plasticity of the transcriptional network controlled by Gaf1. Future studies of those target genes will reveal their mechanism of expression (direct/indirect regulation) and genetic interactions, as well as information about conserved ageing-related processes governed by Gaf1, which other GATA transcription factors may perform downstream of TORC1. These future studies will ultimately contribute to the identification of key components of the fundamental processes that regulate cellular ageing and longevity.

Altogether, the present study demonstrated that Gaf1 is a repressor of non-coding sequences relevant for stress resistance and survival. This is actioned via the direct binding to tRNA genes to repress their expression, providing a mechanism for transcriptional control of global protein translation that prolongs lifespan and reduce translation during TORC1 inhibition that may contribute to lifespan extension. This finding confers Gaf1 a novel transcriptional-based control

of translation and metabolism downstream of TORC1 that is essential to achieve the growth inhibition triggered by reduced TORC1 activity.

7.3. *gaf1*-dependent interactome

Synthetic genetic arrays (SGA) were used for the quantitative and systematic high-throughput screening of genetic interactions between the *gaf1* gene and the non-essential genes of the *S. pombe* genome. This SGA study was performed under optimal nutritional conditions, and was further exploited by introducing chemical genomics using torin1 to inhibit the TOR signalling pathway.

The aim was to elucidate several aspects of *gaf1* including its functional roles *in vivo*, identify candidate genes involved in biochemical pathways/molecular mechanisms directly or indirectly targeted by this compound, elucidate the *gaf1*-dependent interactome in the context of TOR inhibition, and detect the genetic interactions within this network that either reduce or enhance the resistance of *gaf1* Δ mutants to high concentrations of the drug.

These interactions are classified as negative when genes acting in two different pathways that functionally compensate each other, impinge on the same essential biological process, and positive when genes function in a single or linear biochemical pathway, where deleterious mutations in one gene mask the effects of other mutations in the same pathway.

The chemical-genetic screening of single mutants (non-essential genes) in torin1 allowed to explore several functional factors of the fission yeast genome,

including information about the resistance or sensitivity to the compound. The study identified that strains with impaired functions in autophagy-dependent proteolysis showed significant increases in single colony sizes when grown in torin1, suggesting that the increased colony size of the mutants in this context, could be the result of impaired vacuolar function that are unable to complete proteolysis and overall organelle digestion.

Cellular homeostasis in eukaryotic cells requires the coordinated response of different organelles to internal and environmental signals. The yeast vacuole (analogous to the mammalian lysosome) is the degradative compartment of the cell responsible for both proteolysis and for the catabolic process of autophagy. Interestingly, mutants with disrupted autophagy were previously reported to have significantly enlarged vacuoles due to the accumulation of autophagic bodies in the context of nitrogen depletion, suggesting that the increased colony size of the mutants under torin1 treatment detected in the present study, could be the result of impaired vacuolar function that are unable to complete proteolysis and overall organelle digestion.

The current SGA methodology classify positive interactions when there is increased colony size growth recognised by the software, future studies will assess alternative interpretations derived from the remarkable enrichment of vacuolar processes among the 264 disrupted genes identified in the present study, clarifying if the increased colony/spot sizes detected in SGA screenings of TOR inhibitors, particularly in mutants disrupted in vacuolar functions, occurs either because of vacuolar enlargement (rather than increases in cell

proliferation) or due to the capacity of the cells to bypass the restrictive effect of the drugs in proliferation as is the case of *gaf1Δ* cells. This finding introduces a novel parameter to be considered for the interpretation of SGA results.

While the steps and molecular mechanisms responsible for vacuolar fusion have been well described, the molecular drivers of vacuolar fission remain poorly understood. Considering that TORC1 is localised at the vacuoles and its activity negatively regulates autophagy, future studies will establish if a fraction of the 264 genes identified in the present study are involved in molecular mechanisms by which TOR signalling control the process of vacuolar fission/fragmentation in response to stress, particularly in the context of its association with membranes. This will contribute to determine if disruptions in those genes produce enlarged vacuoles and increased cell size (biomass) during TOR inhibition due to their inability to undergo vacuolar fission that lead to increases in colony sizes. Also, this will clarify additional roles of the TOR pathway particularly in the context of its association with membranes.

These results provided additional information regarding the relationship between TOR signalling and vacuolar morphology, introducing new insights into potential candidate genes responsible for vacuolar fragmentation, and suggesting that mutant strains with disruptions in vacuolar functions may present enlarged vacuoles and cell size due to their inability to undergo vacuolar fission in response to TOR inhibition.

While the genetic negative interactions provided more functional information than those obtained from positive interactions, the general profile compiled from both negative and positive interactions integrated with the fitness profile of single mutants, indicated that Gaf1 mainly operates between different pathways that buffer each other, rather than within the same pathways. The synthetic genetic interactions revealed novel networks for this transcription factor to exert its functions in catabolism and overall regulation of protein synthesis, complementing the findings from the transcriptome analyses from chapter 5.

Furthermore, the results revealed that genes with direct or indirect implications in the repression of protein synthesis via regulation of chromatin organisation, transcription and biosynthesis of the ribosomal machinery including tRNAs, provide significant resistance to torin1 when they are not present in the cell. The negative interactions detected in this chemical-genetic screening of double mutants, revealed novel genes that operate in such functions during TOR inhibition, particularly buffering the activity of Gaf1.

The considerable representation of positive interactions identified among double mutants during torin1 treatment, driven by conserved genes enriched in proteolysis, vacuolar function and catabolism, suggest that the examination of their role in other rapamycin-sensitive processes is likely to be fruitful, as the majority of the genes identified in this study are conserved in both budding yeast and humans. The library of haploid single mutants used for these experiments provide 95.3% coverage of the *S. pombe* genome and includes several human cancer genes with over 30% of homology.

Future studies will clarify if the highest levels of resistance to torin1 conferred by mutations in the genes detected here, could be attributed to either increases in cell size due to disruptions in autophagy, or to progression in cell proliferation, as observed in *gaf1* Δ cells, potentially because of interferences with genes that regulate chromatin organisation, transcription and biosynthesis of the ribosomal machinery including tRNAs, which have been proposed as the conveyors of nutrient availability to TORC1.

Since these processes have been described to be regulated by TOR signalling, the elucidation of molecular mechanisms that confer resistance to torin1, and involved in cellular maintenance during TOR inhibition -including differentiated post-mitotic quiescent cells-. This will improve the efficacy of torin1 as an anti-cancer compound, and will provide both comprehensive descriptions of normal cellular physiology, and insights into novel target genes amenable for therapeutic interventions together with the regulatory mechanisms governing several human disorders that involve the loss of adequate lysosomal function, including cancer and neurodegenerative diseases.

The central role of amino acid homeostasis and autophagy in maintaining chronological longevity from yeast to higher organisms, have been attributed to the recycling and removal of cellular damage in the nutrient-limited context of non-dividing cells. These notions have prompted dietary nutritional balance as an alternative strategy for increasing healthy lifespan in humans via “dietary interventions” instead of through caloric restrictions or pharmacological interventions.

Altogether, the SGA analyses produced in this study generated genetic networks linked to *gaf1* in the presence and absence of global TOR inhibition, that provide comprehensive information about individual functional roles of key genes involved in survival and cell cycle regulation, and contributed to elucidate aspects of the complex relationship between genotype and phenotype in *S. pombe*, including the resistance to torin1 treatment potentially applicable to cancer cells. This study represents the first report of a global chemical-genetic screening of non-essential deletion mutants in this model system that produced altered fitness in the presence of torin1 treatment in rich media *in vivo*.

The genes and pathways identified in this dissertation provide valuable insights into the complex relationship between proteolysis, catabolism, vacuolar morphology and TOR signalling. These results introduce new insights into potential candidate genes responsible for vacuolar fission, and open new questions regarding the additional roles that TORC1 may have during its association with membranes.

Bibliography

- Abdel-Sater, F., Iraqui, I., Urrestarazu, A. & André, B., 2004. The external amino acid signaling pathway promotes activation of Stp1 and Uga35/Dal81 transcription factors for induction of the AGP1 gene in *Saccharomyces cerevisiae*. *Genetics*, Apr, 166(4), pp. 1727-39.
- Altschul, S. F. et al., 1997. Gapped BLAST and PSI-BLAST: a new generation of protein database search programs. *Nucleic Acids Research*, 1 Sep, 25(17), pp. 3389-402.
- Araki, T., Uesono, Y., Oguchi, T. & Toh-E, A., 2005. LAS24/KOG1, a component of the TOR complex 1 (TORC1), is needed for resistance to local anesthetic tetracaine and normal distribution of actin cytoskeleton in yeast. *Genes and Genetic Systems*, Oct, 80(5), pp. 325-43.
- Arimbasseri, A. G. & Maraia, R. J., 2016. RNA polymerase III advances: structural and tRNA functional views. *Trends in Biochemical Sciences*, Volume 41, p. 546–559.
- Aris, J. P. et al., 2012. Amino acid homeostasis and chronological longevity in *Saccharomyces cerevisiae*. *Sub-cellular Biochemistry*, Volume 57, pp. 161-186.
- Arita, Y. et al., 2011. Microarray-based target identification using drug hypersensitive fission yeast expressing ORFeome. *Molecular Biosystems*, May, 7(5), pp. 1463-72.
- Arnaoudova, E. et al., 2010. Statistical Phylogenetic Tree Analysis Using Differences of Means. *Frontiers in Neuroscience*, 4(47), pp. 1-7.
- Aronova, S. et al., 2007. Probing the membrane environment of the TOR kinases reveals functional interactions between TORC1, actin, and membrane trafficking in *Saccharomyces cerevisiae*. *Molecular Biology of the Cell*, Aug, 18(8), pp. 2779-94.
- Aspuria, P. J. & Tamanoi, F., 2008. The Tsc/Rheb signaling pathway controls basic amino acid uptake via the Cat1 permease in fission yeast. *Molecular Genetics and Genomics*, May, 279(5), pp. 441-50.
- Atkin, J. et al., 2014. Torin1-mediated TOR kinase inhibition reduces Wee1 levels and advances mitotic commitment in fission yeast and HeLa cells. *Journal of Cell Science*, 127(6), pp. 1346-56.
- Bähler, J. et al., 1998. Heterologous modules for efficient and versatile PCR-based gene targeting in *Schizosaccharomyces pombe*. *Yeast*, Jul, 14(10), pp. 943-51.

Balcazar, N. et al., 2009. mTORC1 activation regulates beta-cell mass and proliferation by modulation of cyclin D2 synthesis and stability. *The Journal of Biological Chemistry*, 20 Mar, 284(12), pp. 7832-42.

Bar-Peled, L. & Sabatini, D. M., 2014. Regulation of mTORC1 by amino acids. *Trends in Cell Biology*, Jul, 24(7), pp. 400-6.

Baryshnikova, A. et al., 2010. Synthetic genetic array (SGA) analysis in *Saccharomyces cerevisiae* and *Schizosaccharomyces pombe*. *Methods in Enzymology*, Issue 470, pp. 145-79.

Bearson, B. L., Lee, I. S. & Casey, T. A., 2009. Escherichia coli O157: H7 glutamate- and arginine-dependent acid-resistance systems protect against oxidative stress during extreme acid challenge. *Microbiology*, Mar, 155(3), pp. 805-12.

Beck, T. & Hall, M., 1999. The TOR signalling pathway controls nuclear localization of nutrient-regulated transcription factors. *Nature*, 9 Dec, 402(6762), pp. 689-92. doi: 10.1038/45287.

Ben-Sahra, I. & Manning, B. D., 2017. mTORC1 signaling and the metabolic control of cell growth. *Current Opinon in cell biology*, Apr, Volume 45, pp. 72-82.

Bicho, C. C. et al., 2010. A genetic engineering solution to the "arginine conversion problem" in stable isotope labeling by amino acids in cell culture (SILAC). *Molecular & Cellular Proteomics*, Jul, 9(7), pp. 1567-77.

Binda, M. et al., 2009. The Vam6 GEF controls TORC1 by activating the EGO complex. *Molecular Cell*, 11 Sep, 35(5), pp. 563-73.

Bioneer, n.d. *Bioneer*. [Online]
Available at: <http://eng.bioneer.com/products/YeastGenome/Spombe-overview.aspx>
[Accessed Feb 2017].

Bitton, D. A. et al., 2015. AnGeLi: A Tool for the Analysis of Gene Lists from Fission Yeast. *Frontiers in Genetics*., 16 Nov, Issue 6, p. 330.

Bjedov, I. et al., 2010. Mechanisms of life span extension by rapamycin in the fruit fly *Drosophila melanogaster*. *Cell Metabolism*, Volume 11, pp. 35-46.

Blagosklonny MV, 2013. MTOR-driven quasi-programmed aging as a disposable soma theory: Blind watchmaker vs. Intelligent designer. *Cell Cycle*, 15 Jun, 12(12), pp. 1842-7.

Bone, N., Millar, J. B., Toda, T. & Armstrong, J., 1998. Regulated vacuole fusion and fission in *Schizosaccharomyces pombe*: an osmotic response dependent on MAP kinases. *Current Biology*, 29 Jan, 8(3), pp. 135-44.

- Boone, C., Bussey, H. & Andrews, B. J., 2007. Exploring genetic interactions and networks with yeast. *Nature Reviews. Genetics*, Jun, 8(6), pp. 437-49.
- Borek, W. E., Zou, J., Rappsilber, J. & Sawin, K. E., 2015. Deletion of Genes Encoding Arginase Improves Use of "Heavy" Isotope-Labeled Arginine for Mass Spectrometry in Fission Yeast. *PLoS One*, 15 Jun, 10(6), p. e0129548.
- Borneman, A. R. et al., 2007. Divergence of transcription factor binding sites across related yeast species. *Science*, 10 Aug, 317(5839), pp. 815-9.
- Brummendorf, T. H. & Balabanov, S., 2006. Telomere length dynamics in normal hematopoiesis and in disease states characterized by increased stem cell turnover. *Leukemia*, Oct, 20(10), p. 1706–1716.
- Buttgereit, F. & Brand, M. D., 1995. A hierarchy of ATP-consuming processes in mammalian cells. *The Biochemical Journal*, 15 Nov, 312(Pt 1), pp. 163-7.
- Campbell, K. J. & White, R. J., 2014. MYC regulation of cell growth through control of transcription by RNA polymerases I and III. *Cold Spring Harbor Perspectives in Medicine*, 1 May, 4(5), p. 4:a018408.
- Chen, B. R. & Runge, K. W., 2009. A new *Schizosaccharomyces pombe* chronological lifespan assay reveals that caloric restriction promotes efficient cell cycle exit and extends longevity. *Experimental Gerontology*, Aug, 44(8), pp. 493-502.
- Chen, D. et al., 2003. Global transcriptional responses of fission yeast to environmental stress. *Molecular Biology of the Cell*, Jan, 14(1), p. 214–29.
- Chen, D. et al., 2008. Multiple pathways differentially regulate global oxidative stress responses in fission yeast. *Molecular Biology of the Cell*, Jan, 19(1), p. 308–317.
- Cheng, Y. et al., 2016. Protective Effects of Arginine on *Saccharomyces cerevisiae* Against Ethanol Stress. *Scientific Reports*, Issue 6, p. 31311.
- Chia, K. H. et al., 2017. Ragulator and GATOR1 complexes promote fission yeast growth by attenuating TOR complex 1 through Rag GTPases. *Elife*, 4 Dec, Volume 6, p. pii: e30880.
- Chica, N. et al., 2016. Nutritional Control of Cell Size by the Greatwall-Endosulfine-PP2A-B55 Pathway. *Current Biology*, 8 Feb, 26(3), pp. 319-30.
- Chorev, M. & Carmel, L., 2012. The Function of Introns. *Frontiers in Genetics*, 13 Apr, Volume 3, p. 55.
- Cohen, A., Kupiec, M. & Weisman, R., 2014. Glucose activates TORC2-Gad8 protein via positive regulation of the cAMP/cAMP-dependent protein kinase A

(PKA) pathway and negative regulation of the Pmk1 protein-mitogen-activated protein kinase pathway. *The Journal of Biological Chemistry*, 1 Aug, 289(31), pp. 21727-37.

Colman, R. J. et al., 2009. Caloric restriction delays disease onset and mortality in rhesus monkeys. *Science*, 10 Jul, 325(5937), pp. 201-4.

Cooper, S. J. et al., 2010. High-throughput profiling of amino acids in strains of the *Saccharomyces cerevisiae* deletion collection. *Genome Research*, Sep, 20(9), pp. 1288-96.

Corkins, M. E. et al., 2013. Zinc finger protein Loz1 is required for zinc-responsive regulation of gene expression in fission yeast. *Proc. Natl. Acad. Sci. USA.*, 17 Sept, 110(38), p. 15371–1.

Costanzo, M. et al., 2016. A global genetic interaction network maps a wiring diagram of cellular function. *Science*, 23 Sep, Issue 353, p. 6306. pii: aaf1420.

Costanzo, M. et al., 2010. The genetic landscape of a cell. *Science*, 22 Jan, 327(5964), pp. 425-31.

Costanzo, M. et al., 2019. Global Genetic Networks and the Genotype-to-Phenotype Relationship. *Cell*, 21 Mar. pp. 177(1):85-100.

Costello, G., Rodgers, L. & Beach, D., 1986. Fission yeast enters the stationary phase G0 state from either mitotic G1 or G2. *Current Genetics*, Volume 11, p. 119–125.

David, L., Clauder-Münster, S. & Steinmetz, L. M., 2014. High-density tiling microarray analysis of the full transcriptional activity of yeast. *Methods in Molecular Biology*, Volume 1205, pp. 257-73.

de Magalhães, J. P. et al., 2012. Genome-environment interactions that modulate aging: powerful targets for drug discovery. *Pharmacological Reviews*, Jan, 64(1), pp. 88-101.

Dimitrov, K. & Sazer, S., 1998. The role of fnx1, a fission yeast multidrug resistance protein, in the transition of cells to a quiescent G0 state. *Molecular and Cellular Biology*, 01 Sep, 18(9), pp. 5239-5246.

Dixon, S. J. et al., 2009. Systematic mapping of genetic interaction networks. *Annual Review of Genetics*, Issue 43, pp. 601-25.

Dixon, S. J. et al., 2008. Significant conservation of synthetic lethal genetic interaction networks between distantly related eukaryotes. *Proceedings of the National Academy of Sciences of the United States of America*, 28 Oct, 105(43), pp. 16653-8.

Dobson, A. J. et al., 2018. Tissue-specific transcriptome profiling of *Drosophila* reveals roles for GATA transcription factors in longevity by dietary restriction. *NPJ aging and mechanisms of disease*, 17 Apr.4(5).

Doi, A. et al., 2015. Chemical genomics approach to identify genes associated with sensitivity to rapamycin in the fission yeast *Schizosaccharomyces pombe*. *Genes to Cells*, Apr, 20(4), pp. 292-309.

Dubois, E., Hiernaux, D., Grennon, M. & Wiame, J. M., 1978. Specific induction of catabolism and its relation to repression of biosynthesis in arginine metabolism of *Saccharomyces cerevisiae*. *Journal of Molecular Biology*, 15 Jul, 122(4), pp. 383-406.

Duncan, C. D. S. et al., 2018. General amino acid control in fission yeast is regulated by a nonconserved transcription factor, with functions analogous to Gcn4/Atf4. *Proceedings of the National Academy of Sciences of the United States of America*, 20 Feb, 115(8), pp. E1829-E1838.

Dunn, T., Gable, K. & Beeler, T., 1994. Regulation of cellular Ca²⁺ by yeast vacuoles. *The Journal of Biological Chemistry*, 11 Mar, 269(10), pp. 7273-8.

Đúranová H, et al., 2019. Fission yeast *Schizosaccharomyces pombe* as a model system for ultrastructural investigations using transmission electron microscopy. *Journal of Microbiology, Biotechnology and Food Sciences*, 9(1), pp. 160 - 165.

Du, X. et al., 2006. The homologous putative GTPases Grn1p from fission yeast and the human GNL3L are required for growth and play a role in processing of nucleolar pre-rRNA. *Molecular Biology of the Cell*, 17(1), pp. 460-474.

Egel, R., 2004. *The Molecular Biology of Schizosaccharomyces pombe: Genetics, Genomics and Beyond*. s.l.:Springer.

Emerson, R. & Thomas, J. H., 2009. Adaptive Evolution in Zinc Finger Transcription Factors. Jan, 5(1), p. e1000325.

Fabrizio, P., Li, L. & Longo, V. D., 2005. Analysis of gene expression profile in yeast aging chronologically. *Mechanisms of Ageing and Development*, Jan, 126(1), pp. 11-6.

Fabrizio, P. & Longo, V. D., 2003. The chronological life span of *Saccharomyces cerevisiae*. *Aging Cell*, Volume 2, pp. 73-81.

Fantes, P. & Creanor, J., 1984. Canavanine resistance and the mechanism of arginine uptake in the fission yeast *Schizosaccharomyces pombe*. *Journal of General Microbiology*, Dec, 130(12), pp. 3265-73.

- Fantes, P. & Hoffman, C., 2016. A Brief History of *Schizosaccharomyces pombe* Research: A Perspective Over the Past 70 Years. *Genetics*, Jun, 203(2), pp. 621-9.
- Fantes, P. & Nurse, P., 1977. Control of cell size at division in fission yeast by a growth-modulated size control over nuclear division. *Experimental Cell Research*, Jul, 107(2), pp. 377-86.
- Fay, D., Keenan, S. & Han, M., 2002. *fzr-1* and *lin-35/Rb* function redundantly to control cell proliferation in *C. elegans* as revealed by a nonbiased synthetic screen. *Genes & Development*, 15 Feb, 16(4), pp. 503-17.
- Filer, D. et al., 2017. RNA polymerase III limits longevity downstream of TORC1. *Nature*, 552(7684), pp. 263-267.
- Fingar, D. C. et al., 2002. Mammalian cell size is controlled by mTOR and its downstream targets S6K1 and 4EBP1/eIF4E. *Genes Dev*, 15 Jun, 16(12), pp. 1472-87.
- Fontana, L., Partridge, L. & Longo, V. D., 2010. Extending healthy life span--from yeast to humans. *Science*, 16 Apr, 328(5976), pp. 321-6.
- Forsburg, S. L., 2011. Fission Yeast Cell Cycle. *PombeNet Forsburg Lab USC*.
- Forsburg, S. & Rhind, N., 2006. Basic Methods for Fission Yeast. *Yeast*, 23((3)), p. 173–183.
- Frias, M. A. et al., 2006. mSin1 is necessary for Akt/PKB phosphorylation, and its isoforms define three distinct mTORC2s. *Current Biology*, 19 Sep, 16(18), pp. 1865-70.
- Geissmann, Q., 2013. OpenCFU, a new free and open-source software to count cell colonies and other circular objects. *PLoS One*, 8(2), p. e54072.
- Gems, D. & Partridge, L., 2013. Genetics of longevity in model organisms: debates and paradigm shifts. *Annual Review of Physiology*, Volume 75, pp. 621-44.
- Georis, I., Tate, J., Cooper, T. G. & Dubois, E., 2011. Nitrogen-responsive Regulation of GATA Protein Family Activators Gln3 and Gat1 Occurs by Two Distinct Pathways, One Inhibited by Rapamycin and the Other by Methionine Sulfoximine. *Journal of Biological Chemistry*, 30 Dec, 286(52), pp. 44897-912.
- Godard, P. et al., 2007. Effect of 21 different nitrogen sources on global gene expression in the yeast *Saccharomyces cerevisiae*. *Molecular and Cellular Biology*, Apr, Volume 8, pp. 3065-86.

- Gonzalez, S. & Rallis, C., 2017. The TOR signaling pathway in Spatial and Temporal control of cell size and growth. *Frontiers in Cell and Developmental Biology*, 5(61).
- Goranov, A. I. et al., 2013. Changes in cell morphology are coordinated with cell growth through the TORC1 pathway. *Current Biology*, 22 Jul, 23(14), pp. 1269-79.
- Graczyk, D., Cieśla, M. & Boguta, M., 2018. Regulation of tRNA synthesis by the general transcription factors of RNA polymerase III—TFIIIB and TFIIIC, and by the MAF1 protein. *Biochimica et Biophysica Acta. Gene Regulatory Mechanisms*, Apr, 1861(4), pp. 320-329.
- Graczyk, D. et al., 2011. Casein kinase II-mediated phosphorylation of general repressor Maf1 triggers RNA polymerase III activation. *Proceedings of the National Academy of Sciences USA*, 22 Mar, 108(12), pp. 4926-31.
- Grech, L. et al., 2019. Fitness Landscape of the Fission Yeast Genome. *Molecular Biology and Evolution*, 1 Aug, 36(8), pp. 1612-1623.
- Gromak, N., 2012. Intronic microRNAs: a crossroad in gene regulation. *Biochemical Society Transactions*, 40(4), p. 759–761.
- Hara, K. et al., 2002. Raptor, a binding partner of target of rapamycin (TOR), mediates TOR action. *Cell*, 26 Jul, 110(2), pp. 177-89.
- Hardy, S., Legagneux, V., Audic, Y. & Paillard, L., 2010. Reverse genetics in eukaryotes. *Biology of the Cell*, 102(10), pp. 561-580.
- Harris, M. et al., 2013. FYPO: the fission yeast phenotype ontology. *Bioinformatics*, 29(13), pp. 1671-1678.
- Hartman, J. L., Garvik, B. & Hartwell, L., 2001. Principles for the buffering of genetic variation. *Science*, 9 Feb, 291(5506), pp. 1001-4.
- Hartmuth, S. & Petersen, J., 2009. Fission yeast Tor1 functions as part of TORC1 to control mitotic entry through the stress MAPK pathway following nutrient stress. *Journal of Cell Science*, 1 Jun, Volume 11, pp. 1737-46.
- Hartwell, L. et al., 1997. Integrating genetic approaches into the discovery of anticancer drugs. *Science*, 7 Nov, 278(5340), pp. 1064-8.
- Hayashi, T. et al., 2007. Rapamycin sensitivity of the *Schizosaccharomyces pombe* tor2 mutant and organization of two highly phosphorylated TOR complexes by specific and common subunits. *Genes to Cells*, Dec, 12(12), pp. 1357-70.

Hedges, S., 2002. The origin and evolution of model organisms. *Nature Reviews, Genetics*, Nov, 3(11), pp. 838-49.

Heitman, J., Movva, N. R. & Hall, M. N., 1991. Targets for cell cycle arrest by the immunosuppressant rapamycin in yeast. *Science.*, 23 Aug, 253(5022), pp. 905-9.

Hillson O, G. S. R. C., 2018. Prospects of Pharmacological Interventions to Organismal Aging. *Biomolecular Concepts*, 31 Dec, 9(1), pp. 200-215. doi: 10.1515/bmc-2018-0018.

Hillson, O., 2018. *Involvement of the fission yeast GATA transcription factor Gaf1 in TOR-dependent stress and nutrient responses.* [Online] Available at: <https://repository.uel.ac.uk/item/846z4> [Accessed 20 Jun 2019].

Hoe, K. L. et al., 1998. Molecular cloning of *gaf1*, a *Schizosaccharomyces pombe* GATA factor, which can function as a transcriptional activator. *Gene*, 30 Jul, 215(2), pp. 319-28.

Hoffman, C., Wood, V. & Fantes, P. A., 2015. An Ancient Yeast for Young Geneticists: A Primer on the *Schizosaccharomyces pombe* Model System. *Genetics*, Oct, 201(2), p. 403–423.

Hofman-Bang, J., 1999. Nitrogen Catabolite Repression in *Saccharomyces cerevisiae*. *Molecular Biotechnology*, Aug, 12(1), pp. 35-73.

Hummel , G., Warren, J. & Drouard , L., 2019. The multi-faceted regulation of nuclear tRNA gene transcription. *IUBMB Life*, Aug, 71(8), pp. 1099-1108.

Iadevaia, V., Liu, R. & Proud, C. G., 2014. mTORC1 signaling controls multiple steps in ribosome biogenesis. *Seminars in Cell & Developmental Biology*, Volume 36, p. 113–120.

Ikai, N., Nakazawa, N., Hayashi, T. & Yanagida, M., 2011. The reverse, but coordinated, roles of Tor2 (TORC1) and Tor1 (TORC2) kinases for growth, cell cycle and separase-mediated mitosis in *Schizosaccharomyces pombe*. *Open Biology*, Nov, 1(3), p. 110007.

Ishiguro, A. et al., 2000. The Rpb6 subunit of fission yeast RNA polymerase II is a contact target of the transcription elongation factor TFIIS. *Molecular and cellular biology*, Feb, 20(4), pp. 1263-70.

Jacinto, E. et al., 2004. Mammalian TOR complex 2 controls the actin cytoskeleton and is rapamycin insensitive.. *Nat Cell Biol.*, Nov, 6(11), pp. 1122-8.

- Janus, A., Robak, T. & Smolewski, P., 2005. The mammalian target of the rapamycin (mTOR) kinase pathway: its role in tumourigenesis and targeted antitumour therapy. *Cellular & Molecular Biology Letters*, 10(3), pp. 479-98.
- Jasnos, L. & Korona, R., 2007. Epistatic buffering of fitness loss in yeast double deletion strains. *Nature Genetics*, Apr, 39(4), pp. 550-4.
- Jeffares, D. C., Penkett, C. J. & Bähler, J., 2008. Rapidly regulated genes are intron poor. *Trends in Genetics*, Aug, 24(8), pp. 375-8..
- Jeffares, D. C., Rallis, C., Rieux, A. & Bähler, J., 2015. The genomic and phenotypic diversity of *Schizosaccharomyces pombe*. *Nature Genetics*, 47(3), pp. 235-241.
- Jiang, B. H. & Liu, L. Z., 2008. Role of mTOR in anticancer drug resistance: perspectives for improved drug treatment. *Drug Resistance Updates*, Jun, 11(3), pp. 63-76.
- Kaeberlein, M. & Kennedy, B. K., 2011. Hot topics in aging research: protein translation and TOR signaling. *Aging Cell*, Apr, 10(2), pp. 185-90.
- Kaizuka, T. et al., 2010. Tti1 and Tel2 are critical factors in mammalian target of rapamycin complex assembly. *The Journal of Biological Chemistry*, 25 Jun, 285(26), pp. 20109-16.
- Kamada, Y. et al., 2010. Tor directly controls the Atg1 kinase complex to regulate autophagy. *Molecular and cellular biology*, Feb, 30(4), pp. 1049-58.
- Kapahi, P. et al., 2010. With TOR, less is more: a key role for the conserved nutrient-sensing TOR pathway in aging. *Cell Metabolism*, 9 Jun, 11(6), pp. 453-65.
- Karagiannis, J., Saleki, R. & Young, P. G., 1999. The pub1 E3 ubiquitin ligase negatively regulates leucine uptake in response to NH₄(+) in fission yeast. *Current Genetics*, Jul, 35(6), pp. 593-601.
- Katewa D and Kapahi P, 2010. Dietary restriction and aging. *Aging Cell*, Apr, 9(2), p. 105–12.
- Kawai, M. et al., 2001. Fission yeast tor1 functions in response to various stresses including nitrogen starvation, high osmolarity, and high temperature. *Current Genetics*, May, 39(3), pp. 166-74.
- Kawashima, S. A., Takemoto, A., Nurse, P. & Kapoor, T. M., 2012. Analyzing fission yeast multidrug resistance mechanisms to develop a genetically tractable model system for chemical biology. *Chemistry & Biology*, 27 Jul, 19(7), pp. 893-901.

- Kenyon, C. J., 2010. The genetics of ageing. *Nature*, 25 Mar, 464(7288), pp. 504-12.
- Kig, C. & Temizkan, G., 2009. Nitric oxide as a signaling molecule in the fission yeast *Schizosaccharomyces pombe*. *Protoplasma*, Dec, 238(1-4), pp. 59-66.
- Kim, D. U. et al., 2010. Analysis of a genome-wide set of gene deletions in the fission yeast *Schizosaccharomyces pombe*. *Nature Biotechnology*, Volume 28, pp. 617-23.
- Kim, J. et al., 2016. AMPK activators: mechanisms of action and physiological activities. *Experimental & Molecular Medicine*, 1 Apr, Volume 48, p. e224.
- Kim, L. et al., 2012. The fission yeast GATA factor, Gaf1, modulates sexual development via direct down-regulation of *ste11+* expression in response to nitrogen starvation. *PLoS One*, 7(8), p. e42409.
- Kirkegaard, T. & Jäättelä, M., 2009. Lysosomal involvement in cell death and cancer. *Biochimica et Biophysica Acta*, Apr, 1793(4), pp. 746-54.
- Klass, M. R., 1983. A method for the isolation of longevity mutants in the nematode *Caenorhabditis elegans* and initial results. *Mechisms of Ageing Development*, Jul-Aug, 22(3-4), pp. 279-86.
- Kohda, T. A. et al., 2007. Fission yeast autophagy induced by nitrogen starvation generates a nitrogen source that drives adaptation processes. *Genes to Cells*, Feb, 12(2), pp. 155-70.
- Ko, L. J. & Engel, J. D., 1993. DNA-binding specificities of the GATA transcription factor family. *Molecular Cellular Biology*, Jul, 13(7), pp. 4011-22.
- Kowalczyk, K. M. & Petersen, J., 2016. Fission Yeast SCYL1/2 Homologue Ppk32: A Novel Regulator of TOR Signalling That Governs Survival during Brefeldin A Induced Stress to Protein Trafficking. *PLoS Genetics*, 18 May, 12(5), p. e1006041.
- Krishna, S. S., Majumdar, I. & Grishin, N. V., 2003. Structural classification of zinc fingers: survey and summary. *Nucleic Acids Research*, 15 Jan, 31(2), pp. 532-50.
- Kristell, C. et al., 2010. Nitrogen depletion in the fission yeast *Schizosaccharomyces pombe* causes nucleosome loss in both promoters and coding regions of activated genes. *Genome Research*, 20(3), pp. 361-3.
- Kulkarni, A., Buford, T. D., Rai, R. & Cooper, T. G., 2006. Differing responses of Gat1 and Gln3 phosphorylation and localization to rapamycin and methionine sulfoximine treatment in *Saccharomyces cerevisiae*. *FEMS Yeast Research*, Mar, 6(2), pp. 218-29.

- Kume, K. et al., 2017. Identification of three signaling molecules required for calcineurin-dependent monopolar growth induced by the DNA replication checkpoint in fission yeast. *Biochemical and Biophysical Research Communications*, 30 Sep, 491(4), pp. 883-889.
- Kuroda, K. et al., 2019. Critical roles of the pentose phosphate pathway and GLN3 in isobutanol-specific tolerance in yeast. *Cell Systems*, 18 Dec, 9(6), p. 534–547.e5.
- Kuzmin, E., Costanzo, M., Andrews, B. & Boone, C., 2016. Synthetic Genetic Arrays: Automation of Yeast Genetics. *Cold Spring Harbor Protocols*, 1 Apr, 2016(4), p. pdb.top086652.
- Laboucarié, T. et al., 2017. TORC1 and TORC2 converge to regulate the SAGA co-activator in response to nutrient availability. *EMBO Reports*, Dec, 18(12), pp. 2197-2218.
- Lai, Y. C. et al., 2014. A small-molecule benzimidazole derivative that potently activates AMPK to increase glucose transport in skeletal muscle: comparison with effects of contraction and other AMPK activators. *The Biochemical Journal*, 15 Jun, 460(3), pp. 363-75.
- Laor, D., Cohen, A., Kupiec, M. & Weisman, R., 2015. TORC1 regulates developmental responses to nitrogen stress via regulation of the GATA transcription factor Gaf1. *mBio*, 7 Jul, 6(4), p. e00959.
- Laor, D. et al., 2014. Isp7 Is a Novel Regulator of Amino Acid Uptake in the TOR Signaling Pathway. *Molecular and Cellular Biology*, 34(5), pp. 794-806.
- Laplante, M. & Sabatini, D. M., 2012. mTOR signaling in growth control and disease. *Cell*, 149(2), p. 274-293.
- Lefrançois, P., Gallagher, J. E. & Snyder, M., 2014. Global analysis of transcription factor-binding sites in yeast using ChIP-Seq. *Methods in Molecular Biology*, Volume 1205, pp. 231-55.
- Lewinska, A., Macierzynska, E., Grzelak, A. & Bartosz, G., 2011. A genetic analysis of nitric oxide-mediated signaling during chronological aging in the yeast. *Biogerontology*, Aug, 12(4), pp. 309-20.
- Li, B., Mendenhall, J. & Meiler, J., 2019. Interfaces Between Alpha-helical Integral Membrane Proteins: Characterization, Prediction, and Docking. *Computational and Structural Biotechnology Journal*, 25 May, Volume 17, pp. 699-711.
- Lie, S. et al., 2018. The contribution of non-essential *Schizosaccharomyces pombe* genes to fitness in response to altered nutrient supply and target of rapamycin activity. *Open biology*, May, 8(5), p. pii: 180015.

Lindner, P., 1893. Schizosaccharomyces pombe n. sp. neuer Gärungserreger. *Wochenschrift für Brauerei*, Volume 10, p. 1298–1300.

Lin, S. J. & Austriaco, N., 2014. Aging and cell death in the other yeasts, Schizosaccharomyces pombe and Candida albicans. *FEMS Yeast Research*, Feb, 14(1), pp. 119-35.

Li, S. C. & Kane, P. M., 2009. The yeast lysosome-like vacuole: endpoint and crossroads. *Biochimica et biophysica acta*, Apr, 1793(4), p. 650–663.

Ljungdahl, P. O. & Daignan-Fornier, B., 2012. Regulation of amino acid, nucleotide, and phosphate metabolism in Saccharomyces cerevisiae. *Genetics*, Mar, 190(3), pp. 885-929.

Lock, A. et al., 2019. PomBase 2018: user-driven reimplementations of the fission yeast database provides rapid and intuitive access to diverse, interconnected information. *Nucleic Acids Research*, 8 Jan, 47(D1), pp. D821-D827.

Lodish, H. et al., 2004. *Molecular Cell Biology*. 5th ed. New York: W. H. Freeman & Co.

Loenarz, C. et al., 2014. Hydroxylation of the eukaryotic ribosomal decoding center affects translational accuracy. *Proceedings of the National Academy of Sciences of the United States of America*, 18 Mar, 111(11), pp. 4019-24.

Loewith, R. & Hall, M. N., 2011. Target of rapamycin (TOR) in nutrient signaling and growth control. *Genetics*, 189(4), pp. 1177-1201.

López-Otín, C. et al., 2013. The hallmarks of aging. *Cell*, Jun6, 153(6), pp. 1194-217.

Luiking, Y. C., Poeze, M., Ramsay, G. & Deutz, N. E., 2005. The role of arginine in infection and sepsis. *The Journal of Parenteral and Enteral Nutrition*, Jan-Feb, 29(1 Suppl), pp. S70-4.

Lyne, R. et al., 2003. Whole-genome microarrays of fission yeast: characteristics, accuracy, reproducibility, and processing of array data. *BMC Genomics*, 10 Jul, 4(1), p. 27.

Mach, K. E., Furge, K. A. & Albright, C. F., 2000. Loss of Rhb1, a Rheb-related GTPase in fission yeast, causes growth arrest with a terminal phenotype similar to that caused by nitrogen starvation. *Genetics*, Jun, 155(2), p. 611–622.

Madrid, M. et al., 2016. Multiple crosstalk between TOR and the cell integrity MAPK signaling pathway in fission yeast. *Scientific Reports*, 23 Nov, Volume 6, p. 37515.

- Mair, W. & Dillin, A., 2008. Aging and survival: the genetics of life span extension by dietary restriction. *Annual Review of Biochemistry*, Volume 77, pp. 727-754.
- Mak, T., Jones, A. W. & Nurse, P., 2021. The TOR-dependent phosphoproteome and regulation of cellular protein synthesis. *The EMBO Journal*, 16 Aug, 40(16), p. e107911.
- Ma, N. et al., 2013. TORC1 signaling is governed by two negative regulators in fission yeast. *Genetics*, Oct, 195(2), pp. 457-68.
- Mani, R. et al., 2008. Defining genetic interaction. *Proc Natl Acad Sci U S A*, 105(9), pp. 3461-3466.
- Marguerat, S. et al., 2006. The more the merrier: comparative analysis of microarray studies on cell cycle-regulated genes in fission yeast. *Yeast*, 23(4), p. 2612277. doi: 10.1002/yea.1351.
- Martín, R. et al., 2017. A PP2A-B55-Mediated Crosstalk between TORC1 and TORC2 Regulates the Differentiation Response in Fission Yeast. *Curr Biology*, 23 Jan, 27(2), pp. 175-188.
- Mason, J. S., Wileman, T. & Chapman, T., 2018. Lifespan extension without fertility reduction following dietary addition of the autophagy activator Torin1 in *Drosophila melanogaster*. *PLoS One*, 12 Jan, 13(1), p. e0190105.
- Mata, J. & Bähler, J., 2006. Global roles of Ste11p, cell type, and pheromone in the control of gene expression during early sexual differentiation in fission yeast. *Proc. Natl. Acad. Sci. USA*, Volume 103, p. 15517–15522.
- Mata, J., Lyne, R., Burns, G. & Bähler, J., 2002. The transcriptional program of meiosis and sporulation in fission yeast. *Nature Genetics*, Sep, 32(1), pp. 143-7.
- Matsumoto, S. et al., 2002. Role of the Tsc1-Tsc2 complex in signaling and transport across the cell membrane in the fission yeast *Schizosaccharomyces pombe*. *Genetics*, Jul, 161(3), pp. 1053-63.
- Matsuo, T. et al., 2007. Loss of the TOR kinase Tor2 mimics nitrogen starvation and activates the sexual development pathway in fission yeast. *Molecular and Cellular Biology*, Apr, 27(8), pp. 3154-64.
- Ma, X. M. & Blenis, J., 2009. Molecular mechanisms of mTOR-mediated translational control. *Nature Review. Molecular Cell Biology*, Volume 10, p. 307–318.
- Ma, Y. et al., 2015. Tor Signaling Regulates Transcription of Amino Acid Permeases through a GATA Transcription Factor Gaf1 in Fission Yeast. *PLoS One*, 10(12), p. e0144677.

McDowall, J., 2007. *Protein of the Month: Zinc Fingers*. [Online] Available at: https://www.ebi.ac.uk/interpro/potm/2007_3/Page1.htm [Accessed 15 Apr 2017].

McKnight, S. L. & Miller, Q. L. J., 1976. Ultrastructural patterns of RNA synthesis during early embryogenesis of *Drosophila melanogaster*. *Cell*, Jun, 8(2), pp. 305-19.

Mercier, A., Pelletier, B. & Labbé, S., 2006. A transcription factor cascade involving Fep1 and the CCAAT-binding factor Php4 regulates gene expression in response to iron deficiency in the fission yeast *Schizosaccharomyces pombe*. *Eukaryotic Cell*, Nov, 5(11), p. 1866–1881.

Mitchison, J. M. & Nurse, P., 1985. Growth in cell length in the fission yeast *Schizosaccharomyces pombe*. *Journal of Cell Science*, Apr, Volume 75, pp. 357-76.

Miwa, Y. et al., 2011. Ecl1, a regulator of the chronological lifespan of *Schizosaccharomyces pombe*, is induced upon nitrogen starvation. *Biosciences, Biotechnology and Biochemistry*, 75(2), pp. 279-83.

Mizuguchi, T., Barrowman, J. & Grewal, S. I., 2015. Chromosome domain architecture and dynamic organization of the fission yeast genome. *FEBS Letters*, 7 Oct, 589(20 Pt), pp. 2975-86.

Morishita, M. & Shimoda, C., 2000. Positioning of medial actin rings affected by eccentrically located nuclei in a fission yeast mutant having large vacuoles. *FEMS Microbiology Letters*, Jul, 188(1), p. 63–67.

Morris, S. M., 2006. Arginine: beyond protein. *The American Journal of Clinical Nutrition*, Feb, 83(2), pp. 508S-512S.

Mukaiyama, H. et al., 2010. Autophagy in the fission yeast *Schizosaccharomyces pombe*. *FEBS Letters*, 2 Apr, 584(7), pp. 1327-34.

Murai, T. et al., 2009. Distinctive responses to nitrogen starvation in the dominant active mutants of the fission yeast Rheb GTPase. *Genetics*, Oct, 183(2), pp. 517-27.

Nakase, Y. et al., 2013. The fission yeast β -arrestin-like protein Any1 is involved in TSC-Rheb signaling and the regulation of amino acid transporters. *Journal of Cell Science*, 1 Sep, 126(17), pp. 3972-81.

Nakashima A, T. F., 2010. Conservation of the Tsc/Rheb/TORC1/S6K/S6 Signaling in Fission Yeast. *Enzymes*, Volume 28, pp. 167-187.

Nakashima, A. et al., 2006. A starvation-specific serine protease gene, *isp6+*, is involved in both autophagy and sexual development in *Schizosaccharomyces pombe*. *Current Genetics*, Jun, 49(6), pp. 403-13.

Nakashima, A. et al., 2012. Psk1, an AGC kinase family member in fission yeast, is directly phosphorylated and controlled by TORC1 and functions as S6 kinase. *Journal of cell science*, 1 Dec, 125(23), pp. 5840-9.

Nakashima, A., Sato, T. & Tamanoi, F., 2010. Fission yeast TORC1 regulates phosphorylation of ribosomal S6 proteins in response to nutrients and its activity is inhibited by rapamycin. *Journal of Cell Science*, 1 Mar, 123(5), pp. 777-86.

Narayanan, s. et al., 2015. Quantitative Fitness Analysis Identifies *exo1Δ* and Other Suppressors or Enhancers of Telomere Defects in *Schizosaccharomyces pombe*. *PLoS ONE*, 10(7), p. e0132240.

Niccoli, T. & Partridge, L., 2012. Ageing as a risk factor for disease. *Current Biology*, 11 Sep, 22(17), pp. R741-52.

Nishimura, A., Kawahara, N. & Takagi, H., 2013. The flavoprotein Tah18-dependent NO synthesis confers high-temperature stress tolerance on yeast cells. *Biochemical and Biophysical Research Communications*, 4 Jan, 430(1), pp. 137-43.

Obara, K., Sekito, T. & Ohsumi, Y., 2006. Assortment of phosphatidylinositol 3-kinase complexes--Atg14p directs association of complex I to the pre-autophagosomal structure in *Saccharomyces cerevisiae*. *Molecular Biology of the Cell*, 17(4), pp. 1527-1539.

Ohsumi, Y., 1999. Molecular mechanism of autophagy in yeast, *Saccharomyces cerevisiae*. *Philosophical Transactions of the Royal Society of London. Series B, Biological Sciences*, 29 Sep, 354(1389), pp. 1577-80; discussion 1580-1.

Otsubo Y, M. T. N. A. Y. M. Y. A., 2018. tRNA production links nutrient conditions to the onset of sexual differentiation through the TORC1 pathway. *EMBO Reports*, 19(3), p. e44867. doi: 10.15252/embr.201744867.

Otsubo, Y., Kamada, Y. & Yamashita, A., 2020. Novel Links between TORC1 and Traditional Non-Coding RNA, tRNA. *Genes (Basel)*, 19 Aug, 11(9), p. 956.

Otsubo, Y., Nakashima, A., Yamamoto, M. & Yamashita, A., 2017. TORC1-Dependent Phosphorylation Targets in Fission Yeast. *Biomolecules*, 3 July, 7(3), p. pii: E50.

Otsubo, Y. & Yamamoto, M., 2012. Signaling pathways for fission yeast sexual differentiation at a glance. *Journal of Cell Science*, 15 Jun, 125(12), pp. 2789-93.

- Oya, E. et al., 2019. Leo1 is essential for the dynamic regulation of heterochromatin and gene expression during cellular quiescence. *Epigenetics & Chromatin*, 17 Jul, 12(1), p. 45.
- Pancaldi, V. et al., 2012. Predicting the fission yeast protein interaction network. *G3-Genes Genomes Genetics*, 1 Apr, 2(4), pp. 453-67.
- Panchaud, N., Péli-Gulli, M. P. & De Virgilio, C., 2013. Amino acid deprivation inhibits TORC1 through a GTPase-activating protein complex for the Rag family GTPase Gtr1. *Science Signaling*, 28 May, 6(277), p. ra42.
- Papatheodorou, I. et al., 2018. Expression Atlas: gene and protein expression across multiple studies and organisms. *Nucleic Acids Research*, 4 Jan, Volume 46(D1), pp. D246-D251.
- Partridge, L., 2010. The new biology of ageing. *Philosophical transactions of the Royal Society of London. Series B, Biological sciences*, 12 Jan, 365(1537), pp. 147-54.
- Pearce, L. R. et al., 2011. Protor-1 is required for efficient mTORC2-mediated activation of SGK1 in the kidney. *The Biochemical Journal*, 15 May, 436(1), pp. 169-79.
- Pelletier, B., Beaudoin, J., Philpott, C. C. & Labbé, S., 2003. Fep1 represses expression of the fission yeast *Schizosaccharomyces pombe* siderophore-iron transport system. *Nucleic Acids Research*, 1 Aug, 31(15), pp. 4332-44.
- Penkett, C. J., Birtle, Z. E. & Bähler, J., 2006. Simplified primer design for PCR-based gene targeting and microarray primer database: two web tools for fission yeast. *Yeast*, 15 Oct, 23(13), pp. 921-8.
- Pérez-Hidalgo, L. & Moreno, S., 2017. Coupling TOR to the Cell Cycle by the Greatwall-Endosulfine-PP2A-B55 Pathway. *Biomolecules*, 4 Aug, 7(3), p. 59.
- Perez-Hidalgo, L. & Moreno, S., 2016. Nutrients control cell size. *Cell Cycle*, 15(13), p. 1655–1656.
- Persikov, A. V., Osada, R. & Singh, M., 2009. Predicting DNA recognition by Cys2His2 zinc finger proteins. *Bioinformatics*, 1 Jan, 25(1), pp. 22-9.
- Petersen, J. & Nurse, P., 2007. TOR signalling regulates mitotic commitment through the stress MAP kinase pathway and the Polo and Cdc2 kinases. *Nature Cell Biology*, Nov, 9(11), p. 1263– 1272.
- Petersen, J. & Russell, P., 2016. Growth and the Environment of *Schizosaccharomyces pombe*. In: *Fission Yeast: A Laboratory Manual*. New York: Cold Spring Harbor Laboratory Press.

Peterson, T. R. et al., 2009. DEPTOR is an mTOR inhibitor frequently overexpressed in multiple myeloma cells and required for their survival. *Cell*, 29 May, 137(5), pp. 873-86.

Piel, M. & Tran, P. T., 2009. Cell shape and cell division in fission yeast. *Current Biology*, 15 Sep, 19(17), pp. R823-7.

Powers, R. W. et al., 2006. Extension of chronological life span in yeast by decreased TOR pathway signaling. *Genes & Development*, 20(2), p. 174-184.

Prentice, H. L., 1992. High efficiency transformation of *Schizosaccharomyces pombe* by electroporation. *Nucleic Acids Research*, 20(3), p. 621.

Prevorovský, M. et al., 2009. Cbf11 and Cbf12, the fission yeast CSL proteins, play opposing roles in cell adhesion and coordination of cell and nuclear division. *Experimental Cell Research*, 1 May, 315(8), pp. 1533-47.

Querfurth, H. & Lee, H. K., 2021. Mammalian/mechanistic target of rapamycin (mTOR) complexes in neurodegeneration. *Mol Neurodegener*, 2 Jul, 16(1), p. 44.

Rai, R., Tate, J. J., Nelson, D. R. & Cooper, T. G., 2013. gln3 mutations dissociate responses to nitrogen limitation (nitrogen catabolite repression) and rapamycin inhibition of TorC1. *The Journal of Biological Chemistry*, 25 Jan, 288(4), pp. 2789-804.

Rallis, C., Codlin, S. & Bähler, J., 2013. TORC1 signaling inhibition by rapamycin and caffeine affect lifespan, global gene expression, and cell proliferation of fission yeast. *Aging Cell*, Aug, 12(4), pp. 563-73.

Rallis, C. et al., 2014. Systematic screen for mutants resistant to TORC1 inhibition in fission yeast reveals genes involved in cellular ageing and growth. *Biology Open*, 15 Feb, 3(2), pp. 161-71.

Rallis, C., Townsend, S. & Bähler, J., 2017. Genetic interactions and functional analyses of the fission yeast gsk3 and amk2 single and double mutants defective in TORC1-dependent processes. *Scientific reports*, 10 Mar.7(44257).

Ralser, M. et al., 2012. The *Saccharomyces cerevisiae* W303-K6001 cross-platform genome sequence: insights into ancestry and physiology of a laboratory mutt. *Open Biology*, Aug, 2(8), p. 120093.

Raudvere, U. et al., 2019. g:Profiler: a web server for functional enrichment analysis and conversions of gene lists (2019 update). *Nucleic Acids Research*, 2 Jul, 47(W1), p. W191–W198.

Rodríguez-López, M. et al., 2020. The GATA transcription factor Gaf1 represses tRNA genes, inhibits growth, and extends chronological lifespan downstream of fission yeast TORC1. *Cell Reports*, 10 Mar, 30(10), p. 3240–3249.e4.

Rose, A. B., 2019. Introns as Gene Regulators: A Brick on the Accelerator. *Frontiers in Genetics*, 7 Feb, Volume 9, p. 672.

Rose, A. B., Emami, S., Bradnam, K. & Korf, I., 2011. Evidence for a DNA-based mechanism of intron-mediated enhancement. 13 Dec, Volume 2, p. 98.

Roux, A. E., Chartrand, P., Ferbeyre, G. & Rokeach, L. A., 2010. Fission yeast and other yeasts as emergent models to unravel cellular aging in eukaryotes. *The journals of gerontology. Series A, Biological sciences and medical sciences*, Jan, 65(1), pp. 1-8.

Roux, A. E. et al., 2009. Pro-aging effects of glucose signaling through a G protein-coupled glucose receptor in fission yeast. *PLoS Genetics*, Mar, 5(3), p. e1000408.

Roux, A. E. et al., 2006. Regulation of chronological aging in *Schizosaccharomyces pombe* by the protein kinases Pka1 and Sck2. *Aging Cell*, Volume 5, p. 345–357.

Rustici, G. et al., 2004. Periodic gene expression program of the fission yeast cell cycle. *Nature Genetics*, Aug, 36(8), pp. 809-17.

Ryan, C. J. et al., 2012. Hierarchical modularity and the evolution of genetic interactomes across species. *Molecular Cell*, 8 Jun, 46(5), pp. 691-704.

Sabatini, D. M. et al., 1994. RAFT1: a mammalian protein that binds to FKBP12 in a rapamycin-dependent fashion and is homologous to yeast TORs. *Cell*, 15 Jul, 78(1), pp. 35-43.

Sabina J, J. M., 2009. Asymmetric signal transduction through paralogs that comprise a genetic switch for sugar sensing in *Saccharomyces cerevisiae*. *The Journal of Biological Chemistry*, 23 Oct, 284(43), pp. 29635-43. doi: 10.1074/jbc.M109.032102.

Saitoh, S. et al., 2015. Mechanisms of expression and translocation of major fission yeast glucose transporters regulated by CaMKK/phosphatases, nuclear shuttling, and TOR. *Molecular Biology of the Cell*, 26(2), pp. 373-386.

Sancak, Y. et al., 2010. Ragulator-Rag complex targets mTORC1 to the lysosomal surface and is necessary for its activation by amino acids. *Cell*, 16 Apr, 141(2), pp. 290-303.

Sancak, Y. et al., 2008. The Rag GTPases bind raptor and mediate amino acid signaling to mTORC1. *Science*, 13 Jun, 320(5882), pp. 1496-501.

Santos, J., Sousa, M. J. & Leão, C., 2012. Ammonium is toxic for aging yeast cells, inducing death and shortening of the chronological lifespan. *PLoS One*, 7(5), p. e37090.

- Sarbassov, D. D. et al., 2006. Prolonged rapamycin treatment inhibits mTORC2 assembly and Akt/PKB. *Molecular Cell*, Apr, 22(2), pp. 159-168.
- Sarkaria, J. N. et al., 1999. Inhibition of ATM and ATR kinase activities by the radiosensitizing agent, caffeine. *Cancer Research*, 1 Sep, 59(17), pp. 4375-82.
- Sawada, N., Ueno, S. & Takeda, K., 2021. Regulation of inorganic polyphosphate is required for proper vacuolar proteolysis in fission yeast. *The Journal of Biological Chemistry*, 297(1), p. 100891.
- Saxton, R. A. & Sabatini, D. M., 2017. mTOR Signaling in Growth, Metabolism, and Disease. *Cell*, 9 Mar, 168(6), pp. 960-976.
- Scazzocchio, C., 2000. The fungal GATA factors. *Current Opinion in Microbiology*, Apr, 3(2), pp. 126-31.
- Scherens, B. et al., 2006. Identification of direct and indirect targets of the Gln3 and Gat1 activators by transcriptional profiling in response to nitrogen availability in the short and long term. *FEMS Yeast Research*, Aug, 6(5), pp. 777-91.
- Schonbrun, M., Kolesnikov, M., Kupiec, M. & Weisman, R., 2013. TORC2 is required to maintain genome stability during S phase in fission yeast. *The Journal of Biological Chemistry*, 288(27), pp. 19649-19660.
- Schonbrun, M. et al., 2009. TOR complex 2 controls gene silencing, telomere length maintenance, and survival under DNA-damaging conditions. *Molecular and Cellular Biology*, Aug, 29(16), pp. 4584-94.
- Schuch, B. et al., 2014. The exosome-binding factors Rrp6 and Rrp47 form a composite surface for recruiting the Mtr4 helicase. *EMBO Journal*, 1 Dec, 33(23), pp. 2829-46.
- Schutt, K. L. & Moseley, J. B., 2017. Transient activation of fission yeast AMPK is required for cell proliferation during osmotic stress. *Molecular Biology of the Cell*, 1 Jul, 28(13), pp. 1804-1814.
- Selman, C. et al., 2009. Ribosomal protein S6 kinase 1 signaling regulates mammalian life span. *Science*, Volume 326, p. 140–144.
- Shabalina, S. A., Ogurtsov, A. Y., Kondrashov, V. A. & Kondrashov, A. S., 2001. Selective constraint in intergenic regions of human and mouse genomes. *Trends in Genetics*, Jul, 17(7), pp. 373-6.
- Shalon, D., Smith, S. J. & Brown, P., 1996. A DNA microarray system for analyzing complex DNA samples using two-color fluorescent probe hybridization. *Genome Research*, Jul, 6(7), pp. 639-45.

- Shertz, C. A. et al., 2010. Conservation, duplication, and loss of the Tor signaling pathway in the fungal kingdom. *BMC Genomics*, 23 Sep, Volume 11, p. 510.
- Shima, J. et al., 2003. Disruption of the CAR1 gene encoding arginase enhances freeze tolerance of the commercial baker's yeast *Saccharomyces cerevisiae*. *Applied and Environmental Microbiology*, Jan, 69(1), pp. 715-8.
- Shimanuki, M. et al., 2013. Klf1, a C2H2 zinc finger-transcription factor, is required for cell wall maintenance during long-term quiescence in differentiated G0 phase. *PLoS ONE*, 22 Oct, 8(10), p. e78545.
- Sideri, T. et al., 2015. Parallel Profiling of Fission Yeast Deletion Mutants for Proliferation and for Lifespan During Long-Term Quiescence. *G3 Genes Genomes Genetics*, Jan, Volume 5, pp. 145-155.
- Sievers, F. et al., 2011. Fast, scalable generation of high-quality protein multiple sequence alignments using Clustal Omega. *Molecular Systemes Biology*, 11 Oct, Volume 7, p. 539. doi:10.1038/msb.2011.75.
- Simpson-Lavy, K. & Kupiec, M., 2019. Carbon Catabolite Repression in Yeast is Not Limited to Glucose. *Scientific Reports*, Volume 9, p. 6491.
- Singleton, R. S. et al., 2014. OGFOD1 catalyzes prolyl hydroxylation of RPS23 and is involved in translation control and stress granule formation. *Proceedings of the National Academy of Sciences of the United States of America*, 18 Mar, 111(11), pp. 4031-6.
- Sipiczki, M., 2000. Where does fission yeast sit on the tree of life?. *Genome Biology*, 1(2).
- Song, J. Y., Kim, K. D. & Roe, J. H., 2008. Thiol-independent action of mitochondrial thioredoxin to support the urea cycle of arginine biosynthesis in *Schizosaccharomyces pombe*. *Eukaryotic Cell*, Dec, 7(12), pp. 2160-7.
- St Onge, R. P. et al., 2007. Systematic pathway analysis using high-resolution fitness profiling of combinatorial gene deletions. *Nature Genetics*, Feb, 39(2), pp. 199-206.
- Stauffer, B. & Powers, T., 2015. Target of rapamycin signaling mediates vacuolar fission caused by endoplasmic reticulum stress in *Saccharomyces cerevisiae*. *Molecular Biology of the Cell*, 15 Dec, 26(5), pp. 4618-30.
- Stauffer, B. & Powers, T., 2017. Target of rapamycin signaling mediates vacuolar fragmentation. *Current Genetics*, 63(1), pp. 35-42.
- Sun, L. L. et al., 2013. Global analysis of fission yeast mating genes reveals new autophagy factors. *PLoS Genet/CS*, 9(8), p. e1003715.

Sun, X. et al., 2016. Identification of novel secreted fatty acids that regulate nitrogen catabolite repression in fission yeast. *Scientific Reports*, 19 Feb, Volume 6, p. 20856.

Su, S. S. et al., 1996. A nitrogen starvation-induced dormant G0 state in fission yeast: the establishment from uncommitted G1 state and its delay for return to proliferation. *Journal of Cell Science*, Jun, 109(6), pp. 1347-57.

Suzuki, T. et al., 2013. Inhibition of AMPK catabolic action by GSK3. *Molecular Cell*, 9 May, 50(3), pp. 407-19.

Szklarczyk, D. et al., 2015. STRING v10: protein-protein interaction networks, integrated over the tree of life. *Nucleic Acids Research*, Jan, Volume 43(Database issue), pp. D447-52.

Takahara, T. & Maeda, T., 2012. TORC1 of fission yeast is rapamycin-sensitive. *Genes and Cells*, Aug, 17(8), pp. 698-708.

Takeda, K., Starzynski, C., Mori, A. & Yanagida, M., 2015. The critical glucose concentration for respiration-independent proliferation of fission yeast, *Schizosaccharomyces pombe*. *Mitochondrion*, May, Volume 22, pp. 91-5.

Takeshige, K. et al., 1992. Autophagy in yeast demonstrated with proteinase-deficient mutants and conditions for its induction. *The Journal of Cell Biology*, Oct, 119(2), pp. 301-11.

Tanaka, N. et al., 2005. Characterization of O-mannosyltransferase family in *Schizosaccharomyces pombe*. *Biochemical and Biophysical Research Communications*, 13 May, 330(3), pp. 813-20.

Teakle, G. R. & Gilmartin, P. M., 1998. Two forms of type IV zinc-finger motif and their kingdom-specific distribution between the flora, fauna and fungi. *Trends in Biochemical Sciences*, Mar, 23(3), pp. 100-2.

ter Schure, E. G., van Riel, N. A. & Verrips, C. T., 2000. The role of ammonia metabolism in nitrogen catabolite repression in *Saccharomyces cerevisiae*. *FEMS Microbiol Rev*, Jan, 24(1), pp. 67-83.

The Bähler Lab, 2016. *The Bähler Lab-University College London (UCL)*. [Online] Available at: <http://www.bahlerlab.info/resources/>. (Accessed: Dec, 2016) [Accessed Dec 2016].

The Gene Ontology Consortium, 2015. Gene Ontology Consortium: going forward. *Nucleic Acids Research*, 28 Jan, Volume 43(Database issue), p. D1049–D1056.

The UniProt Consortium, 2019. UniProt: a worldwide hub of protein knowledge. *Nucleic Acids Research*, 47(D1), pp. D506-515.

- Thoreen, C. C. et al., 2009. An ATP-competitive mammalian target of rapamycin inhibitor reveals rapamycin-resistant functions of mTORC1. *The Journal of Biological Chemistry*, 20 Mar, 284(12), pp. 8023-32.
- Tisi, R., Rigamonti, M., Groppi, S. & Fiorella, B., 2016. Calcium homeostasis and signaling in fungi and their relevance for pathogenicity of yeasts and filamentous fungi. *AIMS Molecular Science*, 3(4), pp. 505-549.
- Tong, A. H. & et al, 2004. Global mapping of the yeast genetic interaction network. *Science*, 6 Feb, 303(5659), pp. 808-13.
- Tong, A. H. et al., 2001. Systematic genetic analysis with ordered arrays of yeast deletion mutants. *Science*, 14 Dec, 294(5550), pp. 2364-8.
- United Nations, 2002. *World population ageing: 1950 - 2050*, New York: United Nations.
- United Nations, 2013. *World Population Ageing 2013*, New York: United Nations.
- Urano, J. et al., 2005. Identification of novel single amino acid changes that result in hyperactivation of the unique GTPase, Rheb, in fission yeast. *Molecular Microbiology*, Nov, 58(4), pp. 1074-86.
- Urano, J. et al., 2007. Point mutations in TOR confer Rheb-independent growth in fission yeast and nutrient-independent mammalian TOR signaling in mammalian cells. *Proceedings of the National Academy of Sciences of the United States of America*, 27 Feb, 104(9), pp. 3514-9.
- Valbuena, N., Guan, K. & Moreno, S., 2012. The Vam6 and Gtr1-Gtr2 pathway activates TORC1 in response to amino acids in fission yeast. *Journal of Cell Science*, 15 Apr, 125(Pt8), pp. 1920-8.
- Valbuena, N., Rozalén, A. E. & Moreno, S., 2012. Fission yeast TORC1 prevents eIF2a phosphorylation. *Journal of cell science*, 15 Dec, 125(24), pp. 5955-9.
- Valvezan, A. J. & Manning, B. D., 2019. Molecular logic of mTORC1 signalling as a metabolic rheostat. *Nature Metabolism*, Mar, 1(3), pp. 321-333.
- van Slegtenhorst, M. et al., 2004. Tsc1+ and tsc2+ regulate arginine uptake and metabolism in *Schizosaccharomyces pombe*. *The Journal of Biological Chemistry*, 26 Mar, 279(13), pp. 12706-13.
- Viollet, B. et al., 2010. AMPK inhibition in health and disease. *Critical Reviews in Biochemistry Molecular Biology*, Aug, 45(4), pp. 276-95.
- Visigalli, R. et al., 2007. Rapamycin stimulates arginine influx through CAT2 transporters in human endothelial cells. *Biochimica et Biophysica Acta*, Jun, 1768(6), pp. 1479-87.

- Wagih, O. & Parts, L., 2014. gitter: a robust and accurate method for quantification of colony sizes from plate images. *G3 (Bethesda)*, 20 Mar, 4(3), pp. 547-552.
- Wang, L., Harris, T. E., Roth, R. A. & Lawrence, L. C. J., 2007. PRAS40 regulates mTORC1 kinase activity by functioning as a direct inhibitor of substrate binding. *The Journal of Biological Chemistry*, 6 Jul, 282(27), pp. 20036-44.
- Wang, R. et al., 2018. L-Arginine Enhances Protein Synthesis by Phosphorylating mTOR (Thr 2446) in a Nitric Oxide-Dependent Manner in C2C12 Cells. *Oxidative Medicine and Cellular Longevity*, 26 Apr, Volume 2018, p. 7569127.
- Wang, T. et al., 2012. LST8 regulates cell growth via target-of-rapamycin complex 2 (TORC2). *Molecular and Cellular Biology*, Jun, 32(12), pp. 2203-13.
- Weisman, R., 2010. Fission Yeast Tor and Rapamycin. In: H. M. a. T. F, ed. *The Enzymes*. s.l.:Burlington: Academic Press, Elsevier Inc, Academic Press, pp. 251-269.
- Weisman, R. & Choder, M., 2001. The fission yeast TOR homolog, tor1+, is required for the response to starvation and other stresses via a conserved serine. *Journal of Biological Chemistry*, 9 Mar, 276(10), pp. 7027-32.
- Weisman, R., Cohen, A. & Gasser, S. M., 2014. TORC2-a new player in genome stability. *EMBO Mol Med.*, Aug, 6(8), pp. 995-1002.
- Weisman, R., Roitburg, I., Nahari, T. & Kupiec, M., 2005. Regulation of leucine uptake by tor1+ in *Schizosaccharomyces pombe* is sensitive to rapamycin. *Genetics*, 169(2), pp. 539-50.
- Weisman, R. et al., 2007. Opposite effects of tor1 and tor2 on nitrogen starvation responses in fission yeast. *Genetics*, Mar, 175(3), pp. 1153-62.
- Wiame, J. M., Grenson, M. & Arst, H. N., 1985. Nitrogen catabolite repression in yeasts and filamentous fungi. *Advances in Microbial Physiology*, Volume 26, p. 1-88.
- Wilhelm, B. et al., 2008. Dynamic repertoire of a eukaryotic transcriptome surveyed at single-nucleotide resolution. *Nature*, 26 Jun, 453(7199), pp. 1239-43.
- Wilkinson, M. G. et al., 1996. The Atf1 transcription factor is a target for the Sty1 stress-activated MAP kinase pathway in fission yeast. *Genes & Development*, 15 Sep, 10(18), pp. 2289-301.
- Willis, N. & Rhind, N., 2011. Studying G2 DNA damage checkpoints using the fission yeast *Schizosaccharomyces pombe*. *Methods in Molecular Biology*, Volume 782, pp. 1-12.

- Wolfe, S. A., Nekludova, L. & Pabo, C. O., 2000. DNA recognition by Cys2His2 zinc finger proteins. *Annual Review of Biophysics and Biomolecular Structure*, 183-212(29).
- Wood, V. et al., 2002. The genome sequence of *Schizosaccharomyces pombe*. *Nature*, 415(6874), pp. 871-80.
- World Health Organization, 2018. *Global Health and Aging*, s.l.: s.n.
- Wu, G. & Morris, S. M. J., 1998. Arginine metabolism: nitric oxide and beyond. *The Biochemical Journal*, 15 Nov, 336(1), pp. 1-17.
- Xie, Y. et al., 2015. Phosphorylation of GATA-6 is required for vascular smooth muscle cell differentiation after mTORC1 inhibition. *Science Signaling*, Volume 8, p. ra44.
- Xu, S., Zhou, J., Liu, L. & Chen, J., 2011. Arginine: A novel compatible solute to protect *Candida glabrata* against hyperosmotic stress. *Process Biochemistry*, 46(6), pp. 1230-1235.
- Xu, Y. Y. et al., 2018. Activation of AMP-activated protein kinase by compound 991 protects osteoblasts from dexamethasone. *Biochemical and Biophysical Research Communications*, 1 Jan, 495(1), pp. 1014-1021.
- Yang, P., Du, H., Hoffman, C. S. & Marcus, S., 2003. The phospholipase B homolog Plb1 is a mediator of osmotic stress response and of nutrient-dependent repression of sexual differentiation in the fission yeast *Schizosaccharomyces pombe*. *Molecular Genetics and Genomics*, 269(1), pp. 116-25.
- Yang, Q., Inoki, K., Ikenoue, T. & Guan, K. L., 2006. Identification of Sin1 as an essential TORC2 component required for complex formation and kinase activity. *Genes & Development*, 15 Oct, 20(20), pp. 2820-32.
- Yang, T. T. et al., 2008. Integration of protein kinases mTOR and extracellular signal-regulated kinase 5 in regulating nucleocytoplasmic localization of NFATc4. *Molecular Cell Biology*, May, 28(10), pp. 3489-501.
- Young, B. P. & Loewen, C. J., 2013. Balony: a software package for analysis of data generated by synthetic genetic array experiments. *BMC Bioinformatics*, 4 Dec, Volume 14, p. 354.
- Yuan, C. et al., 2015. L-arginine upregulates the gene expression of target of rapamycin signaling pathway and stimulates protein synthesis in chicken intestinal epithelial cells. *Poultry Science*, May, 94(5), pp. 1043-51.
- Zhang, L., Sheng, R. & Qin, Z., 2009. The lysosome and neurodegenerative diseases. *Acta Biochimica et Biophysica Sinica (Shanghai)*, Jun, 41(6), pp. 437-45.

Zhang, Q., Na, Q. & Song, W., 2017. Moderate mammalian target of rapamycin inhibition induces autophagy in HTR8/SVneo cells via O-linked β -N-acetylglucosamine signaling. *Journal of Obstetrics and Gynaecology Research*, Oct, 43(10), pp. 1585-1596.

Zhao, J., Zhai, B., Gygi, S. P. & Goldberg, A. L., 2015. mTOR inhibition activates overall protein degradation by the ubiquitin proteasome system as well as by autophagy. *Proceedings of the National Academy of Sciences of the United States of America*, 29 Dec, 112(52), pp. 15790-7.

Zhao, R. et al., 2008. Loss of both GATA4 and GATA6 blocks cardiac myocyte. *Developmental Biology*, 15 May, 317(2), p. 614–619.

Zhou, D. et al., 2007. PNR1 is a unique nuclear receptor coactivator that stimulates RNA polymerase III-dependent transcription. *Journal of Molecular Signaling*, 5 Jul, Volume 2, p. 5.

Zilio, N. et al., 2014. A novel histone deacetylase complex in the control of transcription and genome stability. *Molecular and Cell Biology*, Sep, 34(18), pp. 3500-14.

Zinzalla, V., Stracka, D., Oppliger, W. & Hall, M. N., 2011. Activation of mTORC2 by association with the ribosome. *Cell*, 4 Mar, 144(5), pp. 757-68.

Zoncu, R., Efeyan, A. & Sabatini, D. M., 2011. mTOR: from growth signal integration to cancer, diabetes and ageing. *Nature Reviews Molecular Cell Biology*, Jan, 12(1), pp. 21-35.

[Appendix]
[Appendix]

[Appendix I - Computational prediction on PPI with Gaf1]

Computational prediction of network interaction for Gaf1 in fission/budding yeast. There is a total of 872 predicted PPIs.					
Protein	Common name	Product	Human	SVM score	RF score
SPAPB18E9.02C	ppk18	serine/threonine protein kinase Ppk18 (predicted)	MAST1 MAST4	0.891087	0.652
SPAC20G8.06	not1	CCR4-Not complex subunit Not1 (predicted)	GATA6	0.887828	0.745
SPBC3B8.02	php5	CCAAT-binding factor complex subunit Php5	GATA6	0.873156	0.702
SPAC25G10.09C	pan1	actin cortical patch component	GATA6	0.866825	0.59
SPBC1709.13C	set10	ribosomal lysine methyltransferase Set10	GATA6	0.864049	0.645
SPBC146.01	med15	mediator complex subunit Med15	GATA6	0.863224	0.62
SPCC285.17	spp27	RNA polymerase I upstream activation factor complex subunit Spp27	NONE	0.862713	0.635
SPBC29A3.08	pof4	elongin-A	GATA6	0.85808	0.642
SPCC16C4.14C	sfc4	transcription factor TFIIIC complex subunit Sfc4	GATA6	0.854164	0.639
SPBC17D1.01	SPBC17D1.01	transcriptional regulatory protein Spp41 (predicted)	GATA6	0.853099	0.617
SPBC8D2.07C	sfc9	transcription factor TFIIIC complex subunit Sfc9 (predicted)	GATA6	0.848122	0.652
SPBC4C3.05C	nuc1	rpa190	GATA6	0.846863	0.614
SPBC1105.06	pmc4	mediator complex subunit Pmc4	GATA6	0.844273	0.677
SPAC29B12.06C	rcd1	RNA-binding protein	GATA6	0.842442	0.704
SPAC2F7.11	nrd1	RNA-binding protein Nrd1	GATA6	0.841375	0.641
SPBC1105.07C	SPBC1105.07C	nuclear pore associated protein Thp1-Sac3 complex subunit (predicted)	GATA6	0.841112	0.603
SPBC23E6.09	ssn6	transcriptional corepressor Ssn6	GATA6	0.839907	0.689
SPAC2F3.12C	plp1	thioredoxin fold protein Plp1 (predicted)	GATA6	0.83548	0.538
SPAC458.07	tfa1	transcription factor TFIIIE alpha subunit	GATA6	0.831653	0.624
SPAC29E6.08	tbp1	Tbp	GATA6	0.831459	0.678
SPAC4G9.08C	rpc2	DNA-directed RNA polymerase III complex subunit Rpc2	GATA6	0.829738	0.652
SPAC222.09	seb1	RNA-binding protein Seb1	GATA6	0.826859	0.594

SPAC6F12.11C	sfc1	transcription factor TFIIIC complex A box associated subunit Sfc1	GATA6	0.826798	0.643
SPCP31B10.03C	med31	soh1	MED31	0.825492	0.573
SPCC553.11C	toa2	transcription factor TFIIA complex small subunit Toa2 (predicted)	GTF2A2	0.825472	0.656
SPAC20G4.01	caf16	CCR4-Not complex subunit Caf16 (predicted)	GATA6	0.823578	0.63
SPBC13E7.10C	brf1	transcription factor TFIIIB complex subunit Brf1	GATA6	0.820077	0.634
SPAC23C11.08	php3	CCAAT-binding factor complex subunit Php3	GATA6	0.819285	0.688
SPAC13G7.13C	msa1	RNA-binding protein Msa1	GATA6	0.816088	0.687
SPBC947.13	rba50	RNA polymerase II associated protein (predicted)	GATA6	0.814678	0.674
SPBC19C7.03	cyr1	adenylate cyclase	GATA6	0.811987	0.643
SPAC4D7.10C	spt20	SAGA complex subunit Spt20	GATA6	0.810998	0.654
SPAC664.03	paf1	RNA polymerase II associated Paf1 complex (predicted)	GATA6	0.809338	0.627
SPAC27E2.09	mak2	histidine kinase Mak2	GATA6	0.809158	0.586
SPBC336.09C	rrn7	RNA polymerase I core factor complex subunit Rrn7	GATA6	0.807418	0.633
SPAC17G8.05	med20	mediator complex subunit Med20	GATA6	0.806862	0.623
SPCC11E10.06C	elp4	elongator complex subunit Elp4 (predicted)	GATA6	0.806013	0.642
SPBC651.08C	rpc1	DNA-directed RNA polymerase III complex large subunit Rpc1 (predicted)	GATA6	0.805639	0.628
SPCC16C4.11	pef1	Pho85/PhoA-like cyclin-dependent kinase Pef1	GATA6	0.805237	0.67
SPAC23H3.10	ssr2	SWI/SNF and RSC complex subunit Ssr2	GATA6	0.80403	0.593
SPBC3B8.11	rrn6	RNA polymerase I transcription factor subunit Rrn6 (predicted)	GATA6	0.802424	0.542
SPBC725.17C	rrn11	RNA polymerase I transcription factor subunit Rrn11 (predicted)	GATA6	0.80187	0.612
SPAC22H10.11C	SPAC22H10.11C	TOR signaling pathway transcriptional corepressor Crf1 (predicted)	GATA6	0.801662	0.599
SPBC800.02	whi5	cell cycle transcriptional repressor Whi5 (predicted)	GATA6	0.801192	0.623
SPBC30B4.07C	tfb4	transcription factor TFIIH complex subunit Tfb4	GATA6	0.800483	0.654
SPCC74.06	mak3	histidine kinase Mak3	NONE	0.799513	0.632
SPAC17G6.10	ssr1	SWI/SNF and RSC complex subunit Ssr1	GATA6	0.799222	0.612

SPAC1486.10	thi1	SPAC6G10.01	GATA6	0.799126	0.662
SPBC1711.02	mat3-Mc	mat3Mc	GATA6	0.798574	0.617
SPAC19E9.03	pas1	cyclin Pas1	GATA6	0.796955	0.635
SPBC19G7.16	iws1	transcription elongation factor complex subunit Iws1 (predicted)	GATA6	0.796555	0.632
SPAC1687.01	rpc19	SPAPYUL23.01	GATA6	0.795943	0.64
SPAC56F8.02	SPAC56F8.02	AMP binding enzyme (predicted)	GATA6	0.795006	0.579
SPAC15A10.02	taf12	transcription factor TFIID complex subunit A/ SAGA complex subunit Taf12	GATA6	0.794883	0.609
SPAPB1A11.04C	mca1	transcription factor	GATA6	0.794841	0.639
SPBC1826.01C	mot1	SPBC6B1.01c	GATA6	0.794611	0.663
SPAC688.03C	SPAC688.03C	human AMMECR1 homolog	GATA6	0.793799	0.596
SPAC23A1.17	SPAC23A1.17	WIP family cytoskeletal protein (predicted)	GATA6	0.79373	0.632
SPAC105.03C	SPAC105.03C	transcription factor (predicted)	GATA6	0.793089	0.657
SPAC18G6.11C	rrn3	ribosomal DNA (rDNA) transcription factor Rrn3	GATA6	0.791865	0.697
SPAC139.03	toe2	transcription factor	GATA6	0.791819	0.621
SPAC25B8.11	SPAC25B8.11	transcription factor (predicted)	GATA6	0.791677	0.635
SPBC725.08	pir2	zf-C2H2 type zinc finger protein	GATA6	0.79167	0.56
SPBC16G5.17	SPBC16G5.17	transcription factor	GATA6	0.791468	0.591
SPAPB24D3.01	toe3	transcription factor (predicted)	GATA6	0.790197	0.621
SPAC25G10.03	zip1	transcription factor Zip1	GATA6	0.790115	0.614
SPAC29B12.11C	SPAC29B12.11C	human WW domain binding protein-2 ortholog	GATA6	0.789415	0.504
SPBC336.12C	cdc10	MBF transcription factor complex subunit Cdc10	GATA6	0.789176	0.591
SPAC3F10.12C	SPAC3F10.12C	transcription factor (predicted)	GATA6	0.788248	0.613
SPBC36.07	elp1	elongator subunit Elp1 (predicted)	GATA6	0.787812	0.605
SPAC3C7.09	set8	lysine methyltransferase Set8 (predicted)	GATA6	0.787331	0.62
SPAC1002.10C	sgt1	SGT1 family transcriptional regulator Sgt1	GATA6	0.78662	0.601
SPBC15D4.13C	SPBC15D4.13C	human ASCC1 ortholog	GATA6	0.786545	0.61
SPAC1783.07C	pap1	transcription factor Pap1/Caf3	GATA6	0.786211	0.669

SPAC3C7.04	SPAC3C7.04	transcription factor (predicted)	GATA6	0.785864	0.696
SPCC965.10	SPCC965.10	transcription factor (predicted)	NONE	0.78572	0.659
SPCC16A11.14	sfh1	RSC complex subunit Sfh1	GATA6	0.785625	0.606
SPAC22E12.19	snt1	Set3 complex subunit Snt1	GATA6	0.785507	0.621
SPBC30B4.04C	sol1	SWI/SNF complex subunit Sol1	GATA6	0.784779	0.625
SPAC1F7.11C	SPAC1F7.11C	transcription factor	GATA6	0.784581	0.674
SPAC56E4.04C	cut6	acetyl-CoA/biotin carboxylase	GATA6	0.784105	0.505
SPBP4H10.09	rsv1	transcription factor Rsv1	GATA6	0.783937	0.691
SPBC2D10.06	rep1	MBF transcription factor activator Rep1	GATA6	0.78392	0.604
SPAC16E8.01	shd1	cytoskeletal protein binding protein Sla1 family	GATA6	0.783875	0.612
SPAC1A6.07	sle1	eisosome assembly protein Seg1	GATA6	0.783775	0.59
SPAC11E3.06	map1	MADS-box transcription factor Map1	GATA6	0.78375	0.592
SPBP8B7.30C	thi5	transcription factor Thi5	GATA6	0.783445	0.64
SPAC6G10.12C	ace2	transcription factor Ace2	GATA6	0.783379	0.603
SPAC343.11C	mcs1	multi-copy suppressor of Chk1	GATA6	0.782382	0.623
SPAC1399.05C	toe1	transcription factor	GATA6	0.781978	0.63
SPCC330.13	rpc37	DNA-directed RNA polymerase III complex subunit Rpc37 (predicted)	POLR3E	0.781844	0.622
SPBC1773.16C	SPBC1773.16C	transcription factor	GATA6	0.78122	0.6
SPAC144.02	iec1	Ino80 complex subunit Iec1	GATA6	0.781015	0.622
SPBC19F8.07	mcs6	crk1	GATA6	0.78094	0.598
SPCC18.06C	caf1	CCR4-Not complex CAF1 family ribonuclease subunit Caf1	GATA6	0.780918	0.734
SPAC1327.01C	SPAC1327.01C	SPAC18G6.16c	GATA6	0.780477	0.694
SPBC19C7.10	bqt4	bouquet formation protein Bqt4	GATA6	0.780062	0.632
SPBC29A10.12	SPBC29A10.12	DUF1014 family protein	GATA6	0.779788	0.607
SPCC1919.14C	bdp1	transcription factor TFIIIB complex subunit Bdp1 (predicted)	BDP1	0.779522	0.614
SPAC3H8.08C	SPAC3H8.08C	transcription factor (predicted)	GATA6	0.779317	0.612

[Appendix II – Genes downregulated in *gaf1Δ* relative to the wild type during torin1 treatment]

Lists of genes that are ≥ 1.5 fold-differentially expressed in <i>gaf1Δ</i> compared to wildtype cells following 60 min treatment with 20 μM torin1		
Systematic ID	Gene name	Product description
SPAPJ760.03c	adg1	Schizosaccharomyces specific protein Adg1
SPCC18.01c	adg3	beta-glucosidase Adg3 (predicted)
SPBC428.05c	arg12	argininosuccinate synthase Arg12
SPBC1539.03c	arg41	argininosuccinate lyase (predicted)
SPBC56F2.09c	arg5	arginine specific carbamoyl-phosphate synthase subunit Arg5
SPCC63.08c	atg1	autophagy serine/threonine protein kinase Atg1
SPBC1773.02c	bcp1	thioredoxin peroxidase Bcp1
SPAC2E1P3.04	cao1	copper amine oxidase Cao1
SPBP26C9.02c	car1	arginase Car1
SPAC19G12.03	cda1	chitin deacetylase Cda1
SPBC3E7.12c	cfh4	chitin synthase regulatory factor Cfh4 (predicted)
SPAC29B12.08	clr5	Clr5 protein
SPAC24C9.08	cps1	vacuolar carboxypeptidase (predicted)
SPBC23E6.01c	cxr1	splicing factor Cxr1
SPAC1F7.09c	dal2	allantoicase Dal2
SPBC1198.02	dea2	adenine deaminase Dea2
SPAC12G12.02	efg1	rRNA processing protein Efg1 (predicted)
SPBC1105.05	exg1	cell wall glucan 1,6-beta-glucosidase Exg1
SPBC354.15	fap1	L-pipecolate oxidase
SPCC1393.08	fil1	transcription factor, zf-GATA type
SPAC1399.03	fur4	plasma membrane uracil transmembrane transporter
SPCC622.12c	gdh1	NADP-specific glutamate dehydrogenase Gdh1 (predicted)
SPAC23H4.06	gln1	glutamate-ammonia ligase Gln1
SPAPB1E7.07	glt1	glutamate synthase Glt1
SPAC30D11.01c	gto2	alpha-glucosidase (predicted)
SPBC2F12.14c	gua1	IMP dehydrogenase Gua1
SPAC1834.03c	hhf1	histone H4 h4.1
SPBC8D2.03c	hhf2	histone H4 h4.2
SPBC1105.12	hhf3	histone H4 h4.3
SPAC1834.04	hht1	histone H3 h3.1
SPBC8D2.04	hht2	histone H3 h3.2
SPBC1105.11c	hht3	histone H3 h3.3
SPAC23C11.13c	hpt1	guanine/xanthine/hypoxanthine phosphoribosyltransferase Hpt1
SPCC622.08c	hta1	histone H2A alpha
SPAC19G12.06c	hta2	histone H2A beta
SPCC622.09	htb1	histone H2B Htb1
SPBC29B5.02c	isp4	plasma membrane OPT oligopeptide transmembrane transporter family Isp4
SPAC1039.09	isp5	amino acid transmembrane transporter Isp5
SPAC4A8.04	isp6	vacuolar serine protease Isp6
SPCC1322.05c	lap2	vacuolar aminopeptidase Lap2

SPAC4A8.07c	lcb4	sphingoid long chain base kinase (predicted)
SPAPB8E5.03	mae1	plasma membrane malate/succinate:proton symporter Mae1
SPAC17C9.16c	mfs1	plasma membrane spermidine transmembrane transporter Mfs1 (predicted)
SPAPYUG7.03c	mid2	medial ring protein, anillin Mid2
SPBC2G2.04c	mmf1	mitochondrial matrix protein
SPAC1783.07c	pap1	transcription factor Pap1/Caf3
SPCC338.12	pbi2	vacuolar proteinase B inhibitor Pbi2
SPAP7G5.06	per1	plasma membrane amino acid transmembrane transporter Per1
SPBC83.11	pet2	Golgi phosphoenolpyruvate transmembrane transporter Pet2
SPBP4G3.02	pho1	acid phosphatase Pho1
SPCC736.15	pil1	eisosome BAR domain protein Pil1
SPAPB2B4.04c	pmc1	vacuolar calcium transporting P-type ATPase P2 type, Pmc1
SPBC713.11c	pmp3	plasma membrane proteolipid Pmp3 (predicted)
SPBC3D6.06c	prs5	ribose-phosphate pyrophosphokinase Prs5 (predicted)
SPBC13A2.04c	ptr2	plasma membrane PTR family peptide transmembrane transporter Ptr2
SPCC70.03c	put1	proline dehydrogenase Put1 (predicted)
SPBC24C6.04	put2	delta-1-pyrroline-5-carboxylate dehydrogenase Put2 (predicted)
SPBC16G5.02c	rbk1	ribokinase Rbk1 (predicted)
SPAC23G3.03	sib2	ornithine N5 monooxygenase (predicted)
SPBC1347.11	sro1	stress responsive orphan 1
SPBC16D10.10	tad2	tRNA specific adenosine deaminase subunit Tad2
SPAPYUK71.03c	tcb3	C2 domain protein (phospholipid binding) ER-plasma membrane tethering protein
SPAC22F3.13	tsc1	hamartin
SPAC1399.04c	uck2	uracil phosphoribosyltransferase Uck2
SPCC1795.05c	ura6	uridylate kinase Ura6
SPAC1002.19	urg1	GTP cyclohydrolase II Urg1 (predicted)
SPAC1002.17c	urg2	uracil phosphoribosyltransferase (predicted)
SPAC1002.18	urg3	DUF1688 family fungal protein, implicated in uracil or riboflavin metabolism
SPBC1683.06c	urh1	uridine ribohydrolase Urh1 (predicted)
SPCC162.11c	urk1	uridine kinase/uracil phosphoribosyltransferase (predicted)
SPCC1223.09	uro1	uricase Uro1
SPCC576.01c	xan1	alpha-ketoglutarate-dependent xanthine dioxygenase Xan1
SPAC1F7.12	yak3	aldose reductase ARK13 family YakC, implicated in cellular detoxification
SPCC830.08c	yop1	ER membrane protein DP1/Yop1
SPAC1039.01		amino acid transmembrane transporter (predicted)
SPAC1039.02		extracellular 5'-nucleotidase, human NT5E family (predicted)
SPAC1039.06		D-serine ammonia-lyase activity (predicted)
SPAC1039.07c		possible transaminase, implicated in amino acid or cofactor metabolism
SPAC1039.08		serine acetyltransferase (predicted)
SPAC11D3.15		5-oxoprolinase (ATP-hydrolyzing) (predicted)
SPAC1327.01c		transcription factor, zf-fungal binuclear cluster type (predicted)

SPAC1399.02		transmembrane transporter (predicted)
SPAC1805.16c		purine nucleoside phosphorylase (predicted)
SPAC1A6.03c		lysophospholipase (predicted)
SPAC1F7.10		hydantoin racemase family (predicted)
SPAC212.10		pseudogene malic acid transport protein
SPAC25B8.10		trans-aconitate 3-methyltransferase (predicted)
SPAC26H5.09c		oxidoreductase involved in NADPH regeneration (predicted)
SPAC3H1.06c		transmembrane transporter (predicted)
SPAC521.03		short chain dehydrogenase, human DHRS7 family(predicted)
SPAC56E4.03		aromatic aminotransferase (predicted)
SPAC56F8.15		Schizosaccharomyces pombe specific protein
SPAC6B12.04c		2-aminoadipate transaminase/kynurenine-oxoglutarate transaminase
SPAC806.06c		nicotinamide mononucleotide (NMN) adenylyltransferase (predicted)
SPBC1271.03c		NLI interacting factor family phosphatase (predicted)
SPBC1271.14		acetyl-CoA:L-glutamate N-acetyltransferase (predicted)
SPBC1683.05		transmembrane transporter family (predicted)
SPBC1683.11c		isocitrate lyase (predicted)
SPBC1861.05		bifunctional pseudouridylate synthase/pseudouridine kinase (predicted)
SPBC21C3.15c		aldehyde dehydrogenase, implicated in cellular detoxification (predicted)
SPBCPT2R1.10		pseudogene
SPBPB7E8.01		Schizosaccharomyces specific protein, predicted GPI anchor
SPBPB7E8.02		PSP1 family protein
SPCC11E10.01		cystathionine beta-lyase (predicted)
SPCC1620.06c		ribose-phosphate pyrophosphokinase (predicted)
SPCC576.02		hydantoin racemase family, implicated in amino acid, or derivative metabolism
SPNCRNA.1193		intergenic RNA (predicted)
SPNCRNA.600		translationally silent transcript from tco1 locus

[Appendix III - Genes upregulated in *gaf1Δ* relative to the wild type during torin1 treatment]

Lists of genes that are ≥ 1.5 fold-differentially expressed in <i>gaf1Δ</i> compared to wildtype cells following 60 min treatment with 20 μM torin1		
Systematic ID	Gene name	Product description
SPCC736.11	ago1	argonaute
SPAC3H1.07	aru1	arginase Aru1
SPAC30C2.04	asc1	cofactor for cytoplasmic methionyl-and glutamyl-tRNA synthetases (predicted)
SPAC13G6.10c	asl1	cell wall protein Asl1, predicted O-glucosyl hydrolase
SPBC800.05c	atb2	tubulin alpha 2
SPBC31F10.15c	atp15	F1-FO ATP synthase epsilon subunit (predicted)
SPCC1840.06	atp5	F1-FO ATP synthase delta subunit (predicted)
SPCC645.10	cca2	ATP 3'tRNA nucleotidyltransferase Cca2
SPBC29A10.01	ccr1	NADPH-cytochrome p450 reductase
SPBC646.11	cct6	chaperonin-containing T-complex zeta subunit Cct6
SPBC16A3.19	eaf7	histone acetyltransferase complex subunit Eaf7
SPAC13G7.12c	eki1	choline/ethanolamine kinase Eki1 (predicted)
SPAC1B2.03c	elo2	fatty acid elongase Elo2
SPAC13A11.02c	erg11	sterol 14-demethylase Erg11
SPAC630.08c	erg25	C-4 methylsterol oxidase Erg25 (predicted)
SPBC28E12.05	esf2	U3 snoRNP-associated protein Esf2 (predicted)
SPBC20F10.01	gar1	box H/ACA snoRNP complex subunit Gar1
SPAC19B12.02c	gas1	cell wall protein 1,3-beta-glucanosyltransferase Gas1 (predicted)
SPBC2G5.06c	hmt2	sulfide-quinone oxidoreductase
SPAC926.04c	hsp90	Hsp90 chaperone
SPAC4F8.15	itr1	myo-inositol transmembrane transporter Itr1
SPAC343.16	lys2	homoaconitate hydratase Lys2
SPBC1105.02c	lys4	homocitrate synthase
SPBC1734.11	mas5	DNAJ domain protein Mas5 (predicted)
SPBC428.11	met17	homocysteine synthase Met17
SPBC1826.01c	mot1	TATA-binding protein-associated transcription initiation repressor
SPBP8B7.15c	mpe1	mRNA cleavage ubiquitin-protein ligase E3 Mpe1 (predicted)
SPBC16A3.08c	oga1	Stm1 homolog Oga1
SPCC1281.06c	ole1	acyl-coA desaturase (predicted)
SPAC1F8.07c	pdc101	pyruvate decarboxylase (predicted)
SPAC17D4.01	pex7	peroxin-7 (predicted)
SPBC16H5.02	pfk1	6-phosphofructokinase pfk1
SPAC1A6.04c	plb1	phospholipase B homolog Plb1
SPAPB1A10.14	pof15	F-box protein (predicted)
SPNCRNA.32	pri32	non-coding RNA, poly(A)-bearing (predicted)
SPAC1002.13c	psu1	cell wall beta-glucosidase Psu1 (predicted)
SPAC20H4.07	rad57	RecA family ATPase Rad57/Rhp57
SPBC17G9.10	rpl1102	60S ribosomal protein L11 (predicted)
SPAC23A1.11	rpl1602	60S ribosomal protein L13/L16 (predicted)
SPBC29B5.03c	rpl26	60S ribosomal protein L26 (predicted)
SPAC9G1.03c	rpl3001	60S ribosomal protein L30 (predicted)

SPBC83.02c	rpl4302	60S ribosomal protein L37a (predicted)
SPBC18H10.12c	rpl701	RNase MRP subunit, ribosomal protein L7-like Rpl701
SPAC3H5.07	rpl702	60S ribosomal protein L7b involved in cytoplasmic translation
SPAC1F7.13c	rpl801	60S ribosomal protein L8/L2 (predicted)
SPBC2F12.07c	rpl802	60S ribosomal protein L8/L2 (predicted)
SPAC1071.08	rpp203	60S acidic ribosomal protein A2
SPAC31G5.17c	rps1001	40S ribosomal protein S10 (predicted)
SPBP22H7.08	rps1002	40S ribosomal protein S10 (predicted)
SPAC13G6.02c	rps101	40S ribosomal protein S3a
SPAC31G5.03	rps1101	40S ribosomal protein S11 (predicted)
SPAC144.11	rps1102	40S ribosomal protein S11 (predicted)
SPCC962.04	rps1201	40S ribosomal protein S12 (predicted)
SPBC18H10.13	rps1402	40S ribosomal protein S14 (predicted)
SPBC839.05c	rps1701	40S ribosomal protein S17 (predicted)
SPBC649.02	rps1902	40S ribosomal protein S19 (predicted)
SPBP4H10.13	rps2302	40S ribosomal protein S23 (predicted)
SPAC806.03c	rps2601	40S ribosomal protein S26 (predicted)
SPAC25G10.06	rps2801	40S ribosomal protein S28 (predicted)
SPBC16G5.14c	rps3	40S ribosomal protein S3 (predicted)
SPAC19B12.04	rps3001	40S ribosomal protein S30 (predicted)
SPAC18G6.14c	rps7	40S ribosomal protein S7 (predicted)
SPBC14F5.05c	sam1	S-adenosylmethionine synthetase
SPAC222.09	seb1	RNA-binding and 3'-end processing protein Seb1
SPAC10F6.01c	sir1	sulfite reductase beta subunit Sir1
SPCC1739.13	ssa2	heat shock protein Ssa2
SPAC664.11	ssc1	mitochondrial (2Fe-2S) cluster assembly chaperone Ssc1
SPBC27.08c	sua1	sulfate adenylyltransferase
SPCC1450.04	tef5	translation elongation factor EF-1 beta subunit, guanyl-nucleotide exchange factor
SPBC1E8.04	Tf2-10	retrotransposable element/transposon Tf2-type
SPAC1006.07	tif1	translation initiation factor eIF4A tif1
SPBC25H2.07	tif11	translation initiation factor eIF1A
SPAC222.03c	tim10	Tim9-Tim10 complex subunit Tim10 (predicted)
SPAC6F6.16c	tpz1	shelterin complex subunit Tpz1
SPAC22G7.06c	ura1	carbamoyl-phosphate synthase, aspartate carbamoyltransferase
SPBC23E6.04c	utp10	U3 snoRNP-associated protein Utp10 (predicted)
SPBC1778.01c	zuo1	ribosome-associated chaperone, zuotin (predicted)
SPAC25G10.08	tif302	translation initiation factor eIF3b (p84)
SPAC27D7.09c		But2 family protein, similar to cell surface molecules
SPAC27D7.11c		But2 family protein, similar to cell surface molecules
SPAC29A4.02c		translation elongation factor EF-1 gamma subunit
SPAC2H10.01		transcription factor, zf-fungal binuclear cluster type (predicted)
SPAC30C2.03		Schizosaccharomyces specific protein
SPBC15D4.05		conserved CobW/HypB/UreG nucleotide binding domain protein (predicted)
SPBC21C3.14c		chromatin binding protein ortholog
SPBC409.08		spermine family transmembrane transporter (predicted)
SPBP23A10.11c		circularly permuted 1,3-beta-glucanase (predicted)

SPCC1827.06c		aspartate semialdehyde dehydrogenase (predicted)
SPCC1840.05c	pgm2	phosphoglucomutase (predicted)
SPNCRNA.1626		antisense RNA (predicted)

[Appendix IV - Single mutants with decreased fitness]

Systematic ID	Gene name	Product description
SPAC8E11.02c	rad24	14-3-3 protein Rad24
SPAC637.09	rex1	3'-5'- exoribonuclease Rex1 (predicted)
SPBC15D4.15	pho2	4-phosphoerythronate phosphatase/2-phosphoglycolate phosphatase, involved in detoxification of glycolytic by-products
SPBP22H7.08	rps1002	40S ribosomal protein S10 (predicted)
SPAC1071.07c	rps1502	40S ribosomal protein S15 (predicted)
SPBC18H10.14	rps1601	40S ribosomal protein S16 (predicted)
SPAC23C11.02c	rps23	40S ribosomal protein S23 (predicted)
SPAC25G10.06	rps2801	40S ribosomal protein S28 (predicted)
SPAPB1E7.12	rps602	40S ribosomal protein S6
SPCP1E11.09c	rpp103	60S acidic ribosomal protein P1
SPAC23A1.11	rpl1602	60S ribosomal protein L13/L16 (predicted)
SPBC11C11.07	rpl1801	60S ribosomal protein L18
SPCC5E4.07	rpl2802	60S ribosomal protein L27/L28
SPAC9G1.03c	rpl3001	60S ribosomal protein L30 (predicted)
SPBC16C6.11	rpl3201	60S ribosomal protein L32
SPCC970.05	rpl3601	60S ribosomal protein L36
SPAPB17E12.05	rpl3703	60S ribosomal protein L37 (predicted)
SPCC1223.05c	rpl3702	60S ribosomal protein L37 (predicted)
SPBC11C11.09c	rpl502	60S ribosomal protein L5
SPAC3H5.12c	rpl501	60S ribosomal protein L5 (predicted)
SPAC3H5.07	rpl702	60S ribosomal protein L7b involved in cytoplasmic translation
SPAC1F7.13c	rpl801	60S ribosomal protein L8/L2 (predicted)
SPAC4G9.16c	rpl901	60S ribosomal protein L9
SPAC3C7.08c	elf1	AAA family ATPase Elf1
SPBC2D10.18	abc1	ABC1 kinase family ubiquinone biosynthesis ATPase Abc1/Coq8
SPBC56F2.12	ilv5	acetohydroxyacid reductoisomerase (predicted)
SPBP35G2.07	ilv1	acetolactate synthase catalytic subunit
SPCC338.14	ado1	adenosine kinase (predicted)
SPCC306.09c	cap1	adenylyl cyclase-associated protein Cap1
SPAC9E9.09c	atd1	aldehyde dehydrogenase (predicted)
SPAC1039.07c		aminotransferase class-III, possible transaminase, unknown specificity, implicated in amino acid or cofactor metabolism

SPCC4B3.15	mid1	anillin-related medial ring protein Mid1
SPCP1E11.10	dhm1	ankyrin repeat protein, unknown biological role
SPBC56F2.09c	arg5	arginine specific carbamoyl-phosphate synthase subunit Arg5
SPBC428.05c	arg12	argininosuccinate synthase Arg12
SPAC13G7.07	arb2	argonaute binding protein 2
SPAC140.03	arb1	argonaute inhibitor protein 1
SPBC21H7.04	dbp7	ATP-dependent RNA helicase Dbp7 (predicted)
SPCC825.01		ATPase, involved in cytoplasmic translational initiation (predicted)
SPBC1861.05		bifunctional pseudouridylate synthase/pseudouridine kinase (predicted)
SPBC428.02c	eca39	branched chain amino acid aminotransferase Eca39
SPAC25H1.06	pcf3	CAF assembly factor (CAF-1) complex subunit C, Pcf3
SPBC106.10	pka1	cAMP-dependent protein kinase catalytic subunit Pka1
SPCC18.06c	caf1	CCR4-Not complex CAF1 family ribonuclease subunit 7/8
SPBC1105.04c	cbp1	CENP-B homolog
SPAC688.11	end4	Clathrin adaptor End4
SPAC3C7.12	tip1	CLIP170 family protein Tip1
SPBC24C6.05	sec28	coatamer epsilon subunit (predicted)
SPAC17H9.10c	ddb1	Cul4-RING E3 complex subunit Ddb1
SPAC3H8.05c	mms1	Cul8-RING ubiquitin ligase complex subunit Mms1 (predicted)
SPBC1718.01	pop1	cullin 1 adaptor protein Pop1
SPCC16C4.11	pef1	cyclin-dependent protein kinase Pho85/PhoA-like Pef1
SPCC338.10c	cox5	cytochrome c oxidase subunit V (predicted)
SPCC417.02	dad5	DASH complex subunit Dad5
SPCC1223.15c	spc19	DASH complex subunit Spc19
SPBC2G2.13c	dcd1	deoxycytidylate deaminase (predicted)
SPCC794.07	lat1	dihydrolipoamide S-acetyltransferase E2, Lat1 (predicted)
SPAC30D11.10	rad52	DNA recombination protein, Rad51 mediator Rad52 (previously Rad22)
SPAC6B12.02c	mus7	DNA repair protein Mus7/Mms22
SPAC3C7.04		DNA-binding transcription factor (predicted)
SPAC3H1.11	hsr1	DNA-binding transcription factor Hsr1
SPAC25B8.19c	loz1	DNA-binding transcription factor zf-C2H2 type
SPAC4G8.13c	prz1	DNA-binding transcription factor, calcineurin responsive Prz1
SPBC354.05c	sre2	DNA-binding transcription factor, membrane-tethered Sre2

SPAC31A2.11c	cuf1	DNA-binding transcription factor, nutritional copper sensing Cuf1
SPAC1783.07c	pap1	DNA-binding transcription factor, oxidative stress-responsive Pap1/Caf3
SPBP4H10.09	rsv1	DNA-binding transcription repressor Rsv1
SPBC1718.03	ker1	DNA-directed RNA polymerase I complex subunit Ker1
SPBC17A3.05c		DNAJ/DUF1977, human DNAJB12 homolog, Hsp70 co-chaperone (predicted)
SPAC1D4.05c	erd101	Erd1 homolog (predicted)
SPAC323.05c	mtq2	eRF1 methyltransferase Mtq2 (predicted)
SPCC320.04c	gem1	ERMES complex GTPase subunit Gem1 (predicted)
SPAC8C9.19	emr1	Ermes regulator Emr1
SPAC3A11.07	nde1	external mitochondrial NADH dehydrogenase (ubiquinone) Nde1/Nde2 (predicted)
SPAC222.12c	atp2	F1-FO ATP synthase beta subunit Atp2
SPBC13E7.04	atp16	F1-FO ATP synthase delta subunit (predicted)
SPBC1604.07	atp4	F1-FO ATP synthase subunit (predicted)
SPBC29A10.13	atp7	F1-FO ATP synthase subunit D (predicted)
SPCC895.05	for3	formin For3
SPBC24C6.11	cwf14	G10 protein
SPCC417.07c	mto1	gamma tubulin complex linker Mto1
SPBC4F6.10	vps901	GEF Vps901
SPBC32F12.11	tdh1	glyceraldehyde-3-phosphate dehydrogenase Tdh1
SPBC215.05	gpd1	glycerol-3-phosphate dehydrogenase Gpd1
SPAC22E12.03c	sdj1	glyoxylase III Sdj1
SPAC1006.05c	och1	Golgi alpha-1,6-mannosyltransferase Och1
SPBC947.10	dsc1	Golgi Dsc E3 ligase complex subunit Dsc1
SPAC20H4.02	dsc3	Golgi Dsc E3 ligase complex subunit Dsc3
SPAC4D7.11	dsc4	Golgi Dsc E3 ligase complex subunit Dsc4
SPAC22F8.04	pet1	Golgi phosphoenolpyruvate transmembrane transporter Pet1
SPCC790.03	rbd2	Golgi rhomboid protease Rbd2
SPAC3F10.16c		GTP binding protein, HSR1-related (predicted)
SPAC167.07c	hul5	HECT-type ubiquitin-protein ligase E3 (predicted)
SPAC11G7.02	pub1	HECT-type ubiquitin-protein ligase E3 Pub1
SPAC23H3.13c	gpa2	heterotrimeric G protein alpha-2 subunit Gpa2
SPCC162.05	coq3	hexaprenyldihydroxybenzoate methyltransferase Coq3
SPBC31F10.14c	hip3	HIRA interacting protein Hip3

SPBC725.02	mpr1	histidine-containing response regulator phosphotransferase Mpr1
SPCC970.10c	brl2	histone H2B-K119 ubiquitin ligase complex (HULC) subunit, ubiquitin-protein ligase E3 Brl2
SPAPB1E7.06c	eme1	Holliday junction resolvase subunit Eme1
SPBC56F2.11	met6	homoserine O-acetyltransferase Met6
SPAC3G9.08	png1	ING family homolog Png1
SPBC365.10	arp5	Ino80 complex actin-like protein Arp5
SPAC222.04c	ies6	Ino80 complex subunit Ies6
SPCC4B3.10c	ipk1	inositol 1,3,4,5,6-pentakisphosphate (IP5) kinase
SPBC16C6.02c	vps1302	intermembrane lipid transfer protein, chorein family Vps1302 (predicted)
SPAC25B8.17	ypf1	intramembrane aspartyl protease of the perinuclear ER membrane Ypf1 (predicted)
SPAC11G7.03	idh1	isocitrate dehydrogenase (NAD+) subunit 1 Idh1
SPCC1840.03	sal3	karyopherin/importin beta family nuclear import signal receptor Sal3
SPBP4H10.11c	lcf2	long-chain-fatty-acid-CoA ligase
SPBC16A3.07c	nrm1	MBF complex corepressor Nrm1
SPBC21B10.13c	yox1	MBF complex corepressor Yox1
SPBC2F12.11c	rep2	MBF transcription factor activator Rep2
SPAC22F3.09c	res2	MBF transcription factor complex subunit Res2
SPBC12D12.06	srb11	mediator complex cyclin subunit Srb11
SPBC31F10.09c	nut2	mediator complex subunit Med10
SPCC1450.05c	rox3	mediator complex subunit Med19
SPAC17G8.05	med20	mediator complex subunit Med20
SPCP31B10.03c	med31	mediator complex subunit Med31
SPBC409.19c	mtx2	metaxin 2 Mtx2 (predicted)
SPBC3E7.05c	mic60	MICOS complex subunit Mic60 (predicted)
SPBC6B1.04	mde4	microtubule-site clamp monopolin complex subunit Mde4
SPCC736.06	dar2	mitochondrial aspartate-tRNA ligase Dar2 (predicted)
SPBC83.13	yhm2	mitochondrial carrier, tricarboxylic acid Yhm2 (predicted)
SPAC1486.08	cox16	mitochondrial copper chaperone for cytochrome c oxidase Cox16 (predicted)
SPCC1672.04c	cox19	mitochondrial copper chaperone for cytochrome c oxidase Cox19 (predicted)
SPAC1B3.04c	guf1	mitochondrial elongation factor GTPase Guf1 (predicted)
SPAC4G8.11c	atp10	mitochondrial F1-FO ATP synthase chaperone Atp10 (predicted)

SPAC3A12.12	atp11	mitochondrial F1-FO ATP synthase chaperone Atp11 (predicted)
SPAC9.12c	atp12	mitochondrial F1-FO ATP synthase chaperone Atp12 (predicted)
SPBC336.13c	mmp2	mitochondrial inner membrane peptidase complex catalytic subunit 2 (predicted)
SPBC365.16		mitochondrial membrane protein, conserved in yeast and apicomplexa
SPBC713.08	mim1	mitochondrial MIM complex subunit Mim1
SPAC323.01c	pos5	mitochondrial NADH kinase Pos5 (predicted)
SPBC18H10.11c	ppr2	mitochondrial PPR repeat protein Ppr2
SPCC4B3.17	cbp3	mitochondrial respiratory chain complex III assembly protein Cbp3
SPAC1610.02c	mrpl1	mitochondrial ribosomal protein subunit L1 (predicted)
SPBC2G2.07c	mug178	mitochondrial ribosomal protein subunit L51-b (predicted)
SPBC12D12.07c	trx2	mitochondrial thioredoxin Trx2
SPBC1709.09	rrf1	mitochondrial translation termination factor Rrf1
SPAPB1E7.11c	mpa1	mitochondrial translational activator, Mpa1
SPCC16A11.07	coq10	mitochondrial ubiquinone binding protein Coq10
SPBC6B1.09c	nbs1	Mre11 complex BRCT domain subunit Nbs1
SPBC3D6.08c	lsm1	mRNA decapping complex subunit (predicted)
SPBC1921.03c	mex67	mRNA export receptor, Tap, nucleoporin Mex67
SPAC3G6.02	rpn15	multifunctional proteasome assembly, lid subcomplex subunit Rpn15/Dss1
SPBC146.13c	myo1	myosin type I
SPCC1919.10c	myo52	myosin type V
SPBC577.15c	sim3	NASP family CENP-A chaperone
SPBC9B6.07	nop52	nucleolar protein Nop52 family Rrp1 (predicted)
SPAC1486.04c	alm1	nucleoporin Alm1
SPCC830.10	ham1	nucleoside triphosphatase Ham1 (predicted)
SPAC1F7.01c	spt6	nucleosome remodeling protein/ transcription elongation factor Spt6
SPAC56F8.04c	ppt1	para-hydroxybenzoate--polyprenyltransferase Ppt1
SPAP8A3.07c		phospho-2-dehydro-3-deoxyheptonate aldolase (predicted)
SPAC1A6.04c	plb1	phospholipase B homolog Plb1
SPBC2G2.01c	liz1	plasma membrane pantothenate transmembrane transporter Liz1
SPAC3H8.09c	nab3	poly(A) binding protein Nab3 (predicted)

SPCC663.12	cid12	poly(A) polymerase Cid12
SPCC965.06	osr2	potassium channel, beta subunit, aldo-keto reductase (predicted)
SPCC1322.16	phb2	prohibitin Phb2 (predicted)
SPAC29B12.04	snz1	pyridoxal 5'-phosphate synthase (glutamine hydrolysing)
SPAC26F1.03	pda1	pyruvate dehydrogenase e1 component alpha subunit Pda1 (predicted)
SPAC1851.04c	ric1	Rab-specific(Ryh1/Ypt6) Ric1-Rgp1 guanyl-nucleotide exchange factor subunit Ric1/Sat4
SPAC644.14c	rad51	RecA family recombinase Rad51/Rhp51
SPAC11G7.04	ubi1	ribosomal-ubiquitin fusion protein Ubi1 (predicted)
SPAC664.03	paf1	RNA polymerase II associated Paf1 complex
SPBC651.09c	prf1	RNA polymerase II associated Paf1 complex (predicted)
SPAC27D7.14c	tpr1	RNA polymerase II associated Paf1 complex subunit Tpr1
SPCC1393.05	ers1	RNA-silencing factor Ers1
SPAC1F3.07c	rsc58	RSC complex subunit Rsc58
SPBC1921.07c	sgf29	SAGA complex subunit Sgf29
SPBC14C8.17c	spt8	SAGA complex subunit Spt8
SPAC2F3.07c		Schizosaccharomyces pombe specific protein
SPAP27G11.14c		Schizosaccharomyces pombe specific protein
SPAC27E2.11c		Schizosaccharomyces specific protein
SPBC12C2.01c		Schizosaccharomyces specific protein
SPAC17C9.15c	dhm2	Schizosaccharomyces specific protein Dhm2
SPAC8C9.09c	mug129	Schizosaccharomyces specific protein Mug129
SPBC3H7.15	hhp1	serine/threonine protein kinase (CK1 family) Hhp1
SPAC13G6.15c	rcn1	serine/threonine protein phosphatase (calcipressin) regulatory subunit Rcn1 (predicted)
SPCC1223.11	ptc2	serine/threonine protein phosphatase PP2C catalytic subunit Ptc2
SPAC31A2.13c	sft1	SNARE Sft1 (predicted)
SPAC13C5.02	dre4	splicing associated factor Dre4
SPAC9.13c	cwf16	splicing factor Cwf16
SPCC23B6.01c	osh6	sterol transfer protein Osh6
SPBC2G5.06c	hmt2	sulfide-quinone oxidoreductase
SPAC30D11.13	hus5	SUMO conjugating enzyme E2 Hus5
SPBC649.04	uvi15	tail anchored plasma membrane protein Uvi15
SPBC19G7.10c	pdc2	topoisomerase II-associated deadenylation-dependent mRNA-decapping factor Pdc2
SPAC12G12.13c	cid14	TRAMP complex poly(A) polymerase subunit Cid14

SPBP35G2.08c	air1	TRAMP complex zinc knuckle subunit Air1
SPBC19G7.16	iws1	transcription elongation factor complex subunit Iws1
SPAC22H10.11c	crf1	transcriptional corepressor for ribosomal proteins via TOR signaling pathway Crf1 (predicted)
SPAC630.14c	tup12	transcriptional corepressor Tup12
SPAC637.07	moe1	translation initiation factor eIF3d
SPAC821.05	tif308	translation initiation factor eIF3h (p40)
SPBC16A3.17c		transmembrane transporter (predicted)
SPAC19G12.15c	tpp1	trehalose-6-phosphate phosphatase Tpp1
SPAPB18E9.01	trm5	tRNA (guanine(37)-N(1))-methyltransferase activity Trm5 (predicted)
SPBC1306.02	trm734	tRNA (guanosine 34-2'-O)-methyltransferase regulator Trm734
SPBC1A4.09	pus7	tRNA/snRNA/rRNA pseudouridine synthase Pus7 (predicted)
SPCC613.10	qcr2	ubiquinol-cytochrome-c reductase complex core protein Qcr2 (predicted)
SPAC1782.07	qcr8	ubiquinol-cytochrome-c reductase complex subunit 7
SPAC1687.12c	coq4	ubiquinone biosynthesis protein Coq4 (predicted)
SPBC365.06	pmt3	ubiquitin-like protein modifier SUMO
SPAC328.02	dbl4	ubiquitin-protein ligase E3 involved in sporulation Dbl4
SPAC23A1.07	rnf170	ubiquitin-protein ligase E3 Rnf170 (predicted)
SPCC736.07c	uri1	unconventional prefoldin chaperone involved protein complex assembly Uri1 (predicted)
SPAC227.14	yfh7	uridine kinase Yfh7 (predicted)
SPCC126.09	zip2	vacuolar zinc exporter, ZIP family, Zip2 (predicted)
SPAC17H9.19c	cdt2	WD repeat protein Cdt2
SPAC13F5.07c	hpz2	zf PARP type zinc finger protein Hpz2
SPBC1271.05c		zf-AN1 type zinc finger protein, involved in ER membrane translocation
SPAC4F10.19c	hit1	zf-HIT family C/D snoRNP assembly protein Hit1 (predicted)

[Appendix V – Single mutants with increased fitness]

Systematic ID	Gene name	Product description
SPAC25B8.13c	isp7	2-OG-Fe(II) oxygenase superfamily protein
SPAC31G5.17c	rps1001	40S ribosomal protein S10 (predicted)
SPAC17G6.06	rps2401	40S ribosomal protein S24 (predicted)
SPAC959.07	rps403	40S ribosomal protein S4 (predicted)
SPBC23G7.15c	rpp202	60S acidic ribosomal protein P2
SPCC622.18	rpl6	60S ribosomal protein L6 (predicted)
SPAC1952.09c		acetyl-CoA hydrolase (predicted)
SPBC31F10.07	lsb5	actin cortical patch component Lsb5 (predicted)
SPCC550.12	arp6	actin-like protein Arp6
SPAPB2B4.06		acyl-coenzyme A thioesterase
SPAC5H10.13c	gmh2	alpha-1,2-galactosyltransferase Gmh2
SPBC1289.13c	gmh6	alpha-1,2-galactosyltransferase Gmh6
SPCC576.01c	xan1	alpha-ketoglutarate-dependent xanthine dioxygenase Xan1
SPCC777.04		amino acid transmembrane transporter (predicted)
SPBC21B10.08c		antibiotic biosynthesis monooxygenase-like domain (predicted)
SPAPB1A10.09	ase1	antiparallel microtubule cross-linking factor Ase1
SPBC691.03c	apl3	AP-2 adaptor complex alpha subunit Alp3
SPCC18.09c	hnt3	aprataxin Hnt3
SPBC1703.03c	syo2	armadillo repeat protein, involved in nucleocytoplasmic transport Syo2 (predicted)
SPAC20G8.10c	atg6	autophagy associated beclin family protein Atg6
SPACUNK12.02 c	cmk1	calcium/calmodulin-dependent protein kinase Cmk1
SPBP4H10.19c		calreticulin/calnexin homolog (predicted)
SPCC4G3.15c	not2	CCR4-Not complex NOT box subunit 2
SPAC1B3.05	not3	CCR4-Not complex NOT box subunit 3/5
SPAC29B12.06c	rcd1	CCR4-Not complex RNA-binding protein subunit 9
SPAC821.03c	slf1	cell cortex node protein Slf1
SPBC800.02	whi5	cell cycle transcriptional repressor Whi5 (predicted)
SPAC14C4.09	agn1	cell wall glucan endo-1,3-alpha-glucosidase Agn1
SPAC3G6.01	hrp3	CHD family chromatin remodeller Hrp3
SPAC1783.05	hrp1	CHD family chromatin remodeller, CENP-A chaperone Hrp1
SPAC22A12.03c	csn4	COP9/signalosome complex subunit Csn4

SPAC13G6.03	gpi7	CP2 mannose-ethanolamine phosphotransferase GPI anchor biosynthesis protein Gpi7 (predicted)
SPCC1739.09c	cox13	cytochrome c oxidase subunit VIa (predicted)
SPAC4G9.11c	cmb1	cytosine-mismatch binding protein 1
SPBC24C6.04	put2	delta-1-pyrroline-5-carboxylate dehydrogenase Put2 (predicted)
SPCC965.12	dpe2	dipeptidyl peptidase, unknown specificity, implicated in glutathione metabolism (predicted)
SPBC3B8.05	dph1	diphthamide biosynthesis protein Dph1 (predicted)
SPAC1142.08	fhl1	DNA-binding forkhead transcription factor Fhl1
SPCC777.02		DNA-binding transcription factor (predicted)
SPAC821.07c	moc3	DNA-binding transcription factor Moc3
SPCC1223.13	cbf12	DNA-binding transcription factor, CBF1/Su(H)/LAG-1 family Cbf12
SPAC11E3.06	map1	DNA-binding transcription factor, MADS-box Map1
SPBC16G5.16		DNA-binding transcription factor, zf-fungal binuclear cluster type (predicted)
SPAC11D3.07c	toe4	DNA-binding transcription factor, zf-fungal binuclear cluster type (predicted)
SPBC405.06	xdj1	DNAJ protein Xdj1 (predicted)
SPBC1921.04c		dubious
SPAC1002.20		dubious
SPBC16H5.12c		DUF2433 metallo phosphatase superfamily conserved fungal protein
SPCC594.02c		DUF2456 family conserved fungal protein
SPAC767.01c	vps1	dynamain family protein Vps1
SPAC23C4.06c	efm6	elongation factor EF-1 alpha (eEF1A) lysine 390 methylase Efm6 (predicted)
SPBC543.08	fit1	ER membrane CoA pyrophosphatase (FIT) family lipid storage protein Fit1 (predicted)
SPCC16A11.04	snx12	ER-vacuole tethering sorting nexin Snx12 (predicted)
SPCC191.11	inv1	external invertase, beta-fructofuranosidase Inv1
SPCC550.07	fah2	fatty-acid amide hydrolase (predicted)
SPBC1198.14c	fbp1	fructose-1,6-bisphosphatase Fbp1
SPAC732.02c		fructose-2,6-bisphosphate 2-phosphatase activity (predicted)
SPAC3F10.05c	mug113	GIY-YIGT nuclease superfamily protein
SPCC191.09c	gst1	glutathione S-transferase Gst1

SPBC776.05	gpc1	glycerophosphocholine acyltransferase (GPCAT) Gpc1 (predicted)
SPCC757.03c	hsp3101	glyoxylase III Hsp3101
SPCC4B3.02c	got1	Golgi transport protein Got1 (predicted)
SPBC16E9.14c	zrg17	Golgi zinc importer, CDF family, Zrg17
SPBC1778.09		GTPase activating protein (predicted)
SPAC824.09c		GTPase activating protein (predicted)
SPBC16E9.11c	pub3	HECT-type ubiquitin-protein ligase E3 Pub3 (predicted)
SPAC12B10.01c		HECT-type ubiquitin-protein ligase E3, implicated in negative regulation of ubiquitinated chromatin formation (predicted)
SPAC17G8.13c	mst2	histone acetyltransferase Mst2
SPCC132.02	hst2	histone deacetylase, Sirtuin family, NAD-dependent Hst2
SPBC16D10.07c	sir2	histone deacetylase, Sirtuin family, NAD-dependent Sir2
SPAC4G9.06c	chz1	histone H2A-H2B dimer chaperone Chz1 (predicted)
SPBC15D4.03	slm9	histone H3.3 H4 chaperone, WD repeat protein, hira family Slm9
SPAC1834.03c	hhf1	histone H4 h4.1
SPBC19G7.04		HMG box protein
SPAC869.01		hydrolase activity, implicated in cellular detoxification (predicted)
SPBCPT2R1.03		hypothetical protein
SPBC6B1.08c	ofd1	hypoxic oxygen sensor, prolyl-3,4-dihydroxylase Ofd1
SPAC1F12.06c		inosine-containing RNA endoribonuclease (predicted)
SPBC17A3.03c		inositol phosphatase (predicted)
SPACUNK4.12c	iph1	insulinase pombe homologue 1
SPAC328.01c	msn5	karyopherin/importin beta family nuclear import/export signal receptor (predicted)
SPBC543.03c	pku80	Ku domain helicase (human XRCC5 ortholog) Pku80
SPBC36B7.06c	mug20	linear element protein Mug20
SPBC530.13	lsc1	Lsk1 associated cyclin
SPBC16C6.01c		lysine methyltransferase, human SETD6 ortholog (predicted)
SPBP4H10.20	nhm1	m7G(5')pppN diphosphatase Nhm1
SPAPYUG7.02c	sin1	MAP kinase and TOR substrate adaptor Sin1
SPAC7D4.03c	ahk1	MAP kinase cascade scaffold protein Ahk1 (predicted)
SPAC23A1.06c	cmk2	MAPK-activated protein kinase Cmk2
SPCC1322.08	srk1	MAPK-activated protein kinase Srk1
SPBC119.04	mei3	meiosis inducing protein Mei3

SPBC2G2.09c	crs1	meiosis specific cyclin Crs1
SPBC12C2.03c		methionine synthase reductase (predicted)
SPBC12D12.05c		mitochondrial carrier, ATP:ADP antiporter (predicted)
SPAC227.03c	yea6	mitochondrial carrier, NAD Yea6 (predicted)
SPBC11C11.11c	irc3	mitochondrial DNA branch migration helicase Irc3 (predicted)
SPBC1706.03	fzo1	mitochondrial dynamin family fusion GTPase (mitofusin) Fzo1
SPAC13G7.11	mba1	mitochondrial membrane-associated ribosome receptor Mba1 (predicted)
SPAC20G4.05c	fmp40	mitochondrial protein adenylyltransferase SelO
SPAC25B8.18		mitochondrial thioredoxin-related protein (predicted)
SPAC4F10.11	spn1	mitotic septin Spn1
SPAC9G1.11c	spn4	mitotic septin Spn4
SPAC23H4.12	alp13	MRG family Ctr6 histone deacetylase complex subunit Alp13
SPBC1271.07c		N-acetyltransferase (predicted)
SPAC9G1.06c	cyk3	Nebulin-family actin filament anchoring protein Cyk3
SPAC18B11.04	ncs1	neuronal calcium sensor related protein Ncs1
SPAC8F11.09c	nnt1	nicotinamide N-methyltransferase Nnt1 (predicted)
SPCC777.03c		nifs homolog, possible cysteine desulfurase
SPCC70.06	sac32	nuclear export factor Sac32 (predicted)
SPBP35G2.06c	nup131	nucleoporin, WD repeat Nup131
SPAC806.07	ndk1	nucleoside diphosphate kinase Ndk1
SPBC119.03	cmt1	O-methyltransferase, human COMT catechol homolog 1
SPAC23G3.03	sib2	ornithine N5 monooxygenase (predicted)
SPBC725.15	ura5	orotate phosphoribosyltransferase Ura5
SPAC2F7.10	akr1	palmitoyltransferase Akr1 (predicted)
SPBC25H2.03	vac14	PAS complex subunit, involved in phosphoinositide metabolism Vac14 (predicted)
SPBC609.02	ptn1	phosphatidylinositol-3,4,5-trisphosphate3-phosphatase Ptn1
SPCC1450.09c		phospholipase (predicted)
SPAC27E2.09	mak2	phosphorelay sensor kinase Mak2
SPBC1683.03c	amf1	plasma membrane ammonium transmembrane transporter Amf1 (predicted)
SPBC543.05c	bor1	plasma membrane borate efflux transmembrane transporter Bor1 (predicted)

SPAC1639.02c	trk2	plasma membrane potassium ion transmembrane transporter Trk2
SPBC713.11c	pmp3	plasma membrane proteolipid Pmp3 (predicted)
SPBC13A2.04c	ptr2	plasma membrane PTR family peptide transmembrane transporter Ptr2
SPAC227.10	pfd2	prefoldin subunit Pfd2
SPAC3H8.07c	pfd3	prefoldin subunit Pfd3
SPAC3A11.13	pfd6	prefoldin subunit Pfd6
SPAC12B10.14c	tea5	pseudokinase Tea5
SPAC1093.02	pdx3	pyridoxamine 5'-phosphate oxidase Pdx3 (predicted)
SPBC1778.05c	lam2	Ragulator complex Rag GEF subunit
SPAC16.01	rho2	Rho family GTPase Rho2
SPAC26A3.09c	rga2	RhoGAP, GTPase activating protein Rga2
SPBC1709.13c	set10	ribosomal lysine methyltransferase Set10
SPBC1539.10	nop16	ribosome biogenesis protein Nop16 (predicted)
SPAPB21F2.03	slx9	ribosome biogenesis protein Slx9 (predicted)
SPAC1142.01	rqc1	ribosome quality control complex (RQC) complex subunit Rqc1
SPBC16A3.18	cip1	RNA-binding protein Cip1
SPAC17H9.04c	dri1	RNA-binding protein involved in heterochromatin assembly Dri1
SPAC2F7.11	nrd1	RNA-binding protein Nrd1
SPAC17A2.10c		Schizosaccharomyces pombe specific protein
SPBCPT2R1.02		Schizosaccharomyces pombe specific protein
SPAC683.03		Schizosaccharomyces pombe specific protein
SPBC29A3.21		Schizosaccharomyces pombe specific protein
SPAC630.04c		Schizosaccharomyces specific protein
SPBC13E7.07		Schizosaccharomyces specific protein
SPCC1919.07		Schizosaccharomyces specific protein
SPAC3H8.02	csr102	sec14 cytosolic factor family, phospholipid-intermembrane transfer protein Csr102 (predicted)
SPBP35G2.05c	cki2	serine/threonine protein kinase (CK1 family) Cki2
SPAC1782.09c	clp1	serine/threonine protein phosphatase (Cdc14-related) Clp1/Flp1
SPCC31H12.05c	sds21	serine/threonine protein phosphatase PP1 catalytic subunit Sds21
SPBC18H10.06c	swd2	Set1C complex subunit Swd2.1
SPBC18A7.02c		seven transmembrane receptor-like protein (predicted)
SPAC4F8.10c	stg1	SM22/transgelin-like actin modulating protein Stg1

SPAC20G8.08c	fft1	SMARCAD1 family ATPase Fft1 (predicted)
SPCC1235.05c	fft2	SMARCAD1 family ATPase Fft2 (predicted)
SPAC19A8.05c	sst4	sorting receptor for ubiquitinated membrane proteins, ESCRT 0 complex subunit Sst4
SPBC12C2.07c	srm1	spermidine synthase Srm1 (predicted)
SPBC3B9.15c	scp1	Sre1 cleavage activating protein, Scap Scp1
SPBC16H5.04	snd301	SRP-independent ER targeting protein Snd3a (predicted)
SPBC30B4.04c	sol1	SWI/SNF complex subunit Sol1
SPAC13F5.05	mpd1	thioredoxin family protein Mpd1 (predicted)
SPAC2F3.12c	plp1	thioredoxin fold protein Plp1 (predicted)
SPAC2G11.10c	uba42	thiosulfate sulfurtransferase, URM1 activating enzyme E1-type Uba42 (predicted)
SPBC28F2.02	mep33	translation machinery associated protein Mep33
SPBPB10D8.06c		transmembrane transporter (predicted)
SPCC330.07c		transmembrane transporter (predicted)
SPBPB10D8.07c		transmembrane transporter (predicted)
SPCC736.09c	tfx1	TRAX
SPBC29A10.09c	tri1	triman, ribonuclease involved in priRNA formation Tri1
SPAP8A3.12c	tpp2	tripeptidyl-peptidase II Tpp2
SPAC6B12.09	trm10	tRNA m(1)G methyltransferase Trm10
SPBC19C7.08c	ppm2	tRNA methyltransferase Ppm2 (predicted)
SPBC18H10.08c	ubp4	ubiquitin C-terminal hydrolase Ubp4
SPBC1703.12	ubp9	ubiquitin C-terminal hydrolase Ubp9
SPBC1861.02	abp2	unknown protein, may bind replication origins Abp2
SPCC4B3.05c	hem12	uroporphyrinogen decarboxylase Hem12 (predicted)
SPCC1795.02c	vcx1	vacuolar proton/calcium exchanger (predicted)
SPAC14C4.11	vtc2	vacuolar transporter chaperone (VTC) complex polyphosphate synthetase subunit Vtc2/3 (predicted)
SPAC17C9.11c		zf-C2H2 type zinc finger protein/UBA domain protein
SPCC1739.01		zf-CCCH type zinc finger protein
SPBC9B6.03		zf-FYVE type zinc finger protein, involved in endosomal transport
SPAC19B12.07c		zinc finger C2H2-type, human ZNF277 ortholog, implicated in transcriptional regulation

[Appendix VI – Single mutants sensitive to torin1]

Systematic ID	Gene name	Product description
SPBC4.06		acid phosphatase Fmp10 (predicted)
SPBC14F5.09c	ade8	adenylosuccinate lyase Ade8
SPAC227.04	atg10	Atg12 conjugating enzyme Atg10
SPBC15D4.07c	atg9	autophagy associated phospholipid scramblase Atg9
SPAC589.07c	atg1801	autophagy associated WD repeat protein Atg18a
SPBC16G5.11c	bag101	BAG family molecular chaperone regulator Bag101 (predicted)
SPAC19A8.04	erg5	C-22 sterol desaturase Erg5
SPBC800.02	whi5	cell cycle transcriptional repressor Whi5 (predicted)
SPBC25B2.01	hbs1	Dom34-Hbs1 translation release factor complex GTPase subunit Hbs1 (predicted)
SPAC1002.18	urg3	DUF1688 family fungal conserved protein, implicated in uracil or riboflavin metabolism
SPAC17A2.05	osm1	fumarate reductase Osm1 (predicted)
SPAC23C4.07	tht2	karyogamy protein Tht2
SPAC328.01c	msn5	karyopherin/importin beta family nuclear import/export signal receptor (predicted)
SPAC11E3.12		mitochondrial thioredoxin family protein, implicated in sulfur cluster assembly
SPBC947.05c	frp2	plasma membrane ferric-chelate reductase Frp2 (predicted)
SPAC1527.03	slr1	RNA-binding protein, LARP1 family Slr1 (predicted)
SPCC736.02		Schizosaccharomyces specific protein
SPAC167.01	ire1	serine/threonine protein kinase, sensor for unfolded proteins in the ER Ire1
SPCC794.09c	tef101	translation elongation factor EF-1 alpha Ef1a-a
SPAC1002.17c	urg2	uracil phosphoribosyltransferase (predicted)
SPCC1795.02c	vcx1	vacuolar proton/calcium exchanger (predicted)
SPAC3H5.08c	wdr44	WD repeat protein, human WDR44 family

[Appendix VII – Single mutant resistant to torin1]

Systematic ID	Gene name	Product description
SPAC1851.02	slc1	1-acylglycerol-3-phosphate O-acyltransferase Slc1 (predicted)
SPBC3E7.01	fab1	1-phosphatidylinositol-3-phosphate 5-kinase Fab1
SPBC725.04	hac1	2-hydroxyacyl-CoA lyase Hac1 (predicted)
SPACUNK4.15		2',3'-cyclic-nucleotide 3'-phosphodiesterase (predicted)
SPBC19G7.02	abz2	4-amino-4-deoxychorismate lyase Abz2 (predicted)
SPBC1685.02c	rps1202	40S ribosomal protein S12 (predicted)
SPCP1E11.09c	rpp103	60S acidic ribosomal protein P1
SPCC1682.14	rpl1902	60S ribosomal protein L19
SPBC14C8.04	ilv6	acetolactate synthase regulatory subunit Ilv6 (predicted)
SPAC1952.09c		acetyl-CoA hydrolase (predicted)
SPBC887.01	adi1	acireductone dioxygenase family Adi1 (predicted)
SPBC11G11.02 c	end3	actin cortical patch component End3 (predicted)
SPAC25G10.09 c	pan1	actin cortical patch component, with EF hand and WH2 motif Pan1 (predicted)
SPAC9E9.09c	atd1	aldehyde dehydrogenase (predicted)
SPAC3C7.05c	mug191	alpha-1,6- mannanase (predicted)
SPAC27D7.05c	apc14	anaphase-promoting complex subunit Apc14
SPCP1E11.10	dhm1	ankyrin repeat protein, unknown biological role
SPBP26C9.02c	car1	arginase Car1
SPCP1E11.02	ppk38	Ark1/Prk1 family protein kinase Ppk38
SPBC2D10.04	aly2	arrestin-related endocytic ubiquitin ligase substrate adaptor Aly2
SPBC557.05		arrestin, implicated in vesicle-mediated transport
SPAC20G8.10c	atg6	autophagy associated beclin family protein Atg6
SPAC1D4.03c	aut12	autophagy associated protein Aut12 (predicted)
SPBC19C2.10		BAR adaptor protein, human endophilin A1-like ortholog, implicated in endocytosis
SPBC28E12.06c	lvs1	beige protein homolog Lvs1
SPCC594.07c	bqt3	bouquet formation protein Bqt3
SPAC17G6.05c	bro1	BRO1 domain protein Bro1 (predicted)
SPAC29A4.19c	cta5	Ca ²⁺ /Mn ²⁺ transporting P-type ATPase P5 type Cta5
SPAPB2B4.04c	pmc1	calcium transporting P-type ATPase P2 type, Pmc1
SPAC1039.04		carboxylic acid transmembrane transporter (predicted)
SPAC24C9.05c	mug70	CBS and PB1 domain protein, conserved in fungi and plants, implicated in signalling Mug70

SPBC3B8.02	php5	CCAAT-binding factor complex subunit Php5
SPAC13G6.10c	asl1	cell wall protein Asl1, predicted O-glucosyl hydrolase
SPAC9E9.10c	cbh1	CENP-B homolog Cbh1
SPAC1851.03	ckb1	CK2 family regulatory subunit Ckb1
SPBC24C6.05	sec28	coatamer epsilon subunit (predicted)
SPCC4B3.14	cwf20	complexed with Cdc5 protein Cwf20
SPAC23G3.05c		conserved endomembrane protein, RGS domain, implicated in signal transduction, cell polarity, possibly via membrane tethering (predicted)
SPAC29E6.10c	nst1	conserved fungal NST1 family protein
SPAC6B12.14c		conserved fungal protein
SPBC31F10.05	mug37	conserved fungal protein
SPAC4H3.14c	rng8	contractile ring myosin V regulator Rng8
SPBC16E9.09c	erp5	COPII vesicle coat component Erp5/Erp6 (predicted)
SPCC364.05	vps3	CORVET complex WD repeat subunit Vps3 (predicted)
SPAC17A2.06c	vps8	CORVET complex WD repeat subunit Vps8 (predicted)
SPBC354.01	gtp1	cytoplasmic translation associated GTP binding protein Gtp1
SPAC16E8.01	shd1	cytoskeletal protein binding protein Sla1 family, Shd1 (predicted)
SPBC1198.08	dug1	dipeptidase Dug1 (predicted)
SPAPB1E7.02c	mcl1	DNA polymerase alpha accessory factor Mcl1
SPBC12D12.02c	cdm1	DNA polymerase delta subunit Cdm1
SPCC4G3.10c	rhp42	DNA repair protein Rhp42
SPCC18B5.11c	cds1	DNA replication checkpoint kinase Cds1
SPBC1703.14c	top1	DNA topoisomerase I
SPAC25B8.11		DNA-binding transcription factor (predicted)
SPAPB24D3.01	toe3	DNA-binding transcription factor (predicted)
SPBC56F2.05c		DNA-binding transcription factor (predicted)
SPAC11E3.06	map1	DNA-binding transcription factor, MADS-box Map1
SPAC32A11.03c	phx1	DNA-binding transcription factor, stationary phase-specific Phx1
SPBC19C2.09	sre1	DNA-binding transcription factor, sterol regulatory element binding protein Sre1
SPBC1685.01	pmp1	dual-specificity MAP kinase phosphatase Pmp1
SPCC24B10.18		DUF2462 family protein, human Leydig cell tumor 10 kDa protein homolog
SPBC1198.03c		DUF4646 family conserved fungal protein
SPAC767.01c	vps1	dynamain family protein Vps1

SPBC839.14c	efm4	elongation factor EF-1 alpha (eEF1A) methyltransferase Efm4 (predicted)
SPBC1861.07	elc1	elongin C Elc1 (predicted)
SPBC21B10.09		endomembrane system acetyl-CoA transmembrane transporter (predicted)
SPBC36.06c	spo9	ER farnesyl pyrophosphate synthetase Erg20
SPBP16F5.08c	fmo1	ER flavin-containing N,N-dimethylaniline monooxygenase activity Fmo1 (predicted)
SPAC8F11.08c		ER membrane associated esterase/lipase (predicted)
SPBC14F5.07	doa10	ER ubiquitin-protein ligase E3 Doa10 (predicted)
SPAP8A3.03	zip3	ER zinc exporter, ZIP family Zip3 (predicted)
SPAC1B3.07c	vps28	ESCRT I complex subunit Vps28
SPBC651.05c	dot2	ESCRT II complex subunit Dot2
SPBC4B4.06	vps25	ESCRT II complex subunit Vps25
SPBC3B9.09	vps36	ESCRT II complex subunit Vps36
SPBC13G1.12	did2	ESCRT III complex subunit Did2 (predicted)
SPAC4F8.01	did4	ESCRT III complex subunit Did4
SPBC215.14c	vps20	ESCRT III complex subunit Vps20
SPAC1142.07c	vps32	ESCRT III complex subunit Vps32
SPAC6G9.12	cfr1	exomer complex BRCT domain subunit Cfr1
SPBC31F10.16	bch1	exomer complex ChAPs family (Chs5p-Arf1p-binding) protein Bch1
SPBC1604.09c	rex4	exoribonuclease Rex4 (predicted)
SPAC12B10.07	acp1	F-actin capping protein alpha subunit
SPBC3H7.06c	pof9	F-box protein Pof9
SPBC1703.06	pof10	F-box/WD repeat protein Pof10
SPBC24C6.06	gpa1	G-protein alpha subunit
SPAC1142.06	get3	GET complex (ER membrane insertion) ATPase subunit Get3 (predicted)
SPAC15F9.01c	glm1	Glomulin, ubiquitin-protein transferase inhibitor Glm1 (predicted)
SPCC794.01c	gcd1	glucose dehydrogenase Gcd1
SPAPB1E7.07	glt1	glutamate synthase Glt1
SPAC3F10.04	gsa1	glutathione synthetase large and small subunit Gsa1
SPAC824.07	glo2	glyoxalase II
SPAC6F6.13c		Golgi localized Alpha/Beta hydrolase fold, DUF726 family protein
SPAC1F3.05	gga21	Golgi localized Arf binding gamma-adaptin ortholog Gga21

SPBC32F12.12c		Golgi membrane protein involved in vesicle-mediated transport (predicted)
SPBC83.11	pet2	Golgi phosphoenolpyruvate transmembrane transporter Pet2
SPAC5D6.13	gpp74	Golgi phosphoprotein 3 family Vps74 (predicted)
SPBC16E9.14c	zrg17	Golgi zinc importer, CDF family, Zrg17
SPBC405.04c	ypt7	GTPase Ypt7
SPAPB1A10.10c	ypt71	GTPase Ypt71
SPBC215.10	odr1	HAD superfamily hydrolase, unknown role
SPAC1805.15c	pub2	HECT-type ubiquitin-protein ligase E3 Pub2
SPBC16E9.11c	pub3	HECT-type ubiquitin-protein ligase E3 Pub3 (predicted)
SPAC12B10.01c		HECT-type ubiquitin-protein ligase E3, implicated in negative regulation of ubiquitinated chromatin formation (predicted)
SPAC25H1.02	jmj1	histone demethylase Jmj1 (predicted)
SPBC2D10.11c	nap2	histone H2A-H2B chaperone Nap2
SPBC1105.12	hhf3	histone H4 h4.3
SPBC776.03		homoserine dehydrogenase (predicted)
SPAC23H4.14	vam6	HOPS complex Rab GEF subunit Vam6
SPAC19B12.10	sst2	human AMSH/STAMBP protein homolog, ubiquitin specific-protease
SPAC6G10.10c		human mmtag2 ortholog, implicated in splicing
SPBC1709.11c	png2	ING family histone acetyltransferase complex PHD-type zinc finger subunit Png2
SPBC32F12.01c	css1	inositol phosphosphingolipid phospholipase C, Css1
SPAC1093.03	fig4	inositol polyphosphate phosphatase Fig4 (predicted)
SPAC22G7.01c	fra1	iron responsive transcriptional regulator, peptidase family (predicted)
SPAC11G7.03	idh1	isocitrate dehydrogenase (NAD ⁺) subunit 1 Idh1
SPAC22H10.03c	kap114	karyopherin/importin beta family nuclear import signal receptor Kap14
SPCC31H12.06	mug111	major facilitator family transmembrane transporter Mug111 (predicted)
SPAPYUG7.02c	sin1	MAP kinase and TOR substrate adaptor Sin1
SPAC9G1.02	wis4	MAP kinase Wis4
SPCC4B3.13		MatE family transmembrane transporter (predicted)
SPBC32F12.07c		membrane associated ubiquitin-protein ligase E3, MARCH family (predicted)
SPAC607.06c		metallopeptidase (predicted)

SPBC1778.07		methyltransferase, human CARNMT1 ortholog
SPBC21C3.09c	oaa1	mitochondrial acylpyruvase Oaa1 (predicted)
SPBC725.01	maa1	mitochondrial aspartate aminotransferase Maa1 (predicted)
SPAC17H9.08		mitochondrial carrier, coenzyme A (predicted)
SPAC8C9.12c	mrs3	mitochondrial carrier, iron ion Mrs3 (predicted)
SPCC1235.11	mpc1	mitochondrial carrier, pyruvate Mpc1 (predicted)
SPCC24B10.22	pog1	mitochondrial DNA polymerase, gamma subunit Pog1
SPAC3A12.12	atp11	mitochondrial F1-FO ATP synthase chaperone Atp11 (predicted)
SPAC823.13c	she9	mitochondrial inner membrane protein She9 (predicted)
SPBC365.16		mitochondrial membrane protein, conserved in yeast and apicomplexa
SPAC3G6.05		mitochondrial Mpv17/PMP22 family protein 1 (predicted)
SPCC965.09		mitochondrial omega-amidase (predicted)
SPBC2D10.15c	pth1	mitochondrial peptidyl-tRNA hydrolase Pth1 (predicted)
SPAC1556.03	azr1	mitochondrial protein phosphatase Azr1
SPBC4F6.08c	mrpl39	mitochondrial ribosomal protein subunit L33 (predicted)
SPBC800.07c	tsf1	mitochondrial translation elongation factor EF-Ts Tsf1
SPBC25B2.04c	mtg1	mitochondrial translation factor (GTPase) Mtg1 (predicted)
SPAC110.02	pds5	mitotic and meiotic cohesin loader subunit Pds5
SPAC7D4.14c	iss10	MTREC (exosome adaptor) complex proline-rich subunit Iss10/Pir1
SPCC1919.12c	erm2	multi-spanning vacuolar membrane protease (predicted)
SPBC106.07c	nat2	N alpha-acetylation related protein Nat2 (predicted)
SPAPB17E12.0 8	eos1	N-glycosylation protein Eos1 (predicted)
SPBC12C2.04		NAD binding dehydrogenase family protein
SPBC1778.03c		NADH pyrophosphatase (predicted)
SPBC25H2.05	egd2	nascent polypeptide-associated complex alpha subunit Egd2
SPBC1861.03	naa35	NatC N-acetyltransferase complex subunit Naa35
SPBC947.03c	naa38	NatC N-acetyltransferase non-catalytic Sm-like domain subunit Naa38
SPBC17D11.01	nep1	NEDD8 protease Nep1
SPAC1952.11c	ure2	nickel-dependent urease Ure2
SPBC1539.02		nuclear protein, human IK ortholog, implicated in meiotic chromosome segregation in fission yeast, splicing or spindle checkpoint in human
SPAC1002.02	pom34	nucleoporin Pom34

SPBC23G7.06c	nvj2	nucleus-vacuole junction protein Nvj2
SPAC20G4.08	pdc1	P-body assembly protein
SPBC3H7.09	erf2	palmitoyltransferase Erf2
SPBP8B7.13	vac7	PAS complex phosphatidylinositol phosphate kinase activator Vac7 (predicted)
SPBC4F6.12	pxl1	paxillin-like protein Pxl1
SPCC757.05c		peptidase family M20 protein involved in glutathione catabolism (predicted)
SPAPB17E12.0 3	pex12	peroxisomal ubiquitin-protein ligase E3 Pex12 (predicted)
SPBC18H10.19	vps38	phosphatidylinositol 3-kinase complex subunit Vps38
SPBC3D6.05	ptp4	phosphatidate cytidyltransferase Ptp4/Dgk1
SPBC26H8.03	cho2	phosphatidylethanolamine N-methyltransferase Cho2
SPBC409.10	ade7	phosphoribosylamidoimidazolesuccinocarboxamide synthase, SAICAR synthetase, Ade7
SPBC1271.09	tgp1	plasma membrane glycerophosphodiester transmembrane transporter (predicted)
SPAC27F1.08	pdt1	plasma membrane Nramp family manganese ion transmembrane transporter
SPAC29B12.14c		plasma membrane purine transmembrane transporter (predicted)
SPAC1B3.16c	vht1	plasma membrane vitamin H transmembrane transporter Vht1
SPBC23E6.03c	nta1	protein N-terminal amidase Nta1 (predicted)
SPAC11E3.09	pyp3	protein tyrosine phosphatase Pyp3
SPBC17A3.06		protein tyrosine/serine/threonine phosphatase (predicted)
SPAC10F6.12c	mam4	protein-S isoprenylcysteine O-methyltransferase Mam4
SPBC32F12.05c	cwf12	Prp19 complex subunit Cwf12
SPBC30B4.02c	sqs1	R3H and G-patch domain protein Sqs1 (predicted)
SPAC2E1P5.02 c	mug109	Rab GTPase binding protein upregulated in meiosis II (predicted)
SPBC119.14	rti1	Rad22 homolog Rti1
SPBC3H7.12	rav2	RAVE complex subunit Rav2
SPBC409.16c	saw1	recombination protein Saw1 (predicted)
SPAC22F3.12c	rgs1	regulator of G-protein signaling Rgs1
SPBC216.06c	swi1	replication fork protection complex subunit Swi1
SPBC3F6.05	rga1	RhoGAP, GTPase activating protein Rga1
SPBC16C6.03c	rsa1	ribosome assembly protein Rsa1 (predicted)

SPBC16H5.08c		ribosome biogenesis ATPase, Arb family ABCF2-like (predicted)
SPBC1198.11c	reb1	RNA polymerase I transcription termination factor/ RNA polymerase II transcription factor Reb1
SPAC17A2.09c	csx1	RNA-binding protein Csx1
SPAC16E8.06c	nop12	RNA-binding protein Nop12 (predicted)
SPAC22F8.09	rrp16	rRNA processing protein Rrp16 (predicted)
SPBC2A9.11c	iss9	SAC3/GANP/THP3 family protein, human LENG8 ortholog
SPAC17A2.11		Schizosaccharomyces pombe specific protein
SPBC19C2.06c	mug124	Schizosaccharomyces pombe specific protein
SPAC17A2.10c		Schizosaccharomyces pombe specific protein
SPAPB1A10.05		Schizosaccharomyces specific protein
SPAC607.07c		Schizosaccharomyces specific protein
SPCC70.10		Schizosaccharomyces specific protein
SPAC18G6.13		Schizosaccharomyces specific protein
SPBC23G7.14		Schizosaccharomyces specific protein
SPBC887.08		Schizosaccharomyces specific protein
SPCC1393.12		Schizosaccharomyces specific protein
SPBC28E12.04		Schizosaccharomyces specific protein
SPBC4B4.12c		Schizosaccharomyces specific protein
SPBC409.11	meu18	Schizosaccharomyces specific protein Meu18
SPAC57A10.06	mug15	Schizosaccharomyces specific protein Mug15
SPAC24B11.10c	cfh1	SEL1/TPR repeat protein Cfh1 (predicted)
SPBC1289.01c	chr4	SEL1/TPR repeat protein1, 3-beta-glucan synthase regulatory factor Chf3/Chr4
SPBP35G2.05c	cki2	serine/threonine protein kinase (CK1 family) Cki2
SPBC3H7.15	hhp1	serine/threonine protein kinase (CK1 family) Hhp1
SPAC1687.15	gsk3	serine/threonine protein kinase Gsk3
SPBC16E9.13	ksp1	serine/threonine protein kinase Ksp1 (predicted)
SPBP4H10.04	ppb1	serine/threonine protein phosphatase PP2B (calcineurin A) catalytic subunit Ppb1
SPAC521.03		short chain dehydrogenase, human DHRS7 family(predicted)
SPBC3H7.13	far10	SIP/FAR complex FHA domain subunit Far10/Csc1
SPAC2C4.10c	csc4	SIP/FAR complex subunit Csc4
SPAC2F3.18c		small endoribonuclease with 2 transmembrane domains (predicted)
SPAPB17E12.0	yip12	SMN complex subunit Yip12/Gem2

SPAC4G8.10	gos1	SNARE Gos1 (predicted)
SPAC6F12.03c	fsv1	SNARE Stx8
SPAC19A8.05c	sst4	sorting receptor for ubiquitinated membrane proteins, ESCRT 0 complex subunit Sst4
SPAC4A8.07c	lcb4	sphingoid long chain base kinase (predicted)
SPBC3E7.15c	lac1	sphingosine N-acyltransferase Lac1
SPBC1347.11	sro1	stress responsive orphan 1
SPCC330.12c	sdh3	succinate dehydrogenase (ubiquinone) cytochrome b subunit (predicted)
SPAC12B10.06c	emi5	succinate dehydrogenase complex assembly protein Emi5 (predicted)
SPCC320.05		sulfate transmembrane transporter (predicted)
SPAC343.18	rfp2	SUMO-targeted ubiquitin-protein ligase subunit Rfp2
SPAC2F3.12c	plp1	thioredoxin fold protein Plp1 (predicted)
SPAC24H6.02c	tim15	TIM23 translocase complex subunit Tim15 (predicted)
SPAC1142.02c	sgt2	TPR repeat protein Sgt2 (predicted)
SPBC16D10.01c		TPR repeat protein, conserved fungal protein
SPAC25B8.10		trans-aconitate 3-methyltransferase (predicted)
SPAC821.05	tif308	translation initiation factor eIF3h (p40)
SPBC19G7.17	sec6102	translocon subunit Sec61 homolog (predicted)
SPAPB1E7.08c		transmembrane transporter (predicted)
SPCC553.12c		transmembrane transporter (predicted)
SPBPB10D8.04c		transmembrane transporter (predicted)
SPCC1672.12c	get4	TRC complex (ER membrane insertion) subunit Get4 (predicted)
SPBC887.11	pus2	tRNA pseudouridine synthase Pus2 (predicted)
SPBC23G7.07c	cms1	U3-containing 90S preribosome complex subunit Cms1 (predicted)
SPBC83.01	ucp8	UBA/EH/EF hand domain protein Ucp8
SPBC713.02c	ubp15	ubiquitin C-terminal hydrolase Ubp15
SPAC11E3.04c	ubc13	ubiquitin conjugating enzyme E2 Ubc13
SPAC10F6.05c	ubc6	ubiquitin conjugating enzyme E2 Ubc6 (predicted)
SPBC1A4.05	blt1	ubiquitin domain-like protein Blt1
SPAC16A10.03c		ubiquitin-protein ligase E3 involved in vesicle docking Pep5/Vps11-like (predicted)
SPAC6B12.07c	pqr1	ubiquitin-protein ligase E3 with SPX domain Pqr1
SPAC20H4.10	ufd2	ubiquitin-protein ligase E4 Ufd2 (predicted)
SPBC28F2.11	hmo1	upstream binding transcription factor, RNA polymerase I specific, Hmo1

SPAC1399.04c	uck2	uracil phosphoribosyltransferase Uck2
SPAC3A12.09c	ure4	urease accessory protein UreD
SPAC29A4.13	ure6	urease accessory protein UreF
SPCPB16A4.05 c	ure7	urease accessory protein UreG
SPAC3H1.09c	avt3	vacuolar amino acid transmembrane transporter Avt3
SPAC14C4.15c	dpp1	vacuolar dipeptidyl peptidase (predicted)
SPBC713.07c		vacuolar polyphosphatase (predicted)
SPBC8D2.02c	vps68	vacuolar sorting protein Vps68 (predicted)
SPAC13F5.04c	vta1	Vps20 associated protein Vta1 (predicted)
SPBC27B12.05		WD repeat protein Crt10, involved in ribosomal RNA decay (predicted)
SPBC887.04c	lub1	WD repeat protein Lub1
SPBC16H5.13	wdr7	WD repeat protein, human WDR7 ortholog
SPBC2A9.03		WD40/YVTN repeat-like protein
SPBC24C6.10c	dip1	WISH/DIP/SPIN90 ortholog, endocytosis protein Dip1
SPAC25B8.15c	tyw3	wybutosine biosynthesis protein Tyw3 (predicted)
SPBC25B2.03		zf-C3HC4 type zinc finger
SPAC4F10.19c	hit1	zf-HIT family C/D snoRNP assembly protein Hit1 (predicted)

[Appendix VIII –Gene deletions showing reduced fitness when combined with *gaf1*Δ]

Systematic ID	Gene name	Product description
SPAC637.09	<i>rex1</i>	3'-5'- exoribonuclease Rex1 (predicted)
SPBC685.06	<i>rps001</i>	40S ribosomal protein S0A (p40)
SPBP22H7.08	<i>rps1002</i>	40S ribosomal protein S10 (predicted)
SPAC144.11	<i>rps1102</i>	40S ribosomal protein S11 (predicted)
SPCC962.04	<i>rps1201</i>	40S ribosomal protein S12 (predicted)
SPAC3H5.05c	<i>rps1401</i>	40S ribosomal protein S14 (predicted)
SPAC1071.07c	<i>rps1502</i>	40S ribosomal protein S15 (predicted)
SPCC1393.03	<i>rps1501</i>	40S ribosomal protein S15 (predicted)
SPBC839.05c	<i>rps1701</i>	40S ribosomal protein S17 (predicted)
SPCC24B10.09	<i>rps1702</i>	40S ribosomal protein S17 (predicted)
SPAC23C11.02c	<i>rps23</i>	40S ribosomal protein S23 (predicted)
SPAC17G6.06	<i>rps2401</i>	40S ribosomal protein S24 (predicted)
SPBC19G7.03c	<i>rps3002</i>	40S ribosomal protein S30 (predicted)
SPAC13G6.02c	<i>rps101</i>	40S ribosomal protein S3a
SPBC19F8.08	<i>rps401</i>	40S ribosomal protein S4 (predicted)
SPAC328.10c	<i>rps502</i>	40S ribosomal protein S5 (predicted)
SPCC16C4.10		6-phosphogluconolactonase (predicted)
SPBC23G7.15c	<i>rpp202</i>	60S acidic ribosomal protein P2
SPBC30D10.18c	<i>rpl102</i>	60S ribosomal protein L10a
SPBC17G9.10	<i>rpl1102</i>	60S ribosomal protein L11 (predicted)
SPBC839.13c	<i>rpl1601</i>	60S ribosomal protein L13/L16 (predicted)
SPBC2F12.04	<i>rpl1701</i>	60S ribosomal protein L17
SPCC1682.14	<i>rpl1902</i>	60S ribosomal protein L19
SPAC959.08	<i>rpl2102</i>	60S ribosomal protein L21 (predicted)
SPAC3G9.03	<i>rpl2301</i>	60S ribosomal protein L23
SPBC83.02c	<i>rpl4302</i>	60S ribosomal protein L37a (predicted)
SPAC4G9.16c	<i>rpl901</i>	60S ribosomal protein L9
SPBC56F2.12	<i>ilv5</i>	acetohydroxyacid reductoisomerase (predicted)
SPBP35G2.07	<i>ilv1</i>	acetolactate synthase catalytic subunit
SPBC8D2.18c		adenosylhomocysteinase (predicted)
SPAC1782.11	<i>met14</i>	adenylyl-sulfate kinase (predicted)
SPAC9E9.09c	<i>atd1</i>	aldehyde dehydrogenase (predicted)
SPAC637.06	<i>gmh5</i>	alpha-1,2-galactosyltransferase (predicted)
SPCC757.12	<i>aah1</i>	alpha-amylase homolog Aah1 (predicted)
SPBC19F8.06c	<i>meu22</i>	amino acid transmembrane transporter Meu22 (predicted)
SPCC4B3.15	<i>mid1</i>	anillin-related medial ring protein Mid1
SPCP1E11.10	<i>dhm1</i>	ankyrin repeat protein, unknown biological role

SPAC31A2.09c	apm4	AP-2 adaptor complex mu subunit Apm4 (predicted)
SPAC23H3.06	apl6	AP-3 adaptor complex subunit Apl6 (predicted)
SPAC30D11.05	aps3	AP-3 adaptor complex subunit Aps3 (predicted)
SPBC31F10.10c	mub1	Armadillo-type fold protein, zf-MYND type zinc finger protein, Mub1-Rad6-Ubr2 ubiquitin ligase complex Mub1 (predicted)
SPAC23E2.03c	ste7	arrestin family ubiquitin-ligase adaptor Ste7
SPAC26A3.01	sxa1	aspartic protease Sxa1
SPAC6B12.08	epr1	Atg8-interacting ER-phagy receptor Epr1
SPAC6G9.10c	sen1	ATP-dependent 5' to 3' DNA/RNA helicase Sen1
SPBC776.09	ste13	ATP-dependent RNA helicase Ste13/Dhh1
SPAC631.02	bdf2	BET family double bromodomain protein Bdf2
SPCC1235.02	bio2	biotin synthase
SPBC651.02	nit1	bis(5'-adenosyl)-triphosphatase Nit1 (predicted)
SPBC428.02c	eca39	branched chain amino acid aminotransferase Eca39
SPBC582.05c	brc1	BRCT domain protein Brc1
SPCC330.11	btb1	BTB/POZ family ubiquitin-type ligase substrate adaptor Btb1
SPBC21C3.20c	git1	C2 domain protein Git1
SPCC1919.01	ckk2	calcium/calmodulin-dependent (CaMKK) protein kinase Ckk2/Ppk34
SPBP4H10.19c		calreticulin/calnexin homolog (predicted)
SPBC106.10	pka1	cAMP-dependent protein kinase catalytic subunit Pka1
SPAC22G7.06c	ura1	carbamoyl-phosphate synthase (glutamine hydrolyzing), aspartate carbamoyltransferase Ura1
SPAC11D3.18c		carboxylic acid transmembrane transporter (predicted)
SPAC23C11.08	php3	CCAAT-binding factor complex subunit Php3
SPBC3B8.02	php5	CCAAT-binding factor complex subunit Php5
SPAC1B3.05	not3	CCR4-Not complex NOT box subunit 3/5
SPAC821.03c	slf1	cell cortex node protein Slf1
SPBC800.02	whi5	cell cycle transcriptional repressor Whi5 (predicted)
SPBC29A10.08	gas2	cell wall 1,3-beta-glucanosyltransferase Gas2
SPAC11E3.13c	gas5	cell wall protein 1,3-beta-glucanosyltransferase Gas5 (predicted)
SPAC13G6.10c	asl1	cell wall protein Asl1, predicted O-glucosyl hydrolase
SPBC1105.04c	cbp1	CENP-B homolog
SPBC2D10.16	mhf1	CENP-S ortholog, FANCM-MHF complex subunit Mhf1
SPBC17G9.08c	cnt5	Centaurin Cnt5
SPAC1783.05	hrp1	CHD family chromatin remodeller, CENP-A chaperone Hrp1
SPCC1827.02c	pcy1	choline-phosphate cytidyltransferase Pcy1 (predicted)

SPAC13G7.12c	eki1	choline/ethanolamine kinase Eki1 (predicted)
SPBC2G5.02c	ckb2	CK2 regulatory subunit beta isoform 2, Ckb2
SPAC2F7.07c	cph2	Clr6 histone deacetylase associated PHD-finger protein Cph2
SPCC613.12c	raf1	CLRC ubiquitin ligase complex WD repeat subunit Raf1/Dos1
SPAC30C2.04	asc1	cofactor for cytoplasmic methionyl-and glutamyl-tRNA synthetases Asc1
SPAC4A8.09c	cwf21	complexed with Cdc5 protein Cwf21
SPBC16E9.09c	erp5	COPII vesicle coat component Erp5/Erp6 (predicted)
SPAC19E9.03	pas1	cyclin Pas1
SPBC36.04	cys11	cysteine synthase
SPAC4G9.11c	cmb1	cytosine-mismatch binding protein 1
SPAC16E8.01	shd1	cytoskeletal protein binding protein Sla1 family, Shd1 (predicted)
SPBC2G5.03	ctu1	cytosolic thiouridylase subunit Ctu1
SPAC16A10.05c	dad1	DASH complex subunit Dad1
SPBC24C6.04	put2	delta-1-pyrroline-5-carboxylate dehydrogenase Put2 (predicted)
SPCC757.13		dipeptide transmembrane transporter (predicted)
SPAC926.05c	dph4	diphthamide biosynthesis protein Dph4 (predicted)
SPCC553.01c	dbl2	DNA recombination protein Dbl2
SPAC30D11.10	rad52	DNA recombination protein, Rad51 mediator Rad52 (previously Rad22)
SPCC970.01	rad16	DNA repair endonuclease XPF
SPAC6B12.02c	mus7	DNA repair protein Mus7/Mms22
SPAC1556.01c	rad50	DNA repair protein Rad50
SPBC1A4.03c	top2	DNA topoisomerase II
SPAC1142.08	fhl1	DNA-binding forkhead transcription factor Fhl1
SPCC757.04		DNA-binding transcription factor (predicted)
SPAC3H1.11	hsr1	DNA-binding transcription factor Hsr1
SPAC821.07c	moc3	DNA-binding transcription factor Moc3
SPAC6F12.02	rst2	DNA-binding transcription factor Rst2
SPBC1105.14	rsv2	DNA-binding transcription factor Rsv2
SPBC2F12.09c	atf21	DNA-binding transcription factor, Atf-CREB family Atf21
SPCC736.08	cbf11	DNA-binding transcription factor, CBF1/Su(H)/LAG-1 family Cbf11
SPAC11E3.06	map1	DNA-binding transcription factor, MADS-box Map1
SPBC19G7.06	mbx1	DNA-binding transcription factor, MADS-box Mbx1

SPBC354.05c	sre2	DNA-binding transcription factor, membrane-tethered Sre2
SPAPB1A11.04c	mca1	DNA-binding transcription factor, zf-fungal binuclear cluster type Mca1
SPCC1259.03	rpa12	DNA-directed RNA polymerase complex I TFIIIS subunit Rpa12
SPBC1718.03	ker1	DNA-directed RNA polymerase I complex subunit Ker1
SPBC17A3.05c		DNAJ/DUF1977, human DNAJB12 homolog, Hsp70 co-chaperone (predicted)
SPCC594.02c		DUF2456 family conserved fungal protein
SPAC767.01c	vps1	dynamamin family protein Vps1
SPAC2F7.03c	pom1	DYRK family cell polarity protein kinase Pom1
SPAC1A6.07	sle1	eisosome assembly protein Seg1
SPAC4H3.13	pcc1	EKC/KEOPS complex subunit Pcc1 (predicted)
SPAC23C4.06c	efm6	elongation factor EF-1 alpha (eEF1A) lysine 390 methylase Efm6 (predicted)
SPAC30.02c	kti12	elongator complex associated protein Kti12 (predicted)
SPBC18E5.05c	elp5	elongator complex subunit Elp5 (predicted)
SPAC29A4.20	elp3	elongator complex tRNA uridine(34) acetyltransferase subunit Elp3
SPBC29A3.08	pof4	elongin-A, F-box protein Pof4 (predicted)
SPCC613.03		endoplasmic reticulum EF hand protein (predicted)
SPAC222.14c	sey1	ER fusion GTPase, atlastin Sey1
SPAC25H1.07	emc1	ER membrane protein complex subunit Emc1 (predicted)
SPBC83.10	emc7	ER membrane protein complex subunit Emc7 (predicted)
SPBC1E8.02		ER ubiquitin family protein (predicted)
SPBC839.11c	hut1	ER uridine diphosphate-glucose transmembrane transporter Hut1
SPBC337.09	erg28	Erg28 protein (predicted)
SPAC1F5.05c	mso1	exocytic docking protein Mso1
SPAPB1A10.14	pof15	F-box protein (predicted)
SPCC895.05	for3	formin For3
SPBC1198.14c	fbp1	fructose-1,6-bisphosphatase Fbp1
SPAC3F10.05c	mug113	GIY-YIGT nuclease superfamily protein
SPCC794.01c	gcd1	glucose dehydrogenase Gcd1
SPCC825.02	gbs1	glucosidase II beta subunit
SPBC354.12	gpd3	glyceraldehyde 3-phosphate dehydrogenase Gpd3
SPCC757.03c	hsp3101	glyoxylase III Hsp3101
SPAC1006.05c	och1	Golgi alpha-1,6-mannosyltransferase Och1
SPAC824.09c		GTPase activating protein (predicted)

SPBC530.01	<i>gyp1</i>	GTPase activating protein Gyp1 (predicted)
SPCC4G3.09c	<i>gyp3</i>	GTPase activating protein Gyp3 (predicted)
SPAC18B11.11		GTPase activating protein, Tsc2 paralog (predicted)
SPBC26H8.08c	<i>grn1</i>	GTPase Grn1
SPBC3B9.05	<i>hot15</i>	helper of TIM Hot15 (predicted)
SPBC215.04	<i>git11</i>	heterotrimeric G protein gamma subunit Git11
SPAC17G8.13c	<i>mst2</i>	histone acetyltransferase Mst2
SPBC16D10.07c	<i>sir2</i>	histone deacetylase, Sirtuin family, NAD-dependent Sir2
SPAC4G9.06c	<i>chz1</i>	histone H2A-H2B dimer chaperone Chz1 (predicted)
SPAC18B11.07c	<i>rhp6</i>	histone H2B-K119 ubiquitin ligase complex (HULC), ubiquitin conjugating enzyme E2 subunit Rhp6/Rad6
SPBC31F10.13c	<i>hip1</i>	histone H3.3 H4 chaperone, hira family Hip1
SPBC15D4.03	<i>slm9</i>	histone H3.3 H4 chaperone, WD repeat protein, hira family Slm9
SPBC8D2.03c	<i>hhf2</i>	histone H4 h4.2
SPBC19G7.04		HMG box protein
SPBC776.03		homoserine dehydrogenase (predicted)
SPAC13G7.02c	<i>ssa1</i>	Hsp70 family heat shock protein Ssa1
SPBC577.04	<i>tho5</i>	human THOC5 ortholog Tho5 (predicted)
SPAC24B11.13	<i>hem3</i>	hydroxymethylbilane synthase Hem3 (predicted)
SPAC212.03		hypothetical protein
SPBC365.10	<i>arp5</i>	Ino80 complex actin-like protein Arp5
SPAC664.02c	<i>arp8</i>	Ino80 complex actin-like protein Arp8
SPACUNK4.12c	<i>iph1</i>	insulinase pombe homologue 1
SPBC16C6.02c	<i>vps1302</i>	intermembrane lipid transfer protein, chorein family Vps1302 (predicted)
SPAC328.01c	<i>msn5</i>	karyopherin/importin beta family nuclear import/export signal receptor (predicted)
SPAC1F3.03	<i>sro7</i>	Lgl family protein Sro7 (predicted)
SPBP4H10.11c	<i>lcf2</i>	long-chain-fatty-acid-CoA ligase
SPBC16E9.16c	<i>lsd90</i>	Lsd90 protein
SPBC530.13	<i>lsc1</i>	Lsk1 associated cyclin
SPBC16C6.01c		lysine methyltransferase, human SETD6 ortholog (predicted)
SPAPB24D3.10c	<i>agl1</i>	maltose alpha-glucosidase Agl1
SPAC1834.05	<i>alg9</i>	mannosyltransferase complex subunit Alg9 (predicted)
SPAPYUG7.02c	<i>sin1</i>	MAP kinase and TOR substrate adaptor Sin1
SPAC1D4.13	<i>byr1</i>	MAP kinase Byr1
SPBC1D7.05	<i>byr2</i>	MAP kinase Byr2
SPAC31G5.09c	<i>spk1</i>	MAP kinase Spk1

SPAC1565.04c	ste4	MAPK cascade adaptor protein Ste4
SPBC31F10.09c	nut2	mediator complex subunit Med10
SPCP31B10.03c	med31	mediator complex subunit Med31
SPBC119.04	mei3	meiosis inducing protein Mei3
SPCC1682.08c	mpf2	meiotic pumilio family RNA-binding protein Mpf2
SPBC12C2.03c		methionine synthase reductase (predicted)
SPAPB2B4.02	grx5	mitochondrial [2Fe-2S] cluster assembly and transfer glutaredoxin Grx5
SPBC12D12.05c		mitochondrial carrier, ATP:ADP antiporter (predicted)
SPCC1235.11	mpc1	mitochondrial carrier, pyruvate Mpc1 (predicted)
SPAC57A10.12c	ura3	mitochondrial dihydroorotate dehydrogenase Ura3
SPBC1706.03	fzo1	mitochondrial dynamin family fusion GTPase (mitofusin) Fzo1
SPBC11G11.01	fis1	mitochondrial fission protein Fis1 (predicted)
SPAC13F5.03c	gld1	mitochondrial glycerol dehydrogenase Gld1
SPAC13G7.11	mba1	mitochondrial membrane-associated ribosome receptor Mba1 (predicted)
SPBC1703.11	opa3	mitochondrial outer membrane lipid metabolism regulator Opa3
SPAC25B8.18		mitochondrial thioredoxin-related protein (predicted)
SPAC4F10.11	spn1	mitotic septin Spn1
SPAC9G1.11c	spn4	mitotic septin Spn4
SPBC3D6.04c	mad1	mitotic spindle checkpoint protein Mad1
SPBC6B1.09c	nbs1	Mre11 complex BRCT domain subunit Nbs1
SPAC13C5.07	mre11	Mre11 nuclease
SPAC23H4.12	alp13	MRG family Clr6 histone deacetylase complex subunit Alp13
SPAC1006.03c	red1	MTREC (exosome adaptor) complex subunit Red1
SPBC12C2.04		NAD binding dehydrogenase family protein
SPCC330.03c		NADPH-hemoprotein reductase (predicted)
SPBC25D12.02c	dnt1	nucleolar protein Dnt1
SPAC806.07	ndk1	nucleoside diphosphate kinase Ndk1
SPAC1F7.01c	spt6	nucleosome remodeling protein/ transcription elongation factor Spt6
SPAC27E2.03c		Obg-like ATPase, human OLA1 ortholog (predicted)
SPAC4G9.10	arg3	ornithine carbamoyltransferase Arg3
SPBC577.14c	spa1	ornithine decarboxylase antizyme with +1 programmed ribosomal frameshift Spa1
SPAC144.04c	spe1	ornithine decarboxylase Spe1 (predicted)
SPBC725.15	ura5	orotate phosphoribosyltransferase Ura5

SPCC1795.06	map2	P-factor pheromone Map2
SPCC1020.01c	pma2	P-type proton ATPase, P3-type Pma2
SPAC2F7.10	akr1	palmitoyltransferase Akr1 (predicted)
SPAC1B1.04c	pan3	PAN complex protein phosphotransferase subunit Pan3 (predicted)
SPCC757.05c		peptidase family M20 protein involved in glutathione catabolism (predicted)
SPBC609.02	ptn1	phosphatidylinositol-3,4,5-trisphosphate3-phosphatase Ptn1
SPAP8A3.07c		phospho-2-dehydro-3-deoxyheptonate aldolase (predicted)
SPAC1A6.04c	plb1	phospholipase B homolog Plb1
SPAC27E2.09	mak2	phosphorelay sensor kinase Mak2
SPAC13G7.04c	mac1	plasma membrane anchored protein, claudin family, predicted membrane sensor Mac1
SPCC1393.10	ctr4	plasma membrane copper transporter complex subunit Ctr4
SPCC1235.13	ght6	plasma membrane glucose/fructose:proton symporter Ght6
SPAC23D3.12	pho842	plasma membrane inorganic phosphate transmembrane transporter Pho842
SPBC13A2.04c	ptr2	plasma membrane PTR family peptide transmembrane transporter Ptr2
SPBC36.03c	mfs3	plasma membrane spermidine transmembrane transporter Mfs3
SPAC1B3.16c	vht1	plasma membrane vitamin H transmembrane transporter Vht1
SPBC27B12.08	sip1	Pof6 interacting protein Sip1, predicted AP-1 accessory protein
SPAC821.04c	cid13	poly(A) polymerase Cid13
SPAC3H8.07c	pdf3	prefoldin subunit Pdf3
SPAC3A11.13	pdf6	prefoldin subunit Pdf6
SPAC22A12.07c	ogm1	protein O-mannosyltransferase Ogm1
SPBC16C6.09	ogm4	protein O-mannosyltransferase Ogm4
SPAC26F1.10c	pyp1	protein tyrosine phosphatase Pyp1
SPBC32F12.05c	cwf12	Prp19 complex subunit Cwf12
SPCC1682.15	mug122	PX/PXA domain protein
SPAC1093.02	pdx3	pyridoxamine 5'-phosphate oxidase Pdx3 (predicted)
SPAC13A11.06	pdc202	pyruvate decarboxylase (predicted)
SPBC23E6.08	rgp1	Rab-specific(Ryh1/Ypt6) Ric1-Rgp1 guanyl-nucleotide exchange factor subunit Rgp1/Sat1
SPAC1851.04c	ric1	Rab-specific(Ryh1/Ypt6) Ric1-Rgp1 guanyl-nucleotide exchange factor subunit Ric1/Sat4

SPCC330.02	rhp7	Rad7 homolog Rhp7
SPBC337.13c	gtr1	RagA GTPase Gtr1
SPBC1778.05c	lam2	Ragulator complex Rag GEF subunit
SPBC21.05c	ral2	Ras1-Scd pathway protein Ral2
SPAC3C7.03c	rad55	RecA family ATPase Rad55/Rhp55
SPAC20H4.07	rad57	RecA family ATPase Rad57/Rhp57
SPAC2G11.12	rqh1	RecQ type DNA helicase Rqh1
SPBCPT2R1.08c	tlh2	RecQ type DNA helicase Tlh1
SPAC22F3.13	tsc1	Rheb GAP, hamartin Tsc1
SPAC630.13c	tsc2	Rheb GAP, tuberlin Tsc2
SPBC19G7.08c	art1	RhoGEF Art1
SPBC3B9.13c	rpp102	ribosomal protein P1 Rpp102
SPAC1805.12c	ubi2	ribosomal-ubiquitin fusion protein Ubi2
SPBC16H5.08c		ribosome biogenesis ATPase, Arb family ABCF2-like (predicted)
SPAPB21F2.03	slx9	ribosome biogenesis protein Slx9 (predicted)
SPCC31H12.03c	mlo1	RNA binding protein (predicted)
SPBC1198.11c	reb1	RNA polymerase I transcription termination factor/ RNA polymerase II transcription factor Reb1
SPAC3G9.04	ssu72	RNA polymerase II CTD phosphatase Ssu72
SPBC887.05c	cwf29	RNA-binding protein Cwf29
SPAC17H9.04c	dri1	RNA-binding protein involved in heterochromatin assembly Dri1
SPCC320.07c	mde7	RNA-binding protein Mde7
SPAC2F7.11	nrd1	RNA-binding protein Nrd1
SPAC1952.05	gcn5	SAGA complex histone acetyltransferase catalytic subunit Gcn5
SPBP16F5.03c	tra1	SAGA complex/ASTRA complex, phosphatidylinositol pseudokinase Tra1
SPBC29A3.21		Schizosaccharomyces pombe specific protein
SPCC330.19c		Schizosaccharomyces pombe specific protein
SPAC27E2.11c		Schizosaccharomyces specific protein
SPCC1393.12		Schizosaccharomyces specific protein
SPBC1778.10c	ppk21	serine/threonine protein kinase Ppk21 (predicted)
SPBC902.03	nem2	serine/threonine protein phosphatase (Nem1-Spo7 complex) regulatory subunit (predicted)
SPCC31H12.05c	sds21	serine/threonine protein phosphatase PP1 catalytic subunit Sds21

SPBC16H5.07c	ppa2	serine/threonine protein phosphatase PP2A catalytic subunit Ppa2
SPAC4F10.04	ypa1	serine/threonine protein phosphatase PP2A regulatory subunit, PTPA family Ypa1
SPAC1782.05	ypa2	serine/threonine protein phosphatase PP2A regulatory subunit, PTPA family Ypa2
SPBC18H10.06c	swd2	Set1C complex subunit Swd2.1
SPCC1235.09	hif2	Set3 complex subunit Hif2
SPAC4D7.06c	met8	siroheme synthase Met8 (predicted)
SPAP8A3.05	ski7	Ski complex/exosome interacting GTPase Ski7
SPCC1235.05c	fft2	SMARCAD1 family ATPase Fft2 (predicted)
SPAC25A8.01c	fft3	SMARCAD1 family ATPase Fft3
SPAC823.05c	tlg2	SNARE Tlg2 (predicted)
SPBC12C2.07c	srm1	spermidine synthase Srm1 (predicted)
SPBC23E6.01c	cxr1	splicing factor Cxr1
SPAC1610.01	saf5	splicing factor Saf5
SPCC594.04c		steroid oxidoreductase superfamily protein (predicted)
SPBC1348.02	ftm5	sub-telomeric 5Tm protein family Ftm5
SPCC330.12c	sdh3	succinate dehydrogenase (ubiquinone) cytochrome b subunit (predicted)
SPBC27.08c	sua1	sulfate adenylyltransferase
SPCC320.05		sulfate transmembrane transporter (predicted)
SPAC4H3.02c	swc3	Swr1 complex subunit Swc3
SPBC1539.04	tts1	tetra spanning protein 1, Tts1
SPAC2G11.10c	uba42	thiosulfate sulfurtransferase, URM1 activating enzyme E1-type Uba42 (predicted)
SPAC167.04	pam17	TIM23 translocase complex-associated motor subunit Pam17 (predicted)
SPCC1259.07	rxt3	transcriptional regulatory protein Rxt3
SPAC26H5.10c	tif51	translation elongation and termination factor eIF5A (predicted)
SPCC794.09c	tef101	translation elongation factor EF-1 alpha Ef1a-a
SPBC28F2.02	mep33	translation machinery associated protein Mep33
SPBC2G2.03c	sbh1	translocon beta subunit Sbh1 (predicted)
SPCC330.07c		transmembrane transporter (predicted)
SPCC613.02		transmembrane transporter (predicted)
SPBPB10D8.07c		transmembrane transporter (predicted)
SPCC18B5.10c	tex1	TREX complex subunit Tex1 (predicted)
SPBC16A3.06	tad1	tRNA specific adenosine-37 deaminase Tad1 (predicted)

SPAC8E11.07c	alp31	tubulin specific chaperone cofactor A, Alp31
SPBC18H10.07	wbp4	U2-type precatalytic spliceosome WW domain-binding protein Wbp4 (predicted)
SPBP8B7.10c	utp16	U3 snoRNP-associated protein Utp16 (predicted)
SPAC10F6.05c	ubc6	ubiquitin conjugating enzyme E2 Ubc6 (predicted)
SPBC1A4.05	blt1	ubiquitin domain-like protein Blt1
SPAC328.02	dbl4	ubiquitin-protein ligase E3 involved in sporulation Dbl4
SPBC1861.02	abp2	unknown protein, may bind replication origins Abp2
SPAC13G7.03	upf3	up-frameshift suppressor 3 family protein (predicted)
SPBC1685.07c	avt5	vacuolar amino acid transmembrane transporter Avt5
SPBC354.14c	vac8	vacuolar protein-membrane adaptor Vac8 (predicted)
SPBC9B6.03		zf-FYVE type zinc finger protein, involved in endosomal transport

[Appendix IX – Gene deletions showing increased fitness when combined with *gaf1*Δ]

Systematic ID	Gene name	Product description
SPBC56F2.09c	arg5	arginine specific carbamoyl-phosphate synthase subunit Arg5
SPBC428.05c	arg12	argininosuccinate synthase Arg12
SPAC25H1.06	pcf3	CAF assembly factor (CAF-1) complex subunit C, Pcf3
SPAC1805.07c	dad2	DASH complex subunit Dad2
SPAC18B11.03c		ER alcohol acetyltransferase involved in intermembrane phospholipid transfer (predicted)
SPAC167.07c	hul5	HECT-type ubiquitin-protein ligase E3 (predicted)
SPAC22F3.09c	res2	MBF transcription factor complex subunit Res2
SPBC3E7.05c	mic60	MICOS complex subunit Mic60 (predicted)
SPBC25H2.08c	mrs2	mitochondrial inner membrane magnesium ion transmembrane transporter Mrs2 (predicted)
SPCC4B3.17	cbp3	mitochondrial respiratory chain complex III assembly protein Cbp3
SPBC25B2.04c	mtg1	mitochondrial translation factor (GTPase) Mtg1 (predicted)
SPAC222.05c	mss1	mitochondrial tRNA wobble uridine modification GTPase Mss1 (predicted)
SPAC3H8.09c	nab3	poly(A) binding protein Nab3 (predicted)
SPAC2F3.07c		Schizosaccharomyces pombe specific protein
SPBC18H10.04c	sce3	translation initiation factor (predicted)
SPAC227.14	yfh7	uridine kinase Yfh7 (predicted)

[Appendix X – Double mutants sensitive to torin1]

Systematic ID	Gene name	Product description
SPAC1296.06	tah18	CIA machinery NADPH-dependent diflavin oxidoreductase Tah18 (predicted)
SPAC1851.03	ckb1	CK2 family regulatory subunit Ckb1
SPBC56F2.05c		DNA-binding transcription factor (predicted)
SPBC56F2.01	pof12	F-box protein Pof12
SPBC26H8.08c	grn1	GTPase Grn1
SPBC2D10.11c	nap2	histone H2A-H2B chaperone Nap2
SPAC22H10.03c	kap114	karyopherin/importin beta family nuclear import signal receptor Kap14
SPAC110.02	pds5	mitotic and meiotic cohesin loader subunit Pds5
SPAC458.05	pik3	phosphatidylinositol 3-kinase Pik3
SPBC16C6.09	ogm4	protein O-mannosyltransferase Ogm4
SPCC24B10.04		Schizosaccharomyces specific protein

[Appendix XI – Double mutants resistant to torin1]

Systematic ID	Gene name	Product description
SPCC1682.14	rpl1902	60S ribosomal protein L19
SPCP1E11.02	ppk38	Ark1/Prk1 family protein kinase Ppk38
SPCC895.09c	ucp12	ATP-dependent RNA helicase Ucp12, unknown location and role, implicated in mRNA processing (predicted)
SPAC20G8.10 c	atg6	autophagy associated beclin family protein Atg6
SPAC589.07c	atg1801	autophagy associated WD repeat protein Atg18a
SPAC17G6.05 c	bro1	BRO1 domain protein Bro1 (predicted)
SPBC31F10.05	mug37	conserved fungal protein
SPBC16E9.09c	erp5	COPII vesicle coat component Erp5/Erp6 (predicted)
SPCC364.05	vps3	CORVET complex WD repeat subunit Vps3 (predicted)
SPAC17A2.06c	vps8	CORVET complex WD repeat subunit Vps8 (predicted)
SPBC36.06c	spo9	ER farnesyl pyrophosphate synthetase Erg20
SPAC1B3.07c	vps28	ESCRT I complex subunit Vps28
SPBC651.05c	dot2	ESCRT II complex subunit Dot2
SPBC3B9.09	vps36	ESCRT II complex subunit Vps36
SPBC13G1.12	did2	ESCRT III complex subunit Did2 (predicted)
SPBC215.14c	vps20	ESCRT III complex subunit Vps20
SPAC6G9.12	cfr1	exomer complex BRCT domain subunit Cfr1
SPBC1604.09c	rex4	exoribonuclease Rex4 (predicted)
SPAC1142.06	get3	GET complex (ER membrane insertion) ATPase subunit Get3 (predicted)
SPAC26H5.04	gid5	GID complex armadillo repeat subunit Gid5 (predicted)
SPAC5D6.13	gpp74	Golgi phosphoprotein 3 family Vps74 (predicted)
SPBC405.04c	ypt7	GTPase Ypt7
SPBC16E9.11c	pub3	HECT-type ubiquitin-protein ligase E3 Pub3 (predicted)
SPBC776.03		homoserine dehydrogenase (predicted)
SPAC19B12.10	sst2	human AMSH/STAMBP protein homolog, ubiquitin specific-protease
SPBC725.01	maa1	mitochondrial aspartate aminotransferase Maa1 (predicted)
SPBC1861.03	naa35	NatC N-acetyltransferase complex subunit Naa35
SPBC3H7.09	erf2	palmitoyltransferase Erf2
SPAC27F1.08	pdt1	plasma membrane Nramp family manganese ion transmembrane transporter
SPBC16H5.08c		ribosome biogenesis ATPase, Arb family ABCF2-like (predicted)

SPAC17A2.10c		Schizosaccharomyces pombe specific protein
SPBC4B4.12c		Schizosaccharomyces specific protein
SPBC28E12.04		Schizosaccharomyces specific protein
SPBC16E9.13	ksp1	serine/threonine protein kinase Ksp1 (predicted)
SPAC4G8.10	gos1	SNARE Gos1 (predicted)
SPAC6F12.03c	fsv1	SNARE Stx8
SPAC19A8.05c	sst4	sorting receptor for ubiquitinated membrane proteins, ESCRT 0 complex subunit Sst4
SPAC4A8.07c	lcb4	sphingoid long chain base kinase (predicted)
SPCC330.12c	sdh3	succinate dehydrogenase (ubiquinone) cytochrome b subunit (predicted)
SPBC16D10.01c		TPR repeat protein, conserved fungal protein
SPAC11E3.04c	ubc13	ubiquitin conjugating enzyme E2 Ubc13
SPAC16A10.03c		ubiquitin-protein ligase E3 involved in vesicle docking Pep5/Vps11-like (predicted)
SPAC20H4.10	ufd2	ubiquitin-protein ligase E4 Ufd2 (predicted)
SPBC24C6.10c	dip1	WISH/DIP/SPIN90 ortholog, endocytosis protein Dip1
SPBC25B2.03		zf-C3HC4 type zinc finger